UNIVERSITY OF SOUTHAMPTON

FACULTY OF ENGINEERING AND APPLIED SCIENCE

SOUND ATTENUATION IN LINED DUCTS CONTAINING SUBSONIC MEAN FLOWS

by

B.J. Tester, B.Sc., M.Sc.

Thesis submitted for the degree of

Doctor of Philosophy

in the

Institute of Sound and Vibration Research

July, 1972.

ABSTRACT

FACULTY OF ENGINEERING AND APPLIED SCIENCE

INSTITUTE OF SOUND AND VIBRATION RESEARCH

Doctor of Philosophy

SOUND ATTENUATION IN LINED DUCTS CONTAINING SUBSONIC MEAN FLOWS

by Brian John Tester

This investigation is mainly concerned with a theoretical analysis of the inviscid, perturbed or acoustic field, at a particular frequency, in an infinite, two-dimensional duct of constant cross-section in which the fluid properties, other than the mean axial velocity, are constant; one duct wall has a uniform, locally reacting, frequency dependent wall impedance, the other wall is rigid.

The penturbed duct field due to an infinite, uniform line source, or the two-dimensional Green's function, is formally derived for uniform or 'plug' flow in the duct, and is expressed as an infinite sum of non-orthogonal modes.

The optimisation of modal, axial attenuation rates, in the sense defined by Cremer, is examined in detail for zero flow and for 'plug' flow. Cremer's result, for the lowest order mode pair in the absence of flow, is generalised so that the optimum impedance and attenuation rate can now be obtained for any mode pair in ducts of uniform rectangular, circular or annular cross-section. One qualification to Cremer's result emerges in the derivation of the Green's function: at the optimum condition the mode pair degenerates into a single mode with the expected exponential attenuation rate but this is offset by an amplification rate which is directly proportional to the distance from the source. In spite of this effect the axial decay rate of the Green's function can reach a maximum for a wall impedance close to

Cremer's optimum value. The physical mechanism by which this occurs is understood, qualitatively, with the aid of a ray model.

Under certain conditions it is found that not necessarily all the Green's function modes in 'plug' flow decay away from the source : in a particular example it is shown that one mode is spatially amplified in the downstream direction and is a modified form of the well known temporal instability of an incompressible vortex sheet adjacent to a single flexible wall.

An analytical study of the modal field in sheared flow reveals that the pressure and normal particle displacement are constant through a boundary layer of arbitrary profile, in the limit as the boundary layer thickness tends to zero. Thus the physical effects of 'thin' boundary layers on mode solutions are correctly included in the 'plug' flow model. Approximate analytic solutions are obtained for the pressure and normal velocity variations through boundary layers to first order in a parameter proportional to boundary layer thickness and are used to interpret the behaviour of some exact mode solutions.

ACKNOWLEDGEMENTS

The author is grateful to Dr. C.L. Morfey for his guidance and for many helpful ideas and suggestions. Thanks are also due to Professor P.E. Doak and Dr. P. Mungur for interesting discussions and to Professor J.E. Ffowcs Williams for his contribution to one aspect of this work.

CONTENTS

CHAPTER 1

INTRODUCTION

Lining or replacing the interior surfaces of a duct with acoustically absorptive structures is a well established method of reducing the sound radiation from the duct termination. The method has been applied with considerable success to the duct systems of aero-engines that power the Boeing 747, Lockheed Tri-Star and Douglas DC-10 aircraft and will probably be applied to other aircraft engines in the near future*. The total effective cost per aircraft*, however, is not insignificant and there is an urgent need to reduce costs by, for example, improving the noise reduction performance of duct linings and modifying the design to minimise weight and to simplify their manufacture and installation.

The optimisation of aero-engine duct lining design is guided primarily by measurements from duct facilities, scaled aero-engine models and from full-scale tests, either on the test bed or 'in flight'. This in itself is a costly procedure, particularly the full-scale tests, and it is a considerable advantage to have available some form of theoretically based model in order to interpret and correlate test data, to assess the potential of hypothetical design features and to guide the design of linings in project studies and for future testing. The leading aero-engine and aircraft manufacturers have recognised this advantage and now have models in various stages of development; not surprisingly, most of these models are almost identical to one another.

The overall objectives of the present investigation are (i) to

---

*A progress report on the development of duct linings for these and other aircraft engines, together with cost estimates is given in (1).

improve the present understanding of results obtained from the theory on which these models are based, and (ii) to extend the theory in certain respects. To accomplish these objectives and to overcome difficulties experienced with standard methods of formulation it has been necessary to adopt a more fundamental approach than has been usual in this field and to introduce methods from other branches of mathematical and computational physics.

The models referred to above are meant to represent only some of the physical processes encountered in the real problem; the problem can be briefly described as follows. The rotating machinery and the compressible flow field in an unlined duct are responsible for creating part of the sound field existing outside the duct: what is the reduction of this part of the sound field when acoustically absorptive structures are placed within the duct? A typical 'insertion loss' model which provides estimates of this sound reduction is described in Appendix 1A.

The important features and restrictions of the theoretical basis for the part of this 'insertion loss' model which describes physical processes within the duct are listed below. Where possible, with each restriction, references are given to examples of theoretical studies where that particular restriction has been removed. However, in order to pose a soluble problem other unacceptable restrictions have usually been imposed in these studies; for example the duct walls may have to be rigid and/or non-absorptive. Therefore, at present, the following restrictions remain.*

---

*The exception to this is the model developed by the General Electric Co. (USA) (8) in which the restrictions in (3), (6) and (7) are partly or completely relaxed but this model has the restriction that the unperturbed fluid properties cannot vary over the duct cross-section.

1. The propagation of unsteady or perturbed compressible motion (within the duct) is described by the linearised, (2)-(4), inviscid mass, momentum and energy conservation equations.

2. The effect of the acoustically absorptive structures or duct linings on the perturbation field is represented by a frequency dependent, uniform (5), (6), locally reacting (7) impedance boundary condition at the geometric surface of the lining.

3. The duct geometry is two-dimensional (rectangular) of constant width or three-dimensional of constant rectangular, circular or annular cross section, (9). Each surface or wall must have a uniform locally reacting impedance but this can differ between surfaces; for example, each wall of a rectangular duct can have a different impedance.

4. The unperturbed properties of the fluid (e.g. speed of sound, mean velocity) are independent of axial position,* but may vary over the duct cross-section (11).

5. Only steady-state solutions are considered (i.e., the equations for the perturbed field are assumed to have a harmonic time dependence, $\exp[-i\omega t]$).

6. It is assumed that the spatial dependence of the perturbed field can be described by a finite sum of modes; the axial-x dependence of each mode is of the form $\exp[ik_x x]$ where k_x is independent of x and takes a unique value for each mode, (12). In general it is complex so that each mode decays exponentially in either the positive or negative x direction. The value of k_x and the dependence of each mode on the transverse spatial coordinate(s) are determined by the frequency, duct geometry, the unperturbed fluid properties and the impedance boundary conditions.

7. The modes that decay towards the duct termination are usually

---

*Mungur (10) has very recently proposed a method of numerical calculation for overcoming this restriction.

Essentially Chapters 2 and 3 are concerned with certain aspects of the first stage of development, Chapters 4 and 5 with the second stage and Chapter 6 with the third stage although, inevitably, there is some degree of overlap between chapters.

With some exceptions (16) the results from the most recent and complete of these 'insertion loss' models are in good qualitative, and often quantitative, agreement with experimental measurements (see, e.g., Appendix 1A for 'plug flow' model results and references (16a), (57) for shear flow model results) and consequently, in general, the validity of the theoretical framework outlined above need not be questioned, except in special cases. In distinct contrast very little experimental evidence is available which is sufficiently precise to unequivocally establish the validity of the theoretical framework in detailed quantitative terms. To the author's knowledge only two sets of measurements exist which can be regarded as in fully convincingly close quantitative agreement with theoretical results : the measured attenuation rates of the least attenuated mode in a lined rectangular duct containing (sheared) mean flow reported by Kurze and Allen (17) and the measured attenuation rates of various circumferential modes in lined circular and annular ducts, containing a fluid otherwise at rest, obtained by Snow (18). An example of Snow's (18) results is reproduced in Figure (1.1) as his results are not yet available in the open literature. The theoretical attenuation rate shown in Figure (1.1) has been calculated from the equations given by Morse and Ingard (14), using measured impedance values of a sample of the duct lining structure, obtained by the standing wave tube method.

One of the aims of the present work is to investigate the optimisation of theoretical attenuation rates of duct modes, in the particular sense defined by Cremer (19). The relevance of this particular type of optimisation to practical problems is discussed in Appendix 1B. Cremer's (19) result is extended and generalised in Chapters 2 and 4 but in each case this is preceded by the derivation of an expression for a

Green's function, defined as the acoustic or perturbed pressure within an infinite, two-dimensional (rectangular) duct due to a uniform line source of unit strength.

The Green's function has been obtained for three reasons: first it can be used to calculate the acoustic or perturbed field due to any two-dimensional source distribution. Second, the method of derivation shows quite clearly that Cremer's (19) optimum condition is a special case of mode degeneracy. In effect a new mode solution appears at this condition which does not decay in a simple exponential fashion and hence the 'optimum' modal decay rates obtained by Cremer (19) must be modified. This also highlights the point emphasised in Appendix 1B that the optimisation of the axial decay of a perturbed duct field, strictly speaking cannot be carried out without a specification of the source distribution. Nevertheless, the optimum impedance value defined by Cremer (19) and the generalised values given in this work can be used as a guide to the true optimum value in certain practical problems and, where the source distribution cannot be specified (as is often the case), these values are the only guide. In Chapter 2 (zero mean flow) and Chapter 4 (uniform mean flow) the Green's function has been derived by using a fundamental method given by Brekhovskikh (20); it is not essential that this method be used in Chapter 2 although from the physical viewpoint it has some merits over the method used by Morse and Ingard (14). In Chapter 4, however, together with the application of the Lorentz transform, this method has to be employed because the modes no longer exhibit the orthogonality property used by Morse and Ingard (14). The derivation of the two-dimensional Green's function, expressed as a sum of non-orthogonal modes, for a duct containing uniform mean flow is a new theoretical result and is one of the main objectives of the present investigation.

Finally, the third reason for deriving a Green's function is as

follows: the description of the perturbed field in terms of a sum of modes does not allow a simple physical interpretation of why, for example, certain 'optimum' impedance values give rise to a maximum axial decay rate of the perturbed field. Morfey (21) has suggested that a simple interpretation might be possible if the (duct) Green's function is expressed explicitly as the sum of the free-field Green's function and simple functions representing, approximately, the reflection of the free-field by the duct walls. The axial decay of the perturbed field is then realised by a combination of the free-field decay and interference between the free-field and its reflections. Provided this approach leads to a reasonably accurate description of the actual perturbed field it can be used for the purposes of interpretation. It might also be possible to use this as an alternative method of describing duct fields, particularly where the duct geometry and impedance boundary conditions are such that a simple modal description cannot be obtained. In Chapter 3 the accuracy of this approach is assessed with the reflection of the source free-field (by the duct walls) represented by the free-field of an image source (one for each wall) each having a strength given by the plane wave reflection coefficient evaluated at an angle of incidence defined by the ray paths. In other words the influence of the duct walls on the source free-field is described as if each wall existed in isolation. Further refinements to this ray model are also assessed in Chapter 3.

The new Green's function is first derived in Chapter 4 with the implied assumption that the steady-state function exists and that its modulus tends to zero at large distances from the source. Some evidence is presented to support the validity of this Green's function in the form of comparisons between evaluations of this function and of an approximate ray model Green's function (modified to include uniform mean flow).

However, during the course of this work Ffowcs-Williams (22) claimed that the available evidence indicates that a steady-state function cannot exist because the line source triggers one or more modes of the perturbed field which grow with time. This situation has been encountered before, for example, in the study of electron-stream interaction with plasmas, where a procedure has been evolved by Briggs (23) which takes into account temporal instabilities. By using this procedure it is shown in Chapter 4 that provided certain conditions are satisfied it is possible to derive a steady-state Green's function but this now contains at least one spatially amplified mode downstream of the line source.

Chapter 5 is concerned with the (steady-state) energy flows associated with individual modes, particularly those that occur in the Green's function for a duct containing uniform mean flow.

The connection between the perturbed field modes in uniform mean flow and in mean flows with thin boundary layers is established in Chapter 6 with the aid of analytic approximations and numerical solutions of the ordinary differential equations as formulated for the analysis of compressible boundary layer stability (24).

APPENDIX 1A

A Brief Description of a Typical 'Insertion Loss' Model

The purpose of the model is to provide an estimate of the reduction in acoustic energy radiated from a duct termination when a given length of rigid duct wall is replaced by an acoustically absorptive surface. The model is based partly on the theoretical framework outlined in the Introduction but this alone does not allow an insertion loss to be calculated. In place of an extended theoretical framework the following assumptions are made.

1. The modes identified as representing the reflected field at the duct termination, and all 'cut-off' modes, are discarded.

2. The entrance to the lined section is regarded as the excitation plane of the 'cut-on' modes.

3. Each 'cut-on' mode is assigned the same axial energy flow at the excitation plane* both for the unlined and lined duct.

4. The total axial energy flow at the excitation plane is equated with the acoustic energy radiated from the unlined duct.

5. The total axial energy flow at the end of the lined section is equated with the acoustic energy radiated from the lined duct.

A computer program was written by the author while employed by Rolls Royce Ltd., which evaluates this 'insertion loss' model in its second state of development (uniform, subsonic, mean flow). Using this program comparisons between model estimates and measured insertion loss data have been carried out by Wirt (25); a typical comparison is reproduced in Figure (1.2). Two sets of model estimates of insertion loss ("Predicted Duct Attenuation") are shown: the "145/160 dB PREDICTION"

Cross-modal axial energy flow is ignored.

is for liner impedance values, measured by standing wave tube method with the maximum amplitude of the standing wave, at the test frequency, approximately equal to 145/160 dB. The average sound pressure level at the entrance to the lined section was 159 dB and the "prediction" based on the 160 dB impedance values is in good agreement with the measured data.

APPENDIX 1B

Optimisation of the acoustic performance of lined ducts

The close agreement between measured insertion loss and model estimates obtained by Wirt (25) (see Figure (1.2)), supports the validity of the theoretical framework outlined in the Introduction and the assumptions listed in Appendix 1A, but only for the particular experimental facility used by Wirt (25). For example the insertion loss model assigns an identical axial energy flow to each mode (and ignores cross-modal axial energy flows): the agreement with measurements suggests that in Wirt's (25) facility the source distribution over the plane at the lined section entrance is such that modal equipartition of energy flow actually occurs. In other experimental facilities and, particularly, in aero-engine systems, the source distribution may excite a totally different modal energy distribution and unless this can be specified such insertion loss models are of little use.

In spite of this fact it is common practice in the aero-space industry to carry out 'theoretical' optimisation studies, based on this type of insertion loss model, to specify the liner impedance(s) which give the maximum subjectively weighted insertion loss. In practice, therefore, the optimisation of the acoustic performance of lined ducts cannot be carried out without a specification of the frequency spectrum of the acoustic energy radiated from the unlined duct and of the type of required frequency and amplitude subjective weighting.

The optimisation of modal attenuation rates referred to in the Introduction follows on from Cremer's (19) work and is carried out at a particular frequency. This type of optimisation is of academic

interest but it can only be of direct use in 'realistic' optimisation studies if a large insertion loss is required at and near a particular frequency. For example in Figure (12) the results of the present work would indicate how the liner impedance is to be modified to obtain the maximum insertion loss at some frequency near 2000 Hz (MACH +0.3), 1250 Hz (MACH = 0.0) and 1000 Hz (MACH = -0.4).

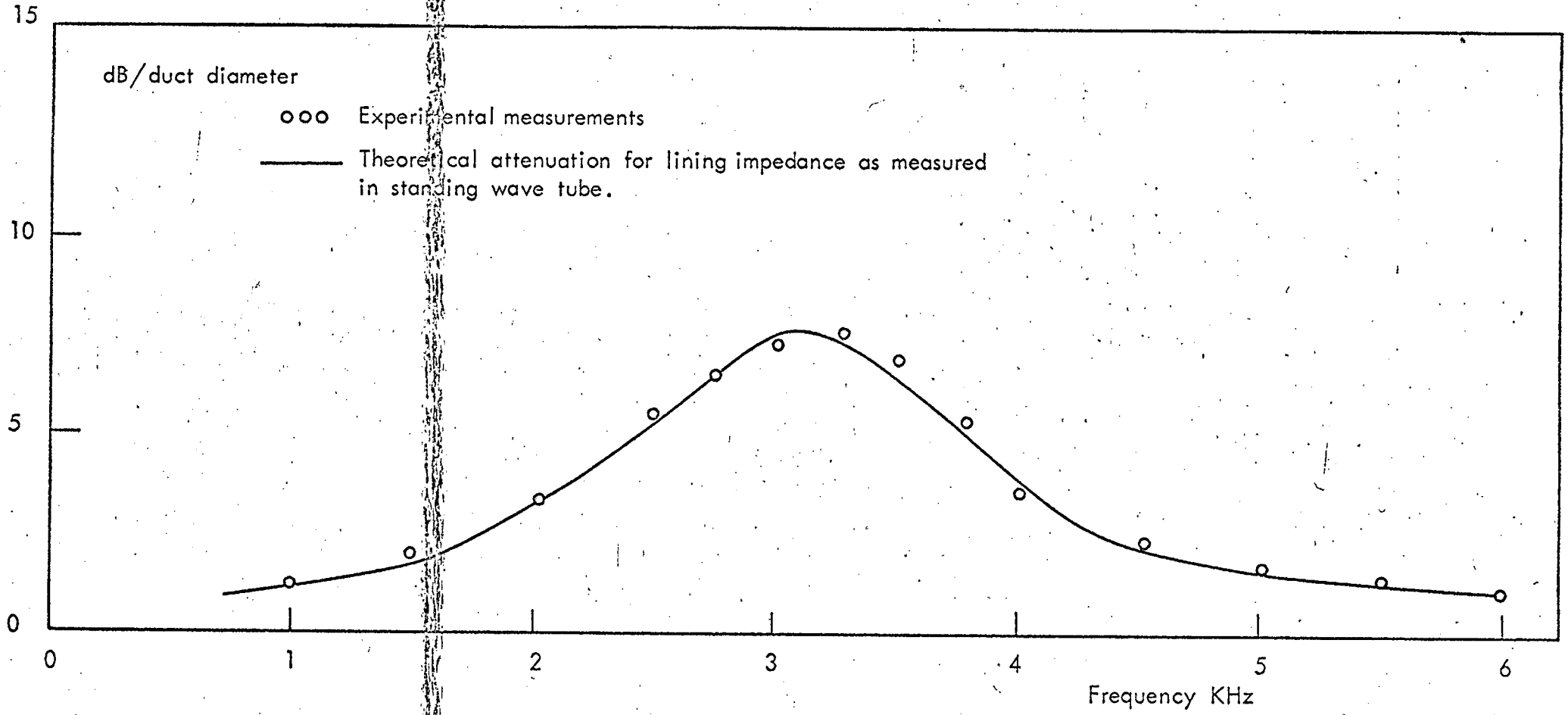

FIG. 1.1 THEORETICAL AND EXPERIMENTAL RESULTS FOR ATTENUATION OF THE ZEROTH ORDER CIRCUMFERENTIAL MODE.

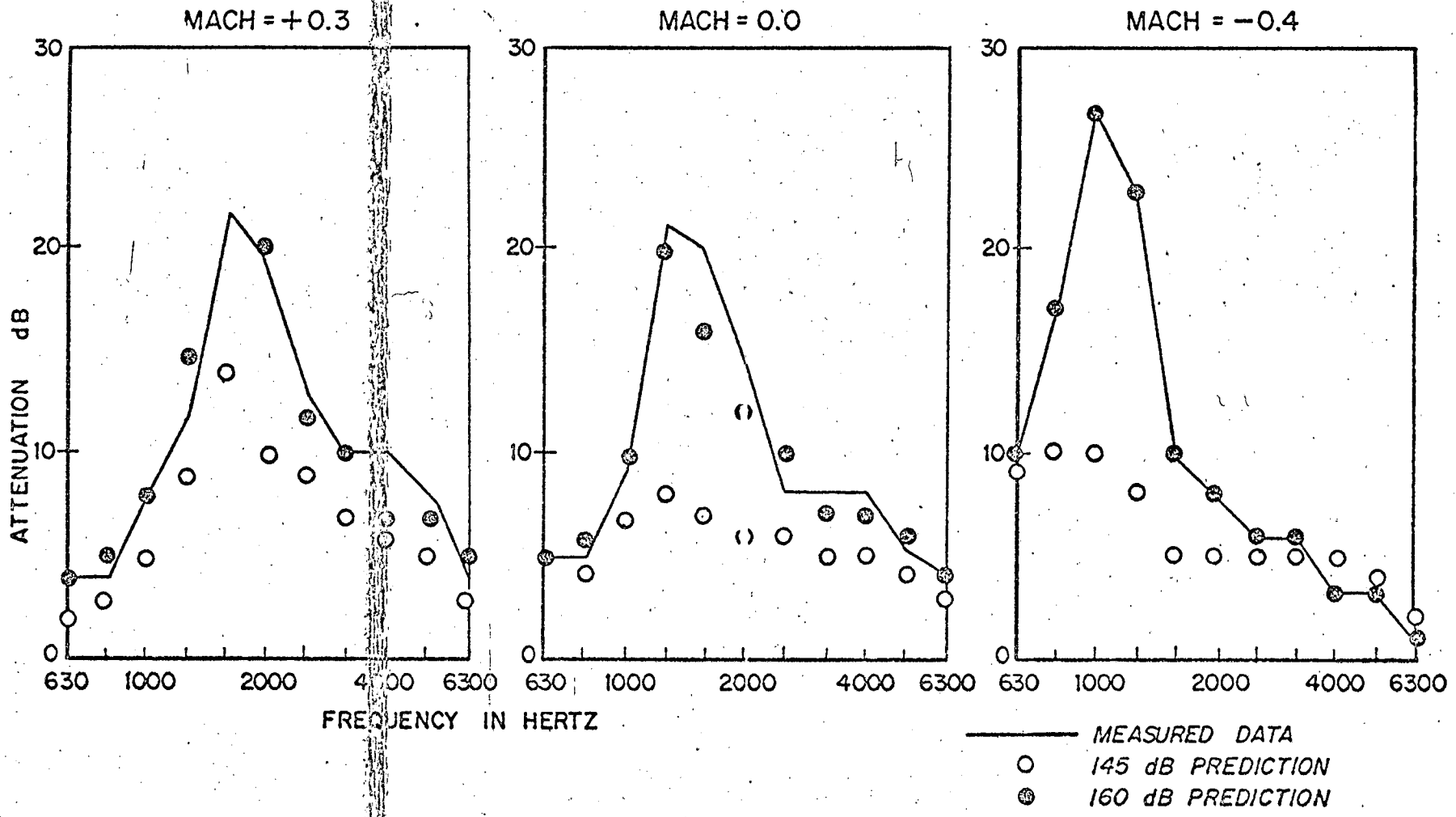

Fig. 1·2 Comparison of Measured and Predicted Duct Attenuation for Various Flow Mach Numbers. The Sound Pressure Level at the Duct Entrance is 159 dB in All Cases. The Duct is Lined Four Feet on Two Sides with Huyck FM 186 Feltmetal Over a One Inch Deep Compartmented Air Space - after Wirt (25).

CHAPTER 2

THE OPTIMISATION OF MODAL SOUND ATTENUATION IN DUCTS, IN THE ABSENCE OF MEAN FLOW

2.1 Discussion

A most intriguing property of theoretical and experimental decay rates of modes in lined ducts, for which there is no obvious explanation, is the existence of maximum decay rates for values of the liner impedance which, at first sight, are arbitrary and totally unconnected with any simple results associated with absorption by reflecting boundaries. For example, the maximum absorption coefficient of a plane wave, incident upon a locally reacting, infinite, plane boundary, is always attained for a purely resistive impedance, irrespective of the wave incidence angle.* In distinct contrast the optimum liner impedance for the maximum attenuation of the least attenuated mode in a lined duct of uniform, rectangular or circular cross-section has a reactive component of the same order of magnitude as the resistive one.

In the early stages of this work a considerable amount of effort was expended in an attempt to explain this apparent anomaly and although the original attempts were largely unsuccessful, a useful by-product emerged in the form of a generalisation of the available results for optimum duct liner impedances, and this is described in section (2.4).

A qualitative explanation of the physical reasons for these

---

*Provided the angle is real.

peculiar optimum impedance values is given in Chapter 3, where it is found to be necessary to specify an acoustic source. Physically, of course, duct modes are generated by a source but it has been common practice in many branches of physics to obtain modal solutions (in itself often a major task) and to make use of these solutions without any specific reference to the source or source distribution.

It became apparent that a complete re-formulation of the classical duct mode problem, with a specified source, was urgently required once it was discovered that the standard Green's function (and hence all solutions for any source distribution) does not exist for the so called optimum impedance values. The method used to derive the standard Green's function consists, in effect, of matching modes to a source distribution, either analytically, using their orthogonality property, or numerically, by an equivalent method. This method which is briefly reviewed in section (2.2) breaks down at optimum conditions.

By adopting a more fundamental approach to the derivation of the Green's function a new mode solution is found which replaces the invalid mode solution responsible for the non existence of the standard Green's function; this derivation is the subject of section (2.3). The method used, which can be found in one particular standard text, is less well known than that based on the orthogonality-matching or expansion procedure. It appears to be completely independent of the properties of the mode functions and, in fact, was introduced to obtain the Green's function as a sum of non-orthogonal modes for a duct with non-locally reacting boundaries. Non-orthogonal modes also occur if the duct contains uniform mean flow and the method is used again in Chapter 4 to obtain the Green's function for this case.

2.2 Review of Standard Theory; the Green's Function for an infinite, Two-dimensional, Lined Duct.

Consider Figure (2.1): a layer of fluid of uniform mean density, ρ_0, and speed of sound, c, is bounded by two infinite planes at y = 0 and at y = h. A line acoustic source, uniform in the z direction with unit strength and a time dependence $\exp[-i\omega t]$ is located at $(\bar{x}_0, y_0)$ where $\bar{x}_0$ is fixed and y_0 can take any value in the interval $0 \leq y_0 \leq h$. The Green's function $G_\omega'(x, y/\bar{x}_0, y_0)$ is defined here as the complex amplitude of the acoustic pressure, due to this source, in the interval $0 \leq y \leq h$. There is no dependence of G_ω' on z because the model is two dimensional.

The acoustic admittance, β_ω, (generally frequency dependent) is also taken to be uniform everywhere at y = h and zero everywhere at y = 0 (rigid wall).

The Green's function satisfies, by definition, the wave equation

$$\{\frac{\partial^2}{\partial x^2} + \frac{\partial^2}{\partial y^2} + (\frac{\omega}{c})^2\} G_\omega'(x, y/\bar{x}_0, y_0) = -\delta(x - \bar{x}_0)\delta(y - y_0) \qquad (2.2.1)$$

and the given admittance boundary conditions at y = 0, h.

The Green's function can be used to calculate the pressure, $p_\omega(x, y)$, due to any 'plane' source distribution $f_\omega(y)$ such that

$$\{\frac{\partial^2}{\partial x^2} + \frac{\partial^2}{\partial y^2} + (\frac{\omega}{c})^2\} p_\omega(x, y) = -f_\omega(y)\, \delta(x - \bar{x}_0)$$

through the relation

$$p_\omega(x, y) = \int_0^h f_\omega(y_0)\, G_\omega'(x, y/\bar{x}_0, y_0)\, dy_0 \qquad (2.2.2)$$

provided the Green's function satisfies the usual law of reciprocity: $G_\omega'(x, y/\bar{x}_0, y_0) = G_\omega'(\bar{x}_0, y_0/x, y)$. The standard procedure for obtaining this Green's function as a solution of equation (2.2.1) is to assume that it can be expanded into an infinite series of orthogonal eigenfunctions

$$G_\omega' = \sum_{n=0}^{\infty} F_n(x)\,\psi_n(y)$$

which, when substituted into equation (2.2.1) for G_ω', gives, after some manipulation (see Morse and Ingard (14))

$$G_\omega'(x,y/\bar{x}_o,y_o) = \frac{-1}{2h} \sum_{n=0}^{\infty} \frac{\psi_n(y)\psi_n(y_o)}{\Lambda_n(ik_{xn})} \exp[ik_{xn}|x - \bar{x}_o|] \qquad (2.2.3)$$

where $$\Lambda_n = \frac{1}{h}\int_0^h \psi_n^2(y)\,dy.$$

To derive equation (2.2.3) the orthogonality property of the functions ψ_n is used, which is defined by

$$\frac{1}{h}\int_0^h \psi_n(y)\psi_m(y)dy = \delta_{mn}\Lambda_{mn} \quad (\delta_{mn} = 0 \quad m \neq n;\ = 1 \quad m = n;\ \Lambda_{nn} \equiv \Lambda_n).$$

If the eigenfunctions ψ_n are simply the solutions of the homogeneous form of equation (2.2.1)

$$\frac{d^2\psi_n}{dy^2} + k_{yn}^2\psi_n = 0 \qquad (2.2.4)$$

where $k_{yn}^2 = k^2 - k_{xn}^2$, $k = \omega/c$

and each satisfies the admittance boundary conditions at the duct walls, defined below, then it can be shown that their orthogonality property depends on the type of admittance which is used.

Multiplying (2.2.4) by ψ_m and also writing the same equation with reversed subscripts m, n $(m \neq n)$

$$\psi_m \frac{d^2\psi_n}{dy^2} + k_{yn}^2 \psi_n\psi_m = 0$$

$$\psi_n \frac{d^2\psi_m}{dy^2} + k_{ym}^2 \psi_n\psi_m = 0$$

and subtracting one from the other, gives

$$\{\psi_m \frac{d^2\psi_n}{dy^2} - \psi_n \frac{d^2\psi_m}{dy^2}\} + (k_{yn}^2 - k_{ym}^2)\psi_n\psi_m = 0 \qquad (2.2.5)$$

The first term can be rewritten as

$$\frac{d}{dy} \{\psi_m \frac{d\psi_n}{dy} - \psi_n \frac{d\psi_m}{dy}\}$$

so that equation (2.2.5) can be integrated directly with respect to y from $y = 0$ to $y = h$ to give

$$\left[\psi_m \frac{d\psi_n}{dy} - \psi_n \frac{d\psi_m}{dy}\right]_0^h + (k_{yn}^2 - k_{ym}^2) \int_0^h \psi_m\psi_n \, dy = 0. \qquad (2.2.6)$$

The boundary conditions at the duct walls are

$$\text{at } y = h: \quad \frac{\partial G_\omega'}{\partial y} = ik\bar{\beta}_\omega G_\omega'; \qquad \text{at } y = 0: \quad \frac{\partial G_\omega'}{\partial y} = 0 \qquad (2.2.7)$$

where $\bar{\beta}_\omega = \beta_\omega \rho_o c$.

$\bar{\beta}_\omega$ is independent of x and if each eigenfunction or mode is to satisfy this boundary condition, then

$$\left[\frac{d\psi_n}{dy} = ik\bar{\beta}_{\omega n}\psi_n\right]_{y=h}; \qquad \left[\frac{d\psi_n}{dy} = 0\right]_{y=0}$$

where $\bar{\beta}_\omega$ has now been allowed to depend on n. Using the first relation the first term of equation (2.2.6) at $y = h$ reduces to

$$\psi_m(h)\{ik\bar{\beta}_{\omega n}\psi_n(h)\} - \psi_n(h)\{ik\bar{\beta}_{\omega m}\psi_m(h)\}$$

which is identically zero provided

$$\bar{\beta}_{\omega n} = \bar{\beta}_{\omega m}$$

that is provided $\bar{\beta}_{\omega}$ is independent of n or say k_{xn}/k, the sine of the 'angle of incidence' of this mode. If this is the case then equation (2.2.6) shows that

$$\int_0^h \psi_n(y)\, \psi_m(y)\, dy = 0 \qquad (m \neq n)$$

and the modes are orthogonal.

If the wall is not locally reacting, then it is not possible to apply an overall boundary condition as in equation (2.2.7), the modes as defined here are not orthogonal and the Green's function cannot be derived on that basis. Nevertheless once the Green's function is found equation (2.2.2) remains valid, that is, the acoustic field can be determined for any source distribution.

The angle-dependent or non-locally reacting admittance boundary condition will not be considered as such but there is another reason why it is necessary to return to a more fundamental derivation of the Green's function, that is, one which does not depend on orthogonal functions. The reason is that for the special condition of optimised modal attenuation, to be discussed in section (2.4) the corresponding normalisation factor Λ_n is zero. The standard Green's function, equation (2.2.3), found in standard texts (14) does not exist under this condition. The Green's function will be rederived to ascertain the reason for this peculiarity and to obtain a solution which does remain finite.

2.3 Fundamental Derivation of the Green's Function with Emphasis on the Optimum Condition.

The principle to be used in this derivation is well known; formally it can be expressed as follows. Given the Green's function, G_ω, for free space (in the absence of all boundaries), then the pressure field in the presence of boundaries as defined above is given by (14),(p.321)

$$p_\omega(x, y) = \int_0^h f_\omega(y_o) G_\omega(x, y/\bar{x}_o, y_o)\, dy_o$$

$$+ \int_{-\infty}^{+\infty} \left[G_\omega(x, y/x_o, h) \frac{\partial p_\omega(x_o, h)}{\partial n_o} - p_\omega(x_o, h) \frac{\partial G_\omega}{\partial n_o}(x, y/x_o, h) \right] dx_o$$

$$+ \int_{-\infty}^{+\infty} \left[G_\omega(x, y/x_o, 0) \frac{\partial p_\omega}{\partial n_o}(x_o, 0) - p_\omega(x_o, 0) \frac{\partial G_\omega}{\partial n_o}(x, y/x_o, 0) \right] dx_o \qquad (2.3.1)$$

where n_o is the normal to the surfaces $y = 0$ and $y = h$, at $x = x_o$, pointing into the fluid.

This expression contains the same integral as in equation (2.2.2) over the given source distribution, but as it now uses the free space Green's function, G_ω, there are an extra two terms which come from a surface integral over the duct boundaries. Physically these terms represent the reflection of the free space field from the duct boundaries. Mathematically these terms also cause the expression for p_ω to become an integral equation in p_ω.

A method of solving this equation for a single surface (say at $y = 0$) is to note, first, that any function $X_\omega(x, y)$ which satisfies the homogeneous wave equation

$$\left\{ \frac{\partial^2}{\partial x^2} + \frac{\partial^2}{\partial y^2} + k^2 \right\} X_\omega(x, y) = 0$$

can be added to the function G_ω. If such a function is chosen so that the modified Green's function, G_ω', has a zero gradient normal to the surface then the pressure field in the presence of a single reflecting boundary is

$$p_\omega(x, y) = \int_0^\infty f_\omega(y_o) G_\omega'(x, y/\bar{x}_o, y_o) dy_o + \int_{-\infty}^{+\infty} G_\omega'(x, y/x_o, 0) \frac{\partial p_\omega}{\partial n_o}(x_o, 0)\, dx_o$$

The function X which ensures that $\partial G_\omega'/\partial n_o = 0$ is well known; it is the Green's function for the image source at $y = -y_o$:

$$X_\omega = G_\omega(x, y/\bar{x}_o, -y_o).$$

If the surface is rigid then $\partial p_\omega/\partial n_o = 0$, and thus

$$p_\omega(x, y) = \int_0^\infty f_\omega(y_o) G_\omega'(x, y/\bar{x}_o, y_o) dy_o; \quad G_\omega' = G_\omega + X_\omega.$$

This is an exact solution for the pressure field due to a source distribution in the presence of a uniform, infinite rigid boundary.

To obtain an expression for the pressure field under the same conditions, but with a locally reacting boundary of admittance $\bar{\beta}_\omega$ (at $y = 0$) introduces a complication which originates from the fact that the reflected field can only be described exactly for an incident field consisting of plane waves. Thus the free space Green's function has to be expressed in terms of plane waves and this can be done by means of the Fourier spatial transform, the formal expression being

$$G_\omega(x, y/\bar{x}_o, y_o) = (2\pi)^{-2} \int_{-\infty}^{+\infty} \int_{-\infty}^{+\infty} \frac{\exp[iK_x(x-\bar{x}_o) + iK_y(y-y_o)]\, dK_x dK_y}{K^2 - k^2} \qquad (2.3.2)$$

where $K^2 = K_x^2 + K_y^2$.

(Note that Morse and Ingard (14) use the opposite sign in the exponential terms). The free space Green's function now consists of plane waves, with wave numbers (K_x, K_y), which are incident on the locally reacting boundary at an angle $-\cos^{-1}(K_y/K)$ and their reflection coefficient, C_r, is

$$C_r = \frac{K_y/K - \bar{\beta}_\omega}{K_y/K + \bar{\beta}_\omega}$$

The image concept is now modified in that an image source is used with a source strength given by the above reflection coefficient. This means that the image source has an angle dependent strength and the simplicity of a simple image source of unit strength is lost. However, an approximate result can still be obtained for $p_\omega(x, y)$ and this result is relevant because it is to be used in Chapter 3, in an attempt to understand the optimum conditions analysed in section (2.4).

By choosing the additive function $X_\omega(x, y)$ to be

$$X_\omega(x, y) = (2\pi)^{-2} \int_{-\infty}^{+\infty} \int_{-\infty}^{+\infty} \frac{C_r \exp[iK_x(x - \bar{x}_o) + iK_y(y + y_o)]}{(K^2 - k^2)} dK_x dK_y$$

(physically the total reflected field) the modified Green's function

$$G_\omega' = G_\omega + X_\omega$$

also satisfies the boundary conditions for the pressure field

$$\frac{\partial G_\omega'}{\partial n_o} = -ik\bar{\beta}_\omega G_\omega'$$

(the minus sign appearing because n_o points into the fluid). Thus the surface integrals in equation (2.3.1) vanish identically and again

$$p_\omega(x, y) = \int_0^\infty f_\omega(y_o)\, G_\omega'(x, y/\bar{x}_o, y_o)\, dy_o$$

(N.B. see below*)

The function X_ω cannot be represented exactly in closed form but, (Morse and Ingard (14), p.371), provided either y or y_o is larger than half a wavelength, a good approximation is, for a point source,

$$G_\omega'(x, y)/\bar{x}_o, y_o) \doteq G_\omega(x, y/\bar{x}_o, y_o) + \frac{\cos\bar{\theta} - \bar{\beta}_\omega}{\cos\bar{\theta} + \bar{\beta}_\omega} G_\omega(x, y/\bar{x}_o, -y_o) \qquad (2.3.3)$$

where $\bar{\theta}$ is defined in Figure (2.2). This is assumed to be a valid approximation for a line source as well.

Apart from introducing the approximate expression in equation (2.3.3) for use in Chapter 3 the above discussion has also served to introduce the fundamental principle by which the Green's function for a duct will be derived. The method is described in detail by Brekhovskikh (20) for a point source but here his method will be used for the line source and a new result will be obtained for the special case, associated with the optimum condition, where the so-called normalisation factor Λ_n found in the denominator of the standard Green's function is equal to zero.

To recapitulate, the Green's function, $G_\omega'(x, y/\bar{x}_o, y_o)$, for an infinite two-dimensional duct is required for a line source at $(\bar{x}_o, y_o)$ which in free space satisfies the wave equation

$$\left\{\frac{\partial^2}{\partial x^2} + \frac{\partial^2}{\partial y^2} + k^2\right\} G_\omega(x, y/\bar{x}_o, y_o) = -\delta(x - \bar{x}_o)\delta(y - y_o) \qquad (2.3.4)$$

G_ω and G_ω' must have a singularity at $x = \bar{x}_o$, $y = y_o$ and G_ω

---

*In fact provided G_ω' satisfies the boundary conditions, either as a whole for a locally reacting boundary, or in terms of its constituent plane waves for non-locally reacting boundaries, the solution $p_\omega = G_\omega'$ causes the surface integrals to vanish identically.

must satisfy the radiation condition that it consists of outgoing waves from the point $(\bar{x}_o, y_o)$.

Defining the Fourier space transform of G_ω

$$G_\omega(K_x, K_y) = (2\pi)^{-2} \int_{-\infty}^{+\infty} \int_{-\infty}^{+\infty} G_\omega(x, y/\bar{x}_o, y_o) \exp[-iK_x x - iK_y y]dxdy$$

with

$$-G_\omega(x, y/\bar{x}_o, y_o) = \int_{-\infty}^{+\infty} \int_{-\infty}^{+\infty} G_\omega(K_x, K_y) \exp[iK_x x + iK_y y)]\, dK_x dK_y$$

and taking the Fourier space transform of equation (2.3.4) and inverting gives

$$G_\omega(x, y/\bar{x}_o, y_o) = (2\pi)^{-2} \int_{-\infty}^{+\infty} \int_{-\infty}^{+\infty} \frac{\exp[iK_x(x - \bar{x}_o) + iK_y(y - y_o)]}{(K^2 - k^2)} dK_x dK_y \qquad (2.3.5)$$

It can be shown [(14), p.366] that the evaluation of this double integral gives a solution for G_ω, satisfying the above conditions, as

$$G_\omega(x, y)/\bar{x}_o, y_o) = \frac{i}{4} H_o^{(1)}(kR) \qquad (2.3.6)$$

where $R^2 = (x - \bar{x}_o)^2 + (y - y_o)^2$.

This solution is now to be modified by the presence of two infinite planes at $y = 0$ and at $y = h$, the boundary conditions being

$$\frac{\partial G_\omega}{\partial y} = ik\beta_\omega G_\omega \quad \text{at } y = h$$

$$\frac{\partial G_\omega'}{\partial y} = 0 \quad \text{at } y = 0$$

In terms of the ratio of the additive function $X_\omega(x, y)$ to $G_\omega(x, y/\bar{x}_o, y_o)$ at these boundaries, the reflection coefficient, these

boundary conditions can be rewritten as

$$C_r = \frac{K_y/K - \bar{\beta}_\omega}{K_y/K + \bar{\beta}_\omega} \quad \text{at} \quad y = h$$

$$C_r = 1 \qquad \text{at} \quad y = 0$$

Before proceeding to take these boundary conditions into account the integration in equation (2.3.5) is carried out with respect to K_y. Writing

$$k_y^2 = k^2 - K_x^2$$

so that the denominator in the integrand becomes

$$(K_y - k_y)(K_y + k_y)$$

it is clear that the integrand has two simple poles in the complex K_y plane, at $K_y = \pm k_y$, where

$$k_y = + \sqrt{k^2 - K_x^2}; \quad |K_x| \leq k$$

$$= + i\sqrt{K_x^2 - k^2}; \quad |K_x| > k$$

When K_x is real and the former condition holds the K_y integration along the $\mathrm{Re}(K_y)$ axis is determined by the two poles at $K_y = \pm k_y$: if $y - y_0 > 0$ the pole $K_y = +k_y$ represents an outgoing wave from the point $(\bar{x}_0, y_0)$ and the pole at $K_y = -k_y$ an incoming wave, and vice versa for $y - y_0 < 0$. The radiation condition can be satisfied, that is, the integral can be determined by the pole representing an outgoing wave, by allowing the wavenumber k to have a small imaginary part*, corresponding to dissipation in the fluid. The imaginary part of k can be set to zero in the final solution. For $|K_x| < |k|$

---

*The sign being such that $|\exp[ikx]| \to 0$ as $x \to +\infty$

the poles are no longer situated on the $Re(K_y)$ axis: the pole with $Re(K_y) > 0$ is situated just above the axis and the pole with $Re(K_y) < 0$, just below. For $y - y_o > 0$ the contour can be closed in the upper half plane, with an infinite semi-circle, without changing the value of the integral, and the integral is evaluated, by the Residue Theorem at the 'outgoing wave pole'. The complete contour is shown in Figure (2.3) where the contour along the $Re(K_y)$ axis is deformed to indicate its path in relation to the poles. For $y - y_o < 0$ the contour is closed in the lower half plane but as the pole is identical, apart from the difference in sign, only one case, $y - y_o > 0$, needs to be considered. The K_y integration is carried out to give

$$G(x, y/\bar{x}_o, y_o) = \frac{i}{4\pi} \int_{-\infty}^{+\infty} \exp[iK_x(x - \bar{x}_o) + ik_y(y - y_o)] \frac{dK_x}{k_y}$$

$$\text{for } (y - y_o) > 0 \qquad (2.3.7)$$

G_ω is now to be modified to satisfy the boundary conditions by considering a plane wave component of G_ω and adding to that component the total reflected field. First ignoring the lower boundary at $y = 0$, the total reflected field is (see Figure (2.4a))

$$\frac{k_y/k - \bar{\beta}_\omega}{k_y/k + \bar{\beta}_\omega} \exp[iK_x(x - \bar{x}_o) + ik_y(2h - y_o - y)].$$

Note that the phase of the reflected field has the same x dependence as the incident field, but the coefficient of k_y is the projection on the y axis of the path traversed by the wave. This is the field due to the image in the upper boundary. To take into account the image in the lower boundary the reflected field is modified to

$$\exp[iK_x(x - \bar{x}_o)]\{C_r \exp[ik_y(2h - y_o - y)] + (1) \exp[ik_y(y + y_o)]\}$$

This second term of course does not satisfy the boundary condition at the upper boundary and the reflection from there (due to the image in the upper boundary of the image in the lower one) (see Figure (2.4b) gives rise to a third term so that the reflected field is now

$$\exp[iK_x(x - \bar{x}_0)]\{C_r \exp[ik_y(2h - y_0 - y)] + (1) \exp[ik_y(y + y_0)]$$

$$+ (1)\ (C_r) \exp[ik_y(2h + y_0 - y)]\}$$

It is emphasised that these leading terms of an infinite series are for the reflection and re-reflection of an incident plane wave at one <u>particular</u> angle $\cos^{-1}(k_y/k)$. The continuous lines in Figures (2.4a) and (2.4b) do not represent this wave or its reflections, as such. They are <u>not</u> lines normal to lines of constant phase as would be the case for the reflection of a spherical wave in the plane (x, y), but simply indicate that, for example, (in Figure (2.4a), line OP) point P receives a contribution from source O, (line O'P), point P receives a contribution from the source image O' and so on. A simple graphical representation of the plane waves is not strictly possible because (see below) in general the 'angle of incidence', $\cos^{-1}(k_y/k)$, is complex.

The total field for the particular plane wave component, including all reflections, can be obtained by repeating the above procedure and the final expression after some manipulation is, (20),

$$\exp[iK_x(x - \bar{x}_0)] \sum_{\ell=0}^{\infty} \{\exp[ik_y(y - y_0)] + \exp[ik_y(y + y_0)]$$

$$+ C_r \exp[ik_y(2h - y - y_0)] + C_r \exp[ik_y(2h - y + y_0)]\}$$

$$\times C_r^{\ell} \exp[2ik_y \ell h]$$

$$= \exp[iK_x(x - \bar{x}_0)].F \quad \text{say}$$

and the total field is

$$G_\omega'(x, y/\bar{x}_o, y_o) = \frac{i}{4\pi} \int_{-\infty}^{+\infty} \exp\,[iK_x(x - \bar{x}_o)]F. \frac{dK_x}{k_y} \qquad (2.3.8)$$

for $(y - y_o) > 0$

The integration variable is now changed to θ where $\theta = \cos^{-1}(k_y/k)$; $K_x = k \sin\theta$; $dK_x = k \cos\theta\, d\theta$ and as

$$\sin\theta = \sin\theta_r \cosh\theta_i + i \cos\theta_r \sinh\theta_i; \quad \theta = \theta_r + i\theta_i$$

$$\cos\theta = \cos\theta_r \cosh\theta_i - i \sin\theta_r \sinh\theta_i ,$$

then the corresponding integration limits are:

$$K_x \to +\infty \qquad \theta \to \frac{\pi}{2} - ia, \qquad a \to \infty$$

$$K_x \to -\infty \qquad \theta \to -\frac{\pi}{2} + ia, \qquad a \to \infty$$

(Note that if k is real then $\theta = \pm\frac{\pi}{2}$ when $K_x = \pm k$)

The chosen contour in the θ plane is shown in Figure (2.5a); the fact that k has a small imaginary part is ignored for the present.

Consider the infinite sum in the function F on this contour

$$S = \sum_{\ell=0}^{\infty} C_r{}^{\ell} \exp[2ikh \cos\theta]^{\ell} = \sum_{\ell=0}^{\infty} X^{\ell} \qquad (2.3.9)$$

Provided $|X| < 1$, S can be given in a closed form

$$S = \{1 - C_r \exp[2ikh \cos\theta]\}^{-1} .$$

Brekhovskikh (20) assumes $|X| < 1$ everywhere on the contour apparently without any detailed justification. Physically, $|X|$ being the reduction in amplitude of a plane wave after one reflection and two traverses of a duct width, it is reasonable to assume that $|X|$ is less than unity. However, it is necessary to digress for a moment

and analyse the behaviour of X on the chosen contour because this may be a crucial point in a similar analysis given in Chapter 4 where mean flow is included.

For a locally reacting boundary, X is simply a function of $\cos\theta$;

$$X = \frac{\cos\theta - \bar{\beta}_\omega}{\cos\theta + \bar{\beta}_\omega} \exp\left[2ikh\cos\theta\right] .$$

Consider first contour BC (see Figure (2.5a)): θ lies in the interval $(-\pi/2, +\pi/2)$, thus

$$0 \leq \cos\theta \leq 1$$

and expressing C_r in terms of the real and imaginary parts of $\bar{\beta}_\omega$:

$$C_r = \frac{\{\cos\theta - \mathrm{Re}(\bar{\beta}_\omega)\} - i\,\mathrm{Im}(\bar{\beta}_\omega)}{\{\cos\theta + \mathrm{Re}(\bar{\beta}_\omega)\} + i\,\mathrm{Im}(\bar{\beta}_\omega)}$$

it can be seen that $|C_r| \leq 1$ if $\mathrm{Re}(\bar{\beta}_\omega) \geq 0$. Thus

$$|X| \leq 1 \text{ on BC if } \mathrm{Re}(\bar{\beta}_\omega) \geq 0$$

as $|\exp[2ikh\cos\theta]| = 1$. The equality $X = 1$ cannot be allowed and this will be dealt with later.

On contours AB and CD

$$\cos\theta = i\sinh a \qquad 0 \leq a \leq \infty$$

and $$X = \frac{\{\mathrm{Re}(\bar{\beta}_\omega) - i(\sinh a - \mathrm{Im}(\bar{\beta}_\omega))\}}{\{\mathrm{Re}(\bar{\beta}_\omega) + i(\sinh a + \mathrm{Im}(\bar{\beta}_\omega))\}} \exp[-2kh\sinh a]$$

As 'a' can tend to zero* $|C_r|$ must be shown to be less than unity. Clearly if $\mathrm{Im}(\bar{\beta}_\omega) \geq 0$, then $|C_r| \leq 1$ but whereas the restriction $\mathrm{Re}(\bar{\beta}_\omega) \geq 0$ on contour BC is a reasonable one (that is, a passive

---

*Also kh can be arbitrarily small.

admittance) this condition is too restrictive. In fact it has arisen because the contour ABCD does not take into account the small imaginary part of k. Corresponding to this complex k value the original contour on the θ plane is changed to Γ_1 as shown in Figure (2.5a), although it remains asymptotic to lines AB and CD. On this 'new' contour AB', θ now takes the value

$$\theta = -\frac{\pi}{2} + \delta + ia \qquad 0 < a \leq \infty$$

and

$$\cos\theta = \sin\delta \cosh a + i\cos\delta \sinh a$$

giving

$$C_r = \frac{\{\sin\delta \cosh a - Re(\bar{\beta}_\omega)\} + i\{\cos\delta \sinh a - Im(\bar{\beta}_\omega)\}}{\{\sin\delta \cosh a + Re(\bar{\beta}_\omega)\} + i\{\cos\delta \sinh a + Im(\bar{\beta}_\omega)\}}$$

or $C_r = 1 + 2i \cot\delta \tanh a$

for the extreme case when $Im(\bar{\beta}_\omega) = -\cos\delta \sinh a$ and $Re(\bar{\beta}_\omega) = 0$. As $a \neq 0$ the exponential factor is less than unity and $|X|$ can be made less than unity by a suitable choice of δ provided that in deforming the contour no singularities of the integrand of equation (2.38) are encountered and provided the contour remains asymptotic to the lines AB and CD. As $a \to \infty$, the exponential factor is small enough to ensure that $|X| \to 0$ as $\delta \to 0$. On contour AB' the equality $|X| = 1$ can be removed because $|\exp[2ikh\cos\theta]| < 1$ with k slightly imaginary. Thus $|X| < 1$ everywhere on the deformed contour provided $Re(\bar{\beta}_\omega) \geq 0$.

Equation (2.3.8) can now be written, with equation (2.3.9) as

$$G_\omega'(x, y/\bar{x}_0, y_0) = \frac{i}{4\pi} \int_{-\frac{\pi}{2}+i\infty}^{\frac{\pi}{2}-i\infty} \{\exp[ik\sin\theta(x - \bar{x}_0)] \; 2\cos iby_0\}$$

$$\times \frac{\{\exp[-b(h-y)] + C_r \exp[b(h-y)]\}}{\exp[-bh] \, (1 - C_r \exp[2bh])} d\theta \qquad (2.3.10)$$

where $b = ik \cos\theta$. The final step leading to the evaluation of this integral is to change the path of integration. Again this is described by Brekhovskikh (20), and in adequate detail, but it is a step which has to be investigated for the purposes of Chapter 4 and thus is outlined briefly here.

Referring to Figure (2.5b) the original integration path ABCD or Γ_1 is seen to be equivalent to a sum of the two contours Γ_2 and Γ_3. It can be shown that the integral, I, over Γ_3 is identically zero. To do so the variable is changed to the 'grazing incidence' angle, α, where

$$\alpha = \frac{\pi}{2} - \theta$$

then

$$I = \frac{i}{4\pi} \int_{-i\infty}^{+i\infty} \{\exp[ik \cos\alpha(x - \bar{x}_0)]\ 2 \cos iby_0 \times \exp[-b(h - y)] + C_r(\alpha) \exp[+b(h - y)]\} / \exp[-bh]\ (1 - C_r(\alpha) \exp[2bh])\ d\alpha \qquad (2.3.11)$$

where $b = ik \sin\alpha$

and

$$C_r(\alpha) = \frac{\sin\alpha - \bar{\beta}_\omega}{\sin\alpha + \bar{\beta}_\omega} .$$

Using

$$C_r(-\alpha) = \frac{1}{C_r(\alpha)}$$

the integrand can be shown to be an odd function of α and hence the integral over Γ_3 is zero.

Finally the contour Γ_2 can be closed in the upper half plane by the infinitely remote path Γ_4, without changing the value of the integral, provided $x - \bar{x}_0 > 0$. Similarly, a closed contour can be

formed in the lower half plane for $x - \bar{x}_o < 0$ but as the poles of the integrand, θ_n, where θ_n satisfies the equation

$$1 - C_r(\theta) \exp[2ikh \cos \theta] = 0 \qquad (2.3.12)$$

are identical in upper and lower planes, apart from the difference in sign, both cases can be covered by writing the $(x - \bar{x}_o)$ dependence as

$$\exp[ik \sin \theta |x - \bar{x}_o|].$$

Thus, by the Residue Theorem, the integral in equation (2.3.10), (over the new contour) is given by

$$G_\omega'(x, y/\bar{x}_o, y_o) = -\tfrac{1}{2} \sum_{n=0}^{\infty} \text{Res}\{\Phi(\theta_n)\} \qquad (2.3.13)$$

where

$$\Phi(\theta) = \frac{\exp[ik \sin \theta |x - \bar{x}_o|] 2 \cos iby_o \{\exp[-b(h - y)] + C_r \exp[b(h - y)]\}}{\exp[-bh] (1 - C_r \exp[2bh])}$$

It is at this point that the analysis of Brekhovskikh (20), which assumes these to be simple poles, needs to be extended to take into account the existence of double poles. The simple pole is clearly the origin of the usual eigenfunction or mode. A pole of order 2, which occurs when two simple poles merge on the complex θ plane, is evidently the reason for the non-existence of the standard solution.

However it is of interest to demonstrate first that the solution given by equation (2.3.13) for simple poles does lead to the solution given in the previous section - a sum of orthogonal modes.

Setting

$$H = 1 - C_r(\theta) \exp[2ikh \cos \theta] \qquad (2.3.14)$$

then near a simple pole, θ_n, H behaves like

$$H \doteq (\theta - \theta_n) \left[\frac{dH}{d\theta}\right]_{\theta=\theta_n}$$

and

$$\text{Res}\{\Phi(\theta_n)\} = \frac{\exp[ik \sin \theta_n |x - \bar{x}_o|] 2 \cos(ib_n y_o)\ 2 \cos(ib_n y)}{[dH/d\theta]_{\theta=\theta_n}} \qquad (2.3.15)$$

where $b_n = ik \cos \theta_n$.

To obtain G_ω' in a suitable form for comparison with the standard solution, the variable is changed to

$$k_y = k \cos \theta \qquad \frac{d}{d\theta} = -k_x \frac{d}{dk_y}$$

$$k_x = k \sin \theta \qquad \frac{dk_x}{dk_y} = -\frac{k_y}{k_x}$$

Then the equation for k_{yn}, $H = 0$, is

$$0 = \frac{-2i \exp[ik_y h]}{k_y h + kh \bar{\beta}_\omega} \{k_y h \sin(h_y h) + ikh \bar{\beta}_\omega \cos(k_y h)\}$$

or

$$-ikh\bar{\beta}_\omega = (k_y h) \tan(k_y h) \qquad (2.3.16)$$

which is the eigenvalue equation first introduced by Morse (13). The value of $dH/d\theta$ at the pole is

$$\left[\frac{dH}{d\theta}\right]_{\theta=\theta_n} = \frac{2ik_{xn}h}{k_{yn}h \sec^2(k_{yn}h)} \left[\frac{d}{d(k_y h)} \{k_y h \tan(k_y h) + ikh\bar{\beta}_\omega\}\right]_{k_y=k_{yn}}$$

or with $\frac{d}{d(k_y h)} \{ikh\bar{\beta}_\omega\} = 0$*

---

*For a locally reacting admittance.

$$\left[\frac{dH}{d\theta}\right]_{\theta=\theta_n} = 2ik_{xn}h \quad \{\frac{\frac{1}{2}\sin(2k_{yn}h)}{k_{yn}h} + 1\}$$

The final expression for the residue at θ_n is

$$\text{Res}\{\Phi(\theta_n)\} = \frac{2\exp[ik_{xn}|x - \bar{x}_o|]\cos(k_{yn}y_o)\cos(k_{yn}h)}{i(k_{xn}h)\{\frac{0.5\sin(2k_{yn}h)}{k_{yn}h} + 1\}}$$

and for the total acoustic field

$$G_\omega'(x,y/\bar{x}_o,y_o) = -\tfrac{1}{2}\sum_{n=0}^{\infty}\frac{\cos(k_{yn}y_o)\cos(k_{yn}y)\exp[ik_{xn}|x-\bar{x}_o|]}{i(k_{xn}h)\,0.5\,[\frac{0.5\sin(2k_{yn}h)}{k_{yn}h} + 1]} \qquad (2.3.17)$$

This expression exhibits the required singularity at $(\bar{x}_o, y_o)$ and is now independent of the sign of $(y - y_o)$ as it remains unchanged when y is interchanged with y_o. It can now be compared directly with the standard expression in equation (2.2.3): choosing the appropriate eigenfunction to be

$$\psi_n(y) = \cos(k_{yn}y)$$

and evaluating Λ_n:

$$\Lambda_n = \frac{1}{h}\int_0^h \cos^2(k_{yn}y)dy = 0.5\,[\frac{0.5\sin(2k_{yn}h)}{k_{yn}h} + 1] \qquad (2.3.18)$$

it can be seen that the expressions for G_ω' are identical.

For a locally reacting admittance $\bar{\beta}_\omega$ it can be shown that all the poles, θ_n, occur in the first quadrant of the complex θ plane so that $\text{Re}(k_x) \geq 0$ and the phase velocity, $\omega/\text{Re}(k_x)$, is positive in the direction of modal decay. This may not be the case for a non-locally reacting admittance which includes in a sense, the mean flow case considered in Chapter 4.

When $\Phi(\theta)$ has a double pole at $\theta = \theta_n$, that is, when H behaves, near θ_n, like

$$H \doteq \frac{(\theta - \theta_n)^2}{2!}\left[\frac{d^2H}{d\theta^2}\right]_{\theta=\theta_n} + \frac{(\theta - \theta_n)^3}{3!}\left[\frac{d^3H}{d\theta^3}\right]_{\theta=\theta_n} \qquad (2.3.19)$$

then the residue is

$$\begin{aligned}\text{Res}\{\Phi(\theta_n)\} &= \lim_{\theta \to \theta_n} \frac{d}{d\theta}\left\{\frac{D}{H}(\theta - \theta_n)^2\right\} \\ &= 2\frac{dD_n}{d\theta}\left\{\frac{d^2H_n}{d\theta^2}\right\}^{-1} - \frac{2}{3}D_n\frac{d^3H_n}{d\theta^3}\left\{\frac{d^2H_n}{d\theta^2}\right\}^{-2} \qquad (2.3.20)\end{aligned}$$

where $D = \exp[ik \sin\theta|x - \bar{x}_o|]\ 2\cos(iby_o)\{\exp[by] + (1 - H)\exp[-by]\}$ and the subscripts n indicate evaluation, after differentiation, at $\theta = \theta_n$. The required quantities take the following values at $\theta = \theta_n$, in the (k_x, k_y) notation

$$D_n = \exp[ik_{xn}|x - \bar{x}_o|]\ 4\cos(k_{yn}y_o)\cos(k_{yn}y)$$

$$\frac{dD_n}{d\theta} = \exp[ik_{xn}|x - \bar{x}_o|]\ 4\cos(k_{yn}y_o)\cos(k_{yn}y)\{ik_{yn}|x - \bar{x}_o| + k_{xn}y_o\tan(k_{yn}y_o) + k_{xn}y\tan(k_{yn}y)\}$$

$$H_n = \left[\frac{-2i\exp[ik_yh]\cos(k_yh)}{k_yh + kh\bar{\beta}_\omega}\right]_{k_y=k_{yn}}$$

$$\frac{dH_n}{d\theta} = -k_{xn}h\,A_n\left[\frac{d}{d(k_yh)}\{(k_yh)\tan(k_yh) + ikh\bar{\beta}_\omega\}\right]_{k_y=k_{yn}} = 0$$

(by definition, for a double pole)

where $A = \dfrac{-2i\exp[ik_yh]\cos(k_yh)}{k_yh + kh\bar{\beta}_\omega}$

$$\frac{d^2H_n}{d\theta^2} = (k_{xn}h)^2 A_n \left[\frac{d^2}{d(k_yh)^2} \{k_yh \tan(k_yh) + ikh\bar{\beta}_\omega\}\right]_{k_y=k_{yn}}$$

$$\frac{d^3H_n}{d\theta^3} = \{-3(k_{xn}h)^3 \frac{dA_n}{d(k_yh)} + 3A_n(k_{xn}h)(k_{yn}h)\} \left[\frac{d^2}{d(k_yh)^2}\{k_yh \tan(k_yh)\right.$$

$$\left. + ikh\bar{\beta}_\omega\}\right]_{k_y=k_{yn}} - (k_{xn}h)^3 A_n \left[\frac{d^3}{d(k_yh)^3} \{k_yh \tan(k_yh) + ikh\bar{\beta}_\omega\}\right]_{k_y=k_{yn}}$$

The values of A_n and the derivatives in these expressions are

$$A_n = 2it^{-1}$$

where $t = \tan(k_{yn}h)$

$$\frac{dA_n}{d(k_yh)} = 2i(1 - t^2)t^{-2}$$

$$\left[\frac{d^2}{d(k_yh)^2} \{k_yh \tan(k_yh)\}\right]_{k_y=k_{yn}} = 2$$

$$\left[\frac{d^3}{d(k_yh)^3} \{k_yh \tan(k_yh)\}\right]_{k_y=k_{yn}} = 4t$$

where use has been made of

$$H_n = 0$$

or

$$k_{yn}h \tan(k_{yn}h) = -ikh\bar{\beta}_\omega$$

$$\frac{dH_n}{d\theta} = 0$$

or

$$\tan(k_{yn}h) + (k_{yn}h) \sec^2(k_{yn}h) = 0$$

and as the admittance is locally reacting

$$\frac{d}{d(k_y h)}(\bar{\beta}_\omega) = 0$$

Thus the final expressions for the quantities required in the residue are

$$\frac{d^2 H_n}{d\theta^2} = (k_{xn}h)^2\, 4it^{-1}$$

$$\frac{d^3 H}{d\theta^3} = \frac{12i(k_{xn}h)}{t^2}\left\{\frac{(k_{xn}h)^2}{3}t^2 + (k_{yn}h)t - (k_{xn}h)^2\right\}$$

so that equation (2.3.20) becomes

$$\begin{aligned}\mathrm{Res}\{\Phi(\theta_n)\} &= 2\{\exp[ik_{xn}|x - \bar{x}_o|].\cos(k_{yn}y_o)\cos(k_{yn}y)\} \\ &\times \left\{\frac{t}{i(k_{xn}h)^2}[ik_{yn}|x - \bar{x}_o| + k_{xn}y_o \tan(k_{yn}y_o) + k_{xn}y \tan(k_{yn}y)]\right. \\ &+ \left.\frac{i}{(k_{xn}h)^3}[(k_{xn}h)^2\frac{t^2}{3} + (k_{yn}h)t - (k_{xn}h)^2]\right\} \qquad (2.3.21)\end{aligned}$$

This expression for the residue at a pole, θ_n, is to be used in place of that given by equation (2.3.15) if the pole is of second order. It is the main result of this section: whereas the standard simple pole solution given by equation (2.3.15) leads to general solutions for the Green's functions which do not exist for the double pole condition, this solution does allow a finite mode amplitude to be calculated.

The question now arises: is this type of solution, containing a mode with an x dependence of the form

$$(Ax + B)\exp[ik_{xn}|x - \bar{x}_o|]$$

associated only with the double pole condition or is it indicative of

the behaviour of two mode solutions near this condition? The answer can be found by taking two modes resulting from two single poles which lie close together on the θ plane, denoted by subscripts m and n, and expanding the normalisation factor about its zero. The field, p_ω, due to these two modes is, from the standard solution (equation (2.3.17), with $y = y_o = \bar{x}_o = 0$

$$p_\omega(x, 0) = \frac{i}{h}\left(\frac{\exp[ik_{xm}x]}{k_{xm}\{\frac{\sin(2k_{ym}h)}{2(k_{ym}h)} + 1\}} + \frac{\exp[ik_{xn}x]}{k_{xn}\{\frac{\sin(2k_{yn}h)}{2(k_{yn}h)} + 1\}}\right) \tag{2.3.22}$$

where the wavenumbers satisfy the equations

$$(k_{ym}h)\tan(k_{ym}h) = (k_{yn}h)\tan(k_{yn}h) = -ikh\bar{\beta}_\omega$$
$$k_{xn} = \{k^2 - k_{yn}^2\}^{\frac{1}{2}}; \qquad k_{xm} = \{k^2 - k_{ym}^2\}^{\frac{1}{2}} \tag{2.3.23}$$

and where, under these conditions, the normalisation factors can be approximated by

$$\frac{\sin(2k_{ym}h)}{(2k_{ym}h)} + 1 \doteq (k_{ym}h - k_{yo}h)\,\frac{2\cos^2(k_{yo}h)}{(k_{yo}h)}$$

and similarly for mode n; subscript zero denotes double pole conditions. Carrying out an expansion of equation (2.3.23) about the same point it is easily shown that

$$(k_{ym}h - k_{yo}h)^2 \doteq (k_{yn}h - k_{yo}h)^2$$

or

$$(k_{ym}h - k_{yo}h) \doteq -(k_{yn}h - k_{yo}h)$$

so that equation (2.3.22) can be rewritten as

$$p_\omega(x, 0) \doteq \frac{i(k_{yo}h)}{h\cos^2(k_{yo}h)} \left\{\frac{\exp[ik_{xm}x]/k_{xm} - \exp[ik_{xn}x]/k_{xn}}{2(k_{ym}h - k_{yo}h)}\right\}$$

The bracketed term, for small values of $(k_{ym}h - k_{yo}h)$, can be approximated by its derivative evaluated at the double pole condition:

$$\frac{d}{d(k_y h)}\left\{\frac{\exp[ik_x x]}{k_x}\right\} = \frac{h(k_{yo}h)}{(k_{xo}h)^3}\exp[ik_{xo}x]\ \{1 - ik_{xo}x\}$$

and thus

$$p_\omega(x, 0) \doteq \frac{i(k_{yo}h)^2}{(k_{xo}h)^3\cos^2(k_{yo}h)}\{1 - ik_{xo}x\}\exp[ik_{xo}x] \qquad (2.3.24)$$

Of course this result has been obtained by using effectively the same procedure as before, but with approximations; nevertheless it does serve as a simple check and at the same time, shows that the linear x dependence does not appear abruptly but is characteristic of the field near the double pole condition. Actually the linear x dependence in equation (2.3.24) is identical to that in the exact solution but the remaining part has some terms missing, the complete solution being (with $y = y_o = \bar{x}_o = 0$)

$$p_\omega(x, 0) = \frac{i(k_{yo}h)^2}{(k_{xo}h)^3\cos^2(k_{yo}h)}\left\{1 + \left(\frac{k_{xo}h}{k_{yo}h}\right)^2\cos^2(k_{yo}h)\right.$$

$$\left. - \frac{(k_{xo}h)^2}{3\cos^2(k_{yo}h)} - ik_{xo}x\right\}\exp[ik_{xo}x] \qquad (2.3.25)$$

which has been obtained from equation (2.3.21) using the equation

$$\tan(k_{yo}h) + (k_{yo}h)\sec^2(k_{yo}h) = 0.$$

The x dependence of the mean square (time averaged) value of this mode is of the form

$$\exp\left[-2\,\mathrm{Im}(k_{xo}h)x/h\right]\left[(1+a)^2+(b+kh(x/h))^2\right]$$

where $k_x h(x/h)$ has been replaced by the high frequency approximation $kh(x/h)$ for the linear x dependence part of the solution; a and b are constants associated with the double pole condition. Thus this mode decays with the usual exponential dependence in the x direction but is also amplified as the result of a sort of interference between two nearly identical modes with amplitudes tending to infinity. This double pole mode is not peculiar to the Green's function: it will occur for any source distribution provided the appropriate wall admittance is present at $y = h$ (see below).

It is at precisely this double pole condition that Cremer (19) deduced, by graphical methods, that $\mathrm{Im}(k_x h)$ attains its maximum value. However, Cremer (19) was apparently unaware of the non-existence of the simple pole solution. It is therefore of interest to evaluate the Green's function at and near a double pole condition, to ascertain the importance of this 'linear amplification' in the correct solution and to assess the relevance of Cremer's (19) result to the optimisation of sound attenuation in ducts.

The Green's function is evaluated for the following conditions: the frequency and duct width are chosen so that $kh = 5$ and the

$$\bar{x}_o = y_o = y = 0 \qquad 2 \leq x/h \leq 20$$

$$(\bar{\beta}_\omega)^{-1} = \bar{Z}_\omega = 1.47816 + j\bar{X}_\omega$$

The reactance, $\bar{X}_\omega$, (note the change to the +j notation) is varied, in steps, between -2.5 and +0.5, one value being close to -1.18441. The impedance $\bar{Z}_\omega = (1.47816 - j\,1.18441)$ is the value which gives rise to the double pole solution and hence the above choice of

resistance. (The method used to determine this impedance is described in section (1.4)) For each impedance value equation (2.3.16) has been solved to obtain the first four $(k_{yn}h)$ values; the corresponding $(k_{xn}h)$ values are obtained from the relation

$$k_{xn}h = \{(kh)^2 - (k_{yn}h)^2\}^{\frac{1}{2}}$$

The imaginary parts of the first two values of $(k_{xn}h)$, multiplied by 8.69 are shown in Figure (2.6a) as a function of $\bar{X}_\omega$. Apart from the double pole condition, clearly shown at $\bar{X}_\omega \doteq -1.2$, Figure (2.6a) gives the individual, axial, modal decay rates of the so called 'cut-on' modes in dB's per duct width.

In Figures (2.6b) and (2.6c) the square of the modulus* of half the Green's function (defined by equation (2.3.17)), in dB, is shown as a function of x/h for 12 reactance values in the specified range. Evaluation of the Green's function is described in Chapter 3**. These graphs contain some interesting features; for example the field, particularly for $\bar{X}_\omega = -2.5$, -2.0 and 0.5 exhibit a distinct, wavy, non-linear decay. This is evidently due to modal interference: the decay (see Figure (2.6a)) of the more rapidly decaying mode is not large enough to remove its influence until $x/h > 12.0$. For the same reason, in effect, non-linear decay also occurs on both sides of the double pole solution although the two sides differ in character due to the asymmetry in decay rates. The field for the reactance value (-1.18) closest to the double pole value is shown as a dashed line on each graph: it is clearly not the best reactance value for the minimisation of the field (at y = 0) in the chosen x/h range. Nor is it necessarily the value corresponding to the maximum decay

---

*That is, twice the time averaged or mean square value.
**In Chapter 3 examples are evaluated for kh = 10 and an identical impedance at y = 0 (in place of a rigid surface); half the Green's function is used here to enable direct comparison with those examples.

rate as is shown in Figure (2.6a), where the actual average decay rate between x/h = 4.0 and 8.0 is superimposed on the modal decay rates*. The two cut-on modes, which completely determine the field in this x/h range, interfere in such a way that the decay rate between x/h = 4.0 and x/h = 8.0 is maximised at a reactance value of approximately -1.4 and exceeds that of the least attenuated mode. At larger distances from the source the decay rate, for this two cut-on mode case, will converge to that of the least attenuated mode except for reactance values at and near the double pole value: here the interference is 'permanent' and is represented by the linear x dependence. Between x/h = 4.0 and x/h = 8.0 this linear amplification results in a degradation of the decay rate from 4.4 dB, due to the exponential factor alone, to 3.3 dB - a reduction of 25%. In spite of this the maximum decay rate at larger distances from the source can be seen in Figure (2.6b) to correspond to the reactance value closest to the double pole value (-1.18). Also the impedance for the maximum decay rate at smaller distances is quite close to the double pole value. It can be concluded that the double pole impedance, $\bar{Z}_{\omega opt}$, which gives rise to the maximum exponential, modal decay rate of the least attenuated mode, at this frequency (kh = 5), is approximately equal to the impedance for the maximum decay and/or decay rate of the Green's function.

Cremer's (19) contribution is the specification of $\bar{Z}_{\omega opt}$ and the corresponding exponential decay rate, both as a function of frequency. Thus, although the actual decay rate corresponding to $\bar{Z}_{\omega opt}$ is somewhat less than Cremer (19) predicted (due to the

---

* Unfortunately it has not been possible to evaluate the acoustic energy flows in these examples. It is preferable to use the axial energy flow rather than the local mean square field value for the reasons given in Chapter 5 but in these examples it is assumed that the latter gives a reasonable indication of the axial energy flow behaviour.

linear amplification) his result is clearly relevant to the particular example evaluated above. Unfortunately it cannot be assumed that the optimum impedance for the decay of an arbitrary source distribution, $f_\omega(y)$, will remain approximately equal to $\bar{Z}_{\omega opt}$, unless it can be established that the associated mode dominates the duct acoustic field, for all impedance values.

The evaluation of the Green's function close to the double pole condition ($\bar{X}_\omega = -1.18$) allows the actual double pole solution of equation (2.3.25) to be checked: the square of the modulus of their ratio, in dB, is shown below as a function of x/h.

x/h	.25	.31	.40	.50	.63	.8	1.00	1.25	1.60	2.00
dB	.08	.08	.09	.07	.08	.07	.06	.07	.05	.05

x/h	2.5	3.15	4.0	5.0	6.3	8.0	10.0	12.5	16.0	20.0
dB	.05	.04	.04	.05	.06	.09	.14	.23	.37	.63

The disagreement up to x/h = 6.3 is attributed to the fact that the solutions must differ as the reactance values are not identical. For larger x/h values the disagreement is probably due to amplification of small errors in the axial mode wavenumbers.

No further use will be made of this double pole solution although it is obviously an important one and should be included in any multimode wave-guide model for a more realistic estimate of the field at and near 'optimum' conditions*.

*Of course at sufficiently small and large distances from the source the double pole solution is asymptotic to one of simple exponential decay; see equation (2.3.25).

2.4 Optimisation of Modal Attenuation Rates

Essentially there are three contributions to be made in this area. In sub-sections 3 and 4 it is shown that Cremer's (19) result can be logically extended to higher order modes in a two-dimensional rectangular duct and to modes in a circular duct. In the next Chapter a simple, duct ray model is constructed on the basis of the approximate source-image ray model for a single wall (noted in the second section of this Chapter). This model is evaluated in an attempt to understand why Cremer's (19) optimum impedance has its particular value and frequency dependence. The extensions are preceded by a detailed description of Cremer's (19) result and in the final sub-section the application of optimum impedance results is discussed with the aid of a simple example.

2.4.1 Discussion

In general the optimum impedance for the maximum attenuation of the local field or of the energy flow depends on the relative mode amplitudes and hence the source distribution, $f_{\omega}(y)$. If the source distribution is not known, mode amplitudes can be measured directly (26) or failing this, source distributions or relative amplitudes can be assumed in the light of appropriate theoretical models.

For example, Tyler and Sofrin (27) show that, under certain conditions, the interaction between rotating and stationary blade rows can produce a single mode. At the other extreme, Dyer's (28) theoretical analysis for "source that is purely random in space" in a hard walled circular duct, shows that, again under certain conditions, all well cut-on modes have equal energy. (See also the analysis by

Morfey [29] for rotating sources.)

(Using a theoretical model based on Dyer's (28) result a computer program written by the author while at Rolls Royce Ltd., was found to be of considerable use by Wirt (25) in interpreting and predicting insertion loss data obtained from the Lockheed California Lined Duct Facility. See Appendix 1A.)

Cremer's [19] result is supposed to be relevant to the Dyer (28) type of source distribution in a rectangular duct. Here Cremer's (19) result is extended to the circular duct and, for the rectangular duct, to all higher order modes in turn, so that the results can be used for the type of source distribution where only one particular mode is preferentially excited.

2.4.2 Cremer's result

To be more precise the definition of optimisation in the present context is the maximisation of the decay or attenuation rate of a mode pair. It is obvious from Figure (2.6a) why the term 'mode pair' should be used although the definition of a mode is arbitrary to some extent and it could be argued that the attenuation of a single mode is being optimised.

The attenuation rate of the mean square modal amplitude (now ignoring the 'linear amplification') is proportional to the imaginary part of the axial wavenumber k_{xn}, and in the usual units the attenuation is

$$8.69\ \mathrm{Im}(k_{xn}h)\ \text{dB per duct width} \qquad (2.4.1)$$

Two parameters determine this quantity: one represents the influence of duct geometry, simply the ratio of the duct width to the sound wavelength in this two-dimensional model, or the reduced frequency

$kh = \omega h/c$. The other is, in general, complex and frequency dependent and is the non-dimensional (locally reacting) wall admittance $\bar{\beta}_\omega$ (or wall impedance $\bar{Z}_\omega = (\bar{\beta}_\omega)^{-1}$) obtained by dividing the actual admittance β_ω by $(\rho_o c)^{-1}$.

The equations which determine $\mathrm{Im}(k_{xn}h)$ from these two parameters were obtained in the previous section; these are

$$j\, kh\bar{\beta}_\omega = (k_y h)\tan(k_y h) \qquad (2.4.2)$$

$$(k_x h) = +\sqrt{(kh)^2 - (k_y h)^2} \qquad (2.4.3)$$

(N.B. In this section $+j$ is used instead of $-i$.)

Apart from the trivial case of $\bar{\beta}_\omega = 0$ (rigid wall at $y = h$) and $\bar{\beta}_\omega \to \infty$ ('pressure release' wall at $y = h$) the solutions, $(k_{xn}h)$ $n = 1, 2, \ldots, \infty$, all have imaginary parts which, in general, are different, there being a minimum value of a sequence of $\mathrm{Im}(k_{xn}h)$ values which increase fairly uniformly with n, without limit. The fact that there is a mode with minimum attenuation rate is extremely useful because provided the source distribution does excite this mode to some extent then at some distance from the source the sound field will consist of just this one mode (except near a termination) and hence the sound attenuation at larger distances will be entirely determined by this minimum value.

At low frequencies the distinction between the mode with the least attenuation and all other modes is fairly clear because the latter are, in general, highly attenuated cut-off modes, where cut-off modes can be loosely defined as those with $k_{yn}h$ values such that

$$|\, k_{yn}h \,| > kh \qquad (2.4.4)$$

With low frequency systems in mind Cremer (19) carried out a

definitive exercise aimed at determining the value of $\bar{\beta}_\omega$ which would optimise the value of this minimum attenuation rate. He obtained the following result in terms of the wall impedance $\bar{Z}_\omega$: the maximum attenuation (for any value of kh) of the least attenuated mode is attained with a wall impedance $\bar{Z}_{\omega_{opt}}$, where

$$\bar{Z}_{\omega_{opt}} = (0.91 - j0.76)\frac{kh}{\pi} \qquad (2.4.5)$$

and this maximum attenuation is calculated using equation (2.4.3) with a $(k_y h)$ value of

$$(k_{yn}h)_{opt} = (2.1 + j1.1) \qquad (2.4.6)$$

Cremer (19) observed that this value of $(k_y h)$ is the point on the complex $(k_y h)$ plane at which modes 0 and 1 merge and become identical in every respect. In other words this optimum condition is identical to the double pole treated in the previous section, although there the complex θ plane was used and then the result was transformed into the $(k_x h)$ and $(k_y h)$ wavenumber parameters.

Morse (13) refers to this point as a branch point of the function $k_y h(jkh\bar{\beta}_\omega)$ and it is necessary to digress at this point to establish that in the context of the previous section this point is a double pole but here it appears as a branch point.

Assume equation (2.4.2) is not satisfied so that

$$f(k_y h) = (k_y h)\tan(k_y h) - j(kh)\bar{\beta}_{\omega_{opt}} \qquad (2.4.7)$$

This function can be expanded about the point $(k_{yn}h)$, where

$$f(k_{yn}h) = 0 = (k_{yn}h)\tan(k_{yn}h) - jkh\bar{\beta}_{\omega_{opt}}$$

$$f(k_yh) = f(k_{yn}h) + (k_yh - k_{yn}h)[f']_{k_{yn}h} + \frac{(k_yh - k_{yn}h)^2}{2!}[f'']_{k_{yn}h} + \ldots$$

If $[f']_{k_{yn}h} \neq 0$ then near $k_{yn}h$, $f(k_yh)$ behaves like

$$f(k_yh) = (k_yh - k_{yn}h)[f']_{k_{yn}h}$$

and the function considered in the previous section, which is essentially $(f)^{-1}$, has a simple pole at $k_yh = k_{yn}h$.

If $[f']_{k_{yn}h} = 0$ then near $(k_{yn}h)$, $f(k_yh)$ behaves like

$$f(k_yh) = \frac{(k_yh - k_{yn}h)^2}{2!}[f'']_{k_{yn}h} \qquad (2.4.8)$$

and the inverse of f has a double pole at $(k_yh) = (k_{yn}h)$, provided $[f'']_{k_{yn}h} \neq 0$. As $[f'']_{k_{yn}h} = 2$ where $[f']_{k_{yn}h} = 0$ the pole cannot be of order greater than 2, that is no more than 2 poles can accumulate in the θ or (k_yh) plane.

Inverting equation (2.4.8) it can be seen that near $(k_{yn}h)$, $(k_yh - k_{yn}h)$ behaves like

$$(k_yh - k_{yn}h)$$

or, treating $(jkh\bar{\beta}_\omega)$ as a variable where

$$jkh\bar{\beta}_\omega = (k_yh)\tan(k_yh)$$

$$(k_yh - k_{yn}h) = \pm\{jkh(\bar{\beta}_\omega - \bar{\beta}_{\omega_{opt}})\}^{\frac{1}{2}}.$$

Thus there is a branch point of (k_yh) when written as a function of

$(jkh\bar{\beta}_\omega)$ at the point defined by the solution of the equation

$$[f']_{k_{yn}h} = 0 = (k_y h) + \tfrac{1}{2}\sin(2k_y h) \qquad (2.4.9)$$

The first solution to this equation is, approximately given by equation (2.4.6).

Evaluation of equations (2.4.2) and (2.4.3) for an infinite duct wave-guide model and an assumed, but fairly uniform excitation of all cut-on modes will lead to overall energy attenuation or insertion loss results with a maximum value for an impedance value at or near the optimum value given by Cremer (19) (equation 2.4.5). His result has been of considerable use in classifying and interpreting trends in theoretical results and, in some cases, experimental results as well.

There are five fairly minor points to be discussed concerning Cremer's (19) result and related matters before proceeding to describe the two extensions.

(a) Cremer's (19) hypothesis centred on the fact that the least attenuated mode was to be optimised for maximum attenuation. To ensure that the mode under consideration was always the least attenuated Cremer (19) carried out a semi-quantitative study of higher order mode attenuation rates which purported to show that these modes always have attenuation rates in excess of the assumed least attenuated one. The analysis was based on approximate solutions of the eigenvalue equation (2.4.2) and it is suggested here that, strictly speaking, these are not adequate for the present purpose. One example which invalidates Cremer's (19) assumption is given here in Figures (2.8) and (2.9). In these figures the attenuation as defined by equation (2.4.1) is shown for the first 6 modes for a (kh) value of 8π (that is $h/\lambda = 4$). In Figure (2.8) the attenuation is plotted as a function

of $\bar{X}_\omega$ with $\bar{R}_\omega$ held constant at its optimum value of 0.93 x 8 = 7.4. In Figure (2.9) the parameters are reversed: the attenuation is a function of $\bar{R}_\omega$ with $\bar{X}_\omega$ = -0.74 x 8 = -5.9. Notice slightly different optimum values have been used from Cremer's (19); in fact those given by Cremer (19) and Morse (13) are slightly in error, the correct values being

$$\bar{Z}_{\omega_{opt}} = (0.929 - j0.744)\frac{kh}{\pi} \qquad (2.4.10)$$

to three significant figures. The method of obtaining these values is described later in section (2.4.1). The method used to solve equation (2.4.2) with (2.4.3) is fairly standard (see, for example, Ko (30)) and was carried out using the computer programme written by the author while at Rolls Royce Ltd., by kind permission of that company. The main purpose of these figures is to demonstrate that the optimisation of the assumed least attenuated (0, 1) mode pair at high frequencies ($kh = 8\pi$) can lead to a situation where almost all the cut-on modes have similar attenuation rates and in fact mode 3 has a smaller attenuation rate. Thus, in general, it cannot be said that either the 0 or 1 mode are least attenuated.

Cremer (19) also implies that his result can be used for a symmetrical duct of twice the width, that is, with an identical impedance at $y = -h$. This is correct provided the source distribution is symmetric about the point $y = 0$. If it is not then odd order modes are excited which have wavenumbers given by solutions of the equation

$$jkh\bar{\beta}_\omega = -(k_y h) \cot (k_y h)$$

As Morfey (31) has pointed out, the lowest order odd mode can also have a similar attenuation rate to that of the lowest order even mode pair

(now referred to as the (0, 2) mode pair) thus providing another qualification to Cremer's (19) result. Nevertheless, the result is still a useful one particularly at lower frequencies where this situation should not arise and also for mode amplitude or energy distributions which decrease with increasing mode order.

(b) In Figures (2.8) and (2.9) and elsewhere the modes have been numbered according to Morse's (13) definition which is based on dividing the complex $(k_y h)$ plane into modal regions by lines of constant phase of $\bar{\beta}_\omega$, the phase value being that of $\bar{\beta}_{\omega_{opt.}}$. In fact any constant property of $\bar{\beta}_{\omega_{opt}}$ can be used: for example, the original Morse chart reproduced by Cremer (19) uses constant $Re(\bar{\beta}_\omega) = Re(\bar{\beta}_{\omega_{opt}})$ as does Plumblee (32). However the constant phase method has the advantage of being recognised in figures of this kind whether the impedance parameter is being used or its inverse, the admittance parameter. Thus in the present context the mode pair (0, 1) are being optimised for maximum attenuation.

(c) The type of graph presented in Figures (2.8) and (2.9) does not represent a complete proof that the optimum impedance equation (2.4.10) is valid, although clearly the peak attenuation of the (0, 1) mode pair does occur at the predicted optimum value. An adequate proof would consist of a sequence of graphs covering the frequency range (0, ∞), each graph showing the complex impedance plane with contours of constant attenuation exhibiting a unique maximum at the optimum impedance point. It has not been possible to carry out such an exhaustive evaluation for the (0, 1) modes, or for higher order modes in the next sub-section, but it will be shown by reference to work published elsewhere that the type of verification given here is, in fact, adequate for the present purpose. Certainly for the (0, 1) mode pair,

Cremer's (19) graphs for 5 values of kh appear to be adequate proof. To give a rough idea of the attenuation dependence away from optimum conditions, in Figure (2.8) the resistance is also set equal to twice and half its optimum value and the resulting attenuation shown for the least attenuated mode.

(d) In any type of optimisation work the initial approach would be to attempt to locate the maximum value of a given function by setting to zero the gradient (s) of the function with respect to the parameter(s). This approach can be used here of course but it would not lead to the present optimum condition. This is not obvious from Cremer's (19) constant attenuation contours on the complex impedance plane but in Figures (2.8) and (2.9) it is clear that the gradient of $\mathrm{Im}(k_x h)$ with respect to $\bar{X}_\omega$ and $\bar{R}_\omega$ is infinite at the optimum condition. (This might also be deduced from the previous analytical description of the optimum condition.) This objection does not apply to the Green's function which, in general, will exhibit stationary maximum values; see, for example, Figure (2.6a).

(e) Finally, it is of interest to record the behaviour of the attenuation (due to the exponential factor alone) at optimum conditions as a function of frequency. This is shown in Figure (2.10) in terms of dB per duct width as a function of h/λ. An approximate formula for this dependence, which is remarkably accurate for all frequencies such that $h/\lambda > 0.5$, can be obtained by taking the first term in the expansion of the square root in equation (2.4.3)

$$k_x h \doteq kh \{1 - \tfrac{1}{2} \frac{(k_y h)^2}{(kh)^2}\}; \qquad kh >> |k_y h|$$

so that

$$\mathrm{Im}(k_x h) = -\mathrm{Re}(k_y h)\mathrm{Im}(k_y h)/(kh)$$

Using equations (2.4.1) and a more exact form of equation (2.4.6) shows that the maximum attenuation of the (0, 1) mode pair is then

$$\text{Attenuation, dB/h} \doteq \frac{3.3}{(h/\lambda)}\ ; \qquad h/\lambda \gtrsim 0.5 \qquad (2.4.11)$$

Equation (2.4.11) is shown evaluated in Figure (2.10). The low frequency approximation is simply

$$k_x h \doteq -jk_y h; \qquad kh << |k_y h|$$

or

$$\text{Attenuation, dB/h} \doteq 18.3; \quad h/\lambda \lesssim 0.1 \qquad (2.4.12)$$

which is clearly the asymptotic limit as $h/\lambda \to 0$ in Figure (2.10).

2.4.3 Optimisation of the attenuation rates of higher order mode pairs

Having considered the optimisation of the attenuation rate of the (0, 1) mode pair in detail, an extension for the next mode pair (1, 2), (2, 3).... (m, m + 1) is straightforward although evidence is required to justify this step.

Equation (2.4.9) is solved for the new branch point values $(k_{ym}h)$; details of the method of solution are given in Appendix 2A. The first three values are,

$$(k_{yo}h) = 2.11 + j\ 1.13$$

$$(k_{y1}h) = 5.36 + j\ 1.55$$

$$(k_{y2}h) = 8.54 + j\ 1.78$$

For large values of m it can be shown that (see Appendix 2A):

$$\lim_{m \to \infty} (k_{ym}h) = (m + \tfrac{3}{4})\pi + j\tfrac{1}{2}\ \ln\{(4m + 3)\pi\} \qquad (2.4.13)$$

In fact equation (2.4.13) is a good approximation for the lowest m values as the table below shows.

m	$\mathrm{Re}(k_{ym}h)$	Eq. (2.4.13)	$\mathrm{Im}(k_{ym}h)$	Eq. (2.4.13)
0	2.106	2.356	1.125	1.22
1	5.356	5.498	1.552	1.540
2	8.537	8.639	1.778	1.771

The corresponding optimum impedance values are

$$\begin{aligned}\bar{Z}_{\omega 0} &= (0.928 - j\,0.744)2h/\lambda \\ \bar{Z}_{\omega 1} &= (0.513 - j\,0.198)2h/\lambda \qquad (2.4.14) \\ \bar{Z}_{\omega 2} &= (0.344 - j\,0.0920)2h/\lambda\end{aligned}$$

For large m, $\mathrm{Im}(k_{ym}h)$ is sufficiently large to permit the approximation

$$\tan(k_{ym}h) \doteq j$$

so that equation (2.4.2) reduces to

$$\bar{Z}_{\omega m} \doteq \frac{kh}{(k_{ym}h)} \doteq \left[(m + \tfrac{3}{4})\pi + j\tfrac{1}{2}\,\ell n\,(4m + 3)\pi\right]^{-1} kh \qquad (2.4.15)$$

The first part of equation (2.4.15) looks interesting because it is of the form

$$\bar{Z}_{\omega m} \cos\theta_m = 1; \qquad \cos\theta_m = (k_{ym}h)/(kh)$$

This is the same condition as for zero reflection of a plane homogeneous wave inclined at angle of incidence θ to a <u>single</u>, uniform, infinite wall of impedance $\bar{Z}_\omega$. However this condition holds for all modes with large [illegible] Im(k_y[illegible]) values and is not peculiar to the optimum condition. Cremer refers to waves of this type as surface waves; they are characterised by large amplitudes at the lined wall. Approximate $\bar{Z}_\omega$ values given by equation (2.4.15) are compared with exact values in the table below.

m	$\mathrm{Re}(\bar{Z}_{\omega m})$	Eq. (2.4.15)	$\mathrm{Im}(\bar{Z}_{\omega m})$	Eq. (2.4.15)
0	.9288	1.087	-.7442	-.5176
1	.5126	.5298	-.1977	-.1484
2	.3440	.3490	-.09197	-.07154

Evidence that this is a valid extension of the optimisation concept is presented in Figures (2.11) - (2.14). As before the real and imaginary parts of $\bar{Z}_\omega$ are held constant in turn, equal to the optimum values given in (2.4.14). Again attenuation rates are shown for the first 6 modes, all for $h/\lambda = 4$. As the arrows indicate, the peak attenuation of the particular mode pair does occur at the predicted optimum impedance values. Notice that although the modal attenuations are continuous functions of impedance, the mode order changes abruptly when the impedance phase equals that of the optimum impedance for that mode pair. (Some changes occur off the graph.)

The frequency dependence of the attenuation (given by the exponential term alone) is shown in Figure (2.15) for the two mode pairs considered. The dashed curves and the horizontal lines at $h/\lambda = 0$ are respectively the high and low frequency approximations equivalent to those given for the (0, 1) mode pair in the previous section. But here the approximate values of $(k_y h)$, as given by equation (2.4.13), have been used. The frequency range for which these high frequency approximations do not apply is now much wider, because of the larger $|k_{ym} h|$ values, and hence these approximations are of little interest.

A discussion of the application of this particular extension is given in sub-section (2.4.5).

2.4.4 Optimisation of modal attenuations in circular ducts

A logical extension of the optimisation concept to circular ducts simply requires the cosine eigenfunction for the two-dimensional duct to be replaced by the Bessel eigenfunction, J_m. The equivalent equations to (2.4.2) and (2.4.3) are then

$$jkb\bar{\beta}_{\omega} = m - \frac{k_r b \, J_{m-1}(k_r b)}{J_m(k_r b)} \quad ; \quad m = 0, 1, 2, \ldots \tag{2.4.16}$$

$$k_x b = + \sqrt{(kb)^2 - (k_r b)^2} \tag{2.4.17}$$

where m defines the order of circumferential variation of the acoustic field, $(k_r b)$ is the non-dimensional radial wavenumber and b is the duct radius.

This extension can be carried out for any m value but here it is confined to the value $m = 0$. Then the branch point coordinates are solutions of

$$\frac{d}{d(k_r b)} \left\{ k_r b \, \frac{J_1(k_r b)}{J_0(k_r b)} \right\} = 0$$

or, after some manipulation

$$J_1(k_r b) = j J_0(k_r b) \tag{2.4.18}$$

The optimum impedance is given (exactly) by

$$\bar{Z}_{\omega_{opt}} = \frac{kb}{k_r b} \tag{2.4.19}$$

(compare this with the previous result for higher order modes in rectangular geometry). A good approximation to the first solution, that is the radial wavenumber which defines the optimum impedance for the radial mode pair (0, 1), can be deduced from the "conformal transformation" in Morse and Ingard (14), p.910. This value

$$(k_{ro} b) \doteq 3.0 - j\,1.3 \tag{2.4.20}$$

and also the approximate optimum impedance value

$$\bar{Z}_{\omega_{opt}} \doteq (.88 - j.38) 2b/\lambda \tag{2.4.21}$$

have been refined by using a 'manual' iteration based on equation (2.4.18)

and a computer sub-routine for Bessel functions with complex arguments (33). However for the present purpose the values given by equations (2.4.20) and (2.4.21) are adequate.

Numerical evidence in support of this extension is lacking as the required computer program was not available, that is, one which computes modal decay rates in circular ducts for arbitrary impedance values. In view of its limited use in the present work the writing of such a program was considered to be unjustified.

A literature review revealed that an attempt to verify this extension using published data would be complicated by the fact that most attenuation data is presented in the form of an energy attenuation summed over a finite number of modes. An exception to this is the work presented by Benzakein et al (34). As Snow (35) has pointed out, it appears likely that a graph of the complex impedance plane (Figure 2.13) with lines of constant attenuation is incorrectly labelled m = 1. All the evidence suggests that this should be for m = 0. If this is the case then this graph, reproduced in Figure (2.16) shows that the optimum impedance is

$$\bar{Z}_{\omega_{opt}} \doteq (2.3 - j1.0) \quad \text{at} \quad 2b/\lambda = 2.6$$

Equation (2.4.21) gives the values

$$\bar{Z}_{\omega_{opt}} \doteq (2.29 - j\,0.99) \quad \text{at} \quad 2b/\lambda = 2.6.$$

Thus it seems likely that this is a graph for m = 0 and if so it provides a verification of the extension of this optimisation concept to circular ducts (for m = 0). The predicted optimum attenuation, using an (approximate) equation of the form given in equation (2.4.11), is approximately 14 dB which agrees with the highest contour values

shown in Figure (2.16). It is also reassuring to note that from Morse and Ingard's (14) chart for $m = 1$ the branch point impedance is

$$(\bar{Z}_{\omega o})_{m=1} \doteq (0.6 - j0.2)\, 2b/\lambda$$

which differs considerably from $(\bar{Z}_{\omega o})_{m=0}$ in magnitude and phase.

2.4.5. Application of optimum impedance results

The main application of Cremer's (19) results and the extensions given in previous sections is to assist in the interpretation (and checking) of theoretical data obtained from multi-modal wave-guide models. The data is usually presented in the form of an energy attenuation, E, where

$$E = 10 \log_{10} \frac{E_{in}}{E_{out}}$$

E_{in} is the acoustic energy summed over a finite number of modes at some reference plane and E_{out} is the energy at a given distance L from that reference plane. The reference plane can be interpreted as the source plane and the latter plane as a duct termination or simply the end of a lined section, reflections being ignored in both cases. E is usually presented as a function of frequency, kh or kb, the 'aspect ratio' L/h and either the wall impedance(s) or parameters which determine the wall impedance, for example the air cavity depth of Helmholtz type liners, the facing sheet resistance and so on.

As far as presently available results are concerned, the most relevant optimum result is that given by Cremer (19) for the (0, 1) mode pair in a rectangular duct and the equivalent result obtained in section (2.4.4) for the circular duct. Although it has been shown that the (0, 1) mode pair is not necessarily the least attenuated, at lower

frequencies (such that $h/\lambda < 4$ say) the higher order modes approach cut-off and Cremer's (19) assumption is valid. It is probably valid up to even higher frequencies if it is assumed that the impedance takes values near the optimum value but not equal to it. Suppose the duct is sufficiently long so that

$$\mathrm{Im}(k_{xn}L) = \mathrm{Im}(k_{xn}h).L/h \qquad n = 2, 3, \ldots.$$

is large enough to cause all the higher order mode energy contributions to E_{out} to be negligible compared with that in the (0, 1) mode pair. Then it is to be expected that the maximum energy attenuation from multi-mode wave-guide models will be found for an impedance close to the optimum value for the (0, 1) mode pair.

This is found to be the case in Rice's (36) results for a circular duct ($m = 0$) where the radial mode amplitudes, and hence the modal energies, have been determined by the condition that the pressure field be uniform for $(0 \leq r \leq b)$ at the reference or source plane. His results are particularly useful because they are given in the form of optimum impedance loci on the complex impedance plane for variable $\eta = D/\lambda$ ($\equiv 2b/\lambda$) and L/D, as shown in Figure (2.17). The value $L/D = 1$ may not be large enough to allow sufficient decay of the high order radial modes; at low frequencies the large difference may also be caused by mode interference. The constant $L/D = 2$ line is closer to the (0, 1) (dashed) line and veers off, as might be expected, at high frequencies; the constant $L/D = 3$ line is closer still. Both $L/D = 2$ and $L/D = 3$ lines, like the one for $L/D = 1$, are probably not asymptotic to the (0, 1) line at low frequencies. The $L/D = 5$ line is asymptotic and does not deviate from the (0, 1) line until $\eta = 3$, although the scales here, and elsewhere, can be rather misleading.

The lack of agreement for low L/D and high n values is not particularly important: L/D values are rarely less than 3 in any practical system and n is usually less than 5 to obtain realistic attenuation rates. Thus, for a practical range of parameters, optimum impedances previously obtained from multi-mode models can now be predicted (and checked) from the type of formulae presented in the previous sub-section.

An obvious extension of this work for aero-engine applications is to include the annular duct case and modes with non-zero m values, which are known to be generated by rotating machinery.

The most obvious application of the results for higher order modes given in Section (2.4.3) is to data from models in which an extreme form of an energy distribution has been used, that is, the energy is confined to one particular mode or mode pair. In a rigid-wall duct modes are easily recognised by their spatial distribution (transverse wavenumber), but as has been shown modes are not generally so well defined in a lined two-dimensional rectangular duct. In lined circular ducts, while the circumferential mode order, m, remains unique and well-defined, the radial modes associated with each particular m value do not. Thus for a rectangular duct, unless the energy is arbitrarily confined to a mode of one particular order (or a pair of adjacent

tive terms. Their value lies mainly in the simple trends exhibited, that of a decreasing resistance and reactance with mode order and proportionality with frequency, kh or kb. As there are no published theoretical results available for rectangular ducts with variable modal energy distributions even approaching the required extremes these particular trends cannot be used at present.

Part of this work in section 4, is summarised in a paper presented at the 7th International Congress on Acoustics (37).

APPENDIX 2A

Approximate, Analytic Branch Point Solutions for High Order Modes in Rectangular Ducts, and the Method Used To Obtain Exact Solutions.

Approximate branch point solutions of the equation

$$\sin(2k_y h) + (2k_y h) = 0 \qquad (2.A.1)$$

for high order modes can be obtained in an analytic form. Inspection of the first three exact solutions reveals that $\mathrm{Re}(k_y h)$ increases uniformly with solution order, m, while $\mathrm{Im}(k_y h)$ increases more slowly so that $\mathrm{Im}(k_y h)/\mathrm{Re}(k_y h) \to 0$ as $m \to \infty$; also $\mathrm{Im}(k_y h) > 1.5$ for $m > 1$. Equation (2.A.1) is split into its real and imaginary parts, using the notation $k_y h = x + jy$;

$$\sin 2x \cosh 2y = -2x \qquad (2A.2)$$

$$\cos 2x \sinh 2y = -2y. \qquad (2.A.3)$$

Dividing equation (2.A.3) by (2.A.2) gives

$$\cot 2x \tanh 2y = y/x \qquad (2.A.4)$$

In view of the trends described above, equation (2.A.4) reduces for large m to

$$\cot 2x \doteq 0$$

$$2x \doteq \frac{\pi}{2}(2m+1) \qquad m = 0, 1, 2, \ldots$$

Inspection of equation (2.A.2) reveals that the even-m solutions are not acceptable so that

$$x \doteq (m + \tfrac{3}{4})\pi \qquad m = 0, 1, 2, \ldots$$

Substituting this solution into equation (2.A.2) and using

$$\cosh^{-1}(2x) = \tfrac{1}{2}\, \ell n\left[2x + \sqrt{(2x)^2 - 1}\,\right]$$

$$\doteq \tfrac{1}{2}\, \ell n\left[4x \right]$$

gives

$$y = \tfrac{1}{2} \ln \{4(m + \tfrac{3}{4})\pi\}$$

or

$$\underset{m \to \infty}{k_y h} = [(m + \tfrac{3}{4})\pi + j \tfrac{1}{2} \ln\{(4m + 3)\pi\}]. \qquad (2.A.5)$$

Using equation (2.A.5) as a starting value the exact solution is obtained by iteration using the standard Newton-Ralphson scheme:

$$(k_y h)_{n+1} = (k_y h)_n - \frac{f[(k_y h)_n]}{f'[(k_y h)_n]}$$

where

$$f[(k_y h)_n] = [\sin(2k_y h) + (2k_y h)]_{k_y h=(k_y h)_n}$$

$$f'[(k_y h)_n] = \left[\frac{d}{d(k_y h)} \{\sin(2k_y h) + (2k_y h)\}\right]_{k_y h=(k_y h)_n}$$

and where $(k_y h)_n$ denotes the n^{th} iteration value of $(k_y h)$. This iteration has always converged, even for $m = 0$ when the starting value is the least accurate.

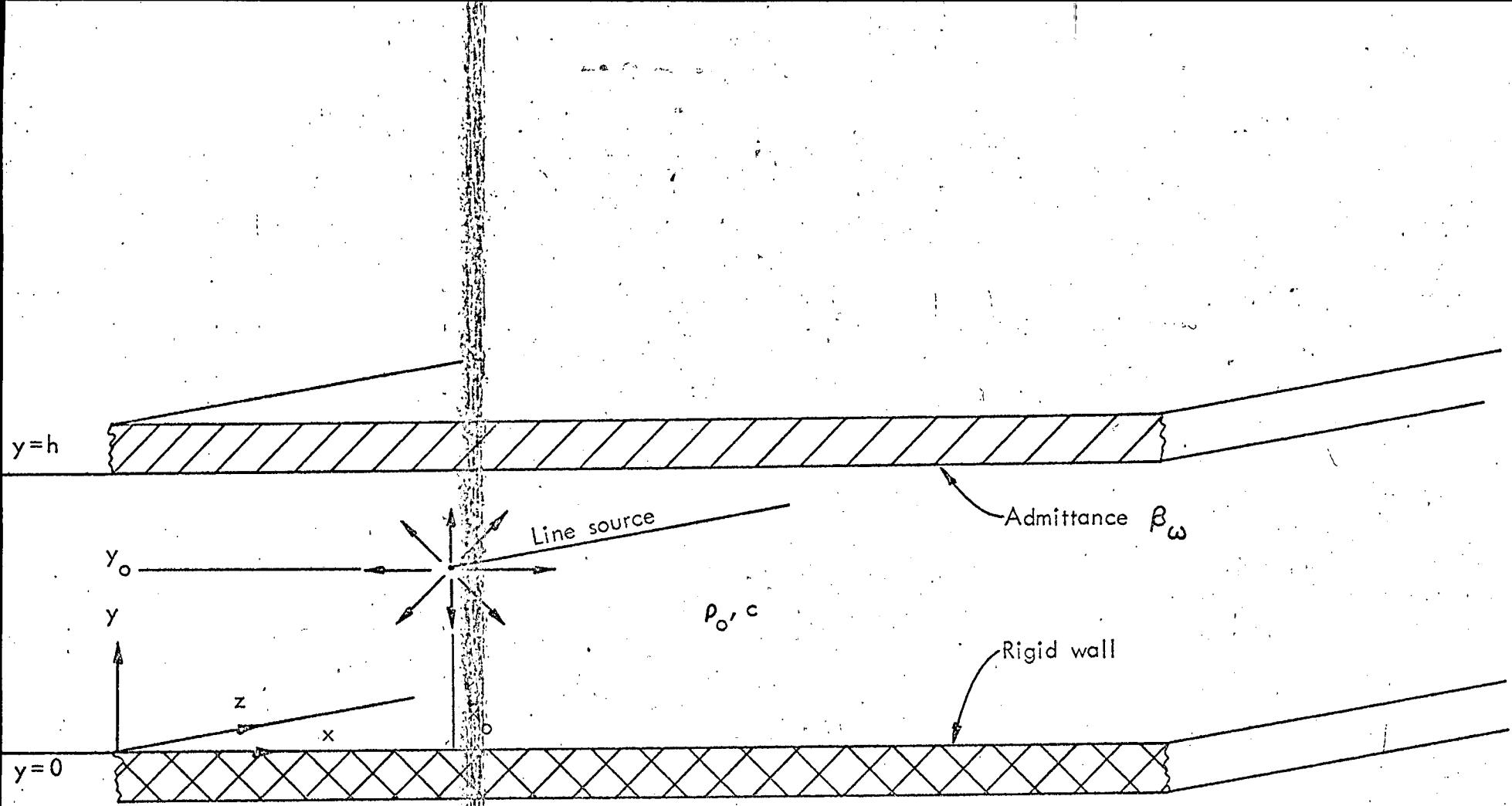

FIG. 2.1 SOURCE AND DUCT GEOMETRY.

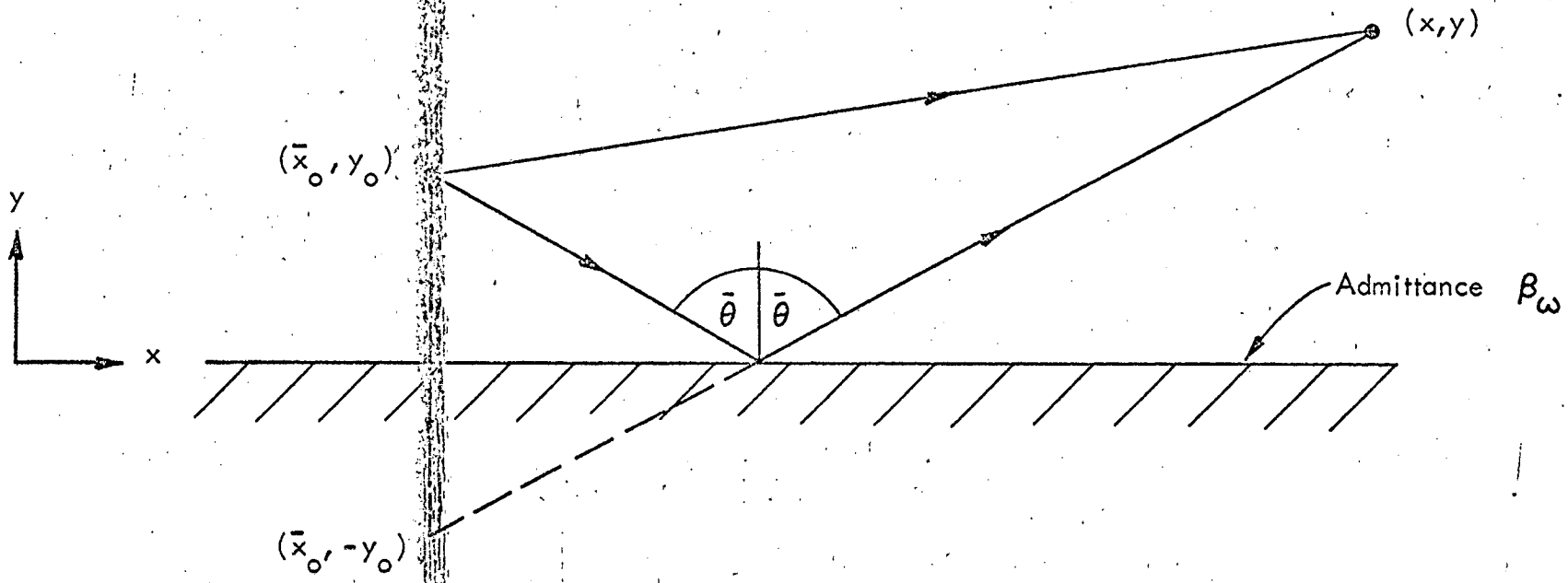

FIG. 2.2 RAY GEOMETRY FOR THE APPROXIMATE GREEN'S FUNCTION.

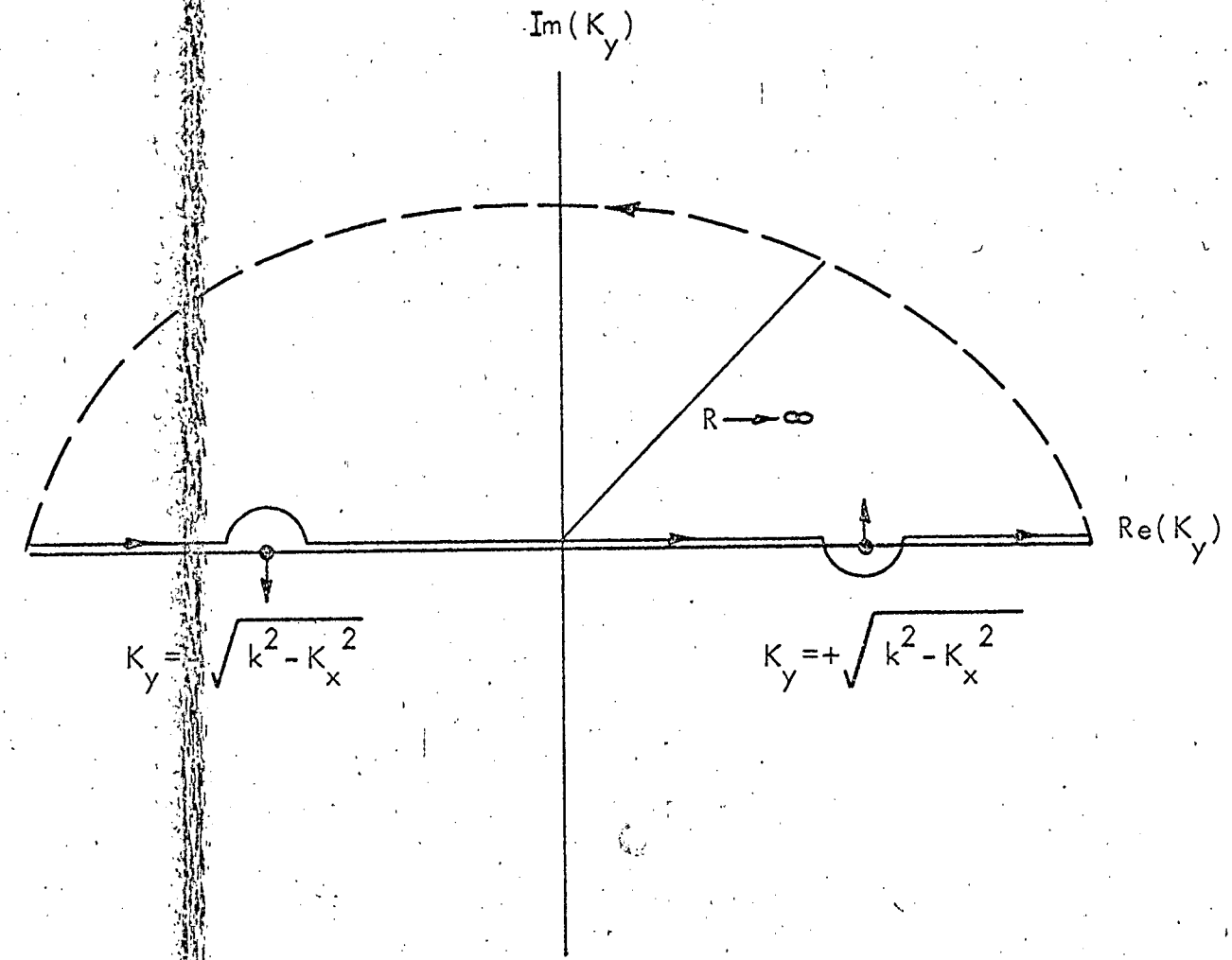

FIG. 2.3 THE K_y INTEGRATION CONTOUR FOR $y - y_o > 0$

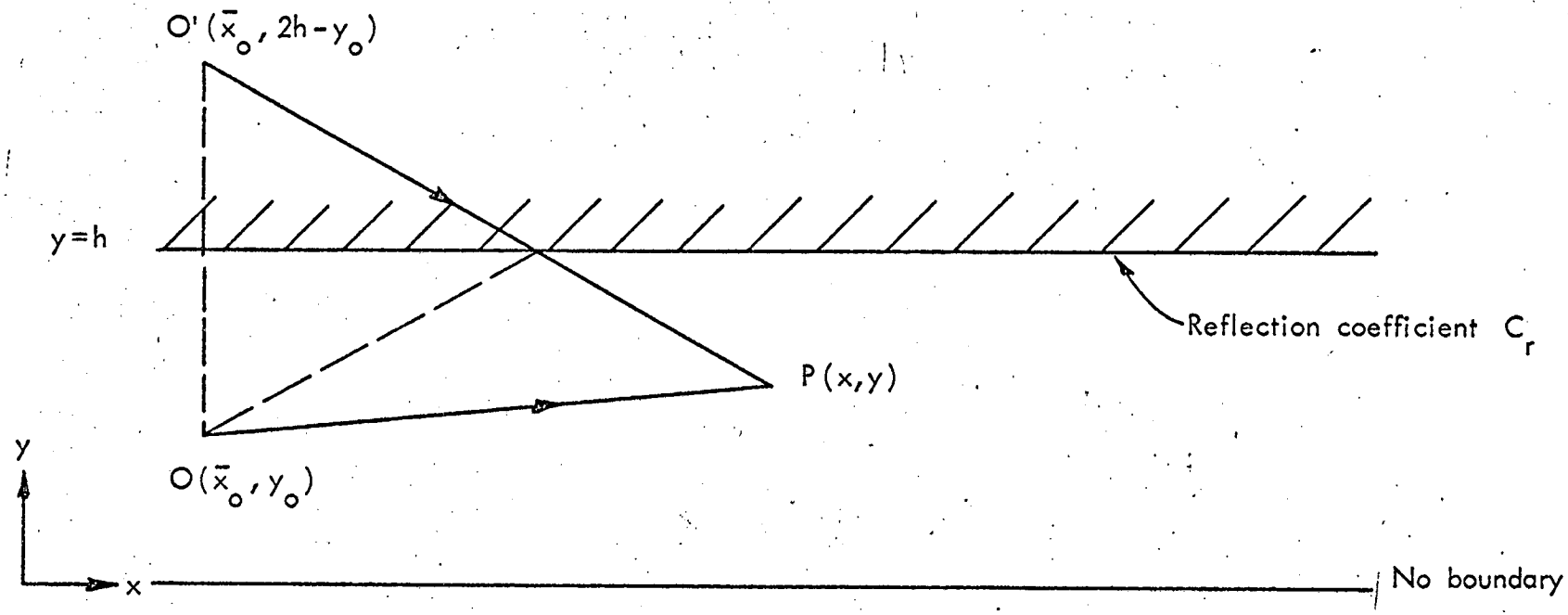

FIG. 2.4a THE FREE FIELD AND A FIRST REFLECTION AT P.

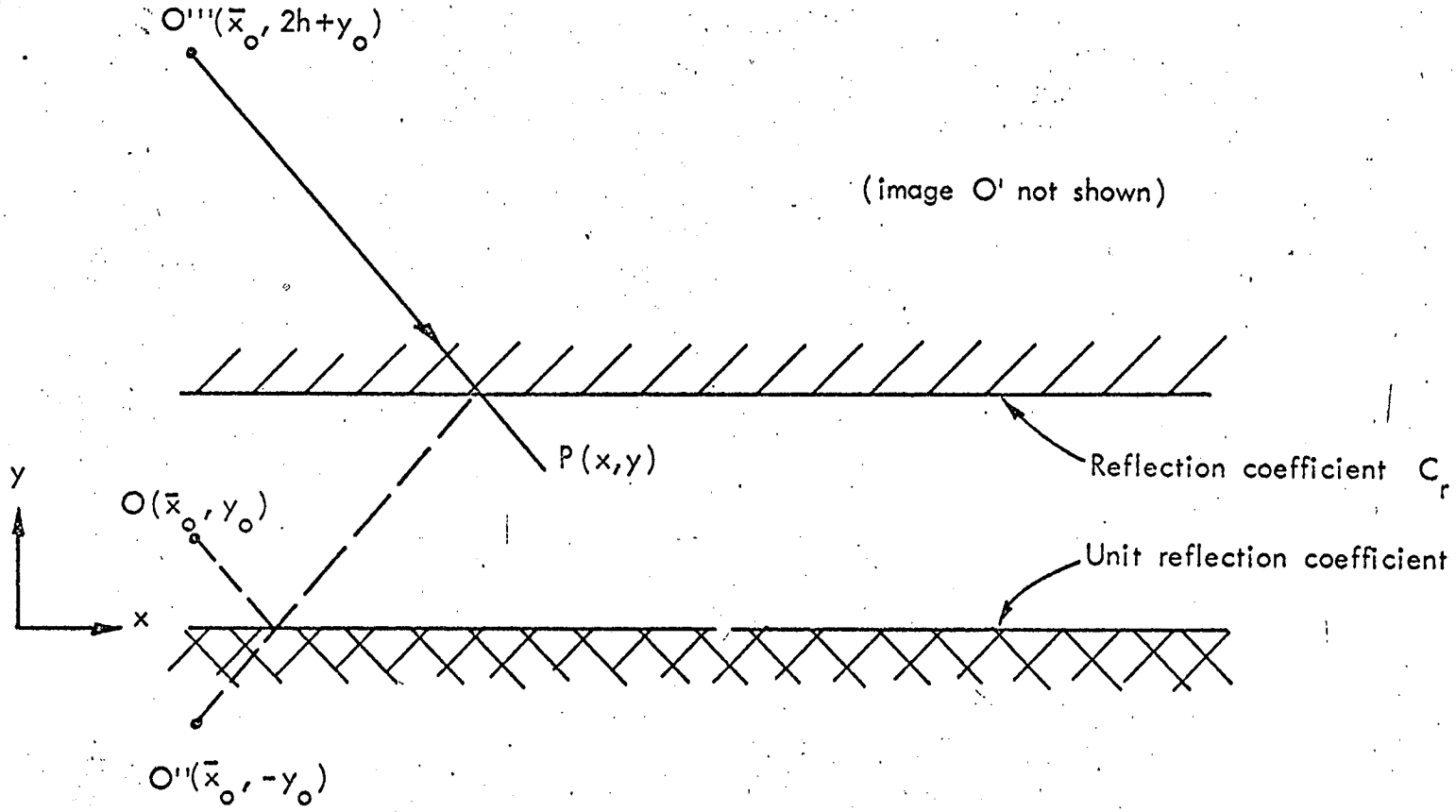

FIG. 2.4b A SECOND REFLECTION AT P.

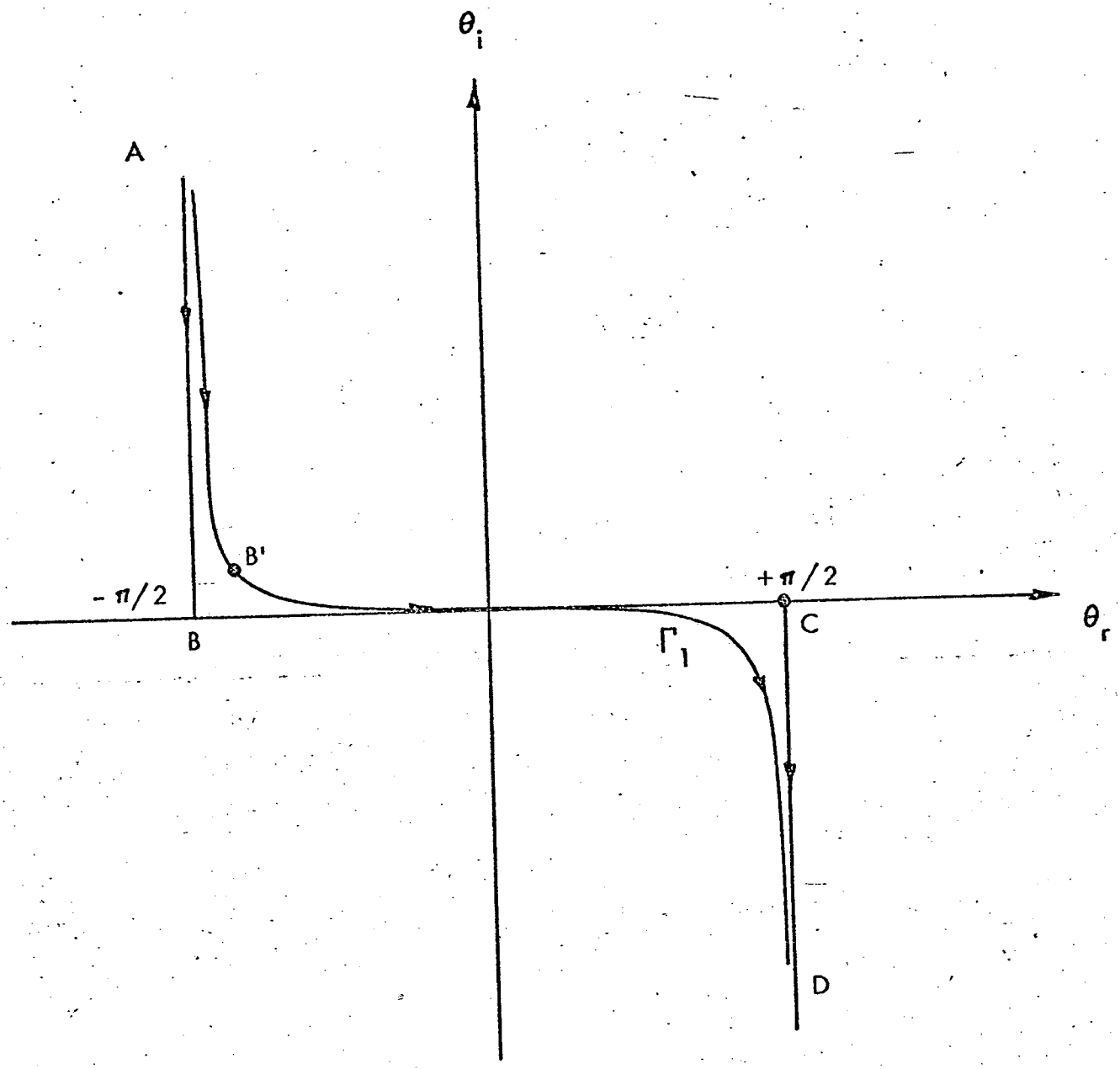

FIG. 2.5a INTEGRATION CONTOURS ON THE COMPLEX θ PLANE.

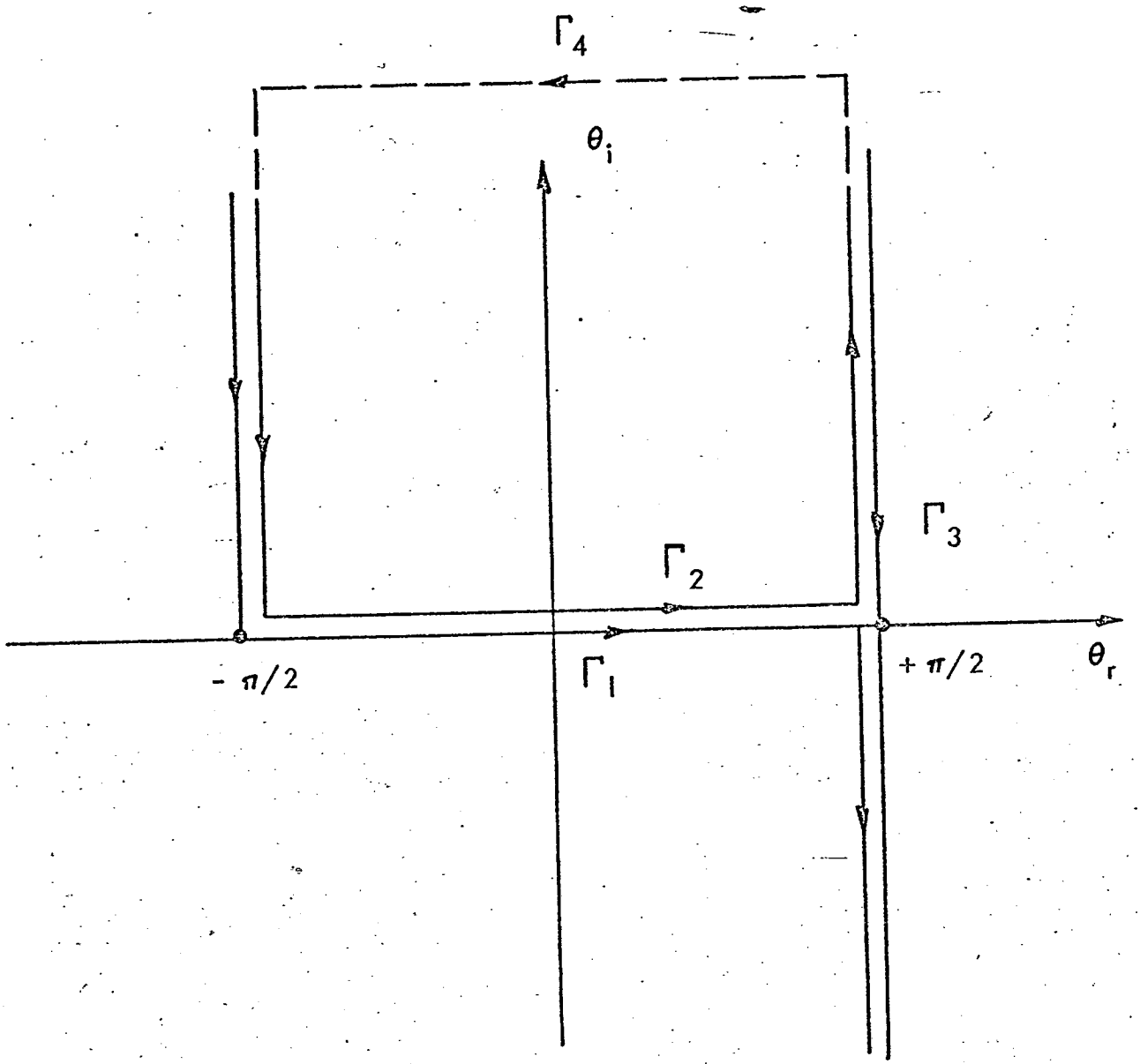

FIG. 2.5b ORIGINAL AND CLOSED CONTOURS.

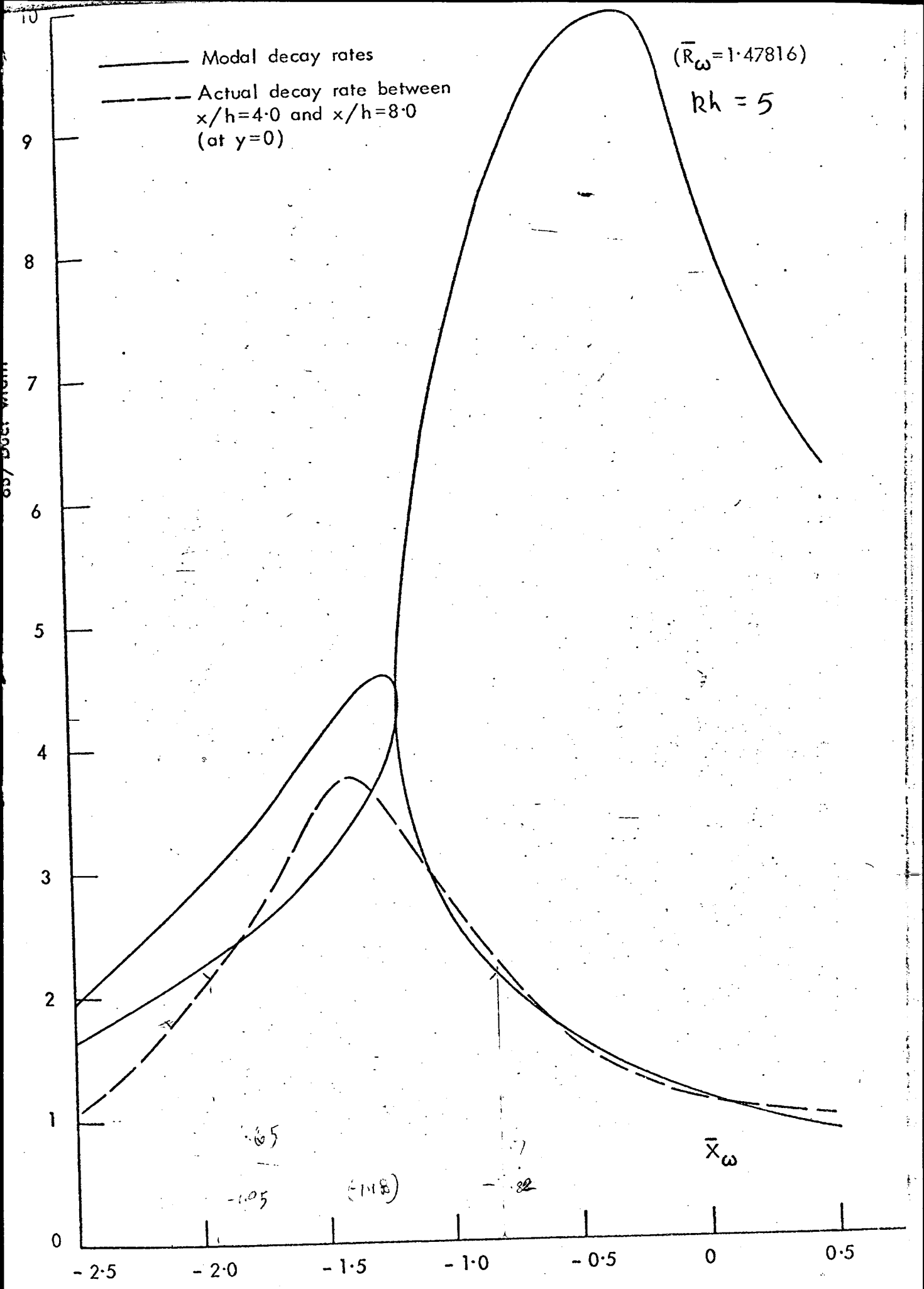

FIG. 2.6a COMPARISON OF MODAL ATTENUATIONS AND ACTUAL DECAY OF GREEN'S FUNCTION BETWEEN x/h = 4·0 AND x/h = 8·0 (4 MODES USED

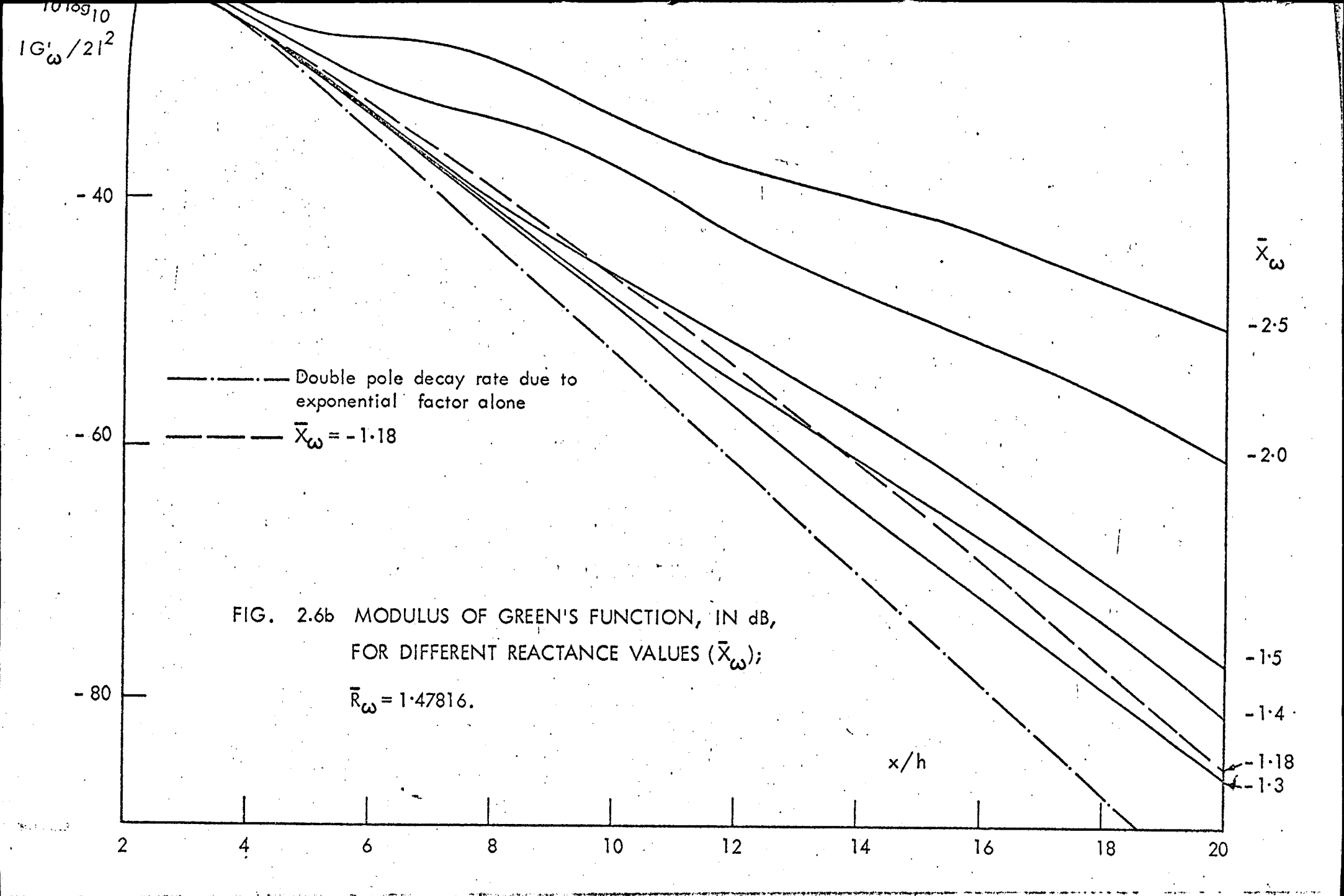

FIG. 2.6b MODULUS OF GREEN'S FUNCTION, IN dB, FOR DIFFERENT REACTANCE VALUES ($\bar{X}_\omega$);

$\bar{R}_\omega = 1{\cdot}47816$.

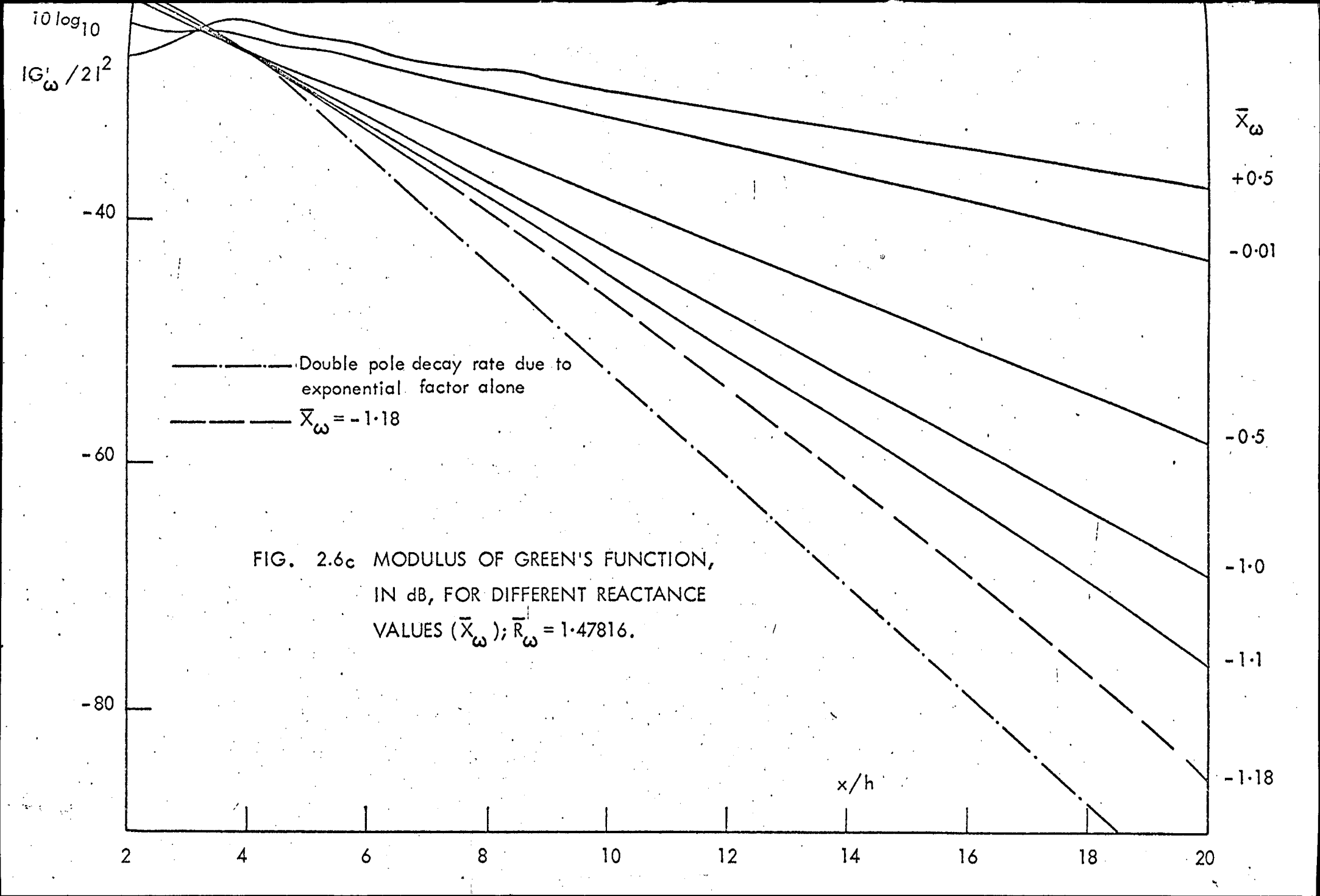

FIG. 2.6c MODULUS OF GREEN'S FUNCTION, IN dB, FOR DIFFERENT REACTANCE VALUES ($\bar{X}_\omega$); $\bar{R}_\omega = 1{\cdot}47816$.

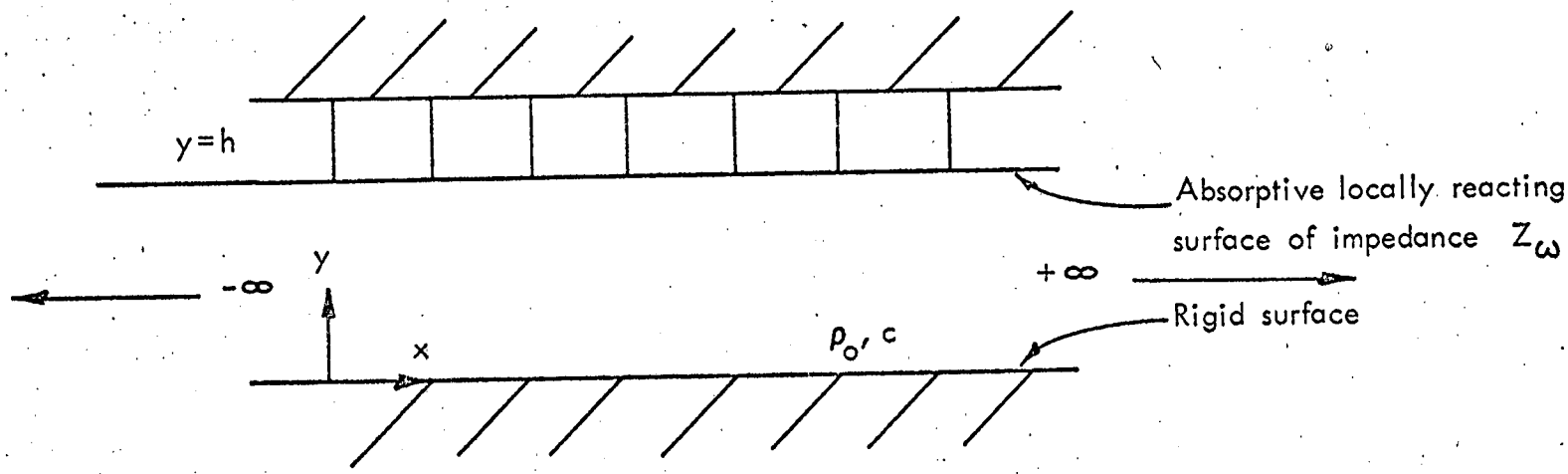

FIG. 2.7 DUCT GEOMETRY

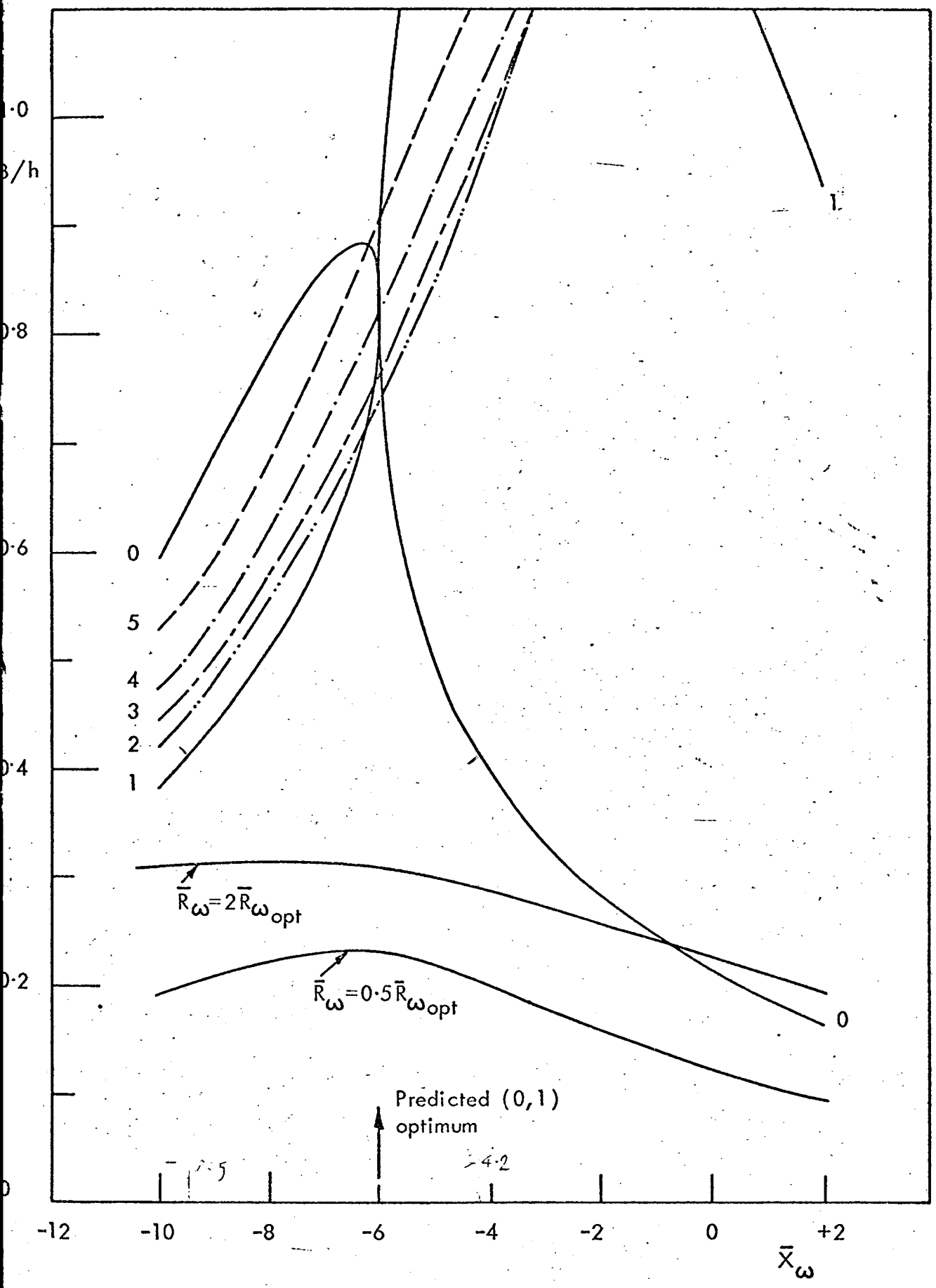

FIG. 2.8 VERIFICATION OF CREMER'S OPTIMUM REACTANCE FOR THE (0,1) MODE PAIR AT $h/\lambda = 4$. (RESISTANCE IS CONSTANT AND EQUAL TO THE OPTIMUM, $(\bar{R}_{\omega_{opt}})$, EXCEPT WHERE INDICATED).

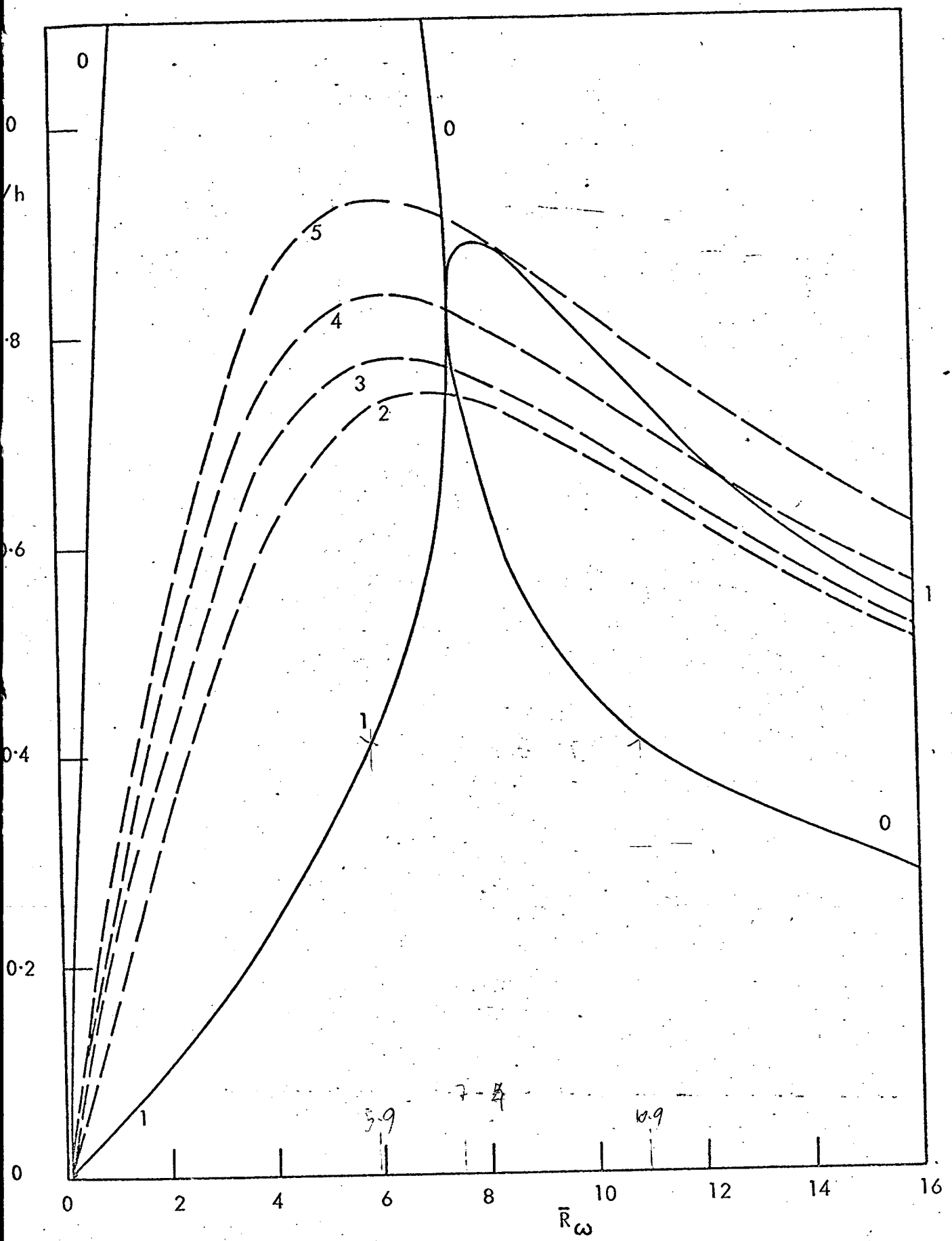

FIG. 2.9 VERIFICATION OF CREMER'S OPTIMUM RESISTANCE FOR THE (0,1) MODE PAIR AT $h/\lambda = 4$. (REACTANCE IS CONSTANT AND EQUAL TO IT'S OPTIMUM VALUE ($\bar{X}_{\omega_{opt}}$))

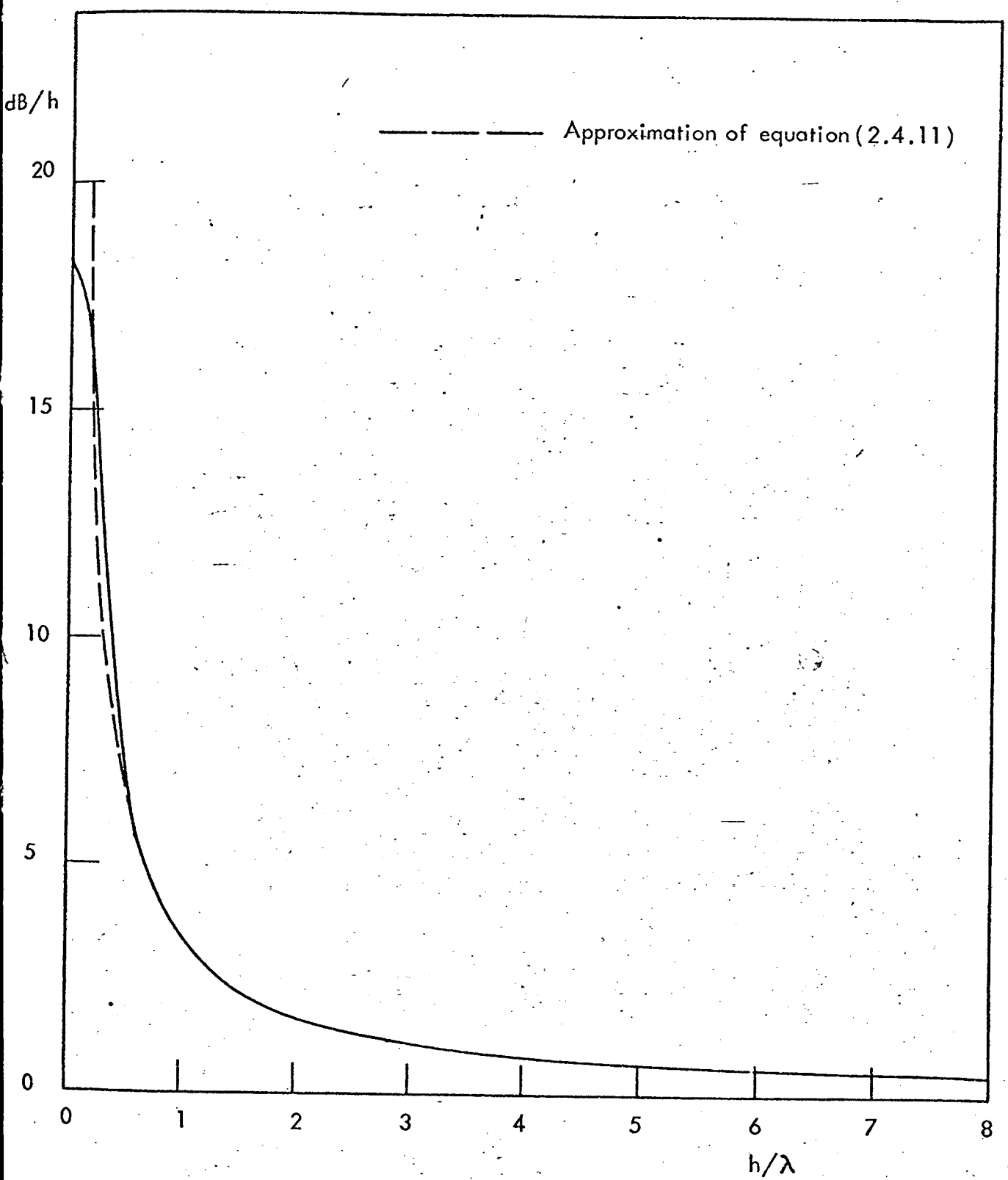

FIG. 2.10 MAXIMUM ATTENUATION RATE OF THE (0,1) MODE PAIR.

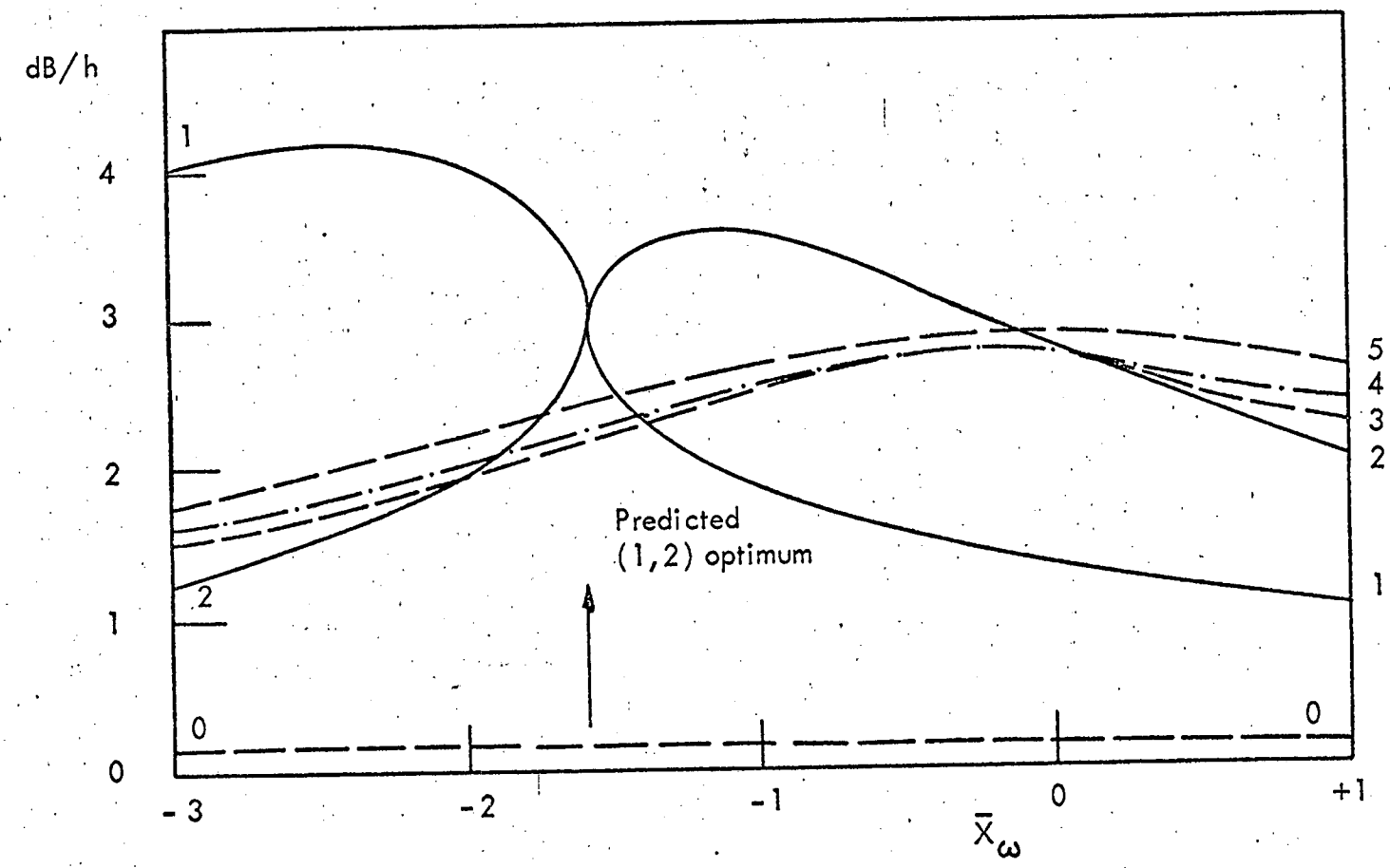

FIG. 2.11 VERIFICATION OF (1,2) OPTIMUM REACTANCE AT $h/\lambda = 4$. (RESISTANCE IS CONSTANT AND EQUAL TO THE OPTIMUM VALUE).

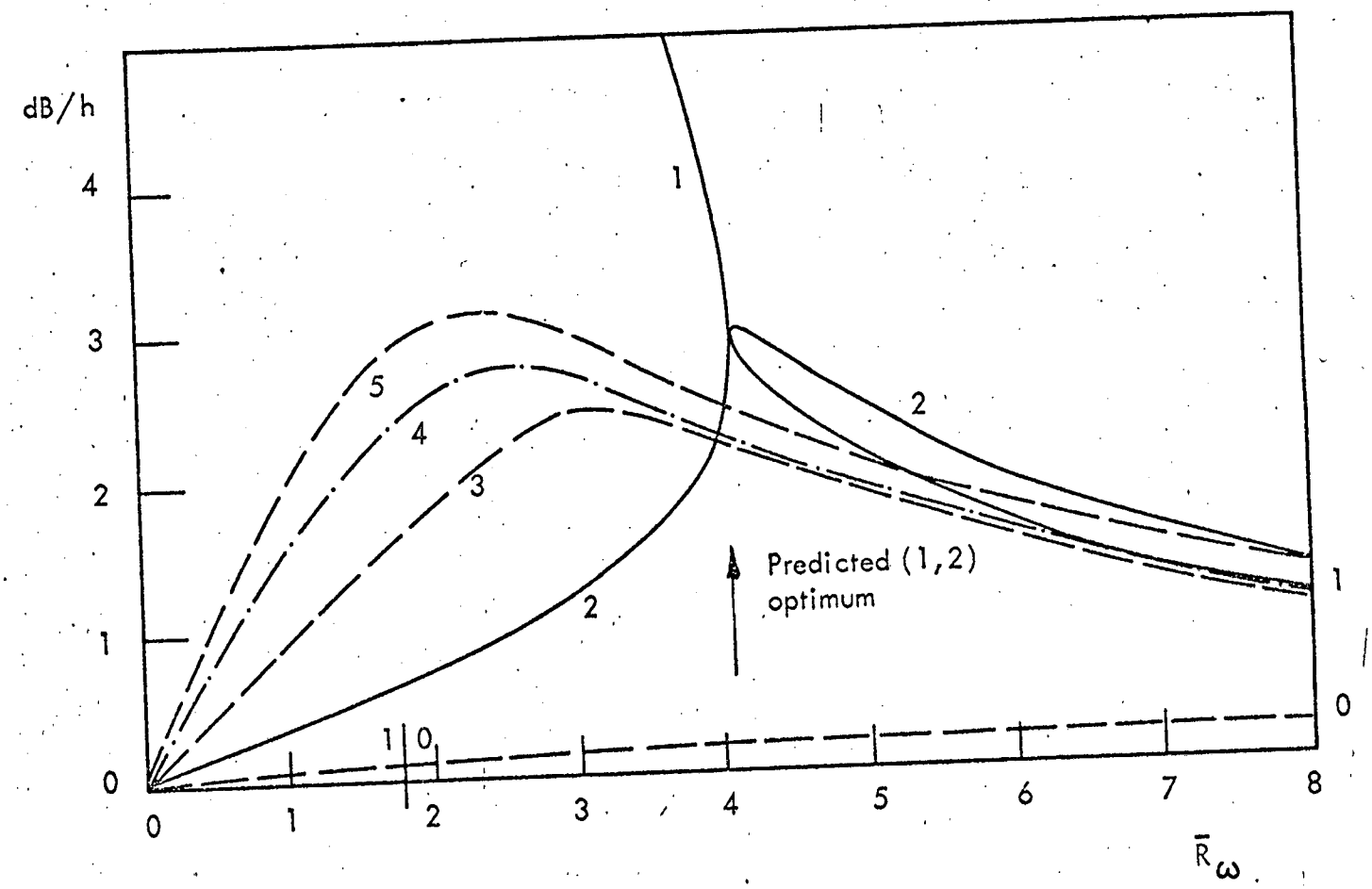

FIG. 2.12 VERIFICATION OF (1,2) OPTIMUM RESISTANCE AT $h/\lambda = 4$. (REACTANCE IS CONSTANT AND EQUAL TO THE OPTIMUM VALUE)

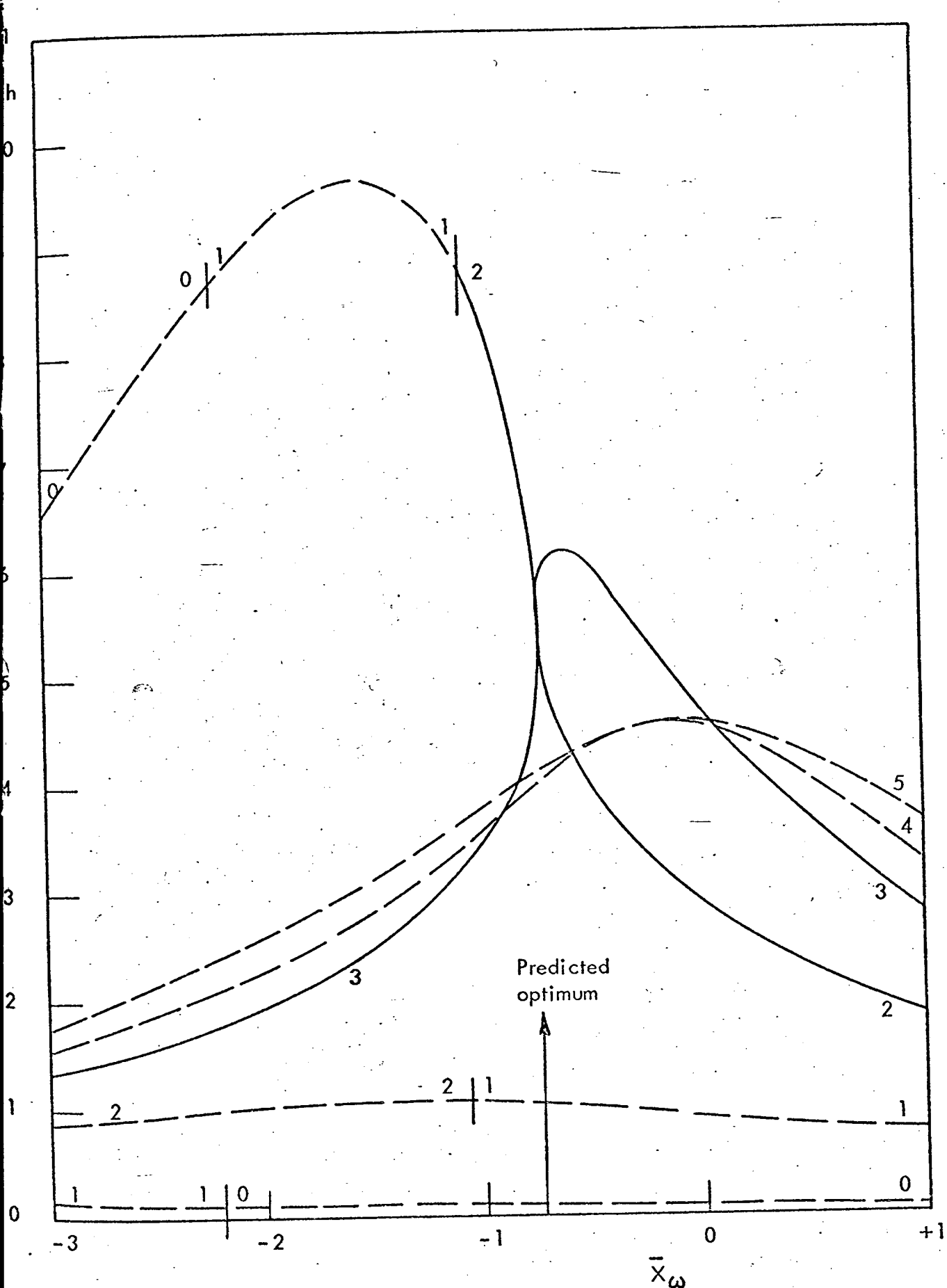

FIG. 2.13 VERIFICATION OF (2,3) OPTIMUM REACTANCE AT $h/\lambda = 4$.
(RESISTANCE IS CONSTANT AND EQUAL TO THE OPTIMUM VALUE)

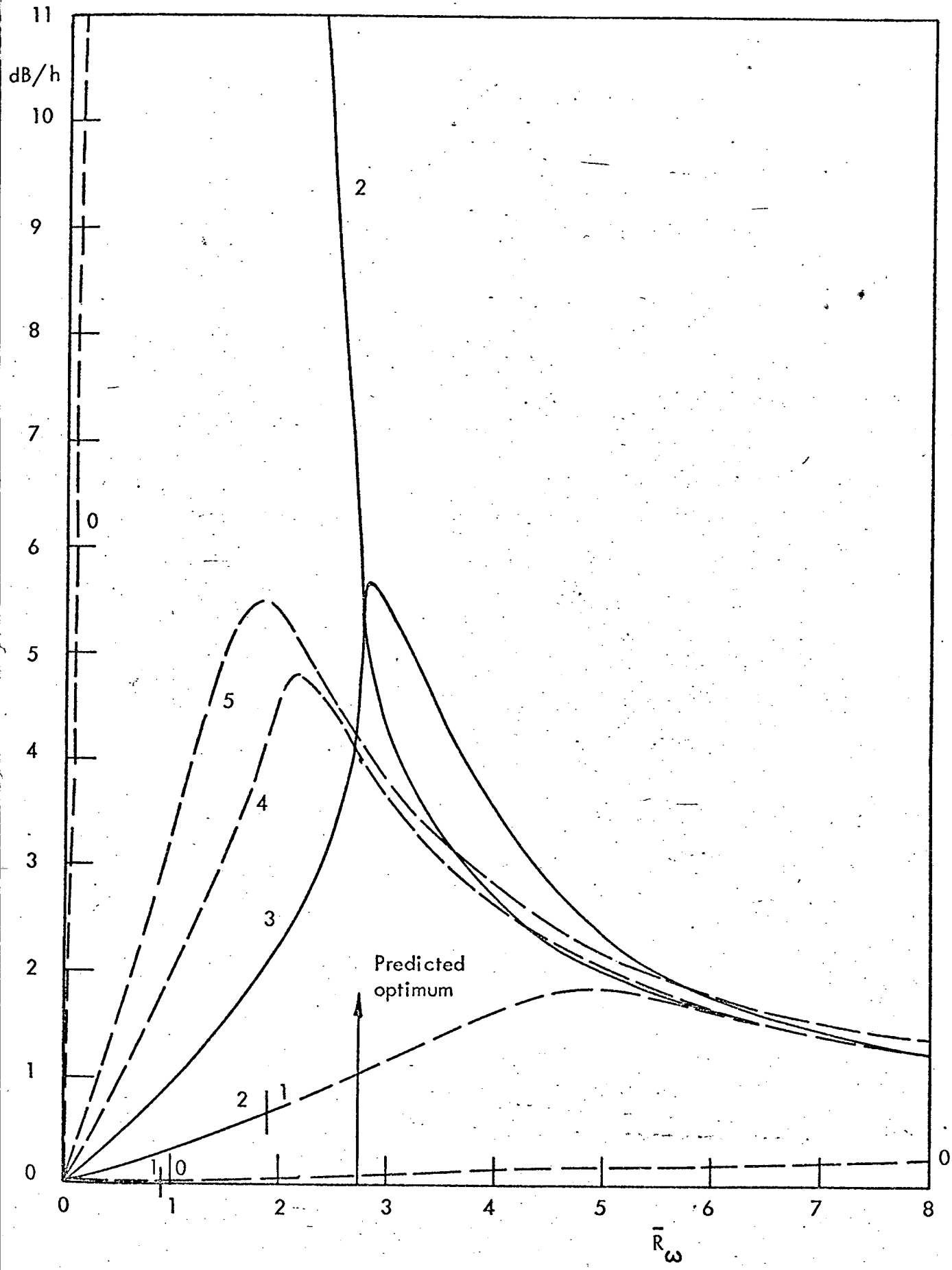

FIG. 2.14 VERIFICATION OF (2,3) OPTIMUM RESISTANCE AT $h/\lambda = 4$.
(REACTANCE IS CONSTANT AND EQUAL TO THE OPTIMUM VALUE).

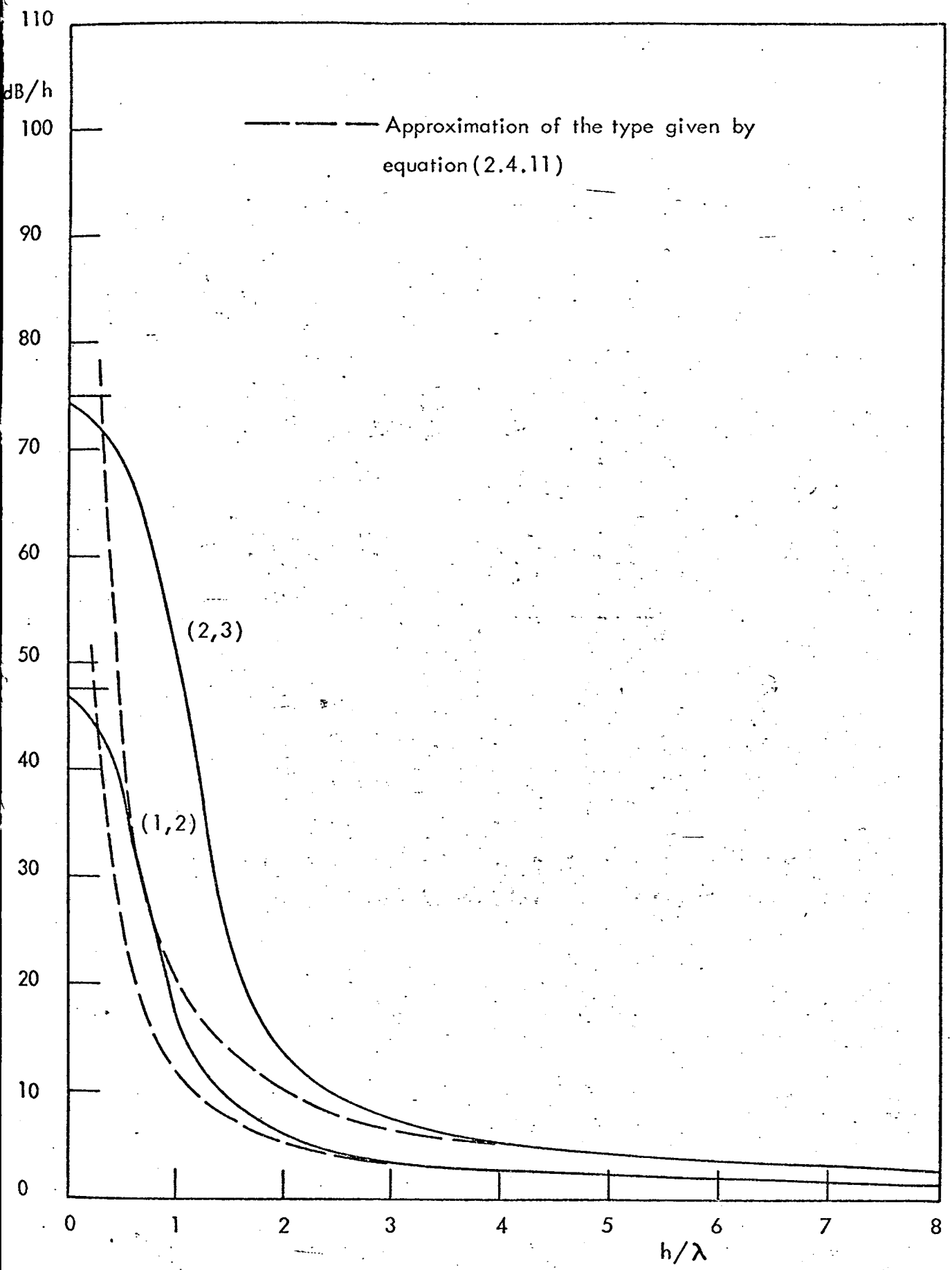

FIG. 2.15 MAXIMUM ATTENUATION RATE OF THE (1,2) AND (2,3) MODE PAIRS.

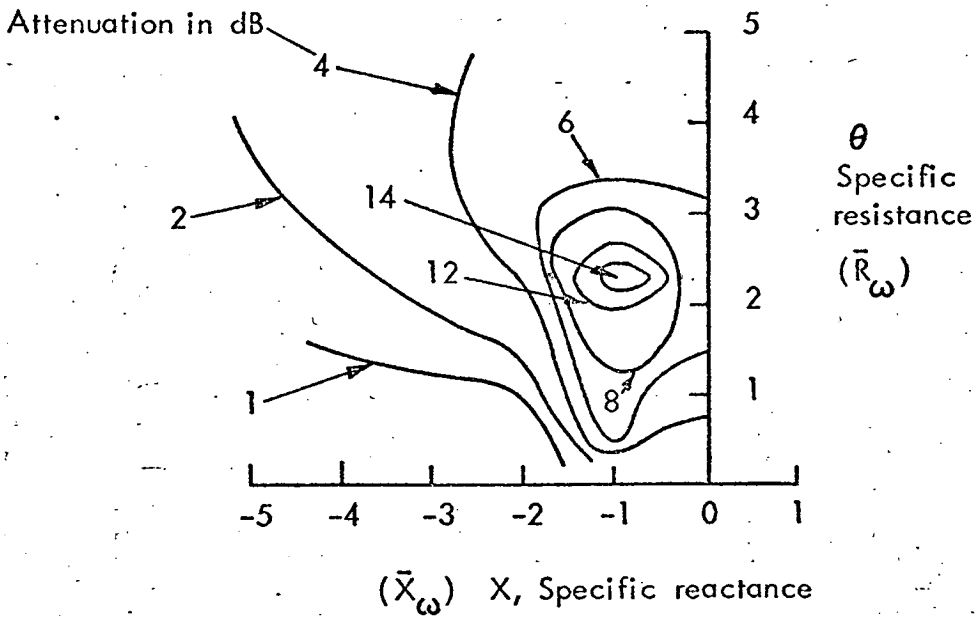

FIG. 2.16 LINES OF CONSTANT ATTENUATION FOR m=0, FIRST RADIAL MODE, FREQUENCY = 1000Hz - AFTER BENZAKEIN ET AL (34)

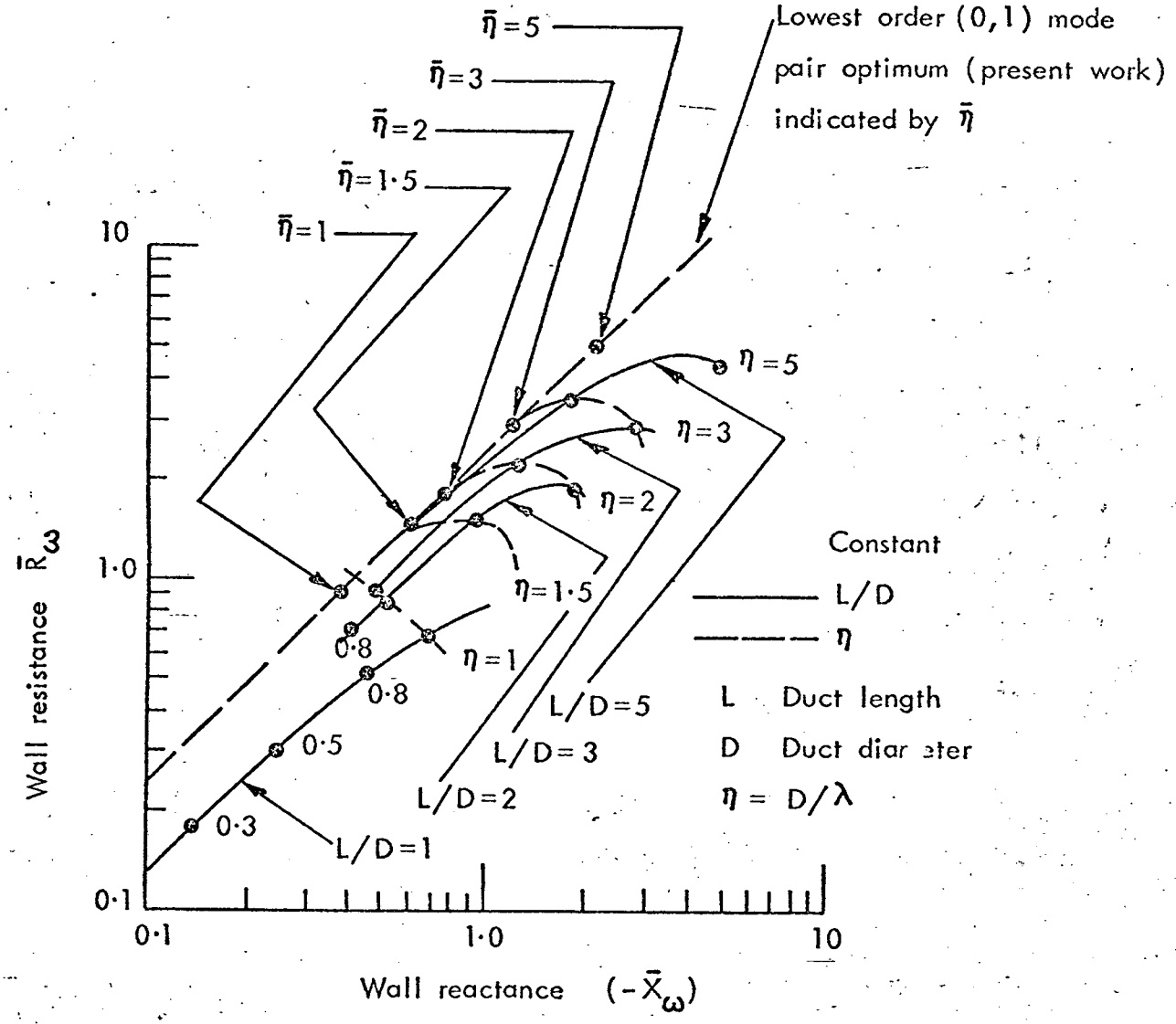

FIG. 2.17 COMPARISON OF THE (0,1) OPTIMUM IMPEDANCE IN A CIRCULAR DUCT WITH RICE'S (36) RESULTS FOR A MULTI-MODAL WAVEGUIDE MODEL.

CHAPTER 3

RAY MODELS FOR SOUND PROPAGATION AND ATTENUATION IN DUCTS, IN THE ABSENCE OF MEAN FLOW

3.1 Discussion

In Chapter 2 the acoustic field due to a line source situated between two infinite planes was constructed on the basis of plane wave reflection from a single infinite plane. The reflection of homogeneous (real angle of incidence) plane waves from a single wall with a locally reacting admittance is well understood apart, perhaps, from the peculiar behaviour as the angle of incidence tends to 90^{o}. Two complications arise when the homogeneous plane wave is replaced by a source and when a second wall is introduced. First, the source field is decomposed into a continuous distribution of homogeneous and inhomogeneous plane waves, and an incident wave of the latter type is not easy to visualise because the angle of incidence has no clear interpretation. The lines of constant amplitude and phase are no longer coincident. Second, there is reflection and re-reflection of these plane waves between the two walls. The resulting field can be represented by an infinite sum of modes but although this is extremely useful in practice, it leads to difficulties in physical interpretation. A good example appears in Chapter 2 where optimum impedances are given for individual mode pairs. The question immediately arises: why, from the physical viewpoint, do these take particular values they do, for example

$$\bar{Z}_{\omega opt} = (0.929 - j0.744)kh/\pi$$

for the lowest order mode pair? Intuitively it appears unlikely that there is a simple, complete answer to such a question but a qualitative physical explanation is clearly desirable.

It has to be recognised, also, that the simple modal result discussed in Chapter 2 has only been derived for a grossly over-simplified system. In practice mathematical models are required for systems with non-uniform impedance boundary conditions and a variety of duct geometries, including those that vary along the duct axis.

In the light of these facts a preliminary study has been made of various approximate models, based on a ray approach suggested by Morfey (21), for representing duct acoustic fields. Such ray models, by virtue of the simplifications employed, avoid the complication of inhomogeneous plane waves by retaining the field due to the source in its original form. Also the simplest version of these models excludes all but the first reflection of the source field in each duct wall, thus allowing the possibility of direct interpretation.

In the first section the accuracy of ray models for a point source between two infinite planes is investigated. A point source is chosen, in the first instance, for the following reason: the only source of error in a multiple reflection ray model is the assumption employed that the reflection of the source field is determined by the specular plane wave reflection coefficient. A correction factor for first order non-specular reflection effects is available, but only for the first reflection of a point source field.

In the second section the line source is re-introduced with particular emphasis on a single reflection, two image ray model. When this model is in reasonable, qualitative agreement with the exact modal model it can be used to interpret the behaviour of the modal field at and near optimum conditions - for the lowest order mode pair.

3.2 Evaluation of Ray Models for the Field Due to a Point Source between Two Infinite Planes

Three ray models are evaluated below for a point source between two infinite planes; the first is represented by Figure (3.1). The field at a point (x, y) is assumed to consist of the direct field from the source at $y = y_o$ and the reflected field, from each wall, due to image sources at $y = -y_o$ and at $y = 2h - y_o$. By using the approximate expression (specular reflection) for the Green's function for a point source in the presence of a single, uniform, infinite wall (14) the Green's function in this case can be written as

$$G_\omega' = \frac{1}{4\pi}\left\{\frac{\exp[ikR_{o1}]}{R_{o1}} + C_{r1}(R_{o2})\,\frac{\exp[ikR_{o2}]}{R_{o2}} + \frac{C_{r2}(R_{o3})\,\exp[ikR_{o3}]}{R_{o3}}\right\} \tag{3.2.1}$$

where

$$C_{r1}(R_{o2}) = \frac{\cos\bar{\theta}_{o2} - \bar{\beta}_{\omega 1}}{\cos\bar{\theta}_{o2} + \bar{\beta}_{\omega 1}}\,; \quad \cos\bar{\theta}_{o2} = \{1 - (\frac{x}{R_{o2}})^2\}^{\frac{1}{2}}, \tag{3.2.2}$$

$$C_{r2}(R_{o3}) = \frac{\cos\bar{\theta}_{o3} - \bar{\beta}_{\omega 2}}{\cos\bar{\theta}_{o3} + \bar{\beta}_{\omega 2}}\,; \quad \cos\bar{\theta}_{o3} = \{1 - (\frac{x}{R_{o3}})^2\}^{\frac{1}{2}}, \tag{3.2.3}$$

$$\begin{aligned} R_{o1} &= \{x^2 + (y - y_o)^2\}^{\frac{1}{2}}, \\ R_{o2} &= \{x^2 + (y + y_o)^2\}^{\frac{1}{2}}, \\ R_{o3} &= \{x^2 + (2h - y_o - y)^2\}^{\frac{1}{2}}. \end{aligned} \tag{3.2.4}$$

Notice that, unlike the model used in Chapter 2, the plane at $y = 0$ has a finite admittance. In all the evaluation examples to be given here $\bar{\beta}_{\omega 1}$ is set equal to $\bar{\beta}_{\omega 2}(= \bar{\beta}_\omega = 1/\bar{Z}_\omega)$ and the source is placed at $y = h/2$ although the relevant computer programs are designed to take unequal admittances and an arbitrary source location.

Under these special conditions the exact Green's function is

$$G_\omega' = \frac{i}{4h} \sum_{n=0}^{\infty} \frac{\cos\{k_{yn}h(y/h - \frac{1}{2})\}\, H_o^{(1)}(k_{xn}x)}{\{\frac{\sin(k_{yn}h)}{(k_{yn}h)} + 1\}} \qquad (3.2.5)$$

where the $(k_{yn}h)$ values are solutions of the equation

$$-\frac{ikh}{2}\,\bar{\beta}_\omega = \frac{(k_y h)}{2} \tan\left(\frac{k_y h}{2}\right) \qquad (3.2.6)$$

and

$$k_{xn} = \{k^2 - k_{yn}^2\}^{\frac{1}{2}}. \qquad (3.2.7)$$

For the present purpose the Hankel function can be replaced by its asymptotic form,

$$H_o^{(1)}(k_{xn}x) = \{\frac{2}{\pi k_{xn} x}\}^{\frac{1}{2}} \exp\left[i(k_{xn}x - \frac{\pi}{4})\right]. \qquad (3.2.8)$$

This is not a valid approximation for the evaluation of modes near the source.

The aim of the present exercise is to evaluate the ray model, described by equations (3.2.1) to (3.2.4), for some values of $\bar{Z}_\omega$ and a fixed value of kh, at selected points within the duct. The accuracy of the model in these examples is determined by a direct comparison with corresponding evaluations of the modal model, described by equations (3.2.5)-(3.2.8). Clearly, for the ray model to be a useful tool it should reproduce the actual field with a fair degree of accuracy, although accuracy requirements will vary with the type of application. If the duct energy flow is the parameter of interest, for example, large errors in the pressure field may not necessarily affect the energy flow to the same degree.

Here comparisons are confined to the mean square (time averaged) value of the field as a function of the axial distance from the source, x, and the distance, y, normal to the axis, from one of the duct walls.

The reduced frequency, kh, is kept equal to 10 through all the examples in this chapter, and the impedance values are chosen to be (1.0 - j.01), (1.0 + j.5) and (1.0 - j1.0). The sound field variation in dB along the duct centre-line (y/h = 0.5) is shown in Figure (3.2) for these impedance values calculated using the mode model. Five modes were used for this evaluation (see Appendix 3A), two 'cut-on' and three 'cut-off'. The field may contain some errors for small x/h values, due to the use of the asymptotic representation of the Hankel function. The ray field, for the same conditions is shown in Figure (3.3). Both fields exhibit the greatest decay and decay rate, beyond x/h = 2.0, for the impedance (1.0 - j1.0); this can be understood in view of the fact that the optimum impedance is approximately (1.5-j1.2). The ray field for the impedance (1.0 - j1.0) falls below the direct field at the smallest x/h value. It is now clear that, at large distances from the source, the ray field attempts to represent the modal decay of the actual field by destructive interference between the direct and reflected rays. Direct comparisons of the two fields are shown in Figures (3.4)-(3.6); the fields are in good agreement, in general, but begin to diverge with increasing distance from the source. These differences become quite large for the impedance value (1.0 - j1.0) beyond x/h = 1.6 and also beyond x/h = 5.0 (not shown). In fact the agreement is the worst overall for this impedance, the best being for (1.0 - j.01). This suggests that the omission of re-reflections for impedance values

that differ from unity is a significant source of error.

Strictly speaking if re-reflections or multiple images are included the ray field will still not converge to the correct value, because the specular reflection coefficient is only an approximation. Furthermore the inclusion of additional images, although a simple procedure, immediately removes much of the simplicity of the ray model and excludes any simple interpretation of the field behaviour.

In the next stage of the investigation the two-image model is retained and the model is improved by including the correction factor for the reflection coefficient given by Brekhovskikh (20), which takes the form

$$\frac{-iN_{o2}}{kR_{o2}} \quad \text{or} \quad \frac{-iN_{o3}}{kR_{o3}}$$

where

$$N_{o2} = \tfrac{1}{2}\{ \left[\frac{d^2C_r}{d\theta^2}\right]_{\theta = \bar{\theta}_{o2}} + \cot \bar{\theta}_{o2} \left[\frac{dC_r}{d\theta}\right]_{\theta = \bar{\theta}_{o2}} \}$$

and similarly for N_{o3}. For the locally reacting boundary condition used here N is given by

$$N = \{ \frac{\bar{\beta}_\omega \cos^2 \bar{\theta} - \bar{\beta}_\omega^2 \cos \bar{\theta} - 2\bar{\beta}_\omega}{(\cos \bar{\theta} + \bar{\beta}_\omega)^3} - \frac{\bar{\beta}_\omega \cos \bar{\theta}}{(\cos \bar{\theta} + \bar{\beta}_\omega)^2} \} \quad (3.2.9)$$

Adding this correction factor to the reflection coefficient gives the re-evaluated ray field as shown in Figures (3.4)-(3.6). The results are somewhat disappointing: there is no dramatic improvement in accuracy and where there is some improvement, for certain ranges of x/h, for example Figure (3.6) $1.25 \lesssim x/h \lesssim 4.0$, it appears to be coincidental for beyond $x/h = 4.0$ (not shown) the correction factor increases the inaccuracy. Based on these results and on others, not given here, it

is concluded that the major source of error is the omission of re-reflections and no appreciable improvement in accuracy can be obtained by including this correction factor in a two-image model.

Re-reflections can be described by a generalisation of equations (3.2.1)-(3.24):

$$G_\omega' = \frac{1}{4\pi} \sum_{\ell=0}^{\infty} \left[C_{r1}^{\ell}(R_{\ell 1}) C_{r2}^{\ell}(R_{\ell 1}) \frac{\exp[ikR_{\ell 1}]}{R_{\ell 1}} \right.$$

$$+ C_{r1}^{\ell+1}(R_{\ell 2}) C_{r2}^{\ell}(R_{\ell 2}) \frac{\exp[ikR_{\ell 2}]}{R_{\ell 2}} + C_{r1}^{\ell}(R_{\ell 3}) C_{r2}^{\ell+1}(R_{\ell 3}) \frac{\exp[ikR_{\ell 3}]}{R_{\ell 3}}$$

$$\left. + C_{r1}^{\ell+1}(R_{\ell 4}) C_{r2}^{\ell+1}(R_{\ell 4}) \frac{\exp[ikR_{\ell 4}]}{R_{\ell 4}} \right] , \qquad (3.2.10)$$

$$C_{r1}(R_{\ell m}) = \frac{\cos(\bar{\theta}_{\ell m}) - \bar{\beta}_{\omega 1}}{\cos(\bar{\theta}_{\ell m}) + \bar{\beta}_{\omega 1}} , \quad \cos(\bar{\theta}_{\ell m}) = \{1 - (\frac{x}{R_{\ell m}})^2\}^{\frac{1}{2}} , \qquad (3.2.11)$$

$$m = 1, 2, 3, 4 ,$$

$$C_{r2}(R_{\ell m}) = \frac{\cos(\bar{\theta}_{\ell m}) - \bar{\beta}_{\omega 2}}{\cos(\bar{\theta}_{\ell m}) + \bar{\beta}_{\omega 2}} , \quad \cos(\bar{\theta}_{\ell m}) = \{1 - (\frac{x}{R_{\ell m}})^2\}^{\frac{1}{2}} , \qquad (3.2.12)$$

$$m = 1, 2, 3, 4 ,$$

$$\begin{aligned} R_{\ell 1} &= \{x^2 + (2\ell h + y - y_o)^2\}^{\frac{1}{2}}, \\ R_{\ell 2} &= \{x^2 + (2\ell h + y + y_o)^2\}^{\frac{1}{2}} , \\ R_{\ell 3} &= \{x^2 + (2(\ell + 1)h - y - y_o)^2\}^{\frac{1}{2}} , \\ R_{4} &= \{x^2 + (2(\ell + 1)h + y_o - y)^2\}^{\frac{1}{2}} . \end{aligned} \qquad (3.2.13)$$

These are a generalisation of the relations derived by Brekhovskikh (20). Two ray models are considered: one described by the equations

(3.2.10)-(3.2.13) and the other described by the same equations but with the correction factor included in the first reflection at each wall: that is, the factor is added to $C_{r1}(R_{o2})$ and $C_{r2}(R_{o3})$. The factor has not been included in terms representing re-reflections because it is not clear whether such a procedure is valid. The correction factor, of course, was derived only for the reflection of a point source field by a single wall.

These two models*, termed the multiple image ray model and the corrected multiple image ray model, are compared in turn with the mode model by taking the square of the modulus of their ratio, expressed in dB. Included also is the corrected two-image ray model: the results are shown in Figures (3.7) - (3.9), again for the centre-line field. Both multiple image ray models show a marked improvement over the corrected two-image model, but for the case $\bar{Z}_\omega = (1.0 - j1.0)$ the error still becomes excessive (> 3 dB) at x/h values greater than 4.0. For the other impedance values, the inclusion of multiple reflections keeps the error less than 1½ dB up to x/h = 10. (Errors at small x/h values are probably due to the asymptotic Hankel function approximation but this has not been directly verified.)

With attention confined to the impedance value (1.0 - j1.0), the transverse error variation given by each ray model at axial locations x/h = 0.5, 2.0 and 8.0 is shown in Figures (3.10)-(3.12). The range of y/h is restricted to 0.0 - 0.5 as the fields are symmetric about the centre line (y/h = 0.5)**. The actual mode (field) variation is also shown in each figure (as an inset). Clearly the multiple

---

*In the evaluation of equation (3.2.10) the value of ℓ is incremented until $|G_\omega' h|^2$, in dB, does not change by more than .01 dB; ℓ rarely exceeds 5.

**The fields are actually evaluated at intervals of y/h = 0.1.

image model is more accurate than the corrected two-image model but the corrected multiple image model produces the most significant improvement.

The unmistakable trends in all the results presented so far are that (1) the two-image models undoubtedly provide a qualitative representation of the duct acoustic field in terms of its dependence on the wall impedance, and (2) increased accuracy can be obtained with multiple images and a correction for the specular, plane wave, first reflection coefficient. It is suggested that the inclusion of an appropriate correction factor for re-reflections would probably provide a ray model sufficiently accurate for most purposes. Even with this degree of sophistication the model would be easier to evaluate than the mode model although in terms of computational time much depends on the actual information required and hence the type of application. Ray models, if proven, would probably be superior in most respects to the modal approach for more realistic boundary conditions and variable geometries; an example of the latter is given by Felsen and Yee (38) ("Ray method for sound-wave reflection in an open-ended circular pipe.")

3.3 Evaluation of Ray Models for the Field Due to a Line Source Between Two Infinite Planes; Qualitative Interpretation of Optimum Conditions

Now that the feasibility and limitations of the ray model for a duct containing a point source have been demonstrated it is preferable that the line source be now re-introduced. Apart from the obvious reason that it is the basic source used throughout this work, it is preferable because, at large distances from the source, the characteristic exponential decay of the Green's function can be easily recognised (apart from the decay near optimum conditions); and because Hankel functions with complex arguments in the mode model can be replaced by simple exponential functions. This allows the mode model to be evaluated accurately, if required, near the source without resorting to non-standard computer sub-routines.* Of course, the ray model now contains Hankel functions, but with real arguments, and these can be evaluated with standard sub-routines.

The disadvantages of using a line source are that the correction factor for the reflection coefficient is not available** (to the author's knowledge), and that even the specularly reflected field is not given explicitly in standard texts. However it is reasonable to assume that this is still given by the plane wave reflection coefficient evaluated at the angle defined by the ray paths so that the two-image ray model Green's function is given by (see Figure (3.1))

$$G_\omega' = \frac{i}{4}\{H_o^{(1)}(kR_{o1}) + C_{r1}(R_{o2})H_o^{(1)}(kR_{o2}) + C_{r2}(R_{o3}) \times H_o^{(1)}(kR_{o3})\} \qquad (3.3.1)$$

---

*A sub-routine for Hankel functions with complex arguments is available but it has not been thoroughly tested.

**Although it presumably can be derived without too much difficulty this has not been attempted as the emphasis here is on a qualitative representation of the field for the purposes of interpretation. As the previous section has shown, the correction factor is of little use unless multiple images are included and this immediately precludes any simple interpretation.

where, in some examples, the Hankel function has been replaced by its asymptotic form (see equation (3.2.8)). The exact Green's function is

$$G_\omega' = \frac{i}{2} \sum_{n=0}^{\infty} \frac{\{\cos\ k_{yn}h(y/h - \tfrac{1}{2})\}}{k_{xn}h\ \tfrac{1}{2}\{\dfrac{\sin\ k_{yn}h}{k_{yn}h} + 1\}} \exp[ik_{xn}x] \qquad (3.3.2)$$

where the $k_{yn}h$ and $k_{xn}h$ values are determined from equations (3.2.6) and (3.2.7). Some evaluations of a multiple image ray model are given below, which is described by equations (3.2.10)-(3.2.13) with the factors $\exp[ikR]/4\pi R$ replaced by $\frac{i}{4} H_o^{(1)}(kR)$ (or its asymptotic form).

In the following examples the same impedance values are used as in the previous section but with an extra value, $\bar{Z}_\omega = (1.47816 - j1.0)$, which has a real part exactly equal to the optimum value for the lowest order mode pair and an imaginary part close to its optimum value (= -1.2). The same parameters are evaluated as before except now the Green's function is itself non-dimensional and therefore is not multiplied by the duct width.

The mode centre-line fields are shown in Figure (3.13) and the corresponding two-image ray fields in Figure (3.14): similarity is evident in the region $0.12 \lesssim x/h \lesssim 1.5$ but at larger distances the ray model cannot accurately reproduce the linear decay. Direct comparisons of the two models are shown in Figures (3.15)-(3.18). Nevertheless the ray model correctly describes the tendency (for $x/h > 1.5$) for the field to be reduced as the optimum impedance ratio is approached. The reason for this trend is that this impedance value causes 'permanent' destructive interference to take place nearest the source (at $x/h = 1.7$ - see Figure 3.14)). Thus the

ray model is capable of indicating, qualitatively, the best impedance value(s) for field minimisation but it cannot faithfully reproduce the corresponding decay rates. This is hardly surprising: destructive interference is inevitably sensitive to the exact value of the reflected fields relative to the direct field. As the ray model is improved it must gradually converge to the correct linear decay behaviour, but this is of little interest here. The two-image ray model has provided the information required for a qualitative interpretation of optimum impedance values: the optimum impedance is roughly that value which allows the amplitude and phase of the singly-reflected field to cause the most efficient destructive interference with the direct field.

From this interpretation it will be shown that the reactance $\bar{X}_\omega$ must be negative (in the +j notation) and directly proportional to kh; although it is not possible to deduce an explicit dependence for $\bar{R}_\omega$ on kh it can be deduced that $\bar{R}_\omega$ must be non-zero and should also be a function of kh. According to the two-image ray model the field on the centre-line * (at a sufficient distance from the source so that the Hankel function can be replaced by its asymptotic form) is proportional to (in the +j notation) p, where

$$p \doteq \frac{\exp[-jkx]}{\{kx\}^{\frac{1}{2}}} + \frac{2|C_r|}{\{(kx)^2 + (kh)^2\}^{\frac{1}{4}}} \exp[-j\{(kx)^2 + (kh)^2\}^{\frac{1}{2}} + j\phi] \qquad (3.3.3)$$

and ϕ is the phase of the reflection coefficient.

For $h/x \ll 1$ this reduces to

---

*For the conditions assumed throughout this Chapter, that is, the source is on the centre-line and the walls have equal impedance.

$$p \doteq \frac{\exp[-jkx]}{\{kx\}^{\frac{1}{2}}} \{1 + 2|C_r| \exp [-jkh(h/2x) + j\phi]\} \qquad (3.3.4)$$

where

$$C_r = \{\bar{Z}_\omega(h/x) - 1\}/\{\bar{Z}_\omega(h/x) + 1\}. \qquad (3.3.5)$$

For complete, destructive interference the reflection coefficient must take the value

$$|C_r| = 0.5 \quad \text{and} \quad \phi = \pm \pi + kh(h/2x).$$

Although C_r clearly does not attain this extreme value in the examples evaluated above, the actual values, for large x/h, must be similar near the optimum condition. The phase of the reflection coefficient, when $|\bar{Z}_\omega h/x| \ll 1$, is, from equation (3.3.5)

$$\phi = \tan^{-1}\{-2\bar{X}_\omega (h/x)\}$$

and equating this with the extreme value given above, one obtains, for $kh(h/x) \lesssim 0.5$

$$kh(h/2x) = -2\bar{X}_\omega(h/x)$$

or

$$\bar{X}_\omega = -kh/4.$$

This agrees with the frequency dependence of the optimum impedance, which is

$$\bar{Z}_{\omega_{opt}} = (0.929 - j0.744)\frac{kh}{2\pi}$$

but differs in absolute value by a factor of 2. Of course, in this approximation (small $|\bar{Z}_\omega h/x|$), the modulus of the reflection coefficient is unity and the resistance must take a value, which violates the condition $|\bar{Z}_\omega h/x| \ll 1$, to obtain the extreme value $|C_r| = 0.5$. Also as $\bar{X}_\omega$ increases with kh, $\bar{R}_\omega$ must also change in

order to maintain the required reflection coefficient. Thus $\bar{R}_\omega$ must be non-zero and should be a function of kh but little more can be deduced with this simple approximation.

Finally the accuracy of the two-image model and the multiple image model is indicated, again on the centre-line, for the four impedance values in Figures (3.19)-(3.22). In the first three figures the Hankel functions in the ray models have been replaced by the usual asymptotic approximation but in the last figure the actual Hankel functions have been used. These results have one feature in common: where the two image model is relatively accurate the multiple image model leads to an improvement, in general, but where the two image model fails completely at large distances from the source, so does the multiple image model. In this region reflection coefficient corrections are essential for the actual field decay to be described by the mechanism of destructive interference.

APPENDIX 3A

Evaluation of the Exact, 'Mode' Green's Functions (Point Source and Line Source)

For the value $kh = 10.0$ and the range of x/h and $\bar{Z}_\omega$ values used, the sum of the first four or five modes provides a sufficiently accurate estimate of the Green's functions given by equations (3.2.6) and (3.3.2) for the present purpose. The wavenumber values for these modes, which are solutions of equation (3.2.6) with equation (3.2.7), are given below for each impedance; the mode number is not necessarily equal to the mode order.

Impedance $\bar{Z}_\omega$	Mode No. n	$Re(k_{yn}h)/4$	$Im(k_{yn}h)/4$	$Re(k_{xn}h)/4$	$Im(k_{xn}h)/4$
1.0+j0.5	0	0.687329	0.123099	2.40707	- 0.0351505
	1	2.00629	0.287664	1.56328	-0.369183
	2	3.36282	0.266948	0.395805	-2.26803
	3	4.84143	0.200839	0.234426	-4.14778
	4	6.37290	0.155231	0.168747	-5.86244
1.0-j.01	0	0.752979	0.155117	2.38945	-0.0488815
	1	2.10688	0.503363	1.58497	-0.669112
	2	3.25386	0.471446	0.713364	-2.15040
	3	4.73124	0.292412	0.344071	-4.02088
	4	6.28871	0.210150	0.228996	-5.7715
1.0-j1.0	0	0.961771	0.230183	2.32101	-0.0953824
	1	1.27285	1.24012	2.55896	-0.616848
	2	2.91746	0.201693	0.382456	-1.53856
	3	4.57303	0.133746	0.159686	-3.83017
	4	6.18097	0.0999752	0.109313	-5.65299
1.47816 - j1.0	0	1.31302	0.703702	2.27724	-0.405744
	1	0.891023	0.408750	2.37627	-0.153268
	2	3.00672	0.198239	0.351552	-1.69548
	3	4.62640	0.126776	0.150636	-3.89361

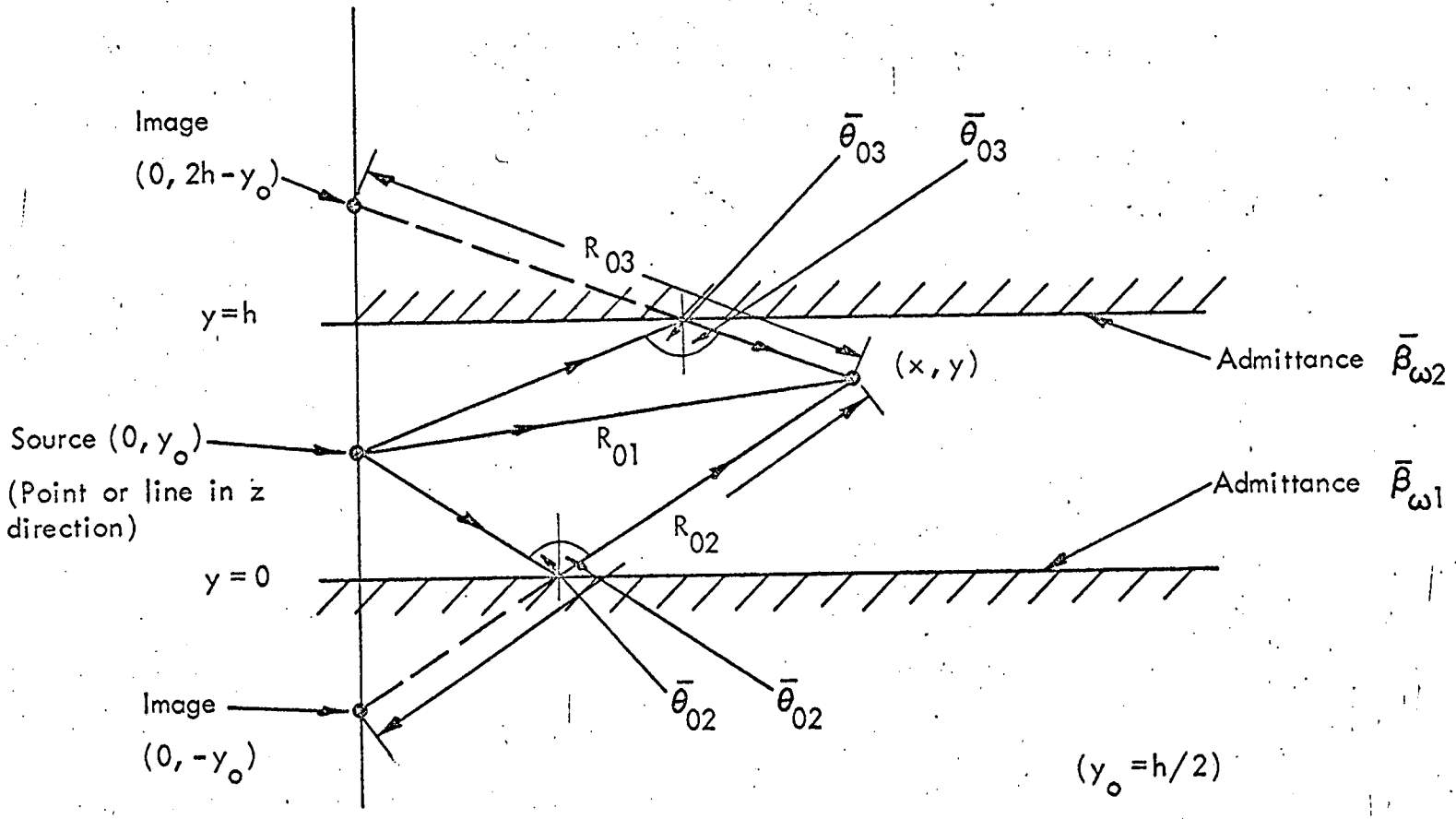

FIG. 3.1 THE TWO-IMAGE RAY MODEL

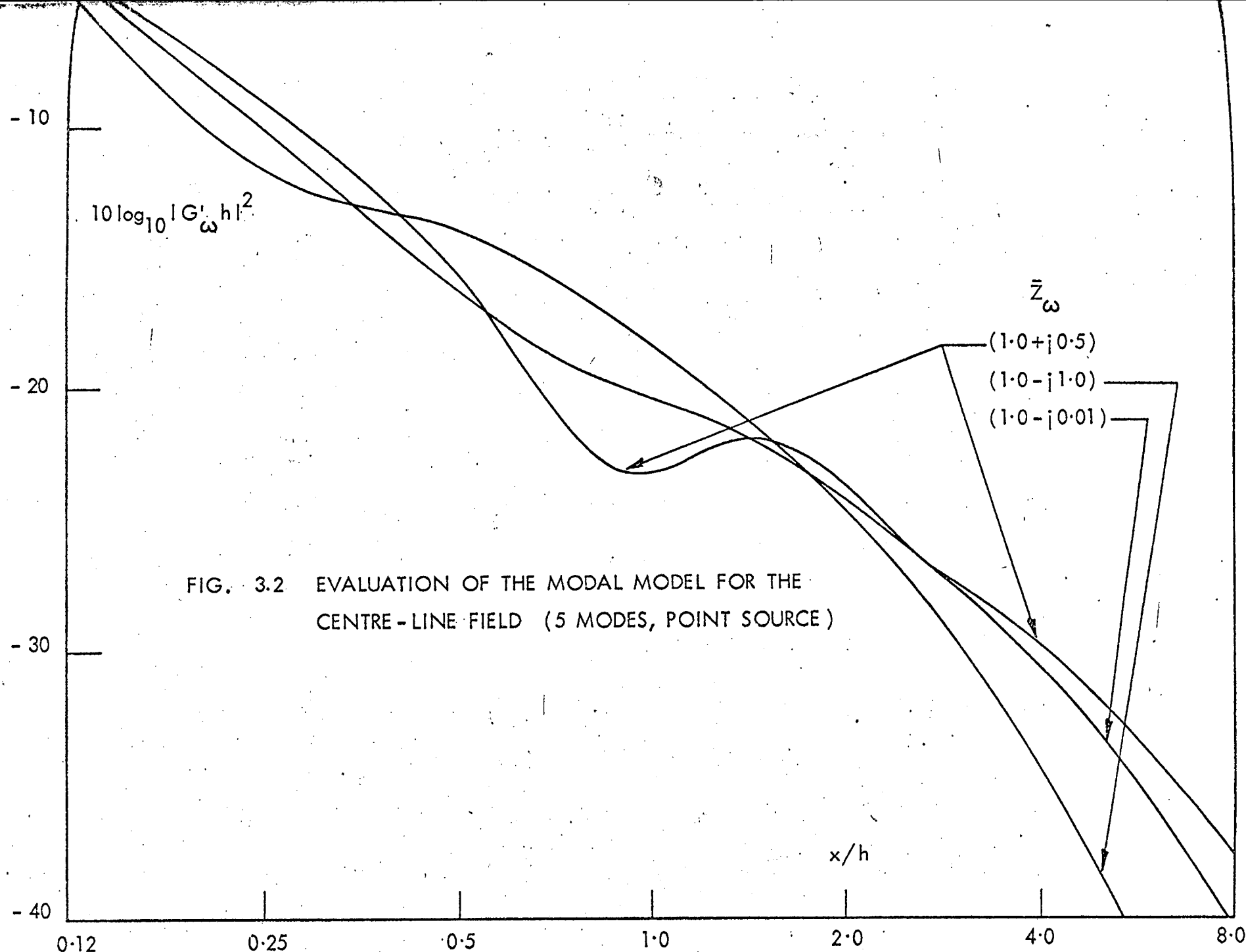

FIG. 3.2 EVALUATION OF THE MODAL MODEL FOR THE CENTRE-LINE FIELD (5 MODES, POINT SOURCE)

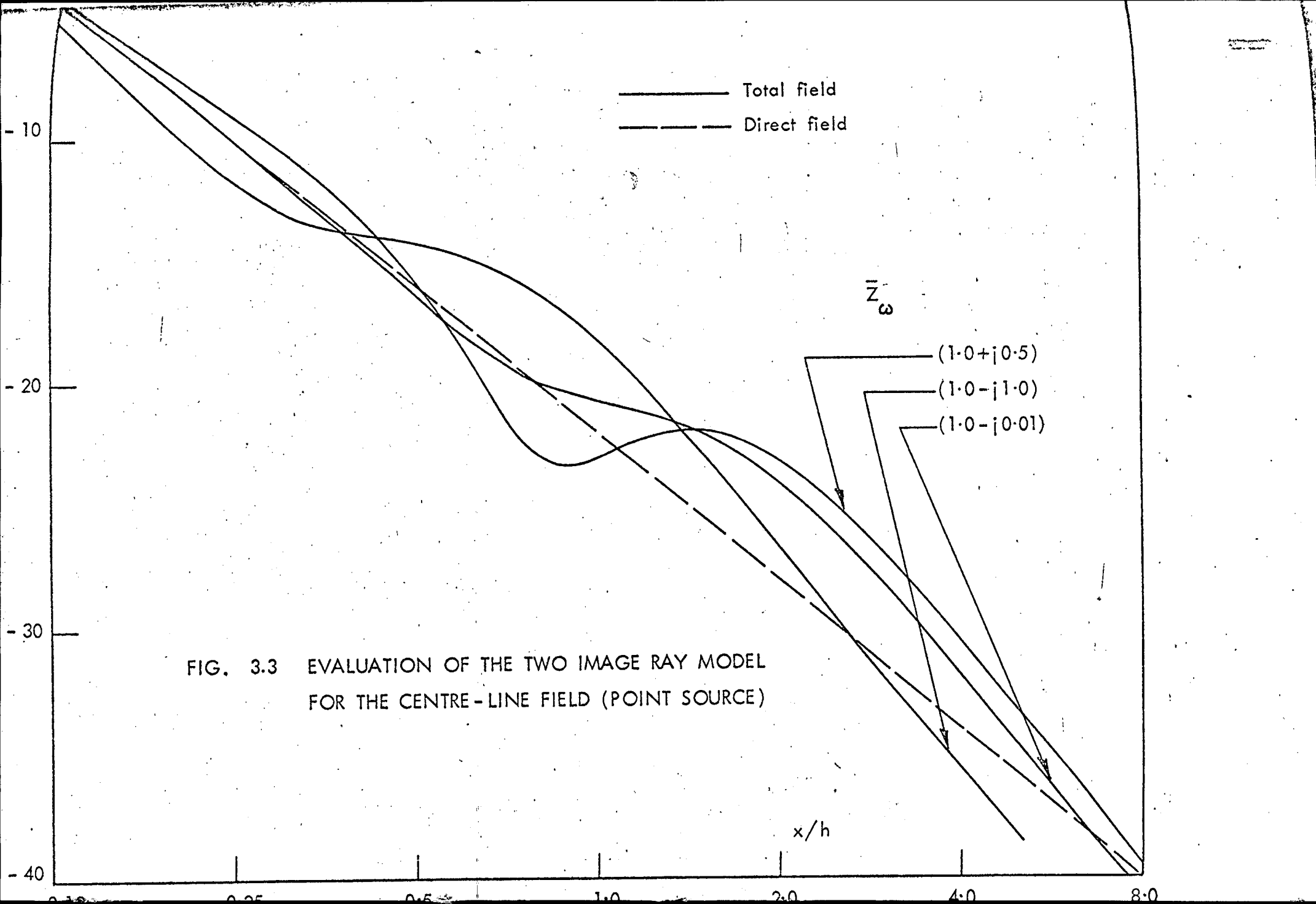

FIG. 3.3 EVALUATION OF THE TWO IMAGE RAY MODEL FOR THE CENTRE-LINE FIELD (POINT SOURCE)

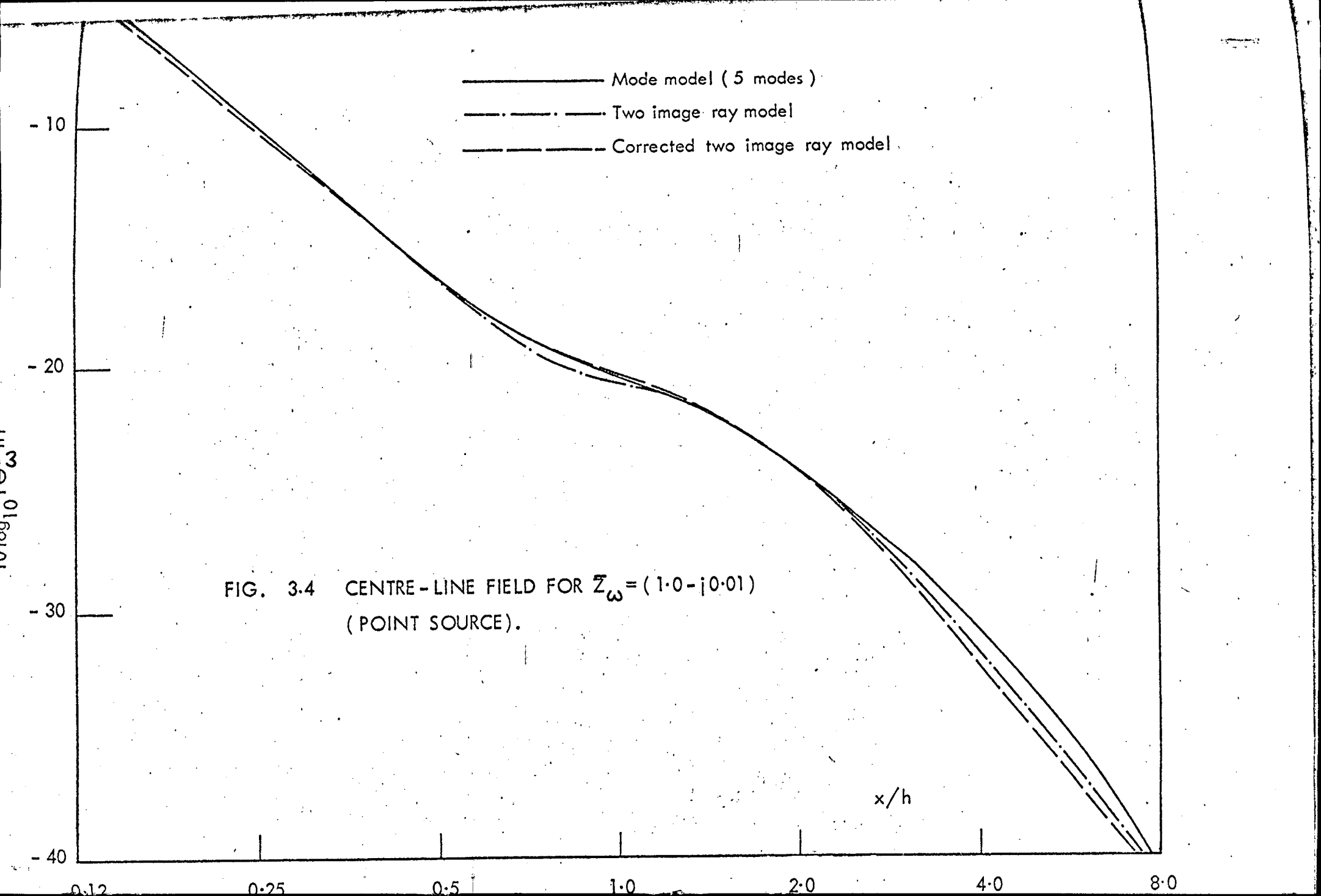

FIG. 3.4 CENTRE-LINE FIELD FOR $\bar{Z}_\omega = (1{\cdot}0 - j0{\cdot}01)$ (POINT SOURCE).

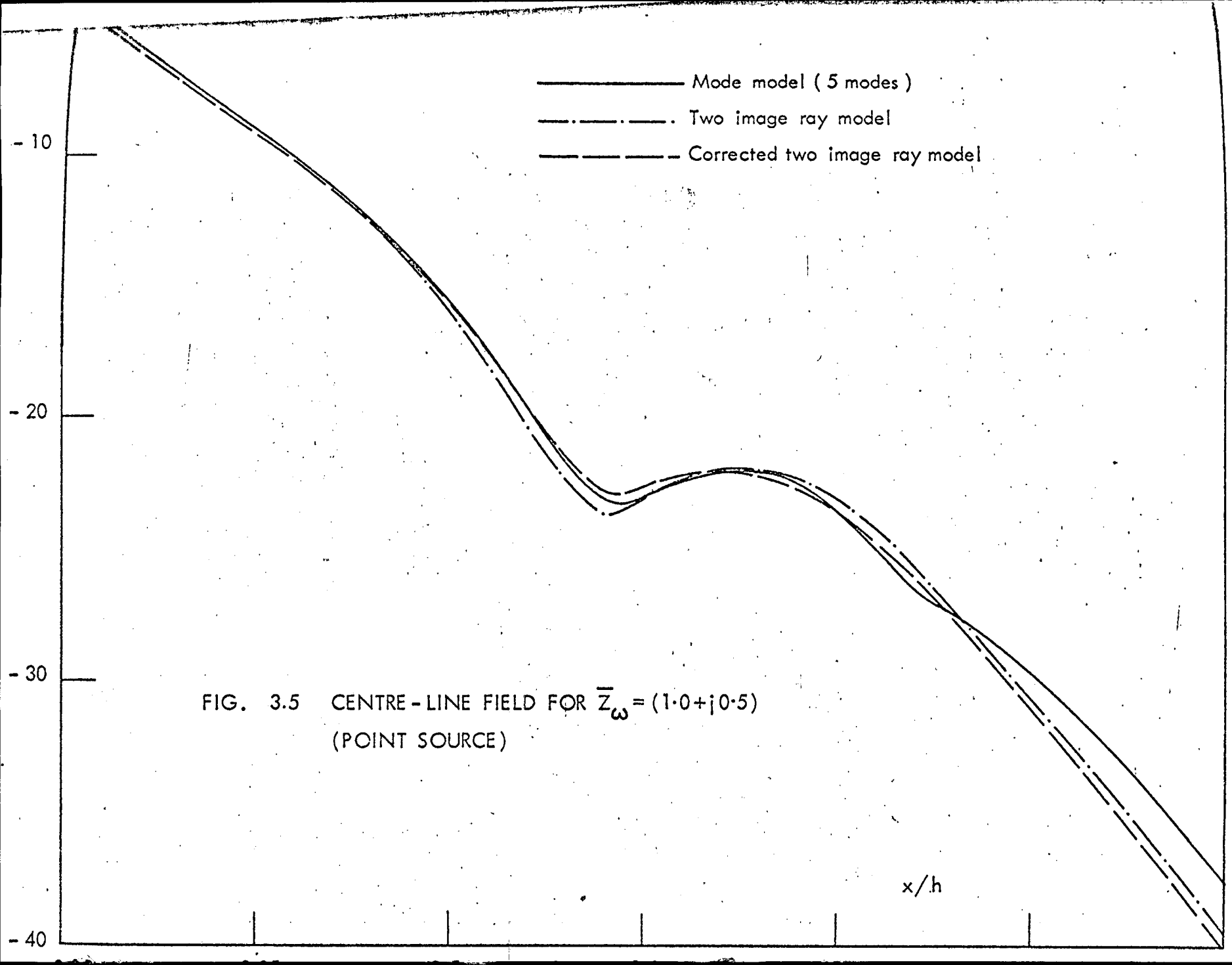

FIG. 3.5 CENTRE-LINE FIELD FOR $\bar{Z}_\omega = (1{\cdot}0 + j0{\cdot}5)$
(POINT SOURCE)

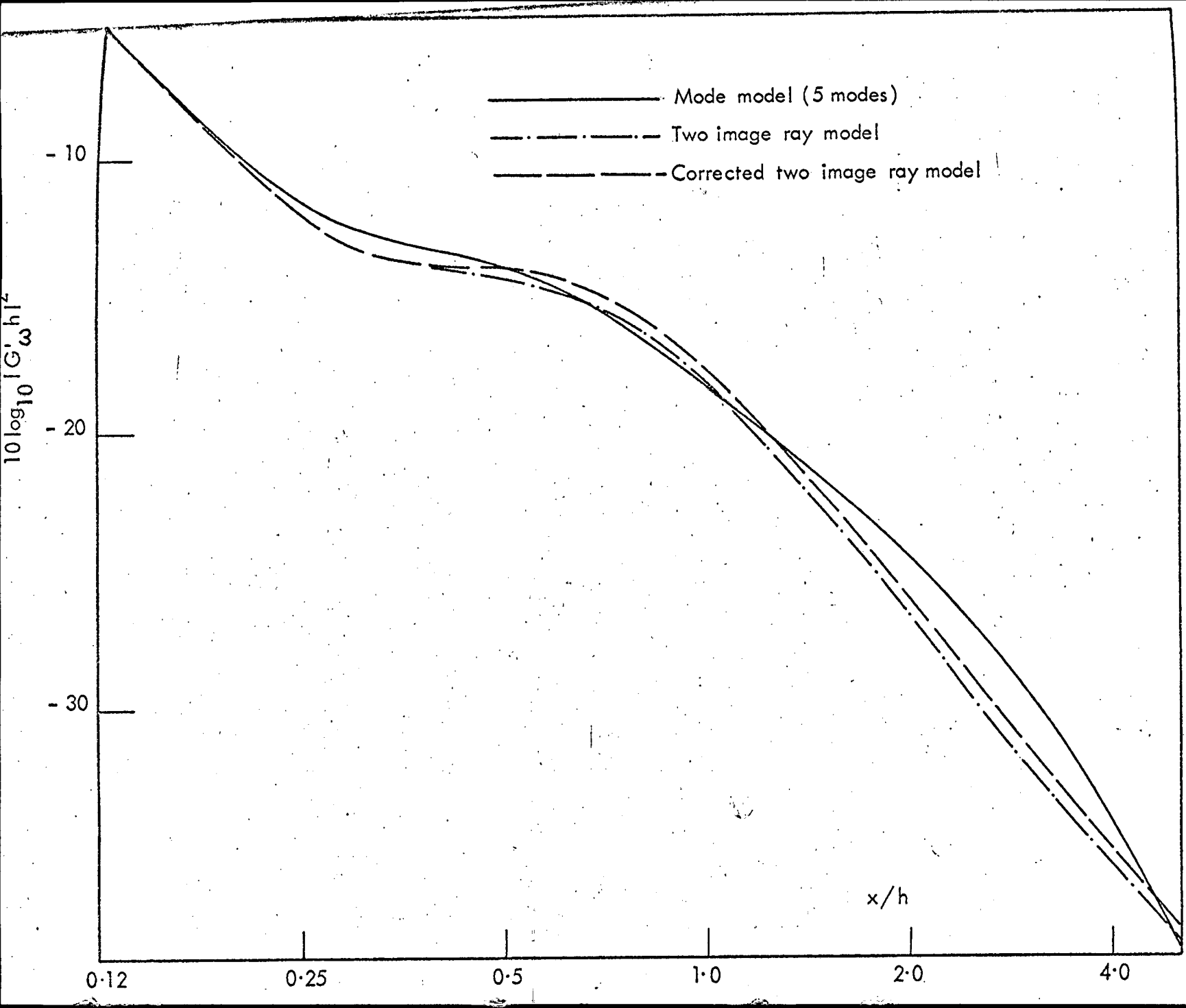
Mode model (5 modes)
Two image ray model
Corrected two image ray model
- 10
- 20
- 30
$10 \log_{10} |G'_3 h|^2$
x/h
0·12
0·25
0·5
1·0
2·0
4·0

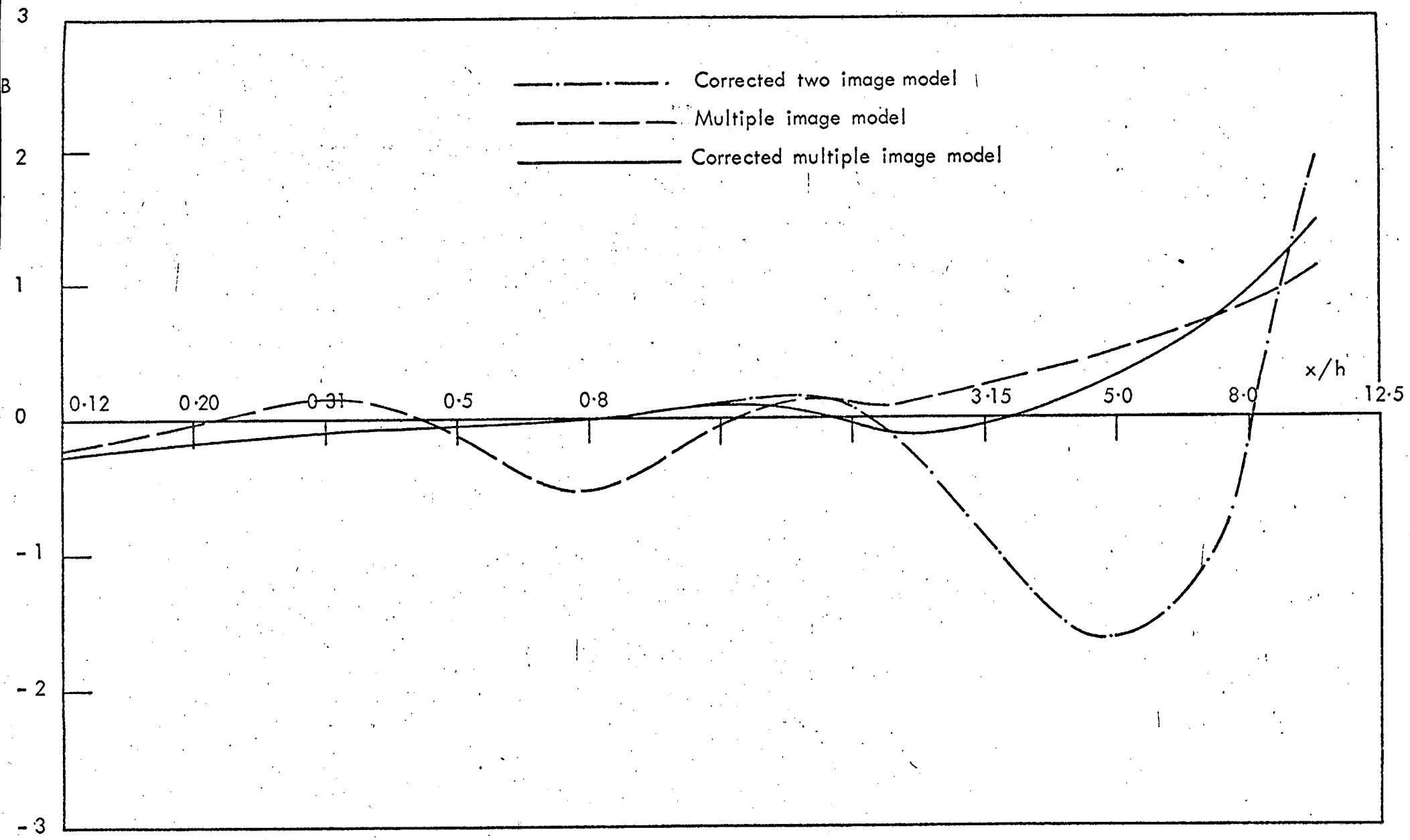

FIG. 3.7 MODULUS SQUARED OF RATIO, IN dB, OF MODE FIELD AND RAY FIELDS ON CENTRE-LINE FOR $\bar{Z}_\omega = (1{\cdot}0 - j0{\cdot}01)$

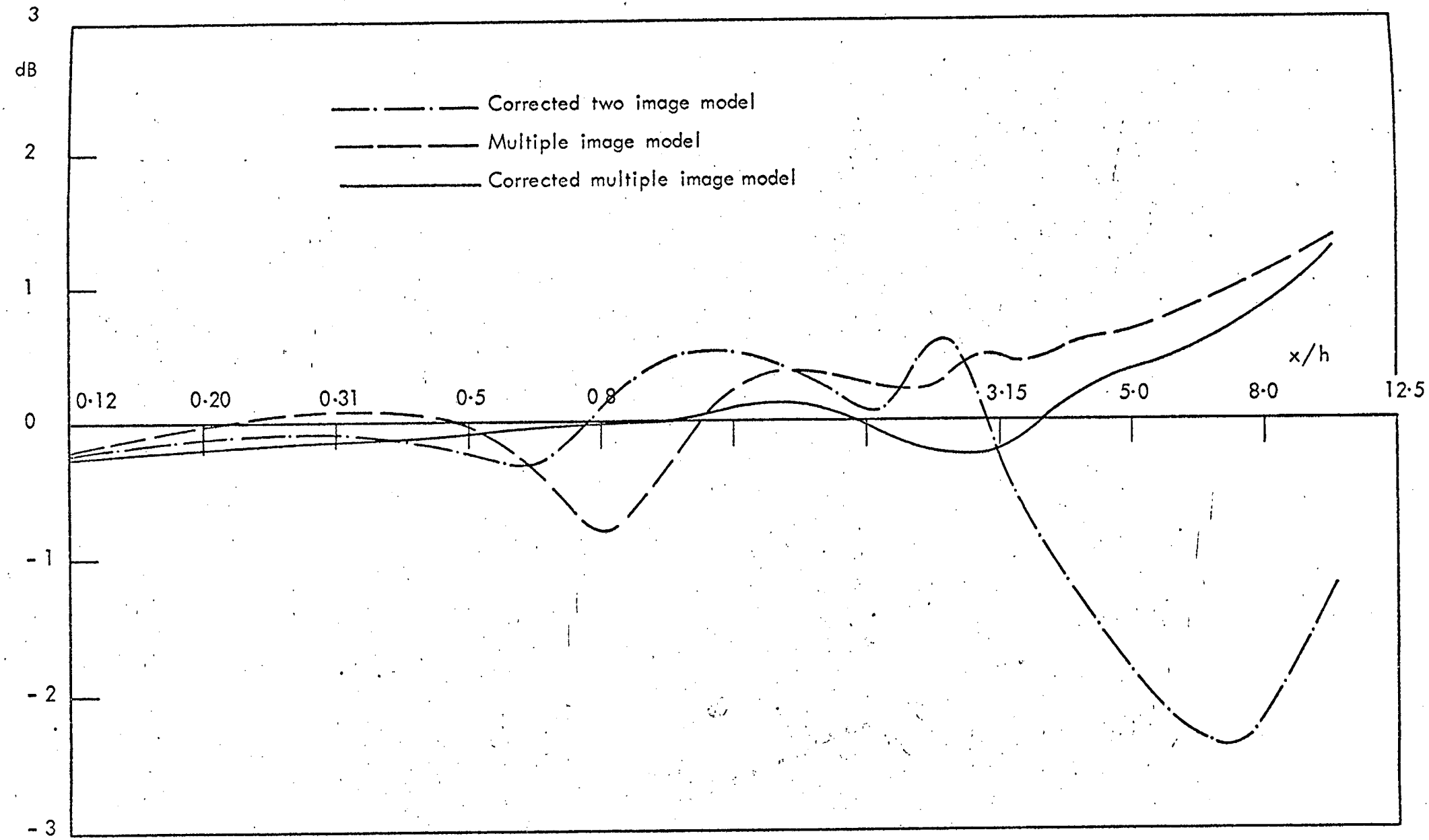

FIG. 3.8 MODULUS SQUARED OF RATIO, IN dB, OF MODE FIELD AND RAY FIELDS ON CENTRE-LINE FOR $\bar{Z}_\omega = (1{\cdot}0 + j0{\cdot}5)$

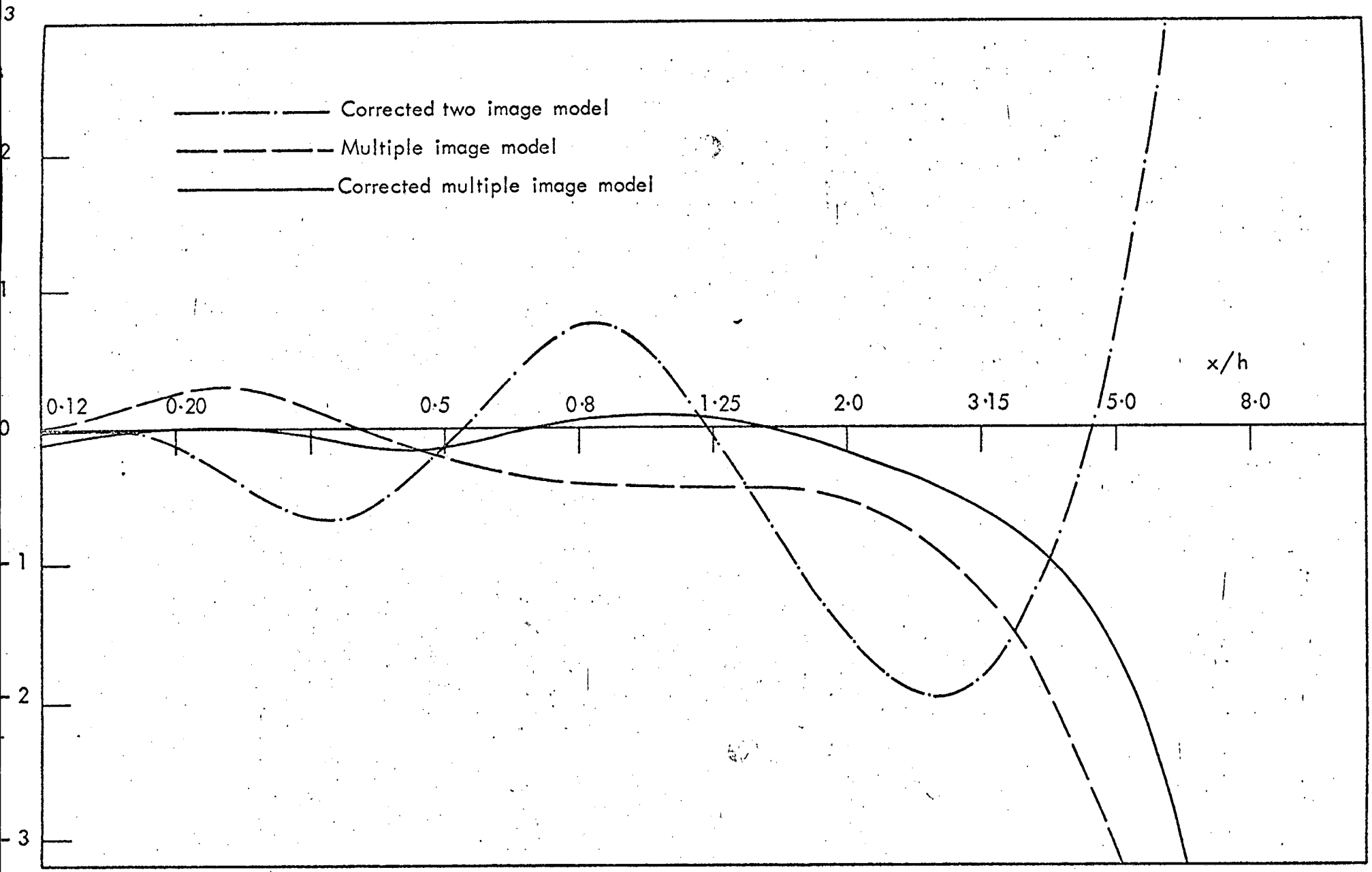

FIG. 3.9 MODULUS SQUARED OF RATIO, IN dB, OF MODE FIELD AND RAY FIELDS ON CENTRE-LINE FOR $\bar{Z}_{(\omega)} = (1{\cdot}0 - j\,1{\cdot}0)$ (5 MODES, POINT SOURCE)

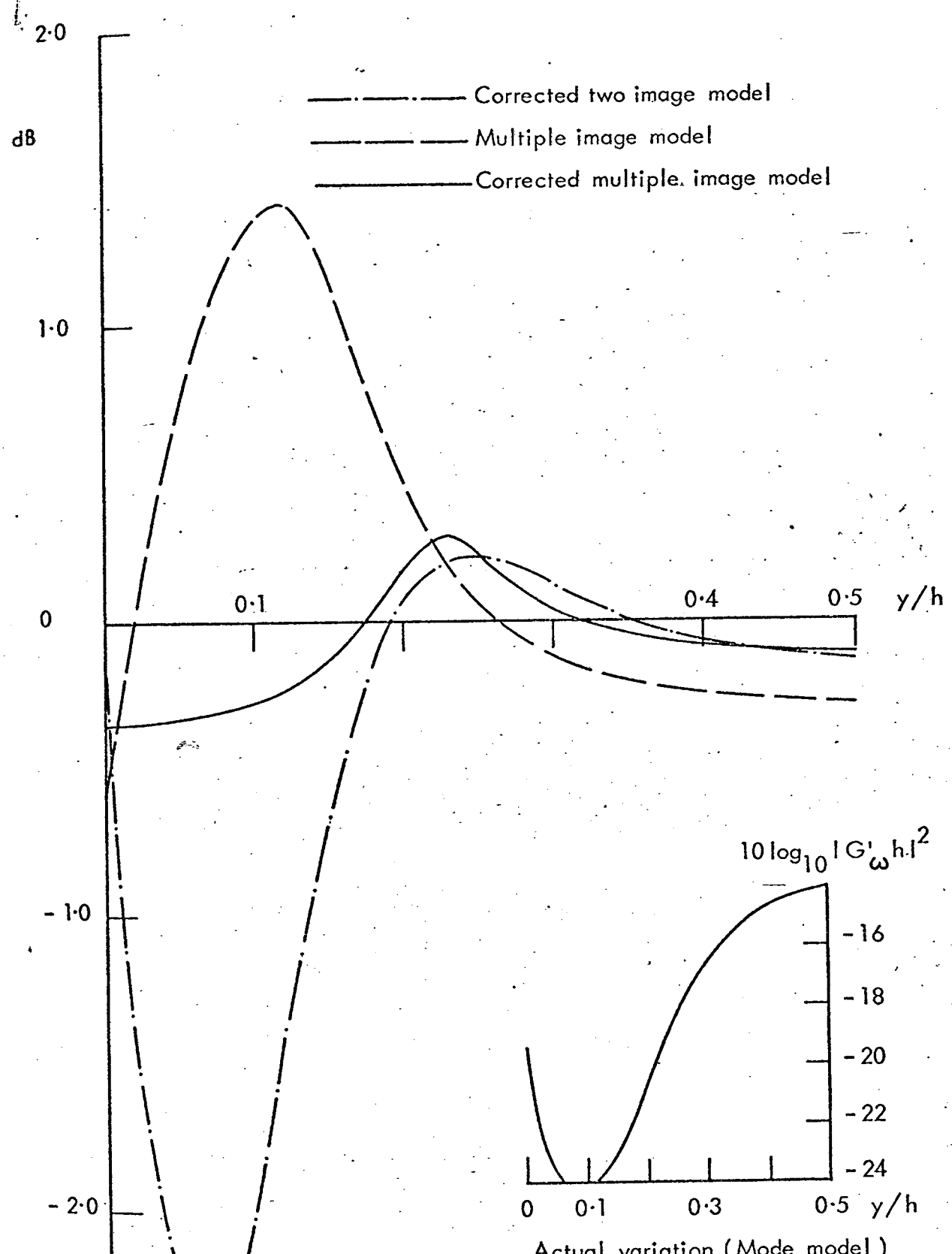

FIG. 3.10 MODULUS SQUARED OF RATIO, IN dB, OF MODE FIELD AND RAY FIELDS AT $x/h = 0{\cdot}5$ FOR $Z_\omega = (1{\cdot}0 - j1{\cdot}0)$ (5 MODES, POINT SOURCE)

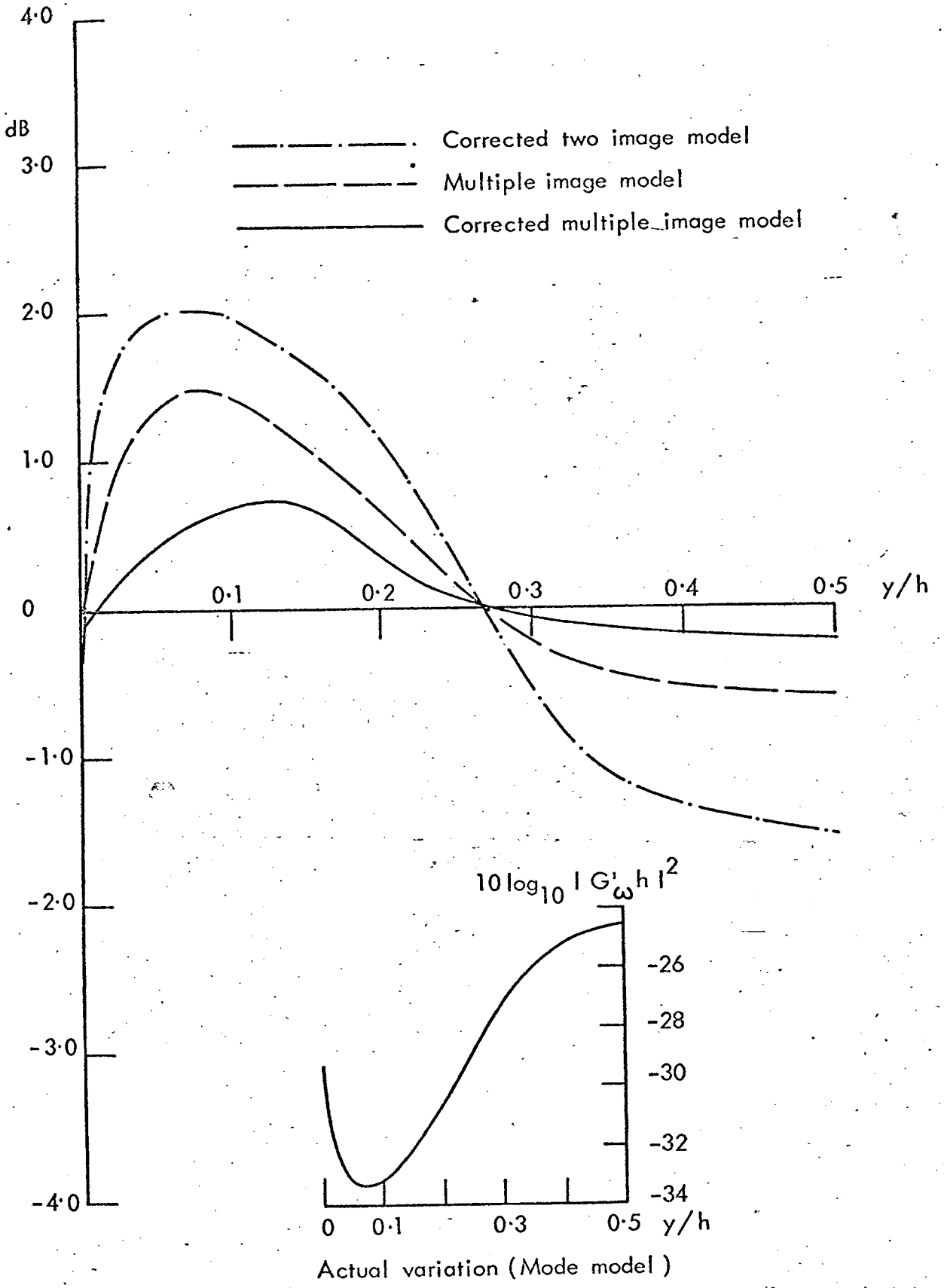

FIG. 3.11 MODULUS SQUARED OF RATIO, IN dB, OF MODE FIELD AND RAY FIELDS AT $x/h = 2{\cdot}0$ FOR $\bar{Z}_\omega = (1{\cdot}0 - j1{\cdot}0)$ (5 MODES, POINT SOURCE)

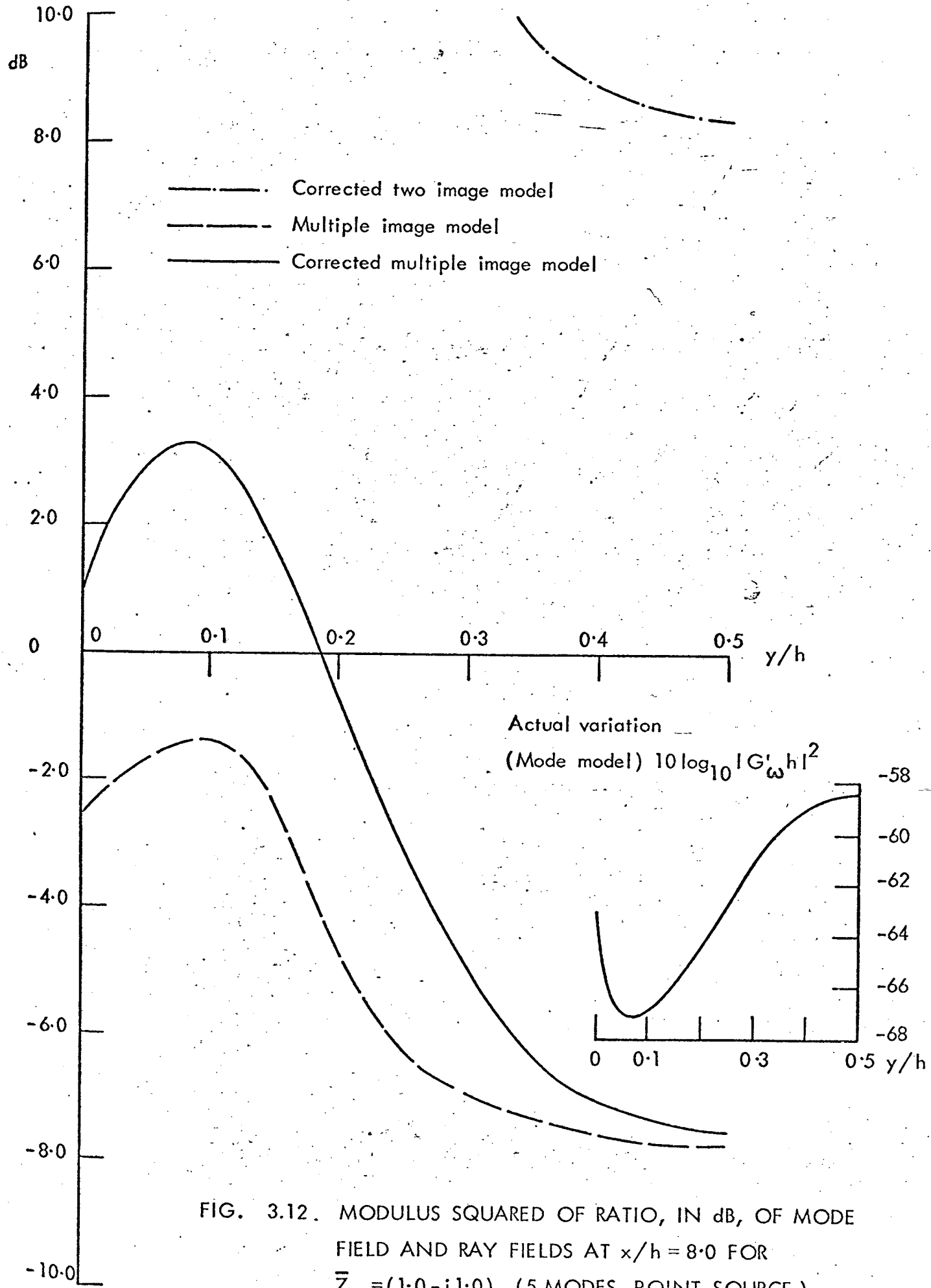

FIG. 3.12. MODULUS SQUARED OF RATIO, IN dB, OF MODE FIELD AND RAY FIELDS AT $x/h = 8{\cdot}0$ FOR $\bar{Z}_{..} = (1{\cdot}0 - i\,1{\cdot}0)$ (5 MODES, POINT SOURCE)

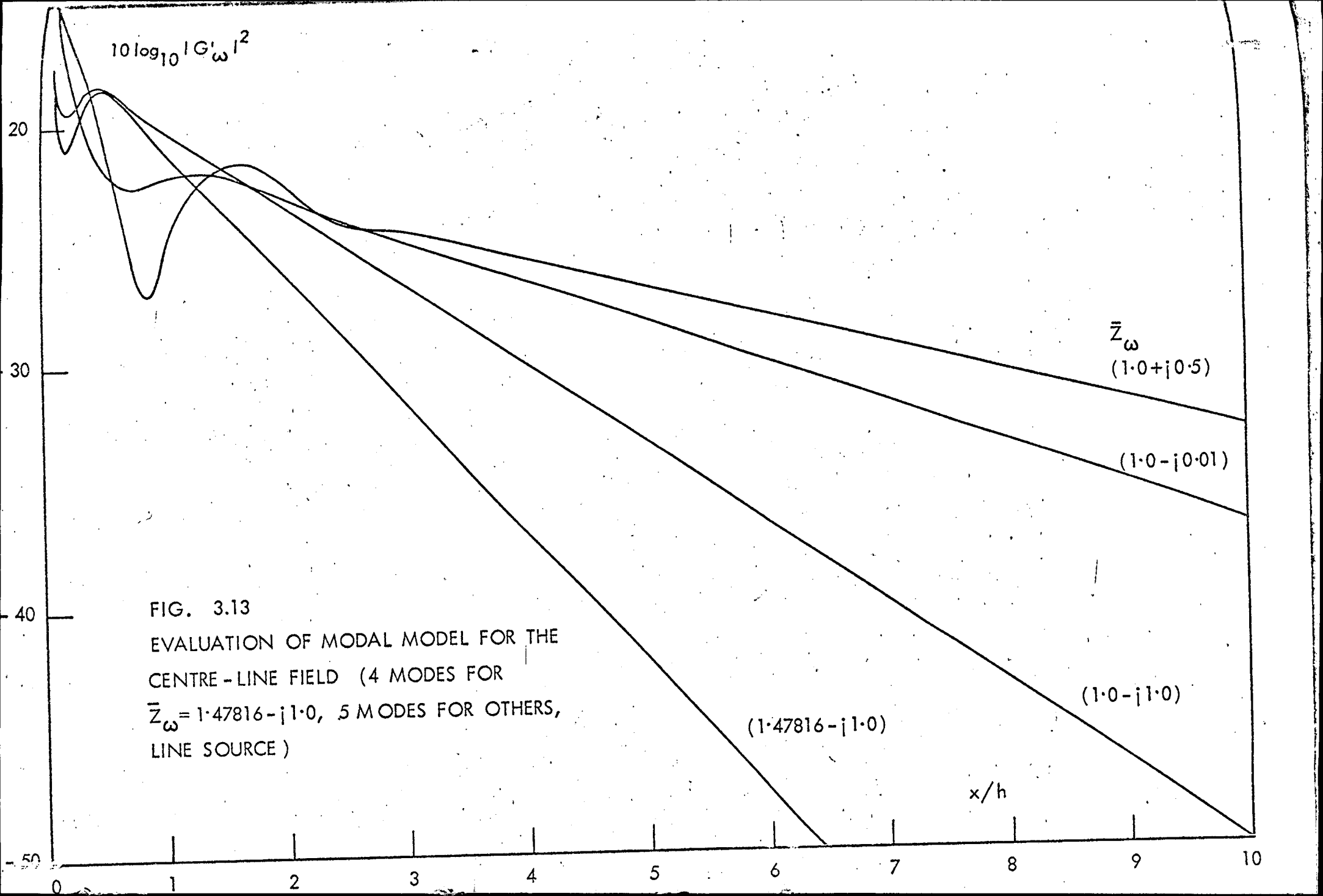

FIG. 3.13
EVALUATION OF MODAL MODEL FOR THE CENTRE-LINE FIELD (4 MODES FOR $\bar{Z}_\omega = 1{\cdot}47816 - j1{\cdot}0$, 5 MODES FOR OTHERS, LINE SOURCE)

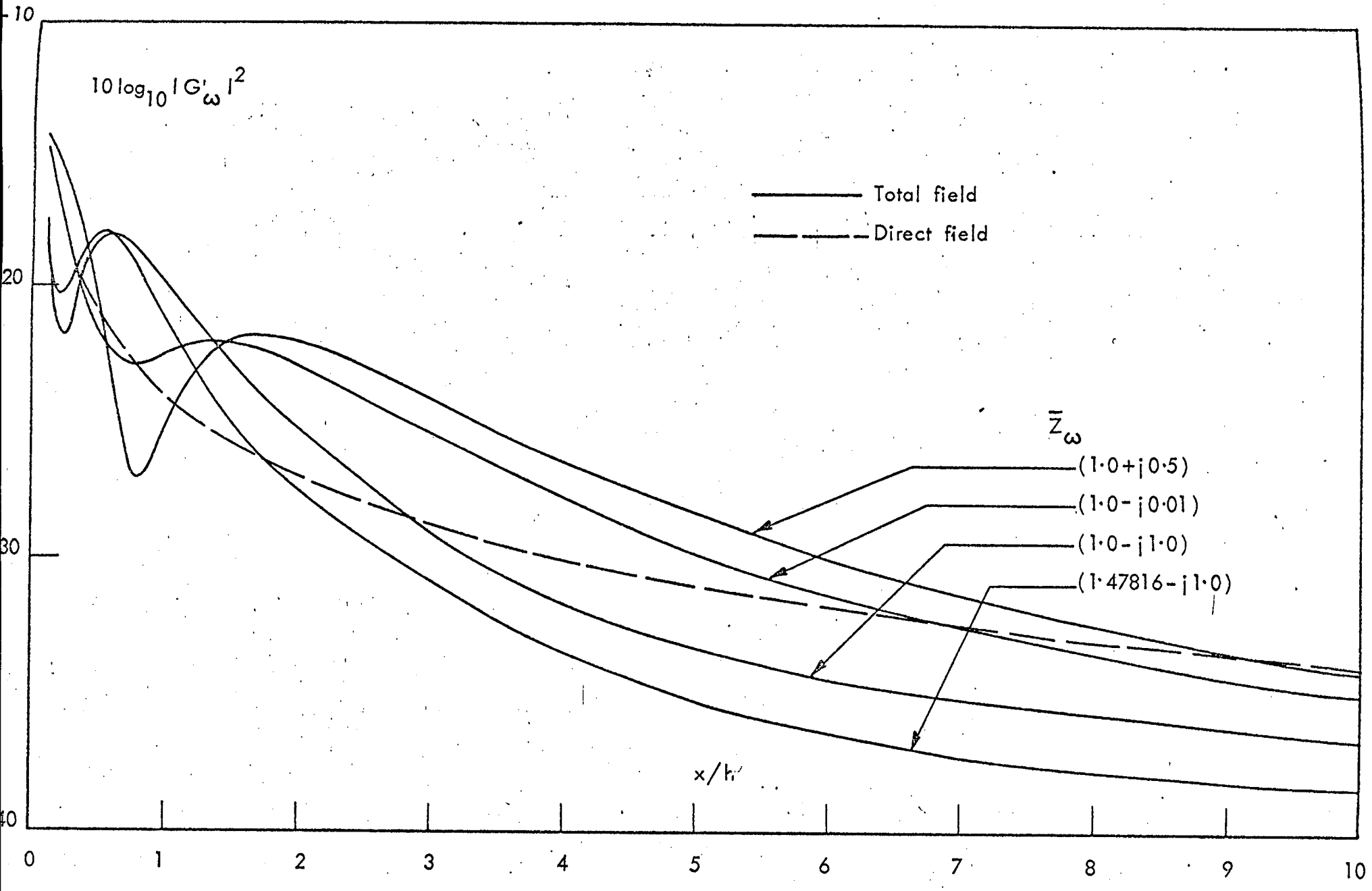

FIG. 3.14 EVALUATION OF TWO IMAGE RAY MODEL FOR THE CENTRE-LINE FIELD (ASYMPTOTIC HANKEL, LINE SOURCE).

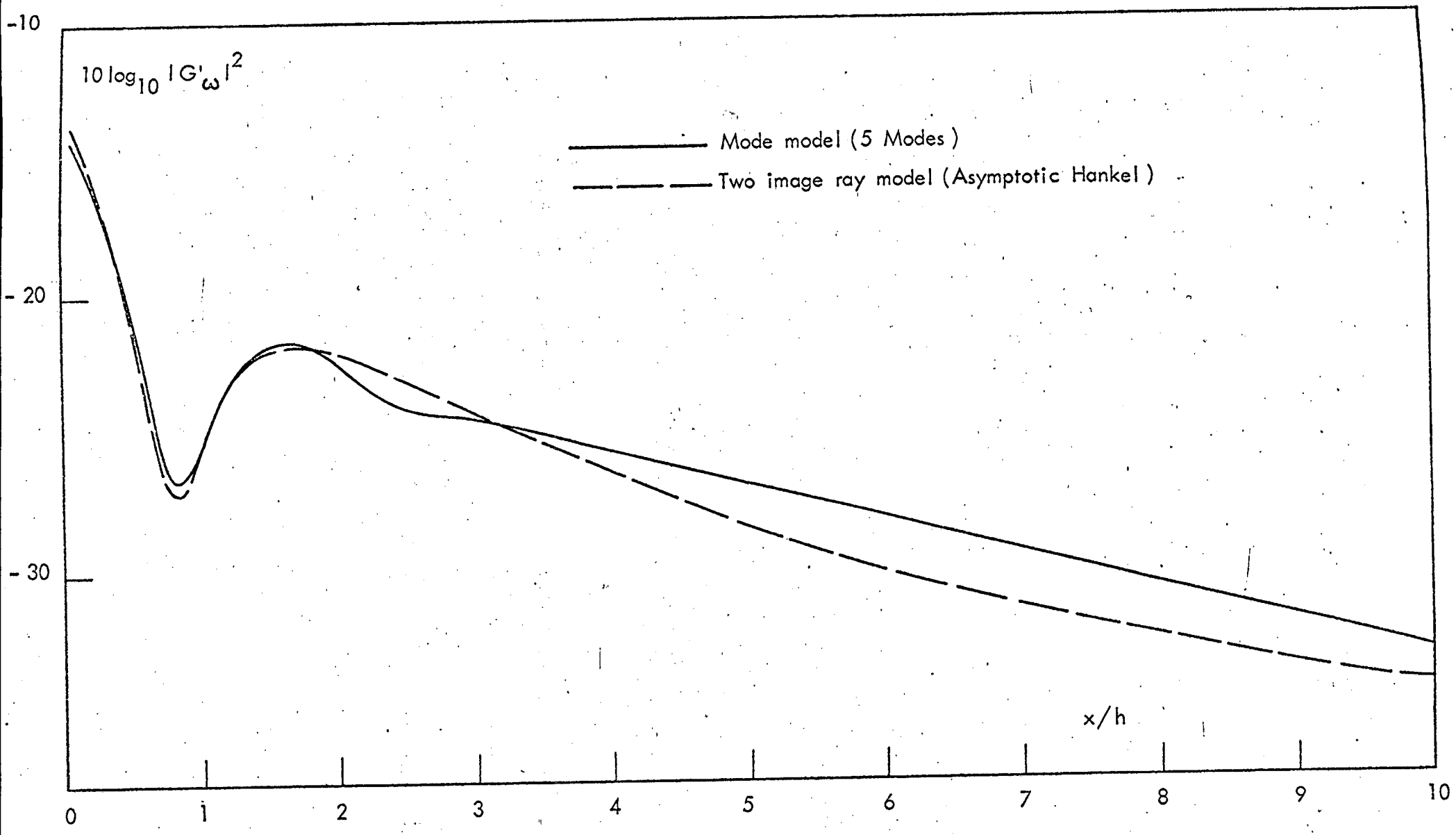

FIG. 3.15 CENTRE-LINE FIELD FOR $\bar{Z}_\omega = (1{\cdot}0 + j0{\cdot}5)$.

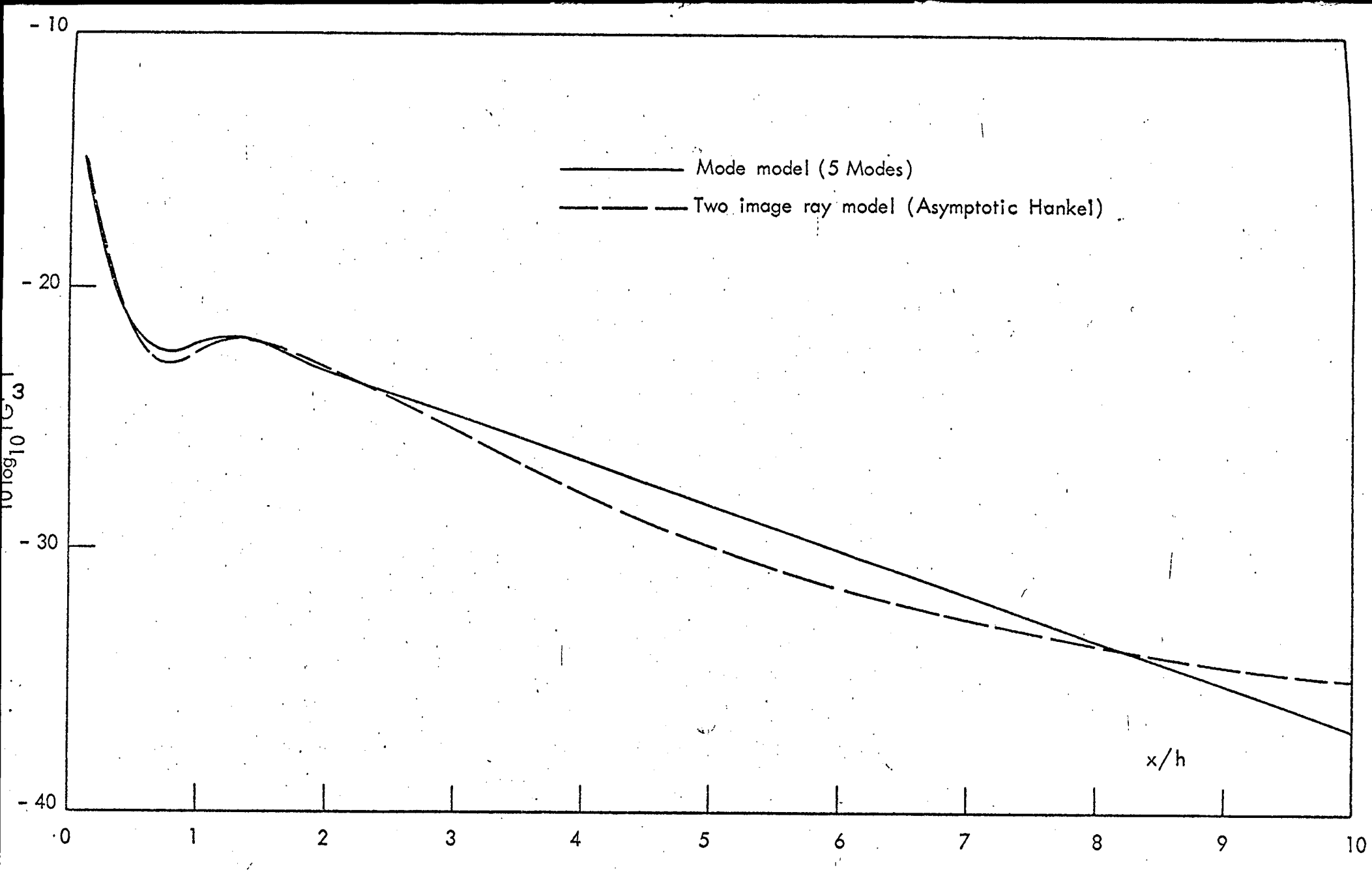

FIG. 3.16 CENTRE LINE FIELD FOR $\overline{Z}_\omega = (1{\cdot}0 - j0{\cdot}01)$.

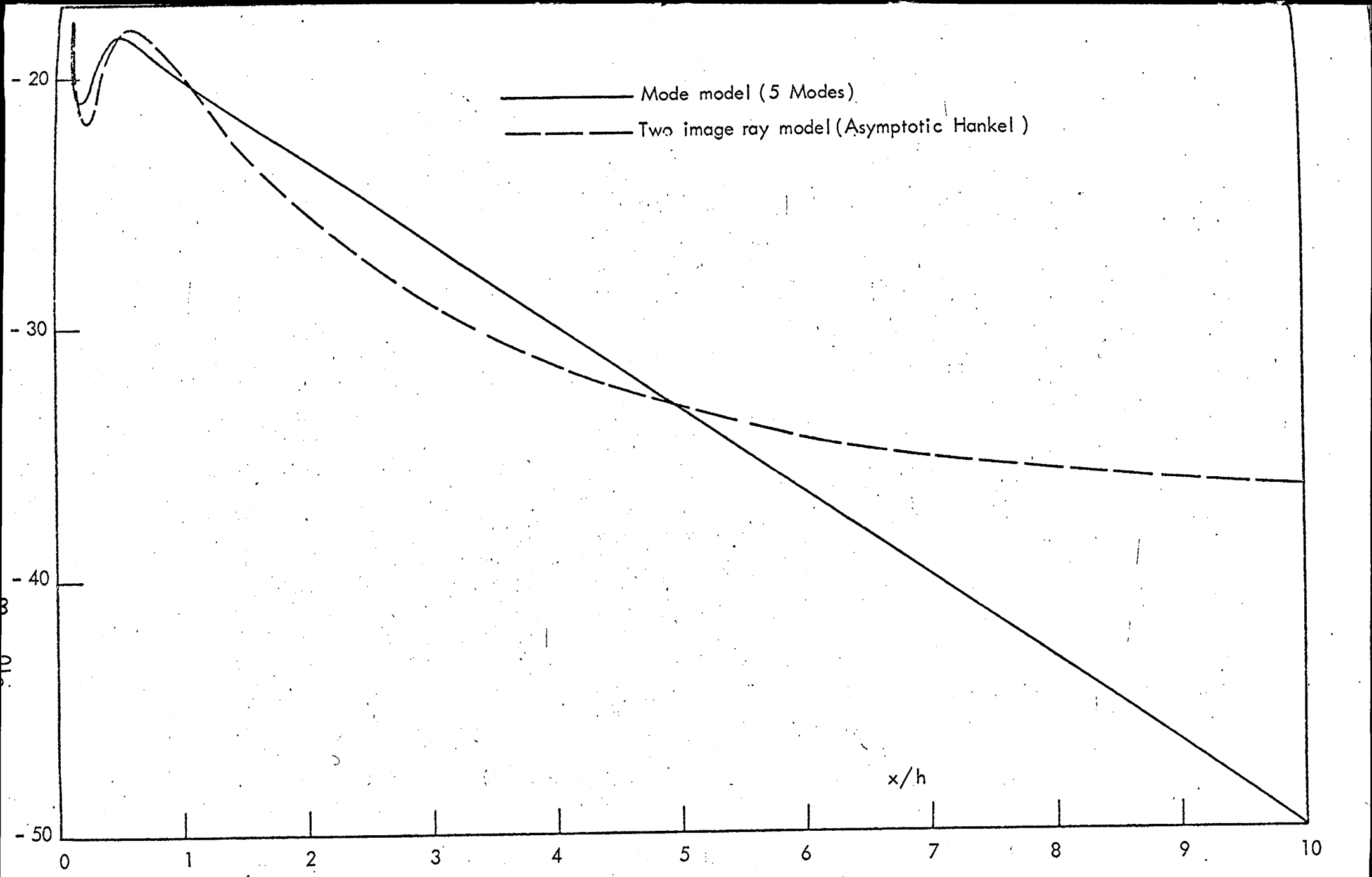

FIG. 3.17 CENTRE-LINE FIELD FOR $\bar{Z}_\omega = (1{\cdot}0 - j1{\cdot}0)$.

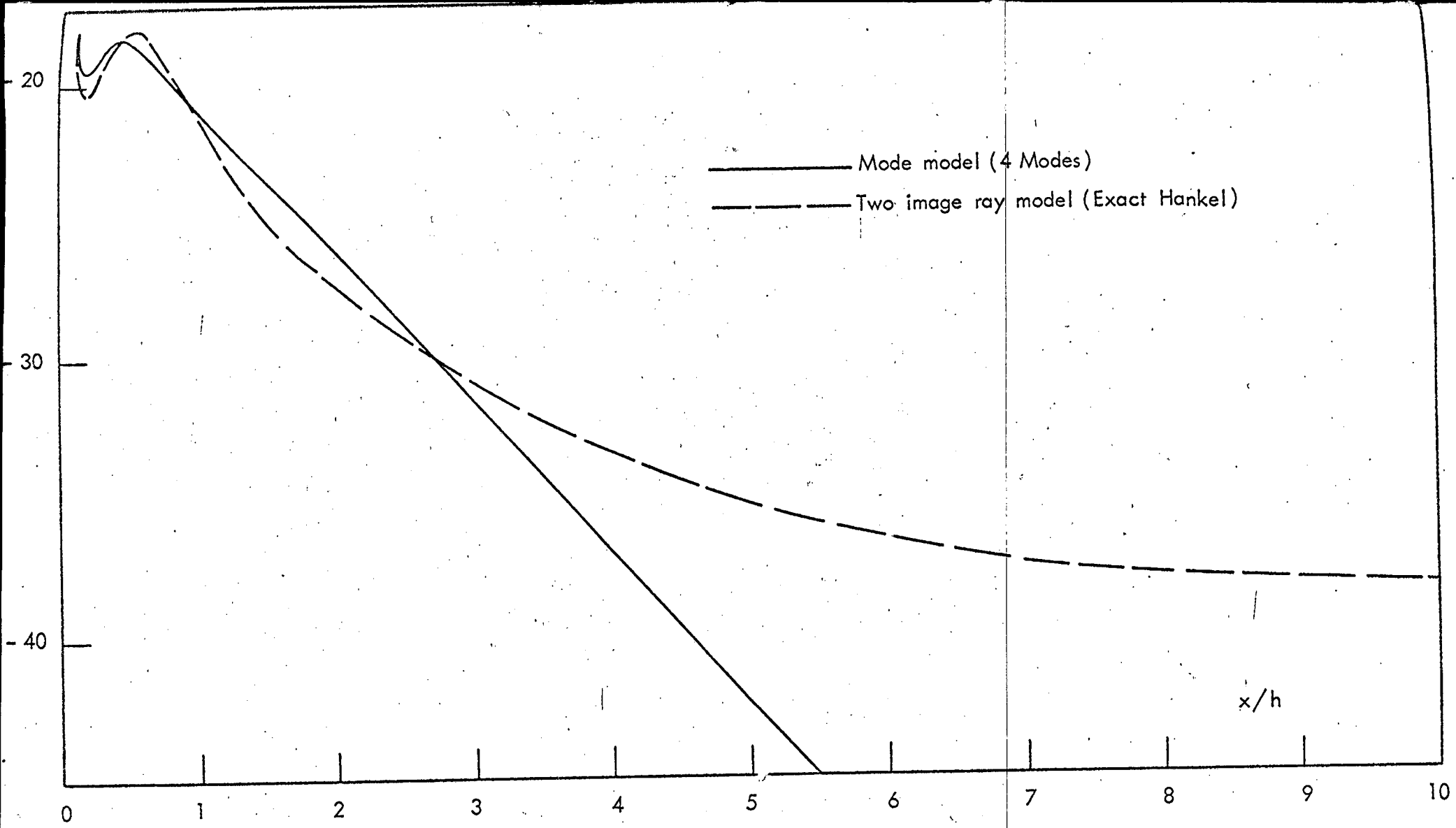

FIG. 3.18 CENTRE-LINE FIELD FOR $\bar{Z}_\omega = (1{\cdot}47816 - j\,1{\cdot}0)$

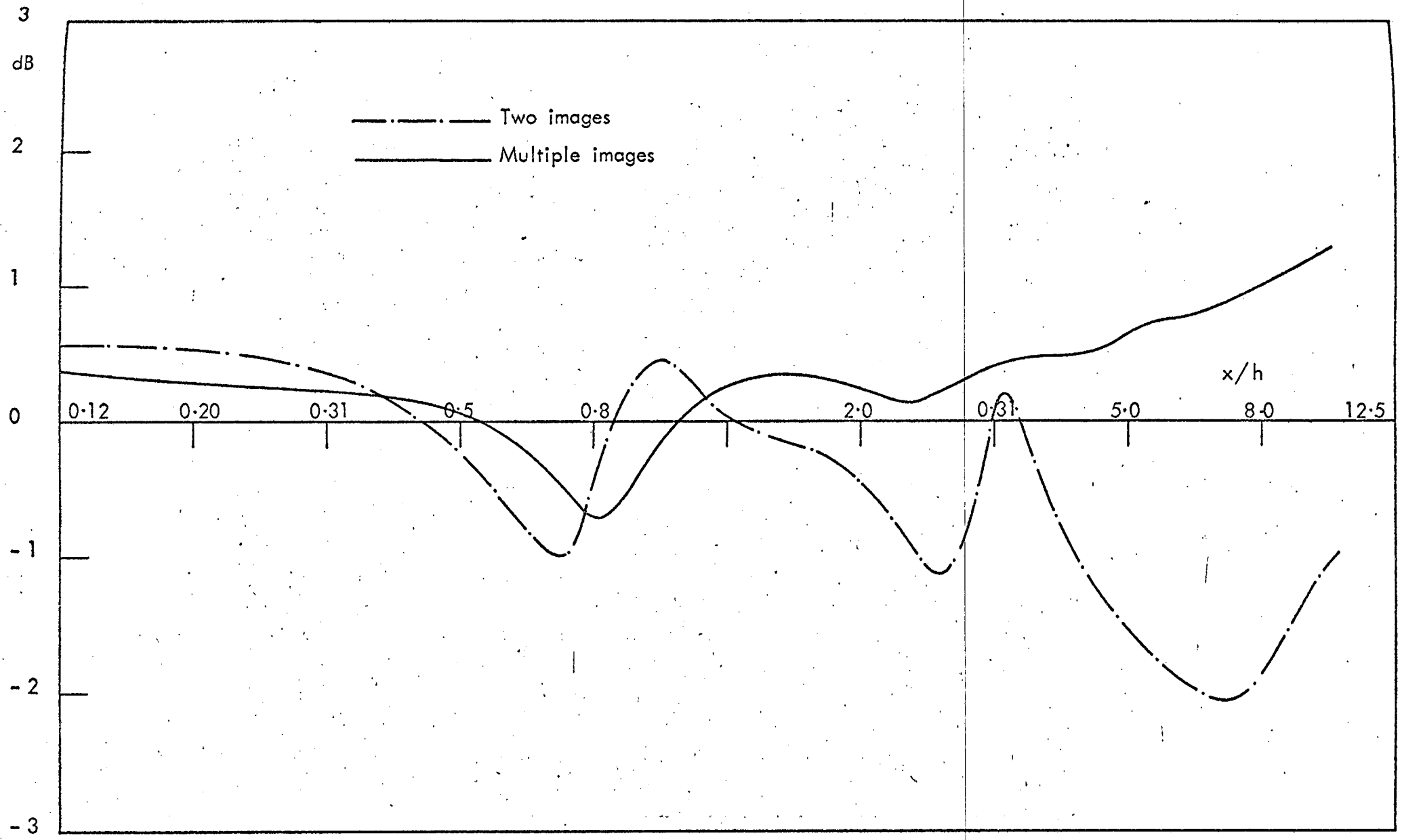

FIG. 3.19 MODULUS SQUARED OF RATIO, IN dB, OF MODE FIELD AND RAY FIELDS ON CENTRE-LINE FOR $\bar{Z}_\omega = (1{\cdot}0 + j0{\cdot}5)$ (5 MODES; ASYMPTOTIC HANKEL, LINE SOURCE).

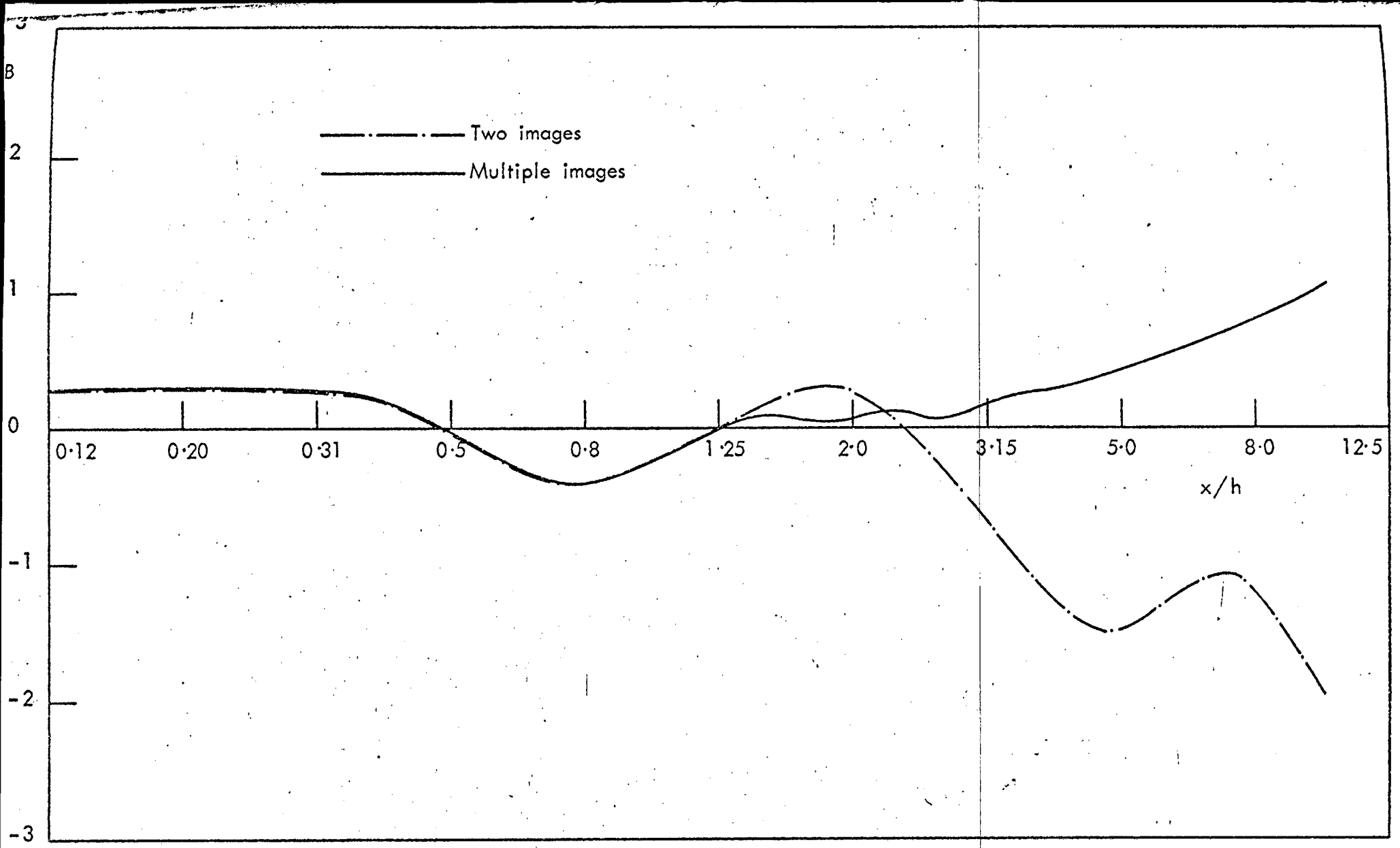

FIG. 3.20 MODULUS SQUARED OF RATIO, IN dB, OF MODE FIELD AND RAY FIELDS ON CENTRE-LINE FOR $\bar{Z}_\omega = (1{\cdot}0 - j0{\cdot}01)$ (5 MODES, ASYMPTOTIC HANKEL, LINE SOURCE).

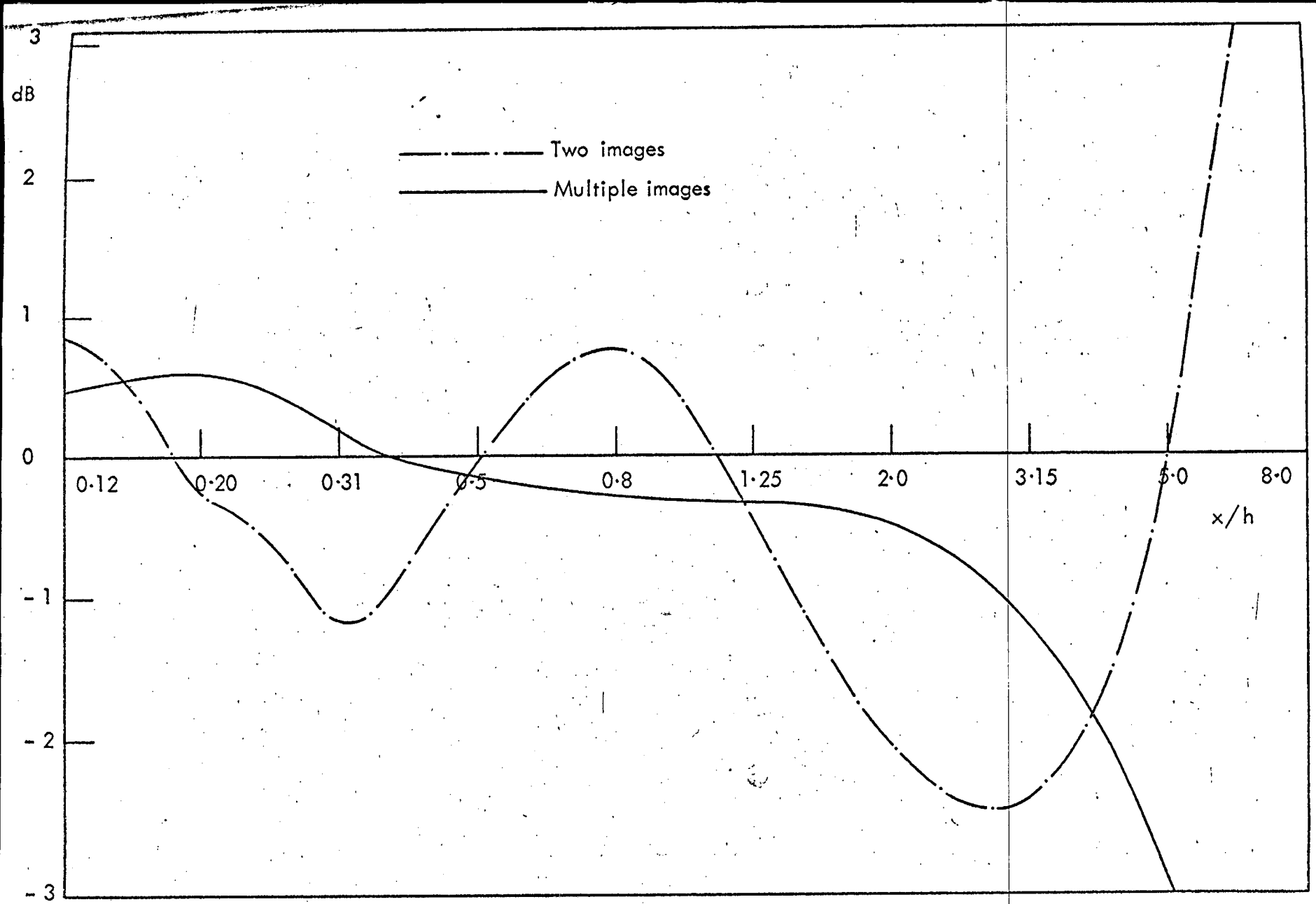

FIG. 3.21 MODULUS SQUARED OF RATIO, IN dB, OF MODE FIELD AND RAY FIELDS ON CENTRE-LINE FOR $\bar{Z}_\omega = (1{\cdot}0 - j1{\cdot}0)$ (5 MODES, ASYMPTOTIC HANKEL, LINE SOURCE).

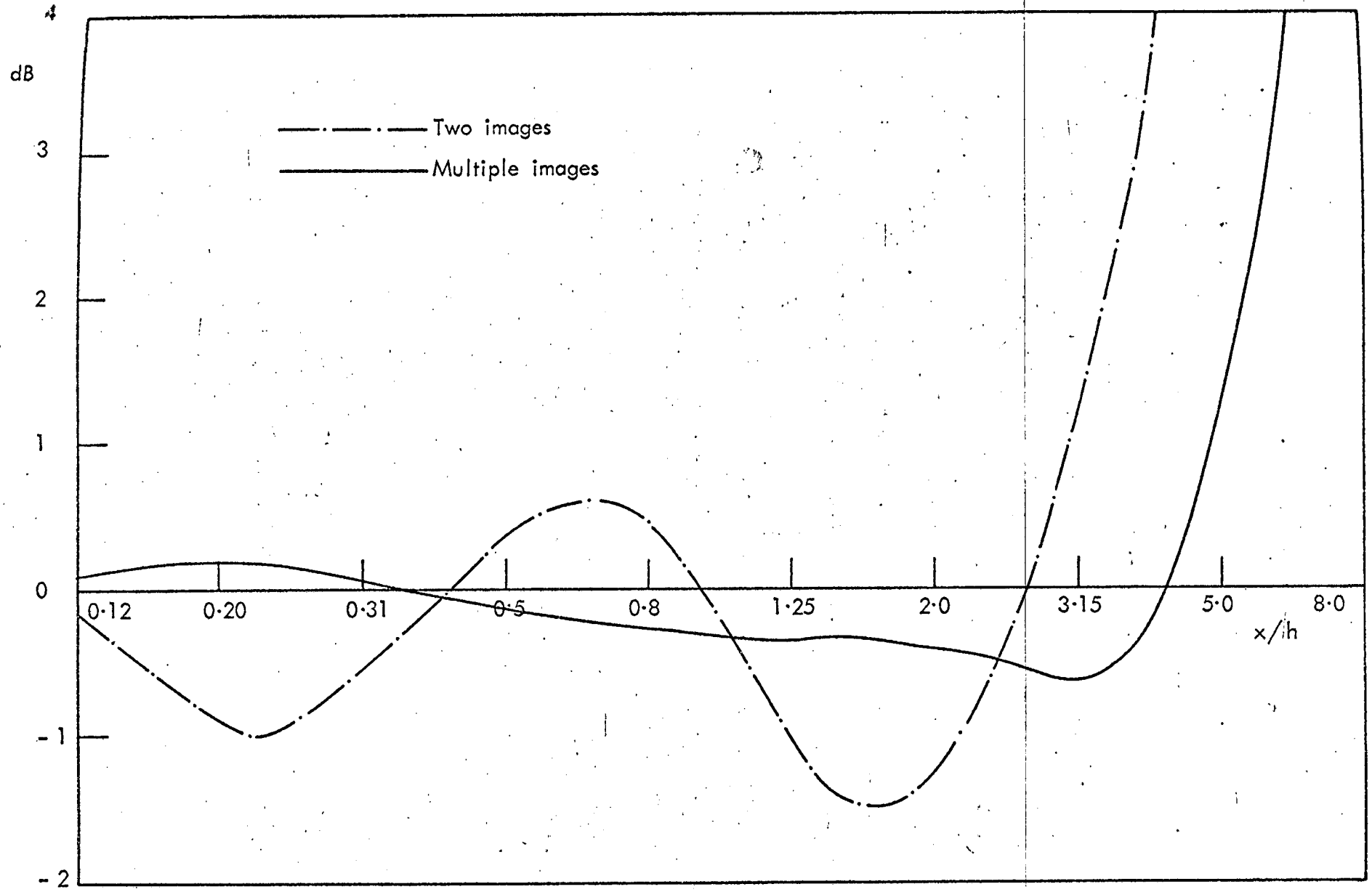

FIG. 3.22 MODULUS SQUARED OF RATIO, IN dB, OF MODE FIELD AND RAY FIELDS ON CENTRE-LINE FOR $\bar{Z}_\omega = (1{\cdot}47816 - j1{\cdot}0)$ (4 MODES, EXACT HANKEL, LINE SOURCE).

CHAPTER 4

THE PROPAGATION AND ATTENUATION OF SOUND IN LINED DUCTS CONTAINING UNIFORM OR 'PLUG' FLOW

4.1 Introduction

In Chapter 2 the line source Green's function has been obtained for an infinite, two-dimensional duct with locally-reacting boundaries in which the unperturbed fluid is at rest relative to the duct walls. Except where the parameter values (reduced frequency and wall admittance) give rise to the double pole condition, the Green's function could have been obtained by the standard method based on the orthogonal properties of the mode- or eigenfunctions*. This method can also be used for three-dimensional duct geometries (e.g. rectangular, circular or annular).

If the unperturbed fluid is not at rest but is in uniform motion relative to the duct walls, the mode functions are no longer orthogonal unless both walls have a zero admittance or impedance. The concept of uniform motion is discussed in section (4.2) and the Green's function for an infinite two-dimensional duct with rigid walls (zero admittance) is derived in section (4.3), using the standard method.

In an attempt to obtain the Green's function for a duct with an arbitrary locally-reacting admittance on one wall (so that the modes are non-orthogonal) the Lorentz type of transformation is applied to the inhomogeneous wave equation (following a suggestion by Morfey (39)) and the Brekhovskikh (20) method is used in exactly the same way as in Chapter 2. This work, described in section (4.4), is incomplete owing to difficulties encountered in establishing the convergence of an integral on a specified contour. Thus the validity of the new Green's function cannot be

---

*Although there may be other methods of dealing with the double pole or degenerate condition.

considered as established; but comparisons with a ray model constructed on the basis of knowledge gained in the work of Chapter 3 suggest that it is correct, at least for the parameter values used in the comparisons. It should be emphasised that the simplicity of the Lorentz-Brekhovskikh approach appears to rest on the absence of the third dimension: in contrast to the zero flow case the Green's function for three-dimensional geometries does not follow directly from the present result.

In section (4.5) the optimisation concepts of Chapter 2 are extended to include uniform flow and some of the results obtained therein are shown to be of practical use. Other results highlight the appearance of what will be referred to as 'strange' modes, defined as modes with phase velocities in the opposite direction to that of decay.

This type of mode can occur for any wall admittance (in uniform flow) and, indeed, even if both walls have a zero admittance or impedance; in these special cases the Lorentz phase velocity ($\omega/Re(k_x')$) which determines the direction of axial energy flow* (see Chapter 5) is either zero or positive in the decay direction. However a duct with a finite, but non-zero, wall admittance may have modes with Lorentz phase velocities in the opposite direction to that of decay and hence these 'strange' modes could be interpreted as amplifying modes. The origin of the 'strange' modes is described in section (4.6).

Finally, in section (4.7), it is recognised that an acoustic

---

*Throughout this chapter 'energy flow' is the integral over the duct width of the axial energy flux as defined by Cantrell and Hart (40).

line source, switched on at time $t = 0$, is capable of triggering instabilities that grow in time. These can be the compressible counterparts of the incompressible, modified Helmholtz instabilities that occur in uniform flow adjacent to a single non-rigid wall. The available information suggests that these instabilities are of the convective type and thus, for a particular example, a Green's function has been obtained in the limit at $t \to +\infty$, with the same time dependence as the source and in the form of the usual sum of spatially decaying modes plus a single mode with spatial amplification in the downstream direction. In the upstream direction the Green's function remains as a sum of spatially decaying modes. Both Green's functions differ from the one given in section (4.4), whose correctness depends on there being no instabilities present. The procedures outlined in section (4.7) also establish the true significance of the 'strange' modes.

4.2 Discussion and Definition of the 'Plug' Flow Model and the Associated Boundary Condition

A precise definition of 'plug' flow in a uniform duct is as follows: the steady constant motion of the duct fluid relative to the duct walls is in the axial direction only, that is parallel to the duct walls, at all points in the duct. The fluid velocity retains this constant value even at the duct walls: there is no boundary layer of slower moving fluid and the fluid is said to 'slip'. The boundary condition for the acoustic field in this uniform flow (see, for example, Morse and Ingard (14)), is that the ratio of its pressure and particle displacement normal to the wall must equal the ratio of the pressure and displacement, or the displacement impedance of the duct wall.

However, if it can be shown that the pressure and displacement are constant through a boundary layer of finite thickness which is introduced between the wall and uniform flow region, then the 'plug' flow acoustic boundary condition can also be used for more realistic duct flows. This aspect is considered in detail in Chapter 6.

For the purposes of the following sections this boundary condition needs to be expressed in terms of the ratio of the acoustic pressure gradient normal to the wall and the pressure there, and in terms of the ratio of the incident pressure field and the reflected field. To obtain these expressions explicitly it is necessary to consider the acoustic field to be composed of inhomogeneous or homogeneous waves with wavenumbers k_x, k_y where x, as before, is parallel to the wall and y is normal to it. The plug flow boundary condition is

$$\frac{p_\omega}{\xi_{y\omega}}\Big|_{wall} = Z_d$$

where $\xi_{y\omega}$ is the particle displacement normal to the wall and

$$p_w = -\rho\left[U_x \phi_x + \phi_t\right]$$

$$\frac{\partial p_w}{\partial y} = -\rho\left[U_x \phi_{xy} + \phi_{ty}\right]$$

$$\frac{k_x M_x}{k} = \frac{M^2 \omega}{\beta^2 \omega} M\alpha$$

$$= M^2/\beta^2$$

$$k_x = \alpha$$

$$k = \omega/c$$

$\bar{\beta}_w$ admittance at $y = 0$

$Z_{d\omega}$ is the wall displacement impedance. Alternatively, in terms of the usual admittance parameter β_ω (time dependence $\exp[-i\omega t]$),

$$\left.\frac{-i\omega\xi_{y_\omega}}{p_\omega}\right|_{wall} = \beta_\omega \, .$$

The fluid particle displacement is related to the normal velocity, v, by

$$v = \frac{D\xi_y}{Dt} \; ; \qquad \text{where} \quad \frac{D}{Dt} \equiv \left(\frac{\partial}{\partial t} + U_x \frac{\partial}{\partial x}\right)$$

or

$$v_\omega = (-i\omega + ik_x U_x)\xi_{y\omega} = \left(1 - \frac{k_x M_x}{k}\right)(-i\omega\xi_{y\omega})$$

where $M_x = U_x/c$.

Finally the normal velocity can be related to the normal pressure gradient by the y momentum equation

$$\rho_o \frac{Dv}{Dt} = - \frac{\partial p}{\partial y}$$

or

$$-i\omega\rho_o \left(1 - \frac{k_x M_x}{k}\right) v_\omega = - \frac{\partial p_\omega}{\partial y} \, ,$$

to obtain the required expression

$$\frac{dp_\omega}{dy} = ik\bar{\beta}_\omega \left(1 - \frac{k_x M_x}{k}\right)^2 . p_\omega . \qquad (4.2.1)$$

The effect of plug flow on the boundary condition is to introduce a factor $\left(1 - \frac{k_x M_x}{k}\right)^2$.

Notice that if k_x/k is a large imaginary number such that $|k_x/k| >> M_x^{-1}$ then

$$\frac{dp_\omega}{dy} \doteq ik \left(-\bar{\beta}_\omega\right) \left\{Im\left(\frac{k_x}{k}\right) M_x\right\}^2 p_\omega$$

and the effective admittance appears to have a negative real part

(the sign of the imaginary part of the effective admittance being opposite to that of the wall admittance).

The plane wave reflection coefficient can be obtained directly from equation (4.2.1): when the incident plane wave amplitude at the wall (say at $y = 0$) is denoted as p_i and the reflected as p_r then

$$p_\omega = p_i \exp[ik_x x + ik_y y] + p_r \exp[ik_x x - ik_y y],$$

$$\frac{dp_\omega}{dy} = ik_y\{p_i \exp(ik_x x + ik_y y) - p_r \exp(ik_x x + ik_y y)\}$$

$$= ik\bar{\beta}_\omega(1 - \frac{k_x M_x}{k})^2 . p_\omega,$$

by equation (4.2.1), and thus, where C_r is defined as p_r/p_i,

$$C_r = \frac{k_y/k - \bar{\beta}_\omega(1 - k_x M_x/k)^2}{k_y/k + \bar{\beta}_\omega(1 - k_x M_x/k)^2}$$

or

$$C_r = \frac{\cos\theta - \bar{\beta}_\omega(1 - M_x \sin\theta)^2}{\cos\theta + \bar{\beta}_\omega(1 - M_x \sin\theta)^2} \qquad (4.2.2)$$

where $\cos\theta = k_y/k$, $\sin\theta = k_x/k$.

Equation (4.2.1) is to be used in the direct modal approach discussed in section (4.3), and equation (4.2.2) in the attempt to derive the Green's function for a lined duct in section (4.4).

4.3 The Lorentz Transformation and the Green's function for a Duct with Rigid Walls

As the zero flow duct has been analysed already in Chapter 2, clearly there are advantages in reducing the wave equation for uniform flow to a form identical to that for zero flow, taking due care with the boundary conditions. This can be done for the Green's function wave equation by using the Lorentz type of transformation and, here, this will be performed on the basic time dependent wave equation,

$$\left(\frac{\partial^2}{\partial x^2} + \frac{\partial^2}{\partial y^2}\right)G - \frac{1}{c^2}\frac{D^2G}{Dt^2} = -\delta(x - \bar{x}_0)\delta(y - y_0)\, q(t), \qquad (4.3.1)$$

where $q(t)$ is the time dependence of the line source at $(\bar{x}_0, y_0)$. For the uniform flow region the coordinates are transformed as follows:

$$x' = \gamma^2 x \qquad y' = \gamma y \qquad t' = t + \gamma^2 \frac{M_x}{c}(x - \bar{x}_0);$$

$$\gamma = (1 - M_x^2)^{-\frac{1}{2}}$$

so that

$$\frac{\partial}{\partial x} = \gamma^2 \frac{\partial}{\partial x'} + \gamma^2 \frac{M_x}{c}\frac{\partial}{\partial t'}; \qquad \frac{\partial}{\partial y} = \gamma\frac{\partial}{\partial y'}; \qquad \frac{\partial}{\partial t} = \frac{\partial}{\partial t'}$$

and equation (4.3.1) becomes

$$\frac{\partial^2 G}{\partial x'^2} + \frac{\partial^2 G}{\partial y'^2} - \frac{1}{c^2}\frac{\partial^2 G}{\partial t'^2} = -\gamma\,\delta(x' - \bar{x}_0')\delta(y' - y_0')\, q(t'). \qquad (4.3.2)$$

Now the usual harmonic time dependence can be assumed in the form

$$q(t') = \exp\,[-i\omega t']$$

and the Fourier (time) transform of equation (4.3.2) is

$$\frac{\partial^2 G_{\omega'}}{\partial x'^2} + \frac{\partial^2 G_{\omega'}}{\partial y'^2} + \left(\frac{\omega'}{c}\right)^2 G_{\omega'} = -\gamma\,\delta(x' - \bar{x}_0')\delta(y' - y_0')\delta(\omega' - \omega). \qquad (4.3.3)$$

Equation (4.3.3) is identical to the wave equation for the Green's function used in the zero flow case, apart from the factor $\gamma = (1 - M^2)^{-\frac{1}{2}}$, multiplying the source function, and of course the $\delta(\omega' - \omega)$ factor which was implicitly assumed before. It remains to transform the boundary conditions: the differential relations for these are

$$v = \gamma^2 \{\frac{\partial}{\partial t'} + U_x \frac{\partial}{\partial x'}\} \xi_y$$

or

$$v_\omega = \gamma^2 (1 - \frac{k'M_x}{k'}) (-i\omega' \xi_{y\omega'}),$$

(where it has been assumed that the x dependence of these quantities is $\exp[ik'_x x']$), and

$$\gamma \rho_o (\frac{\partial}{\partial t'} + U_x \frac{\partial}{\partial x'}) v = - \frac{\partial p}{\partial y'}$$

or

$$-i\omega' \rho_o \gamma^2 (1 - \frac{k'M_x}{k'}) v_\omega = - \frac{dp_{\omega'}}{dy'} .$$

It follows that

$$\frac{dp_{\omega'}}{dy'} = ik' \bar{\beta}_{\omega'} (1 - \frac{k'M_x}{k'})^2 \gamma^3 p_{\omega'} \qquad (4.3.4)$$

is the modified admittance relationship and the reflection coefficient is now

$$C'_r = \frac{\cos\theta' - \bar{\beta}_{\omega'} \gamma^3 (1 - M_x \sin\theta')^2}{\cos\theta' + \bar{\beta}_{\omega'} \gamma^3 (1 - M_x \sin\theta')^2}, \qquad (4.3.5)$$

where $\cos\theta' = k'_y/k'$, $\sin\theta' = k'_x/k'$ and where it has been assumed that the y dependence is of the form $\exp[\pm ik'_y y']$. These boundary conditions are to be applied at $y' = 0$ and at $y' = h' = \gamma h$.

The solution for $G'_{\omega'}$ can be obtained immediately by expanding

$G'_{\omega'}$ into an infinite series of eigenfunctions:

$$G'_{\omega'} = \sum_{n=0}^{\infty} F_n(x')\psi_n(y').$$

If the functions $\psi_n(y')$ are taken to be solutions of the homogeneous form of equation (4.3.3)

$$\frac{d^2\psi_n}{dy'^2} + (k'^2 - k'^2_{xn})\psi_n = 0,$$

each function satisfying the boundary conditions (see equation (4.3.4))

$$\frac{d\psi_n}{dy'} = ik'\bar{\beta}_{\omega'}(1 - \frac{k'_{xn}M_x}{k'})^2\gamma^3\psi_n \quad \text{at} \quad y' = h',$$

$$\frac{d\psi_n}{dy'} = 0 \quad \text{at} \quad y' = 0,$$

then equation (2.2.6) shows that these functions are not orthogonal:

$$(k'^2_{xm} - k'^2_{xn})\int_0^{h'} \psi_m\psi_n dy' = \left[\psi_m \frac{d\psi_n}{dy'} - \psi_n \frac{d\psi_m}{dy'}\right]_0^{h'}$$

$$= \psi_m(h')\psi_n(h')\, ik'\bar{\beta}_{\omega'}\gamma^3\left[(1 - \frac{k'_{xn}M_x}{k'})^2 - (1 - \frac{k'_{xm}M_x}{k'})^2\right].$$

The right hand side does not equal zero unless $\bar{\beta}_{\omega'} = 0$ or $\bar{Z}_{\omega'} = 0$*.

For the case of a rigid walled duct ($\bar{\beta}_{\omega'} = 0$) the Green's function is, by virtue of equation (2.2.4),

$$G'_{\omega'}(x', y'/\bar{x}'_o, y'_o) = \delta(\omega' - \omega)\frac{\gamma i}{2h'}\sum_{n=0}^{\infty}\frac{\psi_n(y')\psi_n(y'_o)}{\Lambda_n k'_{xn}}\exp[ik'_{xn}|x' - \bar{x}'_o|]. \tag{4.3.6}$$

(For a non-zero admittance at $y' = 0$ and/or at $y' = h'$ the Green's function cannot be obtained directly in terms of the functions $\psi_n(y')$.) Note, that in this case

---

*Then $\psi_m = \psi_n = 0$ at $y' = h'$.

$$\Lambda_n' = \frac{1}{h'} \int_0^{h'} \psi_n^2(y')dy'$$

and the appropriate eigenfunction is

$$\psi_n(y') = \cos(k'_{yn}y'), \qquad k'_{xn} = + \sqrt{(\omega'/c)^2 - (k'_{yn})^2},$$

$$k'_{yn}h' = n\pi.$$

Inversion with respect to the Fourier time transformation and returning to the original coordinates gives

$$G'_\omega(x, y/\bar{x}_o, y_o) = \frac{i}{2h} \sum_{n=0}^{\infty} \frac{\cos(k'_{ym}\gamma y)\cos(k'_{yn}\gamma y_o)}{k'_{xn}\Lambda'_n} \exp[ik'_{xn}|x - \bar{x}_o|\gamma^2]$$

$$\exp[-i\omega\{t + \gamma^2 \frac{M_x}{c}(x - \bar{x}_o)\}]$$

or

$$G'_\omega(x, y/\bar{x}_o, y_o) = \frac{i}{2h} \sum_{n=0}^{\infty} \frac{\cos(k_{yn}y)\cos(k_{yn}y_o)}{k'_{xn}\Lambda_n} \exp[ik_{xn}|x - \bar{x}_o| - i\omega t] \qquad (4.3.7)$$

where $k_{yn} = \gamma k'_{yn}$, $\Lambda_n = \Lambda'_n$,

and

$$k_{xn} = \frac{-sgn(x - \bar{x}_o)kM_x + \sqrt{k^2 - k_{yn}^2(1 - M_x^2)}}{(1 - M_x^2)} \qquad (4.3.8)$$ *

Equation (4.3.8) is the familiar relationship between wavenumbers that would have been obtained by applying the same approach directly to the original equation (4.3.1) without utilising the Lorentz transformation. However, because this transformation yields a wave equation which is identical in form to that for zero flow, a possibly arguable assumption has been glossed over in obtaining the solution (4.3.6) to

---

*If the $x - x_o$ dependence is written as $\exp[ik_{xn}(x - \bar{x}_o)]$ then

$$k_{xn} = \{-kM_x + sgn(x - \bar{x}_o)\sqrt{k^2 - k_{yn}^2(1 - M_x^2)}\}/(1 - M_x^2).$$

equation (4.3.3).

This assumption concerns the choice of signs in the solution for the x dependence of the modal solution, which satisfies the equation

$$\frac{d^2F_n(x')}{dx'^2} + (k'^2 - k_{yn}'^2)F_n(x') = -\gamma\psi_n(y_o') \frac{\delta(x' - \bar{x}_o')\delta(\omega' - \omega)}{k'\Lambda_n'}$$

but for clarity the original form of this equation will be used, that is,

$$(1 - M_x^2) \frac{d^2F_n(x)}{dx^2} + 2ik'M_x \frac{dF_n(x)}{dx} + (k'^2 - k_{yn}^2)F_n(x)$$

$$= \frac{-\psi_n(y_o)\delta(x - \bar{x}_o)\delta(\omega' - \omega)}{h\Lambda_n} \qquad (4.3.9)$$

Clearly the solution of this equation is of the form $(x \neq \bar{x}_o)$

$$F_n(x) = A_n \exp[i(x - \bar{x}_o)(-k'M_x \pm \sqrt{k'^2 - k_{yn}^2(1 - M_x^2)})/(1 - M_x^2)] \qquad (4.3.10)$$

where A_n is a constant.

In the zero flow case $(M_x = 0)$ the solution with the + sign is taken for $x - \bar{x}_o > 0$ and the solution with the minus sign for $x - \bar{x}_o < 0$*; as the solutions are identical apart from the change

---

* As k_{yn} is real (in this rigid wall case) this statement can be taken quite literally if $k_{yn} < k'$. If $k_{yn} > k'$ then it appears that a second choice of sign is called for because, for $x - \bar{x}_o > 0$, say,

$$k_{xn} = + \sqrt{k'^2 - k_{yn}^2} = \pm i(+ \sqrt{k_{yn}^2 - k'^2}).$$

This difficult can be avoided by assuming the duct fluid to be slightly dissipative; then both k' and k_{yn} have small imaginary parts such that, for $k' > k_{yn}$, k_{xn} has a small imaginary part. When $k_{yn} > k'$ "taking the positive or negative sign" is defined as taking the same sign of the imaginary part as appears when $k_{yn} < k'$. Thus the solutions are confined to the same branch of the function $\sqrt{k'^2 - k_{yn}^2}$, irrespective of the relative values of k' and k_{yn}. Of course the imaginary parts of k' and k_{yn} can be set to zero once the choice of sign has been made.

in sign the solution can be written as

$$F_n(x) = A_n \exp[ik_{xn}|x - \bar{x}_o|] \quad \text{where} \quad k_{xn} = + \sqrt{k'^2 - k_{yn}^2}.$$

This expression is then substituted into equation (4.3.9) (with $M_x = 0$) to determine A_n. When the Lorentz transformation is used, of course this procedure is effectively repeated and thus, for example, the solution for $x - \bar{x}_o > 0$ is

$$F_n(x) = A_n \exp[i(x - \bar{x}_o)(-k'M_x + \sqrt{k'^2 - k_{yn}^2(1 - M_x^2)})\gamma(1 - M_x^2)].$$

Superficially the reason for the choice of the sign for the square root in the solutions for zero flow can be said to be based on the requirement that outgoing waves (that is waves with a phase velocity (ω/k_x) directed away from the source) should exist in the duct between the source and the 'termination' at $|x - \bar{x}_o| = \infty$. Applying this boundary or radiation condition to the uniform flow solution does not necessarily determine which square root sign is to be used because of the extra factor $-k'M_x/(1 - M_x^2)$. In fact this type of radiation condition must be rejected on the grounds that it can lead to solutions that grow with x when $k' < k_{yn}(1 - M_x^2)^{\frac{1}{2}}$. There can be no reason for this occurrence: even if it were to be argued that this plug flow model has, in general, unrealistic boundary conditions it is difficult to see why this particular boundary condition of zero normal particle displacement and normal velocity should lead to 'growing modes'.

If, instead of the phase velocity radiation condition, it is argued that the Causality Law should be satisfied, a transient analysis must precede the above 'steady state' analysis. Such an analysis has been carried out by Eversman (41), for identical conditions, but with

the line source replaced by the requirement that the harmonic acoustic field be uniform (in $0 \leq y \leq h$) at $x = \bar{x}_o$. Eversman (41) claims to have shown that as $t \to \infty$ modes with negative phase velocities exist for $(x - \bar{x}_o) > 0$, that is: 'incoming' waves can exist as part of the steady state solution.

If the phase velocity radiation condition used for zero flow is viewed as a requirement that there should be an outward flow of energy from the source (in both directions), then the generalisation to uniform mean flow follows from Chapter 5: the direction of the modal energy flow in uniform mean flow is given by the sign of the factor

$$\mathrm{Re}\{\sqrt{k'^2 - k_{yn}^2(1 - M_x^2)}\} = \mathrm{Re}(k'_{xn})$$

and not $\mathrm{Re}(k_{xn})$.

The energy generalisation is used here to justify the 'continuation' from the zero flow case whereby the (downstream and upstream) mode solutions are chosen according to the sign of $\mathrm{Re}(k'_{xn})$. It is also interesting to note that the factor $-k'M_x/(1 - M_x^2)$ which causes this difficulty is completely independent of the particular mode solutions.

For completeness the constant A_n is determined by integrating equation (4.3.9) from $\bar{x}_o - \alpha$ to $\bar{x}_o + \alpha$ and then letting $\alpha \to 0$: the right hand side is simply $-\psi_n(y_o)/h\Lambda_n$ and the left hand side is

$$(1 - M_x^2)\left[\frac{dF_n(x)}{dx}\right]_{\bar{x}_o-\alpha}^{\bar{x}_o+\alpha} + 2ik'M_x\left[F_n(x)\right]_{\bar{x}-\alpha}^{\bar{x}_o+\alpha} + (k'^2 - k_{yn}^2)\int_{\bar{x}_o-\alpha}^{\bar{x}_o+\alpha} F_n(x)dx.$$

The second and third terms are proportional to α as $\alpha \to 0$, leaving

$$\frac{dF_n(\bar{x}_o + \alpha)}{dx} - \frac{dF_n(\bar{x}_o - \alpha)}{dx} = - \frac{\psi_n(y_o)\delta(\omega' - \omega)}{h\Lambda_n(1 - M_x^2)}$$

or, as $\alpha \to 0$,

$$iA_n \left\{ \frac{-k'M + \sqrt{k'^2 - k_{yn}^2(1 - M_x^2)}}{(1 - M_x^2)} - \frac{-k'M - \sqrt{k'^2 - k_{yn}^2(1 - M_x^2)}}{(1 - M_x^2)} \right\}$$

$$= \frac{-\psi_n(y_o)\ \delta(\omega' - \omega)}{h\Lambda_n(1 - M_x^2)} :$$

that is,

$$A_n = \frac{i\psi_n(y_o)\delta(\omega - \omega')}{2k'_{xn}k\ \Lambda_n}$$

which agrees with equation (4.3.7) as it should.

Equation (4.3.7) is the Green's function for a rigid walled duct containing plug flow and has been obtained by utilising the orthogonal property of the eigenfunction solutions of the homogeneous wave equation. For soft walled ducts these eigenfunctions are no longer orthogonal and although it is presumably possible to orthogonalise them and then to continue using the standard method, in the next section Brekhovskikh's (20) analysis will be employed again, together with the Lorentz transformation, as a preferred alternative method of finding the Green's function.

4.4 An Attempt to Derive the Green's Function for a Duct with Non-rigid Walls

As the inhomogeneous wave equation for the Green's function with 'plug' flow has been reduced to a zero flow form, by using the Lorentz transformation, the proposed method of derivation is essentially identical to that given in section (2.3). The reason for referring to it as an attempted derivation is that the wall boundary condition differs in form from that for zero flow and this introduces a problem which has not been fully resolved. If a certain restrictive condition is imposed on the boundary condition then a valid Green's function can be obtained.

The analysis of section (2.3) can be utilised without complication up to the point where the following complete expression is obtained for the Green's function in a lined duct, with walls having reflection coefficients C_r' at $y' = h'$ and unity at $y' = 0$:

$$G_\omega'(x',y'/\bar{x}_o', y_o') = \gamma\delta(\omega' - \omega)\frac{i}{4\pi}\int_{-\infty}^{+\infty}\exp[iK_x'(x' - \bar{x}_o')]\sum_{\ell=0}^{\infty}\{\exp[ik_y'(y' - y_o')] + \exp[ik_y'(y' + y_o')] + C_r'\exp[ik_y'(2h' - y' - y_o')] + C_r'\exp[ik_y'(2h' - y' + y_o')]\}C_r'^{\ell}\exp[2ik_y'h'\ell]\frac{dK_x'}{k_y'},$$

where $k_y' = +\sqrt{k'^2 - k_x'^2}$, $\qquad y' - y_o' > 0.$

Again the integration variable is transformed to θ' where

$$K_x' = k'\sin\theta', \qquad k_y' = k'\cos\theta',$$

and the same contour is chosen as before (see Figure 2.5a).

The difficulty mentioned above now arises in the convergence of

the infinite sum

$$\sum_{\ell=0}^{\infty} C_r'^{\ell} \exp[2ik'h'\ell \cos\theta'] = \sum_{\ell=0}^{\infty} X^{\ell}$$

on the chosen contour, where

$$C_r' = \frac{\cos\theta' - \bar{\bar{\beta}}_{\omega'} \{1 - M_x \sin\theta'\}^2}{\cos\theta' + \bar{\bar{\beta}}_{\omega'} \{1 - M_x \sin\theta'\}^2}, \qquad \bar{\bar{\beta}}_{\omega'} = \gamma^3 \bar{\beta}_{\omega'}.$$

On contour BC where $-\frac{\pi}{2} < \mathrm{Re}(\theta') < \frac{\pi}{2}$ then, approximately,

$$0 < \cos\theta' \leq 1, \qquad -1 < \sin\theta' < +1$$

and

$$C_r' = \frac{\{\cos\theta' - \mathrm{Re}(\bar{\bar{\beta}}_{\omega'})(1 - M_x\sin\theta')^2\} - i\{\mathrm{Im}(\bar{\bar{\beta}}_{\omega'})(1 - M_x\sin\theta')^2\}}{\{\cos\theta' + \mathrm{Re}(\bar{\bar{\beta}}_{\omega'})(1 - M_x\sin\theta')^2\} + i\{\mathrm{Im}(\bar{\bar{\beta}}_{\omega'})(1 - M_x\sin\theta')^2\}}.$$

It can be seen that provided $\mathrm{Re}(\bar{\bar{\beta}}_{\omega'})(1 - M_x \sin\theta')^2 \geq 0$, $|C_r'|$ is always less than or equal to unity. The reflection coefficient can equal unity because, on the deformed contour, θ' has a small imaginary part and the exponential term ensures that the factor X has a magnitude less than unity.

On contour AB, θ' takes the value

$$\theta' = -\frac{\pi}{2} + \delta + ia, \qquad 0 < a < \infty,$$

so that

$$\cos\theta' = \sin\delta \cosh a + i \cos\delta \sinh a,$$

$$\sin\theta' = -\cos\delta \cosh a + i \sin\delta \sinh a.$$

First let $\delta = 0$; then

$$C_r' = \frac{-\mathrm{Re}(\bar{\bar{\beta}}_{\omega'})\{1 + M_x \cosh a\}^2 + i\{\sinh a - \mathrm{Im}(\bar{\bar{\beta}}_{\omega'})(1 + M_x \cosh a)^2\}}{+\mathrm{Re}(\bar{\bar{\beta}}_{\omega'})\{1 + M_x \cosh a\}^2 + i\{\sinh a + \mathrm{Im}(\bar{\bar{\beta}}_{\omega'})(1 + M_x \cosh a)^2\}}.$$

If $Im(\bar{\bar{\beta}}_{\omega}') \geq 0$ then $|C_r'| \leq 1$; if $Im(\bar{\bar{\beta}}_{\omega}') < 0$, then as before, the expression must be written with a finite δ :

$$(1 - M_x \sin\theta')^2 = \{1 + 2M_x \cos\delta \cosh a + M_x^2 \cos^2\delta \cosh^2 a - M_x^2 \sin^2\delta \sinh^2 a\} + i\{-2M_x \sin\delta \sinh a - 2M_x^2 \cos\delta \sin\delta \cosh a \sinh a\}$$

$$= p + iq, \text{ say,}$$

$$C_r' = \frac{\{\sin\delta \cosh a - pRe(\bar{\bar{\beta}}_{\omega}') + qIm(\bar{\bar{\beta}}_{\omega}')\} + i\{\cos\delta \sinh a - pIm(\bar{\bar{\beta}}_{\omega}') - qRe(\bar{\bar{\beta}}_{\omega}')\}}{\{\sin\delta \cosh a + pRe(\bar{\bar{\beta}}_{\omega}') - qIm(\bar{\bar{\beta}}_{\omega}')\} + i\{\cos\delta \sinh a + pIm(\bar{\bar{\beta}}_{\omega}') + qRe(\bar{\bar{\beta}}_{\omega}')\}}$$

This expression should be analysed to determine whether a value of δ, in the range $0 < \delta < \pi/2$, can be found which ensures that $|X| < 1$ for all possible values of $\bar{\bar{\beta}}_{\omega}'$ when $Im(\bar{\bar{\beta}}_{\omega}') < 0$. The deformed contour must of course remain asymptotic to the original contour and the integrand must not possess any singularities in the region between these two contours. As yet this has not been achieved and thus the final result to be obtained for the Green's function is not necessarily valid for $Im(\bar{\bar{\beta}}_{\omega}') < 0$.

The integration path can now be converted into a closed contour in the upper half θ'' plane for $x - x_0 > 0$ and in the lower half plane for $x - x_0 < 0$. (No difficulties are encountered here as the present reflection coefficient still satisfies the relation $C_r'(-\alpha) = 1/C_r'(\alpha)$, where α is the grazing incidence angle- see Chapter 2.)

The poles of the integrand, θ_n', are given by solutions of the equation (reverting to the k_x', k_y' notation)

$$H = (k_y'h') \tan(k_y'h') + i\, k'h' \bar{\bar{\beta}}_{\omega}' (1 - \frac{k_x'M_x}{k'})^2 = 0.$$

Unlike the zero flow case H is not an even function of θ' and

therefore, as might be expected, the poles differ in magnitude (as well as in sign) for $x - x_o > 0$ and $x - x_o < 0$; thus each case must be treated separately.

For the residue at each pole the factor

$$\left[\frac{dH}{d\theta}\right]_{\theta=\theta_n} = \frac{2i}{(k_{yn}h)\sec^2(k_{yn}h)}(k_{xn}h)\left[\frac{d}{d(k_yh)}\{(k_yh)\tan(k_yh) + ikh\bar{\bar{\beta}}_\omega(1 - \frac{k_xM_x}{k})^2\}\right]_{\theta=\theta_n}$$

will differ because the admittance is multiplied by a function of (k'_xh'). (In the above expression and in the one below the dashed notation of the Lorentz transformation is omitted.) After differentiation it becomes

$$\left[\frac{dH}{d\theta}\right]_{\theta=\theta_n} = 2i(k_{xn}h)\{\frac{\frac{1}{2}\sin(2k_{yn}h)}{(k_{yn}h)} + 1\} - 4\bar{\bar{\beta}}_\omega M_x(1 - k_{xn}M_x/k)\cos^2(k_{yn}h). \quad (4.4.1)$$

Provided no double poles exist (i.e., $\left[dH/d\theta\right]_{\theta=\theta_n} \neq 0$) the final solution follows immediately:

$$G'_\omega(x',y'/\bar{x}_o', y_o') = \delta(\omega' - \omega)\frac{i}{2h'}\sum_{n=0}^{\infty}\frac{\cos(k'_{yn}y_o')\cos(k'_{yn}y')}{k'_{xn}\Lambda_n'}$$

$$\exp[ik'_{xn}(x' - \bar{x}_o')] \qquad (\text{for, say, } x' - \bar{x}_o' > 0)$$

where

$$\Lambda_n' = \frac{1}{2}\{\frac{\frac{1}{2}\sin 2k'_{yn}h'}{k'_{yn}h'} + 1\} + \frac{i\bar{\bar{\beta}}'_\omega M_x}{(k'_{xn}h')}(1 - k'_{xn}M_x/k')\cos^2(k'_{yn}h')$$

or in the original coordinates with time dependence $\exp[-i\omega t]$

$$G'_\omega(x,y/\bar{x}_o,y_o) = \frac{i}{2h}\sum_{n=0}^{\infty}\frac{\cos(k_{yn}y)\cos(k_{yn}y_o)}{k'_{xn}\Lambda_n}\exp[ik_{xn}(x - \bar{x}_o)] \quad (4.4.2)$$

$$(x - \bar{x}_o > 0)$$

where

$$k_{xn} = \frac{-kM_x + k'_{xn}}{(1 - M_x^2)} \qquad (4.4.3a)$$

and

$$k'_{xn} = +\sqrt{k^2 - k_{yn}^2(1 - M_x^2)}, \qquad (4.4.3b)$$

$$\Lambda_n = \tfrac{1}{2}\{\frac{\sin(2k_{yn}h)}{2k_{yn}h} + 1\} + \frac{i\bar{\beta}_\omega M_x \cos^2(k_{yn}h)}{(k'_{xn}h)}(1 - k_{xn}M_x/k). \qquad (4.4.4)$$

The wavenumbers k_{xn}, k_{yn} are solutions of the equation

$$(k_y h)\tan(k_y h) = -ikh\,\bar{\beta}_\omega(1 - \frac{k_x M_x}{k})^2, \qquad (4.4.5)$$

with equation (4.4.3) defining the relation between the wavenumbers.

For $(x - x_0) > 0$, the so called 'cut-on' solutions $(k > |k_y|\sqrt{1 - M_x^2})$ are contained in the first quadrant of the θ' plane, $\theta_r' > 0$, $\theta_i' > 0$, but the 'cut-off' solutions can appear in the second quadrant, $\theta_r' < 0$, $\theta_i' > 0$. When solving equation (4.4.5) with equations (4.4.3) for solutions which undergo the transition from 'cut-on' to 'cut-off' the imaginary part of k_y can change sign (see equations (4.6.9) and (4.6.10)) as

$$k_y \propto k_y' \propto \cos\theta_r' \cosh\theta_i' - i\sin\theta_r' \sinh\theta_i'.$$

The sign of the corresponding k_x' solution must be chosen such that its imaginary part remains positive*, because $\theta_i' > 0$, and

$$k_x' \propto \sin\theta_r' \cosh\theta_i' + i\cos\theta_r' \sinh\theta_i'.$$

---

*This is identical to the definition in section (4.3), that is "take the positive sign for $x - \bar{x}_0 > 0$", but it is worth emphasising here because when $\theta_r' < 0$ the required root may not be the principal value generated by a computer sub-routine.

Notice that the axial wavenumber, k_x, can have a negative real part, not only because of the usual factor $-kM_x/(1 - M_x^2)$ (if $M_x > 0$) but also, when $\theta_r' < 0$, through the real part of k_x'.*

The virtues of the above analysis are that it provides a solution for the Green's function in terms of an infinite series of non-orthogonal modes and shows that modal axial wavenumber solutions with negative real parts in excess of the common factor occur naturally with the 'well behaved' 'cut-on' solutions. Of course this may occur because of the conditions imposed and thus the solutions may be forced to group together. The problem of whether or not a contour can be defined to allow convergence of this solution for $Im(\bar{\beta}_\omega) < 0$ also remains.

4.4.1 Some Evidence to Support the Validity of the New Green's Function

A good test of the validity of the new Green's function, G_ω', is that its sum of modes should converge to the free field Green's function, G_ω, near the source, where the influence of the duct walls is negligible (provided the source is at some finite distance from each wall). However, close to the source a large number of modes would be required and thus this test has been carried out only in a modified

---

* $Re(k_x)$ can also be less than zero for $M_x < 0$.

form described in (i) below. In (ii) the new Green's function is compared with those for the zero flow-lined duct and uniform flow-unlined duct in order to establish the conditions under which its new features are significant. The conditions are chosen accordingly in (iii).

(i) A multiple image ray model has been constructed (see Appendix 4A for details) which, from the zero flow results of Chapter 3, is assumed to give a good estimate of the total reflected field near the source, as well as the exact* direct or free field, in uniform flow. Thus it has been possible to extend this test to points where the reflected field begins to modify the direct field.

(ii) Inspection of the expression for G'_ω (equation 4.4.2) and the associated equations which determine the wavenumbers (equation 4.4.5) and normalisation factor, Λ_n (equation 4.4.4), reveals that G'_ω differs from the Green's functions for the zero flow-lined duct and uniform flow-unlined duct (both walls rigid) through the factor $(1 - k_x M_x/k)^2$ in equation (4.4.5) and the extra term $i\bar{\beta}_\omega M_x \cos^2(k_{yn}h)(1 - k_{xn}M_x/k)/(k'_{xn}h)$ in equation (4.4.4). The former modification is well known (14) but the latter has not appeared elsewhere (to the author's knowledge). In many cases of practical interest this extra term in Λ_n can be insignificant: for example, relative to the 'original' term, it is of order $\bar{\beta}_\omega M_x/\{kh(1 + M_x)\}$ for 'well-cut on' modes when $|\bar{\beta}_\omega kh/(1 + M_x)^2| \ll 1$.

Thus for a meaningful test of this Green's function parameter values are deliberately chosen so that this term is significant for two particular modes. To avoid an impractical example (that is a high Mach number or low frequency, or both) the other term is reduced

---

*Given by an exact evaluation of the Hankel function.

to the same order, but with opposite sign, so that $\Lambda_n \to \delta$, for two modes, where $|\delta|$ is small compared with the modulus of each term. The same 'test' is carried out, for comparison, with $M_x = 0$, and again with $\Lambda_n \to \delta$ for two particular modes.

(iii) As in Chapters 2 and 3, the frequency and duct width are chosen so that $kh = 10$ and two Mach numbers are used: $M_x = +0.4$ and $M_x = -0.3$. Impedance values at $y = 0$ and at $y = h$ satisfying the conditions in (ii) are as follows:

M_x	$\bar{Z}_\omega$	
0	1.47816	-j1.18
+.4	0.866525	-j0.55
-.3	2.83446	-j2.4

The impedance for $M_x = 0$ can be recognised as a value close to the Cremer (19) optimum impedance used in Chapter 2; in the following section the impedances for $M_x = +.4$ and $-.3$ will be shown to be close to the optimum values for uniform mean flow. The Green's function* is evaluated for $y_0/h = y/h = 0.5$ as a function of x/h ($\bar{x}_0 = 0$) in the range $.008 \lesssim x/h \lesssim .25$ and the number of modes is varied from 2 (the 'cut-on' modes), to 19.

The 'ray' and 'mode' Green's functions under these conditions are shown in Figures (4.1a) and (4.1b) for $M_x = 0$. In Figure (4.1a), the real part of the 'mode' G'_ω has not converged at all with 2 modes (for this range of x/h). With 19 modes it converges in the range .020 - .25 and is virtually identical to the 'ray' G'_ω. In Figure (4.1b), the imaginary part converges more rapidly and 8 modes give complete agreement with the 'ray' G'_ω over the entire range.

---

*Equal to that given by equation (4.4.2) multiplied by $\frac{1}{2}$ and with y replaced by $y - h/2$.

The comparison is repeated in Figures (4.2a) and (4.2b) for $M_x = +0.4$ and in Figures (4.3a) and (4.3b) for $M_x = -0.3$. The results are strikingly similar to those for zero flow despite the finite Mach numbers and dissimilar impedance values, but the feature of importance in both cases is the ability of the new Green's function to describe the 'near field' of the line source in uniform flow. The number of modes required for convergence is similar to that required for the zero flow Green's function. These results constitute the major part of the evidence, presented here, in support of the validity of the new Green's function.

The comparison between the 'ray' and 'mode' Greens functions is now extended to large distances from the source, that is for $x/h > 0.25$ and up to $x/h = 10.0$. The ray model, from the previous work in Chapter 3, is known to describe the actual field with only moderate accuracy, the error increasing with x/h. If the accuracy of the ray model for uniform flow is similar to that for zero flow then this can be regarded as tentative evidence that the uniform flow Green's function is correct. Thus in this comparison the accuracy of the ray model for uniform flow is compared with that at zero flow by inspecting the modulus squared of the ratio of the 'ray' and 'mode' Green's functions as a function of x/h (again on the centre-line).

Both Green's functions are evaluated for the following Mach numbers and impedance values (the latter are chosen so that the decay rates of the 'cut-on' modes are approximately the same in each example (see next section)):

Example	M_x Figure	+0.4 $\bar{Z}_\omega$		0.0 $\bar{Z}_\omega$		-0.3 $\bar{Z}_\omega$	
A	4.4	0.866525	-j0.55	1.47816	-j1.18	2.83446	-j2.4
B	4.5	"	-j1.0	"	-j2.0	"	-j4.0
C	4.6	"	-j0.25	"	-j0.5	"	-j1.0

The modulus squared, in dB, is shown as a function of x/h, in the range $.12 \lesssim x/h \lesssim 10.0$, in Figures (4.4)-(4.6). These relative errors (in dB) for uniform flow are quite similar to those for zero flow except for a consistent, relatively large error, for $M_x = +0.4$ in the region $0.25 \lesssim x/h \lesssim 0.4$. It has been verified that this error cannot be eliminated by using more modes in the evaluation of the Green's function (4 being used throughout these examples). No explanation can be given for this error and it is tentatively assumed that it is caused by the ray model and not the 'mode' Green's function.

Apart from this discrepancy, comparison with the ray model in the 'near' and 'far' field of the line source does support the validity of the new Green's function for uniform flow.

4.5 Optimisation of Sound Attenuation

In the first set of examples of the previous sub-section the reduced frequency and impedance values for each Mach number were chosen so that the normalisation factor Λ_n became small. In the limit $\Lambda_n \to 0$, of course, the solution is no longer valid and a new solution should be derived corresponding to the double pole in the θ' plane (as in Chapter 2). This double pole solution has not been derived mainly because it is clear that, from the zero flow results of Chapter 2, the behaviour of such a solution is likely to be adequately described by that of the two single pole solutions which lie close together on the θ' plane.

The double pole solution is of interest because a logical extension of Cremer's (19) result is that this solution should correspond to the maximum exponential decay rate of the associated mode pair. Before attempting to verify this the Green's function is evaluated near, and then away, from the double pole condition to establish the significance of this condition for the decay of a specified source distribution.

In Figure (4.7) the centre-line field, $|G'_\omega|^2$ in dB*, is shown as a function of x/h, for the same conditions, Mach number and impedance values of Example A in the previous sub-section: each impedance is very close to the double pole or 'optimum' value for that particular Mach number. The absolute values and decay rates are all similar and the fields in uniform flow exhibit the same type of deviation from exponential decay as that established for zero flow,

---

*Again with the source on the centre-line, identical impedances at y = 0 and y = h, and kh = 10.0

indicating the expected modal interferences (which is represented by the linear x dependence in zero flow).

Again it is recognised that the double pole impedance does not necessarily lead to the maximum decay of the Green's function, or any other source distribution, between two points in the duct. A detailed investigation of the Green's function decay near this condition is therefore unnecessary. However, as it will be shown that this condition does still define the optimisation of the exponential decay rate it is expected that impedance values which are significantly different from the double pole value will lead to reduced decay rates. This is demonstrated for zero flow in Figure (4.8), the impedance values of Examples A, B and C in the previous sub-section being used. The corresponding behaviour for $M_x = +0.4$ and -0.3 is shown in Figures (4.9) and (4.10). At least for the condition chosen (two-dimensional duct, source on centre-line, $kh = 10$) the approximate double pole impedance is a good guide to the optimum impedance for maximum decay of the Green's function in uniform flow.

On the basis of those results and the arguments put forward in Chapter 2, attention is now focussed on the double pole impedance and its variation with Mach number and the reduced frequency, kh.

4.5.1 Optimisation of modal attenuation

The extension of Cremer's (19) result to ducts containing uniform flow is confined here to mode pairs in the basic two-dimensional rectangular duct with a finite admittance at $y=h$ and a rigid wall at $y = 0$. The branch point values of $k_y h$ are solutions of the equation

$$\left[\frac{dH}{d\theta'}\right]_{\theta'=\theta'_n} = 0$$

or

$$\frac{-2j(k'_{xn}h')}{(k'_{yn}h')\sec^2(k_{yn}h)} \quad \frac{d}{d(k'_yh')}\{(k'_yh')\tan(k'_yh') - jk'h' \stackrel{=}{\beta}_\omega$$

$$\times (1 - \frac{k'M_x}{k})^2\}_{\theta'=\theta'_n} = 0$$

which reduces to* (and reverting to the usual wavenumber notation)

$$\frac{d}{d(k_yh)} \{(1 - \frac{k_xM_x}{k})^{-2} (k_yh)\tan(k_yh)\} = 0 \qquad (4.5.1)$$

where

$$k_x = \{-kM_x \pm \sqrt{k^2 - k_y^2(1 - M_x^2)}\}/(1 - M_x^2). \qquad (4.5.2)$$

Examples of solutions of equation (4.5.1) for the (0, 1) mode pair for $kh = 8\pi$ $(k/\lambda = 4)$ are

$$(k_yh)_o = 2.10 + j1.13 \qquad \text{for } M_x = +0.4,$$

$$= 2.11 + j1.12 \qquad \text{for } M_x = -0.3,$$

where a positive Mach number indicates sound attenuation in the downstream direction, and a negative Mach number sound attenuation in the upstream direction. These values are almost identical to the zero flow value of

$$(k_yh)_o = 2.11 + j1.13 \qquad (\text{for } M_x = 0.0)$$

and this is a common feature of all 'well cut-on' solutions where

$$kh > |k_yh| (1 - M_x^2)^{\frac{1}{2}}.$$

For these solutions equation (4.5.2) is, approximately,

$$k_x \doteq \frac{k}{(1 + M_x)} \qquad (4.5.3)$$

---

*The n subscript denoting a modal solution is now omitted.

and with this value equation (4.5.1) is

$$\frac{d}{d(k_y h)} \{(k_y h)\tan(k_y h)\}(1 + M_x)^2\} \doteq 0$$

which, with the equality sign, is identical to the branch point equation for zero flow. The corresponding optimum impedance is markedly different however, being given by equation (4.4.5), which with equation (4.5.3) is

$$\bar{Z}_\omega \doteq \frac{-jkh}{(k_y h)\tan(k_y h)(1 + M_x)^2} .$$

As the $(k_y h)$ values are virtually identical to the zero flow values the optimum impedance with flow $(\bar{Z}_\omega)_o|_{M_x}$ is clearly given by the simple relation

$$(\bar{Z}_\omega)_o|_{M_x} \doteq \frac{(\bar{Z}_\omega)_o}{(1 + M_x)^2} \qquad (4.5.4)$$

where M_x may be positive or negative. In the present examples $(\bar{Z}_\omega)_o|_{M_x}$ takes the values

$$(\bar{Z}_\omega)_o|_{M_x=.4} = 3.81 - j\ 3.03,$$

$$(\bar{Z}_\omega)_o|_{M_x=-.3} = 15.1 - j\ 12.2$$

(cf. $(\bar{Z}_\omega)_o = 7.43 - j\ 5.95$ from section (2.4)).
The factor $(1 + M_x)^{-2}$ takes the following convenient values: approximately 2 for $M_x = +.4$ and approximately $\frac{1}{2}$ for $M_x = -.3$. Clearly the above impedances obey the approximate law given by equation (4.5.4). The method used to obtain solutions to equation (4.5.1) is described in Appendix 4B.

Verification of this extension of Cremer's (19) optimisation

concept is shown in Figures (4.11) and (4.13) for $M_x = +.4$ and in Figures (4.12) and (4.14) for $M_x = -.3$*. In Figures (4.11) and (4.12) the imaginary part of the impedance is held constant and equal to the optimum value and the real part is varied. In Figures (4.13) and (4.14) the real part is held constant and the imaginary part varied. The impedance scales have been chosen so that distance along the x axis is proportional to $\bar{Z}_\omega (1 + M_x)^2$. The evident similarity of modes (0, 1) in each pair of figures demonstrates the general validity of the above approximations, including the required second approximation for $(k_x h)$ for well 'cut-on' modes:

$$k_x h \doteq \left(\frac{kh}{(1 + M_x)} - j \frac{\mathrm{Re}(k_y h)\mathrm{Im}(k_y h)}{kh}\right), \qquad (4.5.5)$$

that is, the attenuation of well cut-on modes is independent of the flow Mach number for constant $k_y h$. The figures also show the expected trend of deviation from this general rule as the mode order increases and approaches 'cut-off'.

The actual variation of $(\bar{Z}_\omega)_0$ with Mach number and kh (or h/λ) is shown in Figures (4.15) and (4.16): for $h/\lambda \geq 0.5$, $(\bar{Z}_\omega)_0$ remains approximately proportional to $kh(1 + M_x)^{-2}$ but, for example, at $h/\lambda = 0.2$ and $M_x \doteq -0.5$ the real part of $(\bar{Z}_\omega)_0$ is zero and for $M_x < -0.5$ becomes negative. For $h/\lambda = 0.05$, $(\bar{R}_\omega)_0$ is negative over the entire M_x range apart from a small interval centred at $M_x = 0$. This pattern is repeated for all smaller values of h/λ, and similarly for $(\bar{X}_\omega)_0$.

---

*The evaluation of attenuation rates was carried out by using a modified form of the Rolls-Royce computer program.

4.5.2 Interpretation of active optimum impedances and the appearance of 'strange' modes

Values of $(\bar{Z}_\omega)_o$ for which $(\bar{R}_\omega)_o < 0$ are shown as dashed lines in Figures (4.15) and (4.16) because, although these values are continuous with the $(\bar{R}_\omega)_o > 0$ values, they are clearly not the required solutions. Although the mode is well behaved in the sense that its phase velocity (not shown) is in the same direction as that of its decay, active impedances will not be considered here* In fact the solution is the complex conjugate of a required solution, although the latter is no longer the optimum impedance for the (0, 1) mode pair. It corresponds to the (1, 2) branch point for an M_x value of the opposite sign.

To illustrate this point consider the case $h/\lambda = 0.05$, $M_x = -.08$ and $M_x = -.10$ where the relevant parameters take the following values:

	$M_x = -.08$	$M_x = -.10$
$(\bar{Z}_\omega)_o$	.018 - j.260	- .020 - j.323
$(k_y h)_o$	2.77 + j1.52	2.92 + j1.54
$(k_x h)_o$	1.55 - j2.76	1.58 - j2.93

$\mathrm{Re}\{(\bar{Z}_\omega)_o\}$ changes sign somewhere between $M_x = -.08$ and $M_x = -.10$. The complex conjugate of the governing equations

$$kh\left(1 - \frac{k_x M_x}{k}\right)^2 (j\bar{\beta}_\omega) = (k_y h)\tan(k_y h)$$

---

* $\mathrm{Re}(\bar{Z}_\omega)$ or $\mathrm{Re}(\bar{\beta}_\omega) < 0$ also invalidates the analysis leading to the Green's function in section 4.4.

$$k_x h = \{-khM_x + \sqrt{(kh)^2 - (k_y h)^2\,(1 - M_x^2)}\}/(1 - M_x^2)$$

indicates that the conjugate solution is, for $M_x = -.10$,

$$(\bar{Z}_\omega) = .020 - j.323\ ,$$
$$(k_y h) = 2.92 - j1.54\ ,$$
$$(kxh) = 1.58 + j2.93\ .$$

As was noted in the previous section (following equation (4.4.5)), solutions of $(k_y h)$ can be accepted but the sign of the imaginary part of $(k_x h)$ must remain the same; thus the alternative minus sign for the square root in the above wavenumber equation must be used. This changes the solution for $M_x = -.10$ but it is now the solution for $M_x \doteq .10$: that is

$$M_x = +.10$$
$$(\bar{Z}_\omega) = 0.020 - j.323\ ,$$
$$(k_y h) = 2.92 - j1.54\ ,$$
$$(k_x h) = -1.58 - j2.93\ .$$

However this is no longer the branch point solution for the (0, 1) mode pair; at the transition point $(\bar{R}_\omega)_0 \to 0$ another solution emerges, as expected, with a real axial wavenumber (zero attenuation). This is the new (0) mode and hence the above solution corresponds to the (1, 2) branch point. By referring to solutions for this mode pair it is found that (as M_x is increased positively from zero) $(\bar{R}_\omega)_1$ tends to zero at $M_x \doteq .06$. Thus in the range $0.06 < M_x < 0.09$ no branch points exist for a positive $\bar{R}_\omega$ value and hence the present optimisation approach breaks down. Standard, 'zero gradient' optimisation methods could be used for this range but these have not been utilised here.

The attenuation is shown in Figure (4.17) as a function of $\bar{X}_\omega$ for $\bar{R}_\omega = .018$, $M_x = -0.08$ and $\bar{R}_\omega = 0.020$, $M_x = + 0.1$*. The corresponding attenuation curves for the transition point $\bar{R}_\omega = 0.0$, $M_x \doteq \pm 0.09$ should lie close to those shown in Figure (4.17) but with the addition of a new mode with zero attenuation. For $\bar{R}_\omega = 0.020$, $M_x = 0.1$ the attenuation of this mode is quite large, especially for $\bar{X}_\omega > 0$, but it is well below the attenuation of the new (1, 2) mode pair, for the optimum value.

The 'strange' mode solutions which require this type of interpretation are analysed in more detail in the following section where approximate analytic solutions are used to illustrate their origin and general behaviour. It should be emphasised that these solutions are not peculiar to optimum conditions, but they did emerge during a systematic tabulation of branch point solutions.

4.5.3 Application of results

The useful practical result to emerge from this optimisation study for 'plug' flow is the approximate rule that the optimum impedance for a 'plug' flow at Mach number M_x is simply equal to the optimum impedance for zero flow divided by $(1 + M_x)^2$. The result can be used to interpret theoretical predictions, and this is to be demonstrated using a specific example. Also, with a little manipulation, a simple rule will be derived for direct application to attenuation measurements with flow.

As an illustration of predicted flow effects the attenuation rate has been calculated for the least attenuated mode in an infinite, two-dimensional rectangular duct of width h, at the reduced frequency values given in Table (4.1).

---

*Some solutions could not be obtained at this condition.

Table 4.1

No.	1	2	3	4	5	6	7	8	9
kh	2.984	3.730	4.700	5.968	7.460	9.325	11.94	14.52	18.65

No.	11	12	13	14
kh	29.84	37.30	47.00	59.68

The results are shown in Figure (4.18) for $M_x = -0.3$, 0 and 0.3. The duct is lined on both walls (at $y = 0$ and at $y = h$) with a material having an impedance characteristic shown in Figure (4.19); the real part of the impedance is held constant while the imaginary part is taken to be $-\cot(kh/12)$: that is approximately the reactance of a partitioned cavity or Helmholtz resonator liner of depth $h/12$.

As the least attenuated mode is a symmetrical one in this case, h can be considered to be twice the width of the equivalent 'one wall lined' duct considered in the optimisation study; thus the optimum impedance for zero flow is

$$Z_{\omega_{opt}} = (0.929 - j0.744)\frac{kh}{2\pi} .$$

This is shown in Figure (4.19) together with the values at $M_x = \pm 0.3$ given by the above expression divided by $(1 + M_x)^2$.

If it is pre-supposed that the maximum attenuation occurs at the optimum reactance value, irrespective of the resistance value, then from Figure (4.19), this should occur at just below frequency number 6 for zero flow, between 4 and 5 for $M_x = -0.3$ and between 6 and 7 for $M_x = +0.3$. Inspection of Figure (4.18) shows that these are good estimates of the frequency of maximum attenuation. In addition Figure (4.19) indicates that the resistance of two is almost equal to the optimum value for $M_x = -0.3$ and hence the large attenuation shown

in Figure (4.18) is expected*. Without this guide-line of the optimum impedance concept it would be difficult to understand why the maximum attenuation occurs at particular, finite negative reactance values and why these values depend on the Mach number. It also enables sensible ranges of parameter values to be chosen for parametric studies, which are common in the aero-space industry.

The supposition that the maximum attenuation always occurs, approximately, at the optimum reactance value appears to be correct over a wide range of resistances although it has not been proved in the preceding analysis. For example, in Figure (4.20) a graph taken from the multi-modal parametric study by Ko (30) shows that for a large resistance variation the maximum attenuation remains at roughly the same frequency and hence the same reactance.** (The pertinent data for this graph are: $M_x = 0.4$, $h = 7.37"$, duct length, $L = 16"$, $c = 1120$ ft.sec^{-1}.) The impedance formula can be found in reference (30) but to a good approximation it is simply

$$\bar{Z}_\omega = R_* - j \cot(kh/7.37).$$

Adopting this approximate rule, and taking the low frequency approximation of the cavity reactance,

$$- \cot k\ell \doteq - \frac{1}{k\ell}, \qquad k\ell \ll \pi/2,$$

gives the frequency of maximum attenuation, $f(0)$, for the lowest order mode pair as the solution of

$$\frac{1}{k\ell} \doteq 0.744 \frac{kh}{\pi}$$

---

*The maximum attenuation is also large because it occurs at a smaller kh value (see Figure 2.); also the maximum attenuation is no longer completely independent of M_x as the mode is not 'well cut-on'.

**This probably occurs because the reactance changes rapidly with frequency; in other cases the maximum attenuation may change with resistance.

which is $f(0) = \frac{c}{2\pi} \{\frac{\pi}{\ell h 0.744}\}^{\frac{1}{2}}$ for zero flow. For a finite flow Mach number, using the well 'cut-on' approximation being used, the frequency of maximum attenuation is

$$f(M_x) = \frac{c}{2\pi} \{\frac{\pi}{\ell h 0.744}\}^{\frac{1}{2}} (1 + M_x)$$

and the ratio is

$$\frac{f(M_x)}{f(0)} = (1 + M_x). \qquad (4.5.6)$$

This approximate relationship is compared with some experimental results given by Eversman (42) in Figure (4.21).

The exact relationship between frequencies of maximum attenuation is more complicated than that given by equation (4.5.6). Nevertheless it may represent a useful engineering approximation; it should be applicable where $k\ell < \pi/2$ and $kh > 2$, or $2 < kh < h/\ell$.

4.6 Some Approximate, Analytic Examples of 'Strange' Modes

The origin of the 'strange' mode solutions mentioned in previous sections can be investigated by taking some approximate analytic solutions of the governing equations, which can be written as

$$-ikh\left(1 - \frac{k_x M_x}{k}\right)^2 \bar{\beta}_\omega = (k_y h)\tan(k_y h), \tag{4.6.1}$$

$$\left(1 - \frac{k_x M_x}{k}\right)^2 = \left(\frac{k_x}{k}\right)^2 + \left(\frac{k_y}{k}\right)^2 . \tag{4.6.2}$$

From the preceding results it is clear that the appropriate approximation is that the mode is well 'cut-off'. Certain well 'cut-off' modes satisfy the condition

$$\left|\frac{k_x M_x}{k}\right| \gg 1$$

and this will be used to simplify equations (4.6.1) and (4.6.2) to obtain three different types of approximate solution. In every case the left hand side of equation (4.6.2) is, in effect, replaced by $k_x^2 M_x^2/k^2$ so that

$$k_x h \doteq \pm i \frac{k_y h}{\sqrt{1 - M_x^2}},$$

and this relation is used to reduce equation (4.6.1) to one variable. Once this has been solved, a second approximation is obtained by using

$$k_x h \doteq \frac{-khM_x}{1 - M_x^2} \pm i \frac{k_y h}{\sqrt{1 - M_x^2}} \tag{4.6.4a}$$

or

$$\frac{k_x'}{k} = \pm \frac{ik_y}{k\sqrt{1 - M_x^2}} \tag{4.6.4b}$$

in place of equation (4.6.3). This procedure could then be repeated, substituting this second approximation into equation (4.6.1) and so on, with due regard for convergence of this iteration, but this has not been attempted here. It will be shown in the next section that the second approximation solutions are quite accurate for modes which satisfy the condition $|k_x M_x/k| >> 1$. Note that equation (4.6.4b) is identical to equation (4.6.3) with k_x replaced by k_x', and thus the second approximation for k_x/k is identical to the first approximation for k_x'/k which would have been obtained from the Lorentz equivalent of equations (4.6.1) and (4.6.2) with the assumptions $|k_x'/k| >> 1$ and $|k_x' M_x/k| >> 1$.

Substituting for k_x in equation (4.6.1) (using equation (4.6.3)) and retaining only the $k_x^2 M_x^2/k^2$ term, so that

$$(1 - \frac{k_x M_x}{k})^2 \doteq - \left| \frac{(k_y h)^2 M_x^2}{(kh)^2(1-M_x^2)} \right| , \qquad (4.6.5)$$

gives

$$-i \left| \frac{(k_y h)^2 M_x^2}{(kh)^2(1 - M_x^2)} \right| kh(- \bar{\beta}_\omega) \doteq (k_y h)\tan(k_y h). \qquad (4.6.6)$$

If $(k_y h)^2$ is almost real, equation (4.6.6) indicates the reason for the appearance of these 'strange' modes: the passive ($Re(\bar{\beta}_\omega) \geq 0$) wall admittance is now acting like an <u>active</u> admittance because of the minus sign introduced by equation (4.6.5). Conversely an active ($Re(\bar{\beta}_\omega) < 0$) wall admittance can appear to act like a passive one, which accounts for the appearance of negative resistances in the optimum impedance study of section (4.5).

The first two types of approximation are based on the assumption that $(k_y h)^2$ is almost real: one is used when the

modulus of the left hand side of equation (4.6.6) tends to zero, corresponding to $|\bar{\beta}_\omega| \to 0$, and the other where the modulus tends to infinity. The latter limit covers a wide range of $|\bar{\beta}_\omega|kh$ values because the term in square brackets can be indefinitely large.

Denoting the left hand side of equation (4.6.6) by

$$\eta = -i\left[\frac{(k_y h)^2 M_x^2}{(kh)^2(1-M_x^2)}\right] kh(-\bar{\beta}_\omega)$$

the approximate solutions are (see, for example, Doak and Vaidya (43)) for $|\eta| \to 0$

$$k_y h \doteq m\pi + \frac{\eta}{m\pi}, \quad m = 1, 2, \ldots, \infty, \quad m \neq 0 \qquad (4.6.7)$$

and for $|\eta| \to \infty$

$$k_y h \doteq (2n - 1)\frac{\pi}{2}\left(1 - \frac{1}{\eta}\right), \quad n = 1, 2, \ldots, \infty, \; n \neq 0. \qquad (4.6.8)$$

Substituting $m\pi$ for $k_y h$ in η gives a first approximation for $k_y h$ in the limit $|\eta| \to 0$:

$$k_y h \doteq m\pi \left\{1 - \frac{M_x^2 \, Im(\bar{\beta}_\omega)}{kh(1 - M_x^2)} + i\frac{M_x^2 \, Re(\bar{\beta}_\omega)}{kh(1 - M_x^2)}\right\} \qquad (4.6.9)$$

and similarly for $|\eta| \to \infty$

$$k_y h \doteq (2n - 1)\frac{\pi}{2}\left\{1 - \frac{kh(1 - M_x^2)Im(\bar{Z}_\omega)}{M_x^2\{(2n-1)\frac{\pi}{2}\}^2} + \frac{ikh(1 - M_x^2)Re(\bar{Z}_\omega)}{M_x^2\{(2n-1)\frac{\pi}{2}\}^2}\right\} \qquad (4.6.10)$$

These expressions show that provided $Re(\bar{\beta}_\omega)$ (or $Re(\bar{Z}_\omega)$) is positive, the imaginary part of the solutions for $k_y h$ can have a positive sign for well 'cut-off' modes, being normally negative for well 'cut-on' modes. The possibility of this occurrence was noted in section (4.4) (note k_y'h' $= k_y h$) and although there is nothing in the analysis presented there to suggest that this is in any way significant, the corresponding

axial wavenumbers (both $k_x'h'$ and k_xh) can have phase velocities in the opposite direction to that of decay (see below). Thus the approximate solutions above are examples of the 'strange' modes.

Substituting the k_yh expressions into equation (4.6.4a) leads to the second approximation for k_x/k. In terms of k_x'/k this is, for $|n| \to 0$,

$$\frac{k_x'}{k} \doteq \pm \frac{m\pi\sqrt{1 - M_x^2}}{kh} \{\frac{-M_x^2\, Re(\bar{\beta}_\omega)}{kh(1 - M_x^2)} + i(1 - \frac{M_x^2\, Im(\bar{\beta}_\omega)}{kh(1 - M_x^2)})\} \quad (4.6.11)$$

and, for $|n| \to \infty$,

$$\frac{k_x'}{k} \doteq \pm \frac{(2n-1)\pi/2\sqrt{1 - M_x^2}}{kh} \{\frac{-kh(1-M_x^2)Re(\bar{Z}_\omega)}{M_x^2\{(2n-1)\pi/2\}^2}$$

$$+ i(1 - \frac{kh(1 - M_x^2)\, Im(\bar{Z}_\omega)}{M_x^2\{(2n-1)\pi/2\}^2})\}. \quad (4.6.12)$$

Notice that the plus or minus sign cannot be chosen independently for the real and imaginary parts of k_x'/k. According to the analysis of section (4.4) the positive sign is chosen in the above expressions for $x - \bar{x}_0 > 0$ so that the mode decays in the positive x direction, although the phase velocity is quite clearly in the opposite direction if $M_x > 0$:

$$\frac{Re(k_x)}{k} = \{ -M_x + \frac{Re(k_x')}{k} \}/(1 - M_x^2).$$

In the third type of approximation it is assumed that

$$|Im(k_yh)| > 1.5$$

and then the tangent function on the right hand side of equation (4.6.1) can be approximated by

$$\text{isgn } (\text{Im}(k_y h)).$$

Of course the solution obtained for $k_y h$ must be checked to ensure that it satisfies the above condition. Squaring equation (4.6.1) and re-arranging gives

$$(1 - \frac{k_x M_x}{k})^4 \; \bar{\beta}_\omega^{\,2} \doteq (\frac{k_y}{k})^2 \; ;$$

hence, after substituting for $(k_y/k)^2$ from equation (4.6.2),

$$(1 - \frac{k_x M_x}{k})^4 \; \bar{\beta}_\omega^{\,2} \doteq (1 - \frac{k_x M_x}{k})^2 - (\frac{k_x}{k})^2 .$$

Each side is expanded and terms of order zero and one in $k_x M_x/k$ are neglected to give

$$\bar{\beta}_\omega^{\,2}(6M_x^2 - 4\frac{k_x M_x^3}{k} + \frac{k_x^2 M_x^4}{k^2}) \doteq -(1 - M_x^2)$$

or

$$\frac{k_x}{k} \doteq \frac{2}{M_x} \pm \frac{i\sqrt{2M_x^2 + (1 - M_x^2)\bar{Z}_\omega^2}}{M_x^2} . \qquad (4.6.13)$$

In this case, if $\bar{Z}_\omega$ is real, the phase velocity is equal to half the flow velocity and in the same direction. It is completely independent of the decay direction or choice of signs.

The second approximation is

$$\frac{k_x}{k} \doteq -\frac{M_x}{1 - M_x^2} + \frac{2}{M_x} \pm \frac{i\sqrt{2M_x^2 + (1 - M_x^2)\bar{Z}_\omega^2}}{M_x^2} \qquad (4.6.14a)$$

so that

$$\frac{k_x'}{k} \doteq \frac{2(1 - M_x^2)}{M_x} \pm \frac{i(1 - M_x^2)}{M_x^2}\sqrt{2M_x^2 + (1 - M_x^2)\bar{Z}_\omega^2} .$$

If $\bar{Z}_\omega$ is real and $M_x > 0$ the pole responsible for this mode would be located in the first θ' quadrant for $x - \bar{x}_o > 0$, along with the

well 'cut-on' modes (+i), and in the fourth quadrant for $x - \bar{x}_o < 0$ with the other 'strange' modes (-i); but the former does not exist. That is, the solution with the positive sign in equation (4.6.14) must be rejected* as a solution of the above approximate equations due to an inconsistency in signs. This is not immediately apparent because the important sign is lost when equation (4.6.1) is squared. Conversely for $M_x < 0$ (and again if $\bar{Z}_\omega$ is real) the solution with the minus sign is rejected. Thus, from equation (4.6.14a), the direction of the phase velocity is determined by the direction of the flow velocity (for subsonic Mach numbers) and is always in the opposite direction to that of decay.

It is clear from these approximate solutions that the origin of the 'strange' modes lies in the peculiar behaviour of the factor $(1 - k_x M_x/k)^2$ multiplying the admittance, $\bar{\beta}_\omega$, which originates from the boundary conditions used in the 'plug' flow model. It is therefore pertinent to enquire whether the assumed boundary condition is realistic for such modes: this has led to an investigation which is described in Chapter 6.

These solutions are also intriguing from the energy viewpoint because, as was mentioned before, the direction of axial energy flow is given by the sign of the real part of the Lorentz axial wavenumber, which, for the above solutions, can be in the opposite direction to that of the decay. The energy aspect is discussed in detail in Chapter 5.

---

*At least, for real frequencies.

4.7 The Existence of Temporal Instabilities and the Correct Procedure for Obtaining the Green's Function

4.7.1 Introduction

During the course of the attempted derivation of the Green's function (described in section (4.4)) it was suggested by Ffowcs-Williams (22) that the Green's function for a source which emits a pulse at, say $t = 0$ would grow in time even if the source is situated (in uniform flow) at a finite distance from a single absorptive wall. He also pointed out that the fundamental radiation condition is the Causality Law, that is for $t < 0$, with the source switched off, no disturbances can exist anywhere in the region under consideration.*

In the brief literature review which follows, it is shown that the available information supports Ffowcs-Williams' (22) suggestion but possibly with an important qualification. This qualification, if proven for a lined duct containing uniform flow, means that a 'steady state' Green's function for a source-time dependence $\exp[-i\omega t]$ does exist, in a restricted sense, but it is necessary to examine the transient response after the source is switched on. The source must be switched on at, say, $t = 0$ in order to apply the fundamental Causality Law and to obtain the correct result. This procedure also leads to a satisfactory interpretation of the 'strange' modes. However the conclusions given here must be regarded as tentative as the analysis is by no means rigorous: for example it has been assumed (again) that the θ' integrand converges on the specified contours.

4.7.2 Review of information on instability in related problems

The Green's function derived in section (4.4) is based on the reflection of plane waves from a single, infinite, uniform boundary

---

*And not that $|G_\omega'| \to 0$ as $|x' - \bar{x}'| \to \infty$ which is the radiation condition implied in the Brekhovskikh (20) method through the choice of contour on the θ' plane.

which, in effect, is non-locally reacting. Suppose the boundary to be replaced by one whose admittance represents the mean boundary between two semi-infinite streams in relative, uniform motion (see Figure (4.22)). It is well known (44) that for incompressible flows the (unsteady) motion of the fluid interface is unstable (in time) with respect to an imposed spatially periodic disturbance (Helmholtz instability). Of more relevance in the present context is the analysis by Miles (45) for compressible fluids: an initial velocity (normal to the interface) of the form $\exp[ik_x x]$ (k_x real) is imparted to the fluid interface at $t = 0$ and the asymptotic (x, t) dependence (that is, as $t \to \infty$) of the interface displacement is shown to be of the form

$$\exp\left[ik_x\left(x - \frac{\omega}{k_x}t\right)\right]$$

where*

$$\frac{\omega}{ck_x} \equiv \frac{k}{k_x} = \frac{M_x}{2} \pm i\{(M_x^2 + 1)^{\frac{1}{2}} - (M_x/2)^2 - 1\}^{\frac{1}{2}}. \qquad (4.7.1)$$

(These solutions are valid for $M_x < 2\sqrt{2}$ but another neutral solution appears in the range $2 < M < 2\sqrt{2}$).

Thus for subsonic Mach numbers there is always one unstable disturbance (taking the + sign in equation (4.7.1)) following an abrupt displacement of the interface. Equation (4.7.1) is a solution of the equation

$$-ik(1 - k_x M_x/k)^2 \{1 - (\frac{k_x}{k})^2\}^{\frac{1}{2}} - ik_y = 0 \qquad (4.7.2)$$

where

$$k_y = \{(k - k_x M_x)^2 - k_x^2\}^{\frac{1}{2}},$$

---

* Both fluids are taken to have the same speed of sound, c.

which determines the location of the poles in the complex (k/k_x) plane. (The omitted plus and minus signs for the square roots are chosen to satisfy the 'finiteness conditions' at infinity - see Miles (45)).

Clearly the initial condition used by Miles (45) is inconsistent with that which would be caused by a plane wave component of a point or line source field. In Friedland and Pierce's (46) analysis a line source is introduced at a finite distance, h, from the interface, and emits a pulse at $t = 0$ (described by the function $\delta(t)$). In this case the fluid containing the source is at rest - see Figure (4.23a). After a certain time a spatial region develops (in $y < 0$) in which the solution is 'singular', indicating instability in time; this is shown as a shaded region in Figure (4.23b). Each corner of this region moves in the downstream direction with the velocity indicated in Figure (4.23b); these velocities are approximate and valid only for $M_x << 1$. (This region always develops if $M_x < 2\sqrt{2}$ which is consistent with Miles' (45) result.) Thus the unstable region moves away from the source and does not even exist at points (x, y) where $x < h - y$. Although this result will be modified if the fluid containing the source also has a uniform mean velocity, it is a strong indication that the presence of an acoustic source near a fluid interface, switched on at $t = 0$, will trigger a convective instability and not one which grows indefinitely with time at any point: this is the important qualification mentioned above.

Tam (47) assumed this to be the case in his analysis of a model for the influence of pressure fluctuations on the (thin) shear layer at the boundary of a supersonic jet close to the nozzle (see Figure (4.24)). The pressure fluctuations are assumed to be localised at $x = 0$ and to

induce a pressure difference across the shear layer at this point. The fluctuation at (real) frequency ω is switched on at $t = 0$. By using Miles' (45) results and a method developed by Briggs (23), Tam (47) obtains the asymptotic ($t \to \infty$) pressure dependence outside the jet on x, r, θ and t, the latter being simply $\exp[-i\omega t]$; the x dependence is $\exp[ik_x x]$ where k_x is the unstable solution in equation (4.7.1): thus the wave amplifies spatially without limit in the x direction, travelling with phase velocity equal to one half the jet velocity. Of course when the amplitude becomes sufficiently large non-linear effects can no longer be neglected and this solution is invalid. The spatial pressure pattern of this amplifying wave in the x, r plane is shown by Tam (47) to be in excellent agreement with the observed radiation from jets.

Tam's (47) philosophy and Briggs' (23) method are used below, but first it is necessary to re-introduce the real boundary in place of the fluid interface. (It is recognised that this imposes a different boundary condition, not only for the normal particle displacement and pressure, but also for the tangential particle velocity if the fluid is viscous. The effects of viscosity and thermal conductivity are ignored throughout the present work but they may be particularly important in this context.) For an incompressible fluid the modified Helmholtz instability is well known and appears in the 'panel flutter' problem (see, for example, Betchov and Criminale (49)). If the wall impedance is purely reactive and given by

$$Z_\omega = -i(\omega m - \frac{K}{\omega})$$

the solutions of the boundary condition equation,

$$-i\omega(1 - k_x U_x/\omega)^2 \left\{\frac{1}{Z_\omega/\rho_o}\right\} - ik_y = 0 \qquad (4.7.3)$$

where

$$k_y = \{-k_x^2\}^{\frac{1}{2}} = +ik_x \qquad (k_x \neq 0)$$

(compare this with equation (4.7.2))

are

$$\frac{\omega}{k_x} = \frac{U_x \pm i\{k_x\bar{m}\,U_x^2 - (1 + k_x\bar{m})\,\frac{\bar{K}}{k_x}\}^{\frac{1}{2}}}{(1 + k_x\bar{m})} \qquad (4.7.4)$$

where $\bar{m} = m/\rho_o$, $\bar{K} = K/\rho_o$.

For a sufficiently large value of U_x, so that the term within the square root is positive, one of the solutions in equation (4.7.4), for a given spatially periodic disturbance (k_x real), gives rise to amplification with time of that disturbance. For future reference, suppose ω is given and $|k_xU_x/\omega| > 1$; then the approximate solutions of equation (4.7.3) are

$$\frac{k_x}{\omega} \doteq \frac{1}{(U_x/2)}\{1 \pm iZ_\omega/2\rho_oU_x\}. \qquad (4.7.5)$$

This concludes the review of the relevant information in the published literature; it is understood that Ffowcs-Williams and his co-workers are, at present, attempting to analyse a model consisting of a point source (in uniform flow) emitting a pulse at $t = 0$, and located at a finite distance from an absorptive wall.

4.7.3 Instabilities in ducts

In the analysis which follows the duct model is modified in that the source still has a time dependence $\exp[-i\omega t]$, but is switched on at $t = 0$ and following Tam (47), Briggs' (23) method is used to

obtain the Green's function as $t \to +\infty$. The analysis is not complete or rigorous but each important step is outlined and particular attention is given to the contour deformation procedure defined by Briggs (23).

The time dependent, inhomogeneous wave equation now has a source time dependence $\exp[-i\omega t]$ for $t \geq 0$ only, and is zero for $t < 0$. The Laplace transform is used in place of the Fourier transform and all initial conditions are set to zero; consequently the term $\delta(\omega' - \omega)$ is replaced by $\{-i(\omega' - \omega)\}^{-1}$. The major difference in the analysis occurs in performing the inverse transformations, that is, the integrations with respect to ω' and K_x', or θ', to obtain G_ω' as a function of t' and x'. The integration path (AB) for ω' is shown in Figure (4.25), together with the pole at $\omega' = \omega$, the source radian frequency. The value of ε is chosen so that the integration path lies above all the singularities of the integrand to satisfy the Causality Law. That is, the Green's function

$$G_\omega'(x', y'/\bar{x}_o', y_o') = \int_{-\infty+i\varepsilon}^{\infty+i\varepsilon} G_{\omega'}'(x', y'/\bar{x}_o', y_o') \exp[-i\omega' t'] \, d\omega' \tag{4.7.6}$$

where

$$G_{\omega'}'(x', y'/\bar{x}_o', y_o') = \int_{-\infty}^{+\infty} G_{\omega'}'(K_x', y'/\bar{x}_o', y_o') \, dK_x' \tag{4.7.7}$$

must be zero for $t < 0$. Upon rewriting the integrand in equation (4.7.6) as

$$\{G_{\omega'}' \exp[ik' \frac{M_x}{c}(x' - \bar{x}_o')]\} \exp[-i\omega' t] \quad \text{(note that } t' = t + \frac{M_x}{c}(x' - \bar{x}_o')\text{)}, \tag{4.7.8}$$

it is clear that, provided the bracketed term satisfies certain conditions, the integrand vanishes on the infinite semi-circle closing

the integration path in the upper half plane, when $t < 0$. Thus the integral is unaffected by this closure and, by the Residue Theorem, is zero for $t < 0$ provided this contour contains no singularities.

If it could be established that no singularities existed anywhere in the ω' upper half plane then the original contour would be lowered to lie just below the real axis (line A'B' in Figure (4.25)) except for the deformation around the pole at $\omega' = \omega$. Again provided the bracketed term in the expression (4.7.8) satisfies certain conditions, the integrand vanishes on an infinite semi-circle in the lower half plane when $t > 0$ and the integration can be evaluated by the Residue Theorem. If the singularities of the integrand are all simple poles then their contributions are negligible as $t \to +\infty$ except for the simple pole at $\omega' = \omega$. Then of course one obtains the result of section (4.4).

However it is easily shown that singularities can exist in the upper half plane. Suppose the K_x' integration is being evaluated directly on the $\mathrm{Re}(K_x')$ axis so that K_x' takes all real values between $\pm\infty$. The poles of the integrand for the ω' integration are then solutions of the equation

$$-ik'h'(1 - K_x'M_x/k')^2 \bar{\bar{\beta}}_{\omega'} = (k_y'h') \tan (k_y'h') \qquad (4.7.9)$$

where $k_y' = \pm \sqrt{k'^2 - K_x'^2}$.

Suppose that $K_x'^2 >> |k'|^2$ and $|K_x'h'| > 1.5$;

then

$$k_y' \doteq \pm i|K_x|$$

and $\tan(k_y'h') \doteq \tan(\pm i|K_x'h'|) \doteq \pm i|K_x'h'|$.

Equation (4.7.9) then reduces to

$$-ik'(1 - K_x'M_x/k')^2 \bar{\bar{\beta}}_{\omega'} - ik_y' \doteq 0$$

which is identical in form to equation (4.7.3). Equation (4.7.4) can be used directly to obtain the complex frequency poles if $\bar{\beta}_\omega$, is purely reactive. As the imaginary part can be positive it is clear that a transient compressible duct mode can be nearly identical to the single wall, incompressible, Helmholtz time-unstable solution. This mode is almost completely independent of the duct width and (in the y direction) grows exponentially towards the absorptive wall at $y' = h'$.

In physical terms the value of ε must be larger than the largest time growth rate, ε_m, of the unstable (real K_x') duct mode(s) to satisfy the Causality requirement. Here it is assumed that ε_m remains finite but even with this assumption it is clear that the Green's function may still not exist in the asymptotic limit $t \to +\infty$, unless the unstable modes are of a particular type. To quote Briggs (23): "..... two types of instabilities can be distinguished physically: 'convective" instabilities and 'absolute' or 'nonconvective' instabilities. In an infinite system, a pulse disturbance that is initially of finite spatial extent may grow in time without limit at every point in space (an absolute instability) or it may 'propagate along' the system so that its amplitude eventually decreases with time at any fixed point in space (a convective instability).

Unfortunately the field due to a pulse from a source (in uniform flow) in a duct or in the presence of a single wall has not been analysed and thus the unstable modes may be of either type (or may not exist at all due to lack of convergence on the original and/or deformed contours). However it is known, from Friedland and Pierce's (46) analysis, that a line source in the presence of a fluid interface does give rise to convective instability. This result, together

with the absence, in what follows, of any evidence of absolute instabilities (according to Briggs' (23) criteria) is the justification for assuming that the unstable modes are of the convective type and hence that the asymptotic Green's function does exist.

Briggs' (23) procedure originated from a qualitative argument, ascribed to Professor Bers; the procedure and its justification is quoted as follows (modified to the -i notation).

"'To decide whether a given wave with a complex $k_x = k_{xr} - ik_{xi}$ for some real ω is amplifying or evanescent, determine whether or not k_{xi} has a different sign when the frequency takes on a large positive imaginary part. If it does, then the wave is amplifying; otherwise, it is an evanescent wave'.

This statement has a simple physical interpretation if we think of driving the system with a source that is localised in space and has an exponentially increasing sinusoidal time dependence. For a sufficiently large exponential growth in time of the source, the principle of causality would imply that all waves should decay from the source. Therefore, an amplifying wave should have the property that its "growth constant" changes sign as the frequency acquires a sufficiently large positive imaginary part corresponding to exponential growth in time."

Further details of Briggs' (23) procedure need not be given here, apart from outlining the actual steps in evaluating the ω' and K_x' integrations. The integration with respect to K_x' is transformed to the θ' variable ($K_x' = k' \sin \theta'$) and the initial contour on the complex θ' plane is now determined by using the following complex k' value:

$$ck' \equiv \omega' = \omega + i\omega_i$$

where ω is the source (real) radian frequency and ω_i is

sufficiently large such that all amplifying modes at frequency ω have become modes attenuating away from the source. Provided there are no absolute instabilities and the maximum growth rate in time of the most unstable mode is finite, letting $\omega_i \to +\infty$ ensures that all modes decay away from the source. The contour on the θ' plane is shown in Figure (4.26); all the poles of the integrand (in θ') must now be located on the θ' plane, for the value $\omega' = \omega + i\omega_i$, $\omega_i \to +\infty$ particularly with respect to this contour. The θ' integrand is assumed to converge on this contour, in the sense that the infinite sum $\sum_{\ell=0}^{\infty} X^{\ell}$ can be replaced by $(1 - X)^{-1}$, and this is discussed later.

The value of ω_i is then uniformly reduced to zero and the θ' contour and the poles are moved to their (real) source frequency locations but during this process the contour must not cross any pole but must be deformed around it. For $t \to +\infty$ this procedure, in effect, dispenses with the ω' integration, the Causality requirement is satisfied and the Green's function is obtained at frequency ω. If the situation arises where two θ' poles approach the contour from each side so that even with deformation the poles move <u>onto</u> the contour this, according to Briggs (23), means that absolute instabilities <u>are</u> present.

Apart from the question of convergence on the various ω' and θ' contours, it remains to establish the location of the θ' poles with respect to the θ' contour as ω_i is brought from $+\infty$ down to zero. A general investigation is beyond the scope of the present work but a single example will clarify the use of Briggs' (23) procedure and indicate the problems involved.

4.7.4 An example of the derivation of the Green's function taking into account the possible existence of convective instabilities

The first problem to arise is the fact that there is an infinite number of θ' poles. In the first instance only the first ten are considered but a simple pattern emerges which suggests that the location of the remaining poles can be predicted. The second problem concerns the fact that the impedance must now be defined as an explicit function of frequency as its value will change with ω'. For the purposes of this exercise it is assumed that the impedance contains a frequency independent resistance, a simple inertia term and the reactance of a simple cavity of depth ℓ:

$$\bar{Z}_{\omega'} = \bar{R} - i\omega' \bar{m} + i \cot(\omega'\ell/c) \qquad (4.7.10)$$

As $\omega_i \to +\infty$ the cotangent function $\to -i$ but the inertia term increases in direct proportion to ω_i so that the real part of $\bar{Z}_{\omega'}$ increases without limit. To simplify the computation of pole locations it is assumed that for the upper limit of ω_i used ($\doteq 40\omega$) the inertia constant, $\bar{m}$, is sufficiently small such that this term can be neglected. The actual value chosen for $\bar{Z}_{\omega}$ (at the real source frequency) is

$$\bar{Z}_{\omega} = 3.5 + i.4892$$

which with $kh = \pi/10$ corresponds to a cavity depth approximately $3\frac{1}{2}$ times the duct width. (As ω_i increases from zero $\bar{Z}_{\omega'}$ rapidly attains the value 4.5.) This example originates from the low frequency behaviour of the optimum impedance value given in section (4.5). The reactance was originally supposed to be an optimum value for $M_x = 0.5$ and the resistance is similar to its supposed optimum ($\doteq 3.9$). The value $M_x = 0.5$ is used in the present example.

The pole locations (that is the mode solutions) are obtained from the equations

$$-ik'h'\left(1 - \frac{k_x'M_x}{k'}\right)^2 \bar{\beta}_{\omega'} = (k_y'h') \tan(k_y'h'), \qquad (4.7.11)$$

$$k_x'h' = \pm \{(k'h')^2 - (k_y'h')^2\}^{\frac{1}{2}}. \qquad (4.7.12)$$

In practice the solutions are first obtained numerically with

$$k' = \frac{\omega}{c} + i0.0$$

and then the value of the imaginary part of k' is increased in steps to some large but finite value: in this case the upper limit chosen is $\omega_i/\omega = 42$. The solutions obtained at each step are plotted as a function of ω_i/ω and will be given later. The solutions, that is the pole locations, at this upper limit are assumed to correspond to the limit $\omega_i \to +\infty$ and are shown schematically in Figure (4.26). The first ten numerical values of k_x'/k' are shown below.

Table of k_x'/k' values for large ω_i/ω.

n	k'_{xn}/k'		n	k'_{xn}/k'	
0-	-1.004	$-i.1791 \times 10^{-3}$	0+	1.002	$+i.6117 \times 10^{-4}$
1-	3.881	-i12.02	1+	1.026	$+i.1104 \times 10^{-2}$
2-	-1.040	$-i.1755 \times 10^{-2}$	2+	3.881	+i12.02
3-	-1.109	$-i.4719 \times 10^{-2}$	3+	1.086	$+i.3795 \times 10^{-2}$
4-	-1.208	$-i.8751 \times 10^{-2}$	4+	1.179	$+i.7737 \times 10^{-2}$
5-	-1.331	$-i.1348 \times 10^{-1}$	5+	1.298	$+i.1244 \times 10^{-1}$

All the poles that correspond to modal decay in the positive x direction (solutions denoted by a plus sign) are located somewhere in the shaded region 'A' in Figure (4.26), except the (2+) pole. Although it is in the first quadrant its position does not change with ω_i

beyond $\omega_i/\omega \doteq 4$; in distinct contrast the other poles in region A continue to move towards the point $\theta' = \pi/2$ with increasing ω_i/ω. Similarly all the poles that correspond to modal decay in the negative x direction are located somewhere in the shaded region B and are moving towards the point $\theta' = -\pi/2$ with increasing ω_i. The exception is the (1-) pole which does not move beyond $\omega_i/\omega \doteq 3$. It will be shown that further solutions of equations (4.7.11) and (4.7.12) give rise to (+) poles in the first quadrant and (-) poles in the third quadrant, that is, to the right and left of the contour for $\omega_i/\omega \to \infty$ respectively. This completes the first stage of Briggs' (23) procedure.

The second stage is the reduction of ω_i to zero and the final result, $\omega_i = 0$, is shown schematically in Figure (4.27). The contour is now identical to that used in section (4.4) except that it has had to be deformed around the (1-) pole. The (1-) and (2+) poles have hardly moved at all during the reduction of ω_i to zero but it is the former pole which causes the fundamental change in the final result for the Green's function. The (0+) and (0-) stay near the points $\pm \pi/2$ and the remaining 'strange' mode poles take up positions in the second and fourth quadrants.

The analysis of section (4.4) can now be repeated for $x - \bar{x}_o > 0$ and the end result is exactly the same except the Green's function contains an additional mode due to the residue contribution from the (1-) pole. For $x - \bar{x}_o < 0$ the Green's function has 'lost' that same mode. The additional mode is of course a spatially amplifying mode and at some finite distance from the source dominates the entire field. In this example there is no evidence of (two) poles merging onto the contour and thus no absolute instabilities are present, according to Briggs' (23) criterion.

The numerical values of k_x'/k' for $k' = \omega/c$ are given below.

Table of k_x'/k' for $\omega_i/\omega = 0$

n	k_{xn}'/k'		n	k_{xn}'/k'	
0-	-0.798	-i1.18	0+	1.06	+i.120
1-	4.85	-i8.96	1+	-1.57	+i6.67
2-	2.40	-i11.8	2+	-1.83	+i13.7
3-	1.20 (1.16)	-i21.2(-21.6)	3+	-1.20 (-1.16)	+i21.8(21.6)
4-	0.833 (.826)	-i30.1(-30.3)	4+	-0.856 (-.826)	+i30.3(30.3)
5-	0.645 (.643)	-i38.8(-39.3)	5+	-0.660 (-.643)	+i38.9(39.3)

It is important to attain some understanding of these solutions, particularly of poles 3 - 5, to predict the behaviour of further solutions as $\omega_i/\omega \to +\infty$ (the reverse of the correct procedure but it simplifies the following arguments).

The appropriate approximate solution for modes 3-5 is given by equation (4.6.12); the values obtained from this equation, shown in brackets in the above table, improve in accuracy with increasing solution order n. The dependence of $Re(k_x'/k')$ on ω_i/ω is shown in Figure (4.28); the relevant feature here is the abrupt change in sign of $Re(k_x'/k')$ of modes 3-5 for some small value of ω_i/ω, say Δ, where Δ decreases with n. This means that the n^{th} order (+) pole, as $n \to \infty$, moves to the right and into the first quadrant of the θ' plane, and the n^{th} order (-) pole to the left, into the third quadrant, for an infinitesimal value of ω_i/ω. As the contour is always located in the second and fourth quadrants, poles 3-5 and higher order poles are well separated for all values of ω_i/ω. The behaviour of $Re(k_x'/k')$ can be understood by referring to equation (4.6.12) (ignoring $Im(\bar{Z}_{\omega'})$):

$$\frac{k_x'}{k'} \doteq \pm \left\{ \frac{-\mathrm{Re}(\bar{Z}_{\omega'})(1 - M_x^2)^{3/2}}{(2n - 1)\,\pi/2\;\; M_x^2} + i\,\frac{(2n - 1)\,\pi/2\,\sqrt{1 - M_x^2}}{k'h} \right\}. \qquad (4.7.13)$$

Provided $\mathrm{Re}(\bar{Z}_{\omega'})$ remains effectively constant (small ω_i/ω) the first term vanishes as $n \to \infty$ and $\mathrm{Re}(k_x'/k')$ is obtained from the second term, being of the same sign as $\mathrm{Im}(k_x'/k')$. As ω_i/ω increases, Figure (4.28) shows that this equation is no longer valid; $\mathrm{Re}(k_x'/k') \to \pm 1$ and the solution is 'cut-on'. It is suggested that the inclusion of a small but necessarily finite inertia term in the impedance does not affect these trends and, if anything, hastens the convergence of $\mathrm{Re}(k_x'/k') \to \pm 1$, as $\omega_i/\omega \to \infty$. The 'cut-on' solutions (0+) and (0-) for $\omega_i/\omega = 0$ remain 'cut-on' as $\omega_i/\omega \to \infty$ and with two exceptions, all the other solutions converge to these as $\omega_i/\omega \to \infty$. The behaviour of the imaginary parts of these solutions is shown in Figure (4.29), in the form of $(k_x'h)$, indicating that

$$\mathrm{Im}(k_x'h) \to \mathrm{Im}(k'h)$$

for all but two solutions, and thus confirming that

$$\frac{k_x'}{k'} \to \pm 1, \qquad \text{as} \quad \omega_i/\omega \to +\infty.$$

This trend is summarised in Figure (4.27), that is, the movement of poles towards the point $\theta' = \pm \pi/2$ $(k_x'/k' \equiv \sin\theta')$ as $\omega_i/\omega \to +\infty$.

The behaviour of the (1-) and (2+) poles is totally different. The appropriate approximate solution for the (1-) mode is given by equation (4.6.14b)

$$\frac{k_x'}{k'} \doteq \frac{2(1 - M_x^2)}{M_x} \pm i\,\frac{(1 - M_x^2)^{3/2}}{M_x^2}\,\bar{Z}_{\omega'} \qquad (4.7.14)$$

where a further approximation has been made by assuming $2M_x^2 \ll (1 - M_x^2)\bar{Z}_\omega^2$. As noted in the previous section, if $\bar{Z}_\omega$ is real and $M_x > 0$ only the negative sign can be used in this solution <u>if k' is real</u>. In the present example $\bar{Z}_\omega$ is nearly real and $M_x > 0$ and thus one value is obtained for $k' = k$:

$$\frac{k_x'}{k} = 4.27 - i9.09 \qquad (4.85 - i8.96)$$

which is in reasonable agreement with the exact value given in brackets. For certain complex frequencies both signs can be used and with $\bar{Z}_\omega = 4.5$,

$$\frac{k_x'}{k'} = 3.0 \pm i11.7$$

which correspond to the actual solutions for the (1-) and (2+) poles

$$\frac{k_x'}{k'} = 3.88 \pm i12.02.$$

Mathematically the significance of the (1-) pole is that as $\omega_i/\omega \to 0$ it remains at a fixed location on the θ' plane as the contour approaches, and hence the contour must be deformed around it. Physically its important feature, the one which indicates that it represents an amplifying mode, is that the imaginary parts of k_x' and k_x <u>change sign</u> as ω_i/ω is reduced from $+\infty$ to 0, as is shown in Figure (4.29) (for k_x'). It is not difficult to confirm, from equation (4.7.14), that this change of sign must occur at approximately $\omega_i/\omega = 3$ in the present case.

It is clearly no coincidence that the approximate solution, given by equation (4.7.14) which closely describes the behaviour of the unstable solution, is nothing more than the compressible equivalent of the well known solution for incompressible modified Helmholtz

instabilities in the presence of a single absorptive wall. Unfortunately the present limited study does not provide a sufficient basis for concluding that duct instabilities can always be recognised with the aid of equation (4.7.14). For the present the somewhat tedious pole/contour tracking procedure must be carried out as ω_i/ω is varied over a specified range.

With regard to the convergence of the infinite sum

$$\sum_{\ell=0}^{\infty} X^{\ell}; \quad X = C_r' \exp\left[2ik'h \cos \theta'\right]$$

on the θ' contour corresponding to $\omega_i/\omega \to +\infty$, it is interesting to note that as the impedance is then infinite $|C_r| \to 1$, and as $\mathrm{Im}(k') \to +\infty$, $|X|$ is zero everywhere on the contour except at the point $\theta' = 0$ when $|X| \to 1$. Thus there is no doubt as to the convergence of the infinite sum on this contour. This could prove a useful starting point for an attempt to prove that convergence still exists on the contour, for any value of ω_i/ω, including the value zero.

4.7.5 Conclusions

The conclusion drawn from the discussion of temporal instabilities is that the new Green's function (for uniform flow) obtained in section (4.4) is only correct if it can be shown that no instabilities exist for the given values of reduced frequency, wall impedance (including frequency dependence) and Mach number. If instabilities are present the analysis of section (4.4) is incorrect because a steady state has been assumed to exist throughout the interior of the duct ($-\infty < x < \infty$), with $|G_{\omega'}| \to 0$ as $|x' - \bar{x}_0'| \to \infty$, as a result of continuous operation of the source, at a particular frequency for all time. The correct procedure is to start, or switch on, the source at a specified time and allow the

instabilities to develop. If the instabilities are of the convective type it is then still possible to describe the field in terms of modes decaying or amplifying away from the source, at the source frequency, in the asymptotic limit $t \to +\infty$

The practical implications of this result and, indeed, its relevance to practical situations at all, are discussed in the final chapter.

Finally it is worth making the perhaps obvious point that the significance of the 'strange' modes is now clear: in general, despite the fact that both types of phase velocity $(\omega/\mathrm{Re}(k_x), \omega/\mathrm{Re}(k_x'))$ can be in the opposite direction to that of decay, these modes are simply the 'cut-off' modes in uniform flow. In the present example there is one exception to this interpretation: this is a mode which in the steady state analysis of section (4.4) would be identified as a 'strange' mode, decaying in the upstream direction, but which is now recognised as a spatially amplified mode propagating in the downstream direction.

APPENDIX 4A

The Multiple Image Ray Model for the (Duct) Green's Function (Uniform Line Source) in Uniform Flow.

The Green's function, G_ω, with time-dependence $\exp[-i\omega t']$ in the Lorentz frame of reference is given by an appropriate solution of equation (4.3.3) which is

$$G(x', y'/\bar{x}_o', y_o') = \gamma \frac{i}{4} H_o^{(1)}(kR') \exp[-ikM_x(x' - \bar{x}_o')]$$

where $R' = \{(x' - \bar{x}_o')^2 + (y' - y_o')^2\}^{\frac{1}{2}}$.

This multiple image model is described by equations (3.2.10)-(3.2.13), with the factors $\exp[ikR]/4\pi R$ in equation (3.2.10) replaced by the above expression and the reflection coefficients, C_r, by

$$C_r' = \frac{\cos\theta' - \bar{\beta}_\omega \gamma^3 (1 - M_x \sin\theta')^2}{\cos\theta' - \bar{\beta}_\omega \gamma^3 (1 - M_x \sin\theta')^2}.$$

The coordinates x, y, etc. in those equations are replaced by x', y', etc.

APPENDIX 4B

The method used to obtain the exact branch point solutions for uniform flow

The branch points are solutions of (equation (4.5.1)):

$$f\{(k_y h), M_x\} = 0$$

where

$$f \equiv \frac{d}{d(k_y h)} \{(1 - \frac{k_x M_x}{k})^{-2}(k_y h) \tan(k_y h)\}.$$

The solution is known for $M_x = 0$ (see Appendix 2A) and by using this as a starting value, the exact solution is obtained by iteration, for some finite value of M_x, by using the standard Newton-Ralphson scheme:

$$(k_y h)_{n+1} = (k_y h)_n - \frac{f[(k_y h)_n]}{f'[(k_y h)_n]}$$

where

$$f' \equiv \frac{df}{d(k_y h)} .$$

Convergence of this iteration can always be obtained for a sufficiently small value of M_x. Once the exact solution is found the M_x value is incremented and the procedure is repeated.

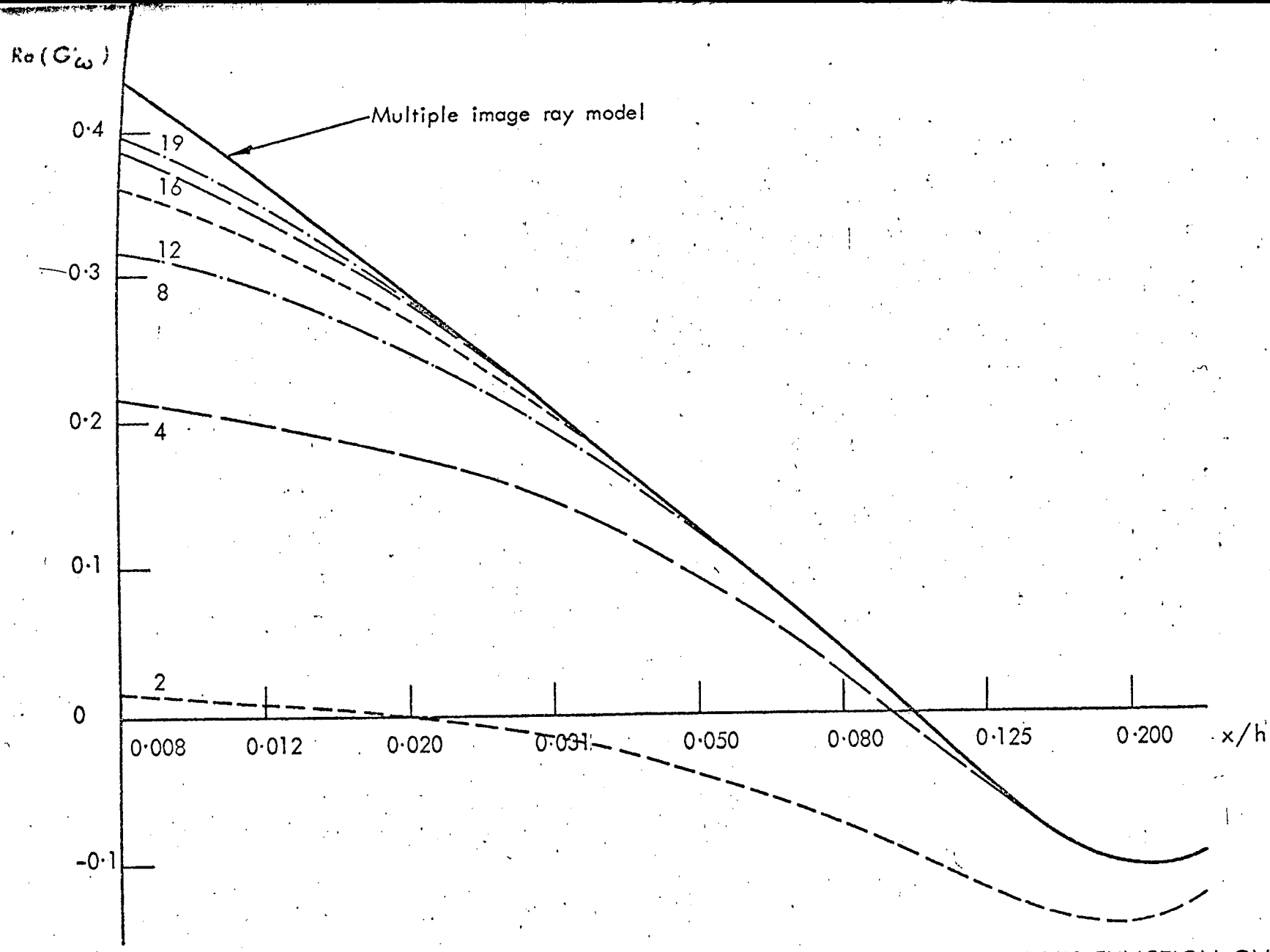

FIG. 4.1a COMPARISON OF 'RAY' GREEN'S FUNCTION AND 'MODE' GREEN'S FUNCTION ON CENTRE-LINE, FOR VARIABLE NUMBER OF MODES, AT $M_x = 0{\cdot}0$.

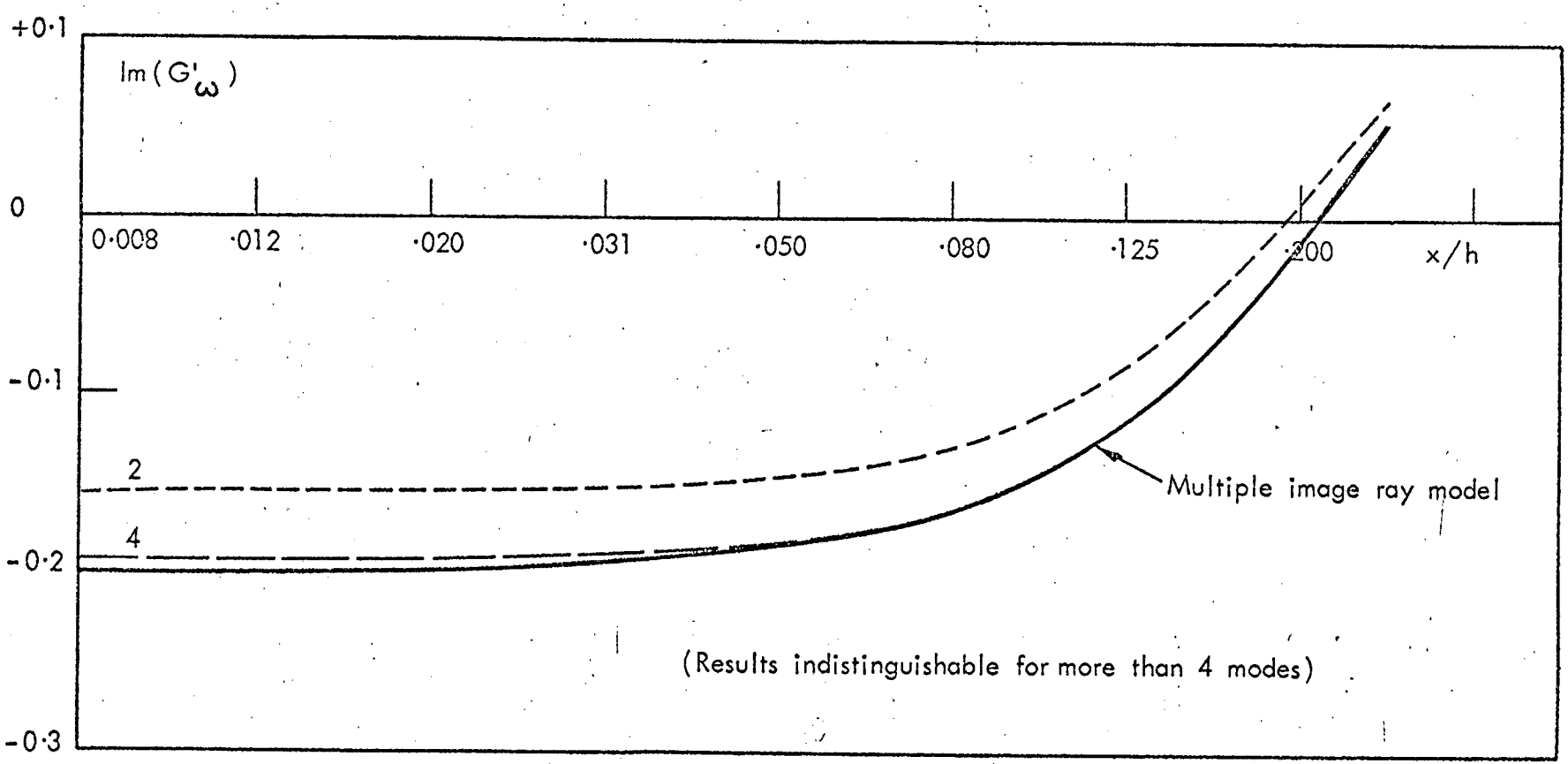

FIG. 4.1b COMPARISON OF 'RAY' GREEN'S FUNCTION AND 'MODE' GREEN'S FUNCTION ON CENTRE LINE, FOR VARIABLE NUMBER OF MODES, AT $M_x = 0{\cdot}0$.

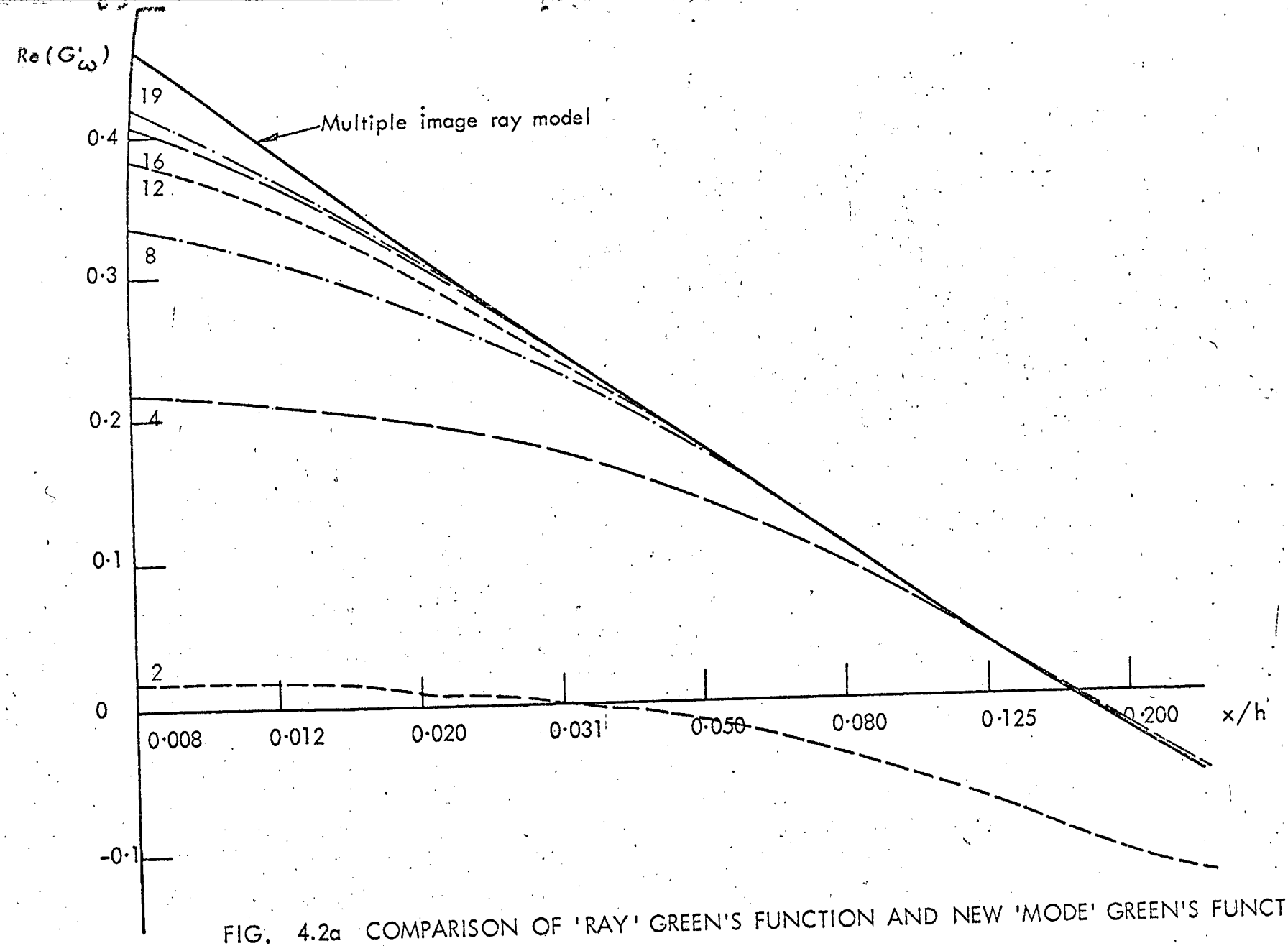

FIG. 4.2a COMPARISON OF 'RAY' GREEN'S FUNCTION AND NEW 'MODE' GREEN'S FUNCTION ON CENTRE-LINE FOR VARIABLE NUMBER OF MODES, AT $M_x = +0{\cdot}4$.

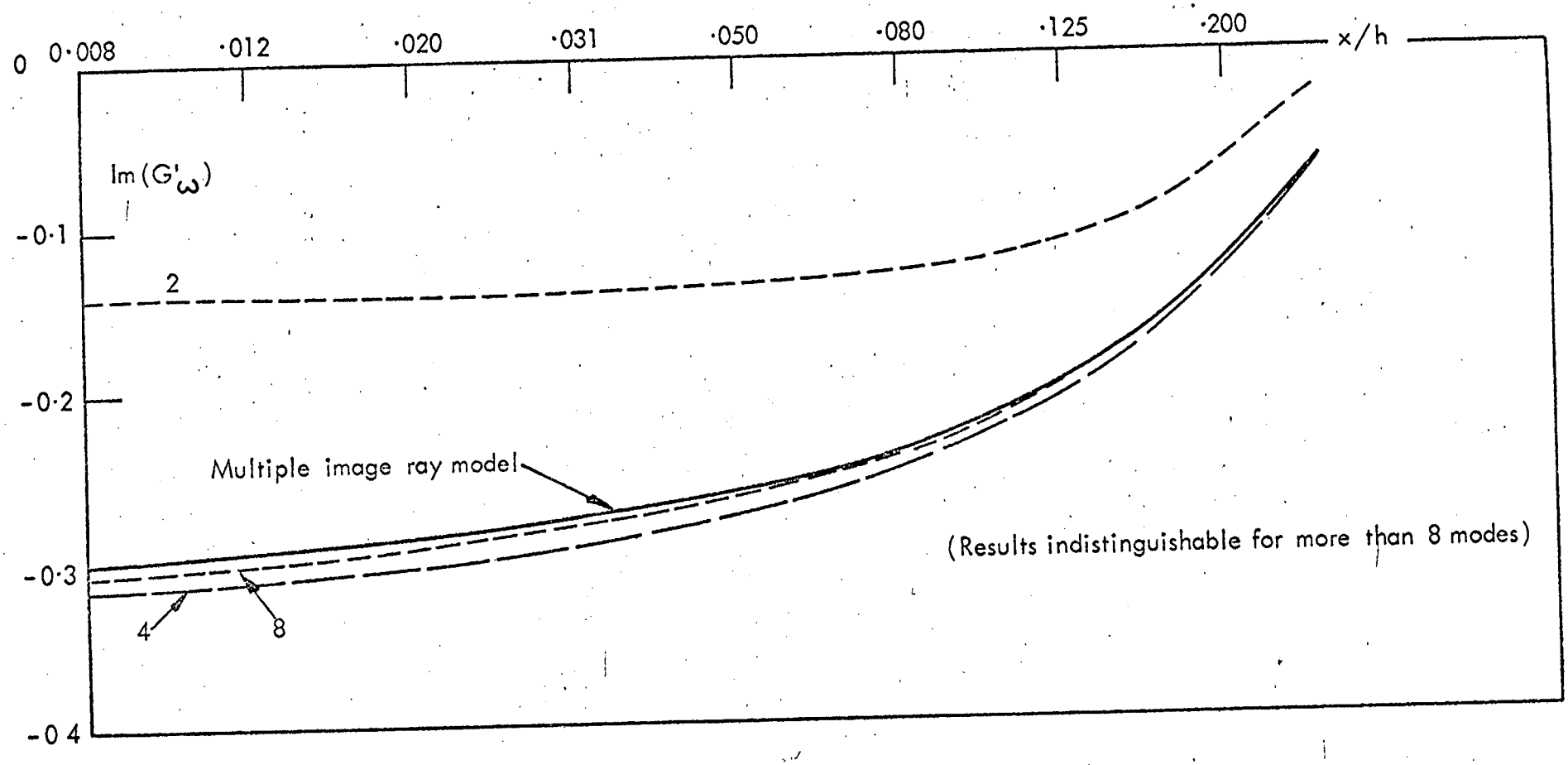

FIG. 4.2b COMPARISON OF 'RAY' GREEN'S FUNCTION AND NEW 'MODE' GREEN'S FUNCTION ON CENTRE-LINE, FOR VARIABLE NUMBER OF MODES, AT $M_x = +0{\cdot}4$.

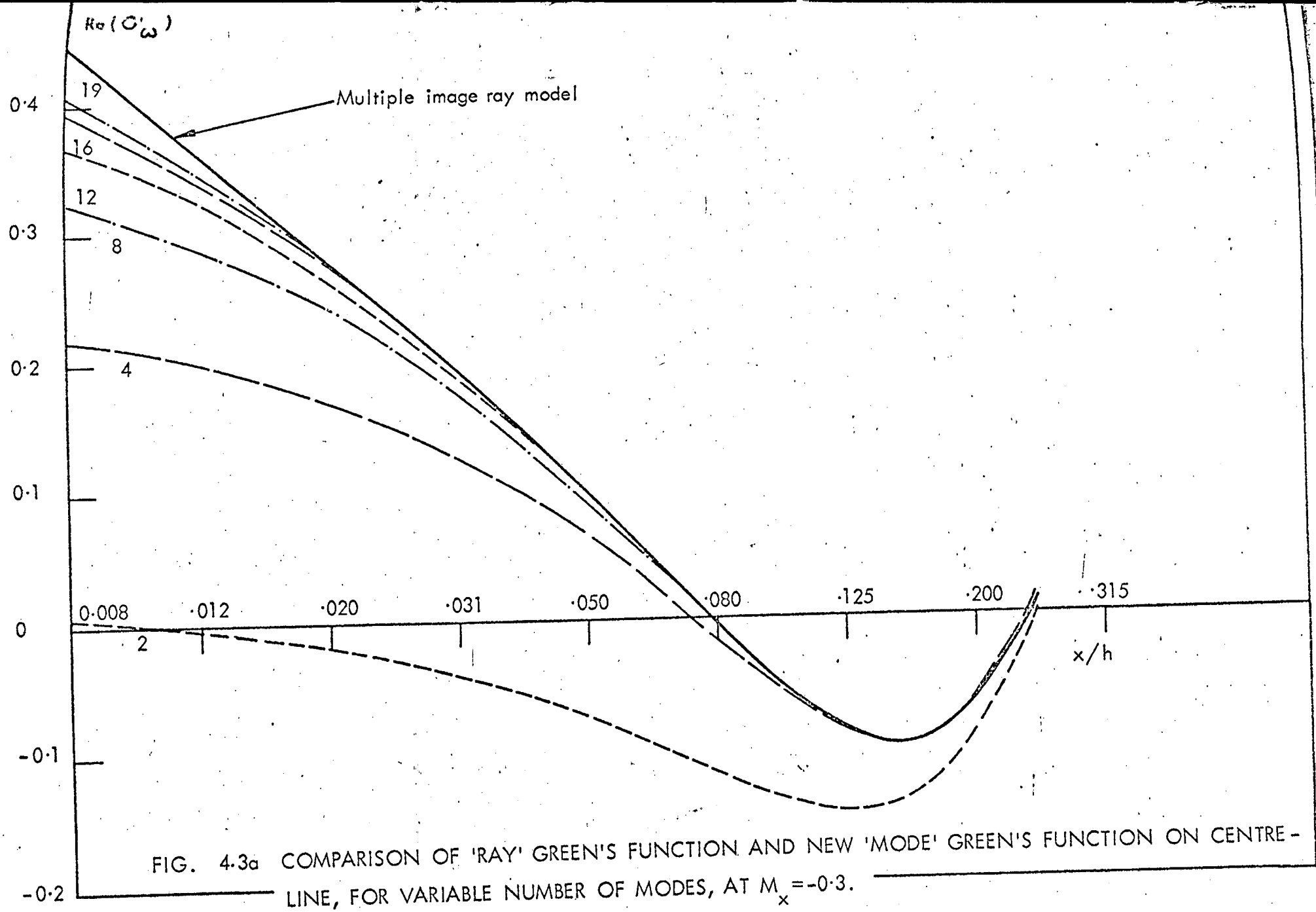

FIG. 4·3a COMPARISON OF 'RAY' GREEN'S FUNCTION AND NEW 'MODE' GREEN'S FUNCTION ON CENTRE-LINE, FOR VARIABLE NUMBER OF MODES, AT $M_x = -0{\cdot}3$.

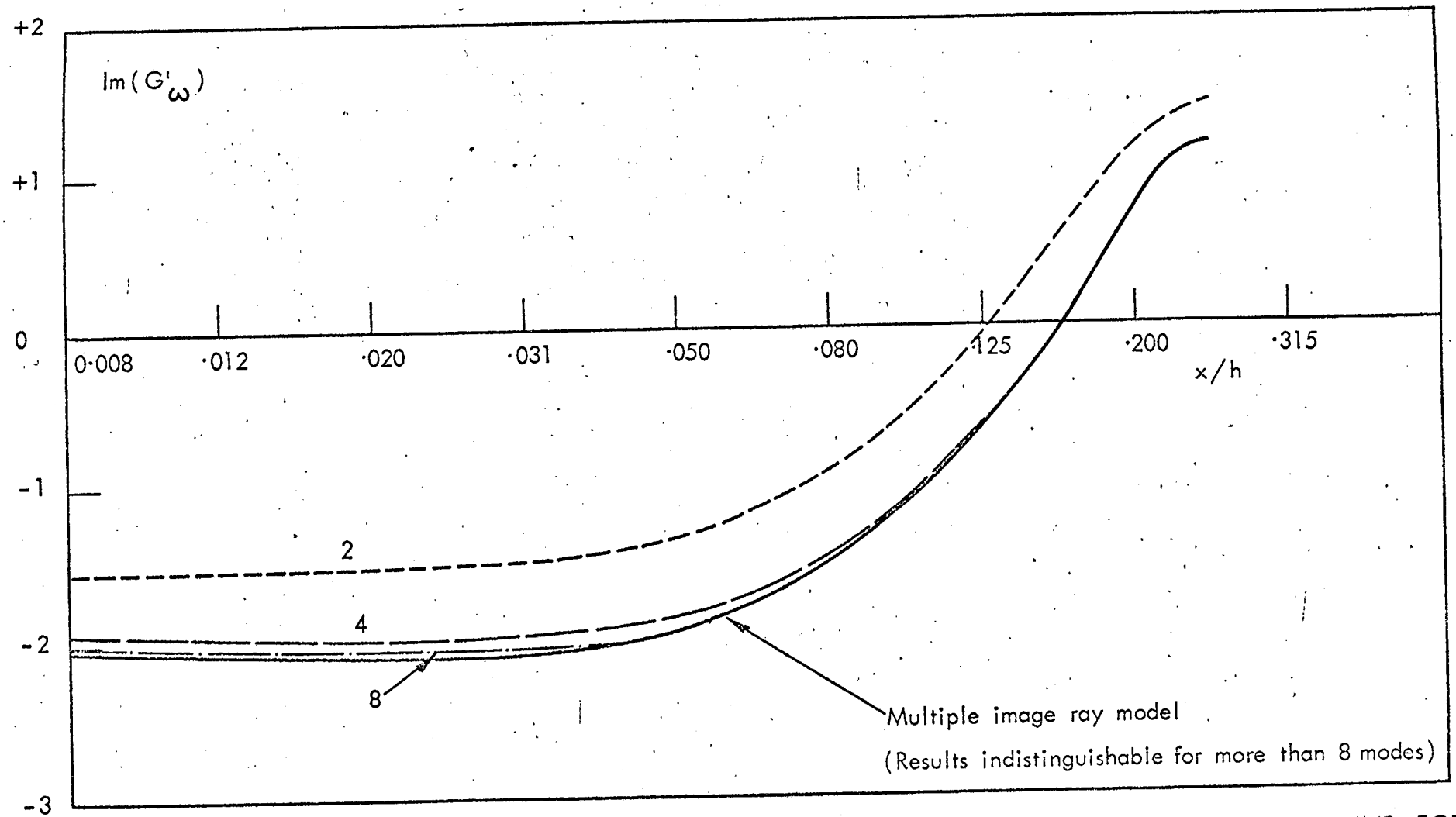

FIG. 4.3b COMPARISON OF 'RAY' GREEN'S FUNCTION AND NEW 'MODE' GREEN'S FUNCTION ON CENTRE-LINE, FOR VARIABLE NUMBER OF MODES, AT $M_x = -0{\cdot}3$

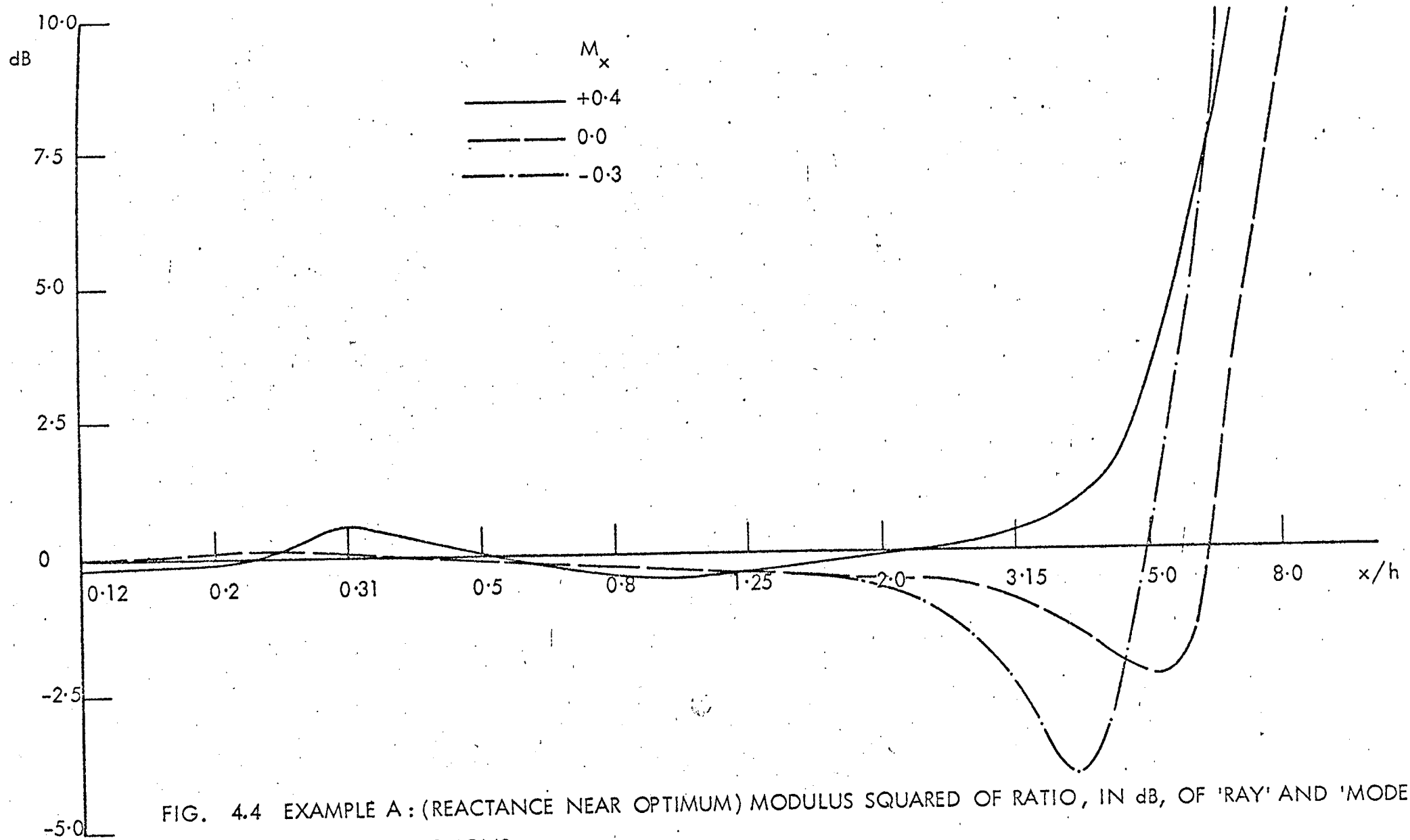

FIG. 4.4 EXAMPLE A : (REACTANCE NEAR OPTIMUM) MODULUS SQUARED OF RATIO, IN dB, OF 'RAY' AND 'MODE' GREEN'S FUNCTIONS.

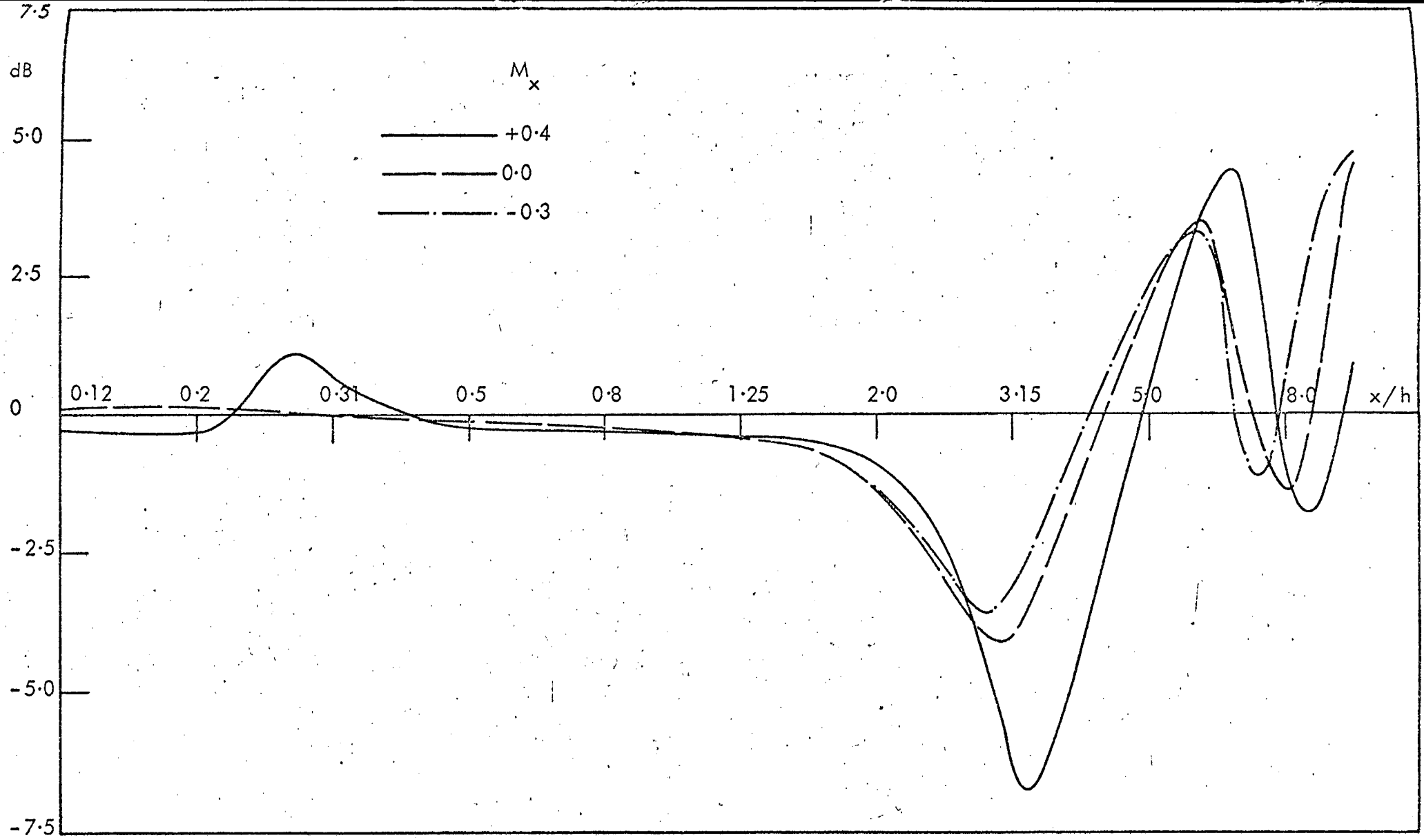

FIG. 4.5 EXAMPLE B : (REACTANCE MAGNITUDE LARGER THAN OPTIMUM) MODULUS SQUARED OF RATIO, IN dB, OF 'RAY' AND 'MODE' GREEN'S FUNCTIONS.

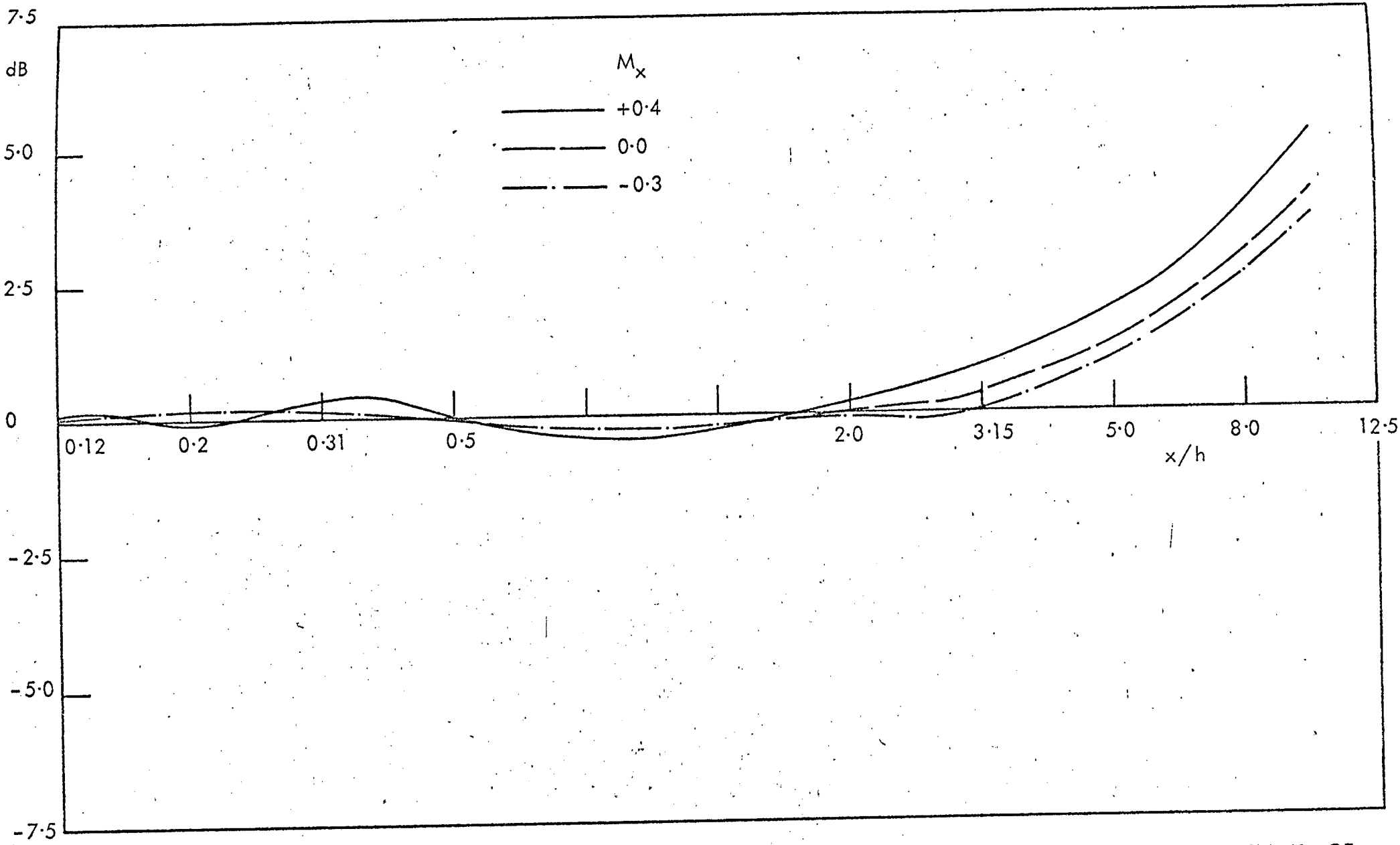

FIG. 4.6 EXAMPLE C : (REACTANCE MAGNITUDE SMALLER THAN OPTIMUM) MODULUS SQUARED OF RATIO, IN dB, OF 'RAY' AND 'MODE' GREEN'S FUNCTIONS.

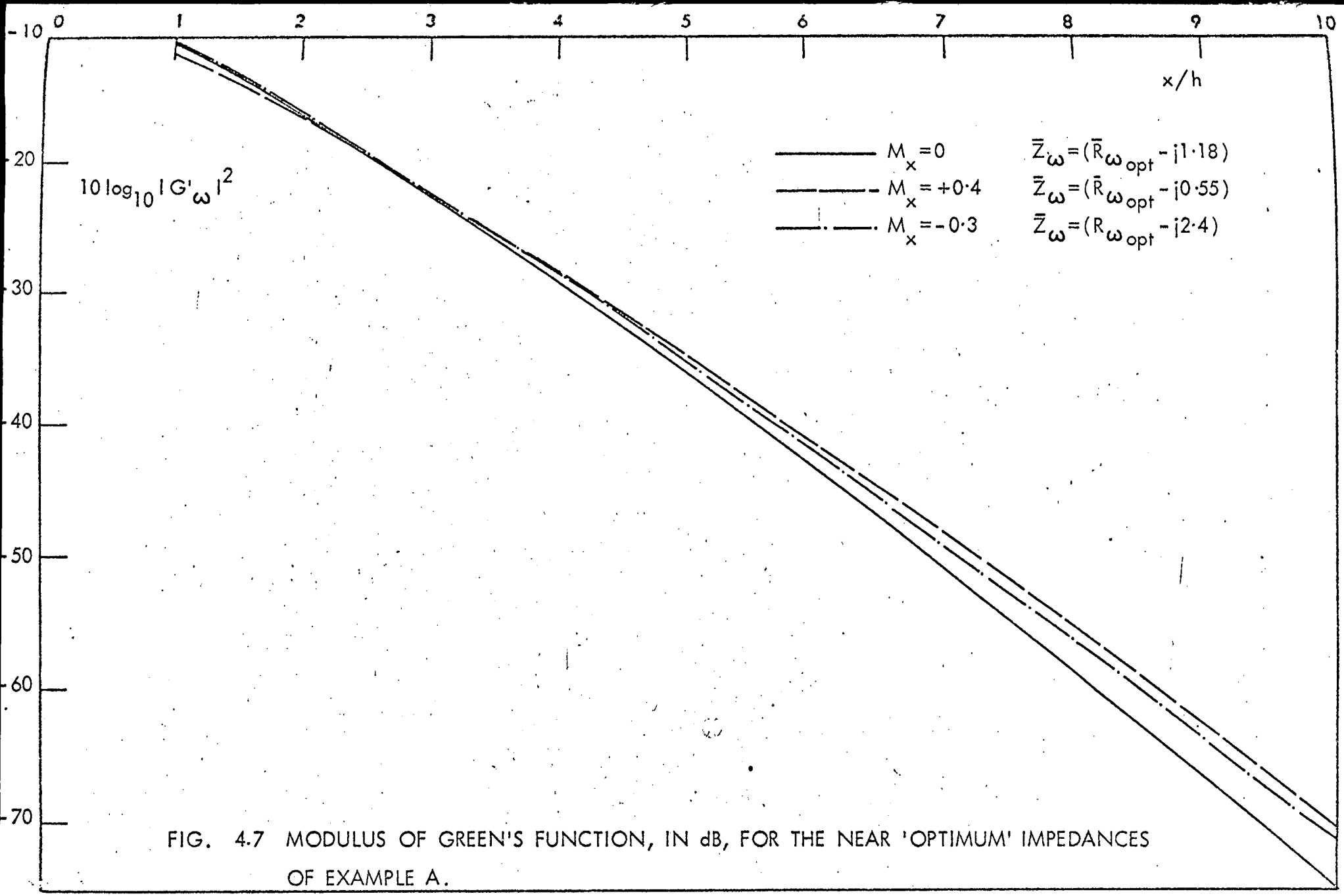

FIG. 4.7 MODULUS OF GREEN'S FUNCTION, IN dB, FOR THE NEAR 'OPTIMUM' IMPEDANCES OF EXAMPLE A.

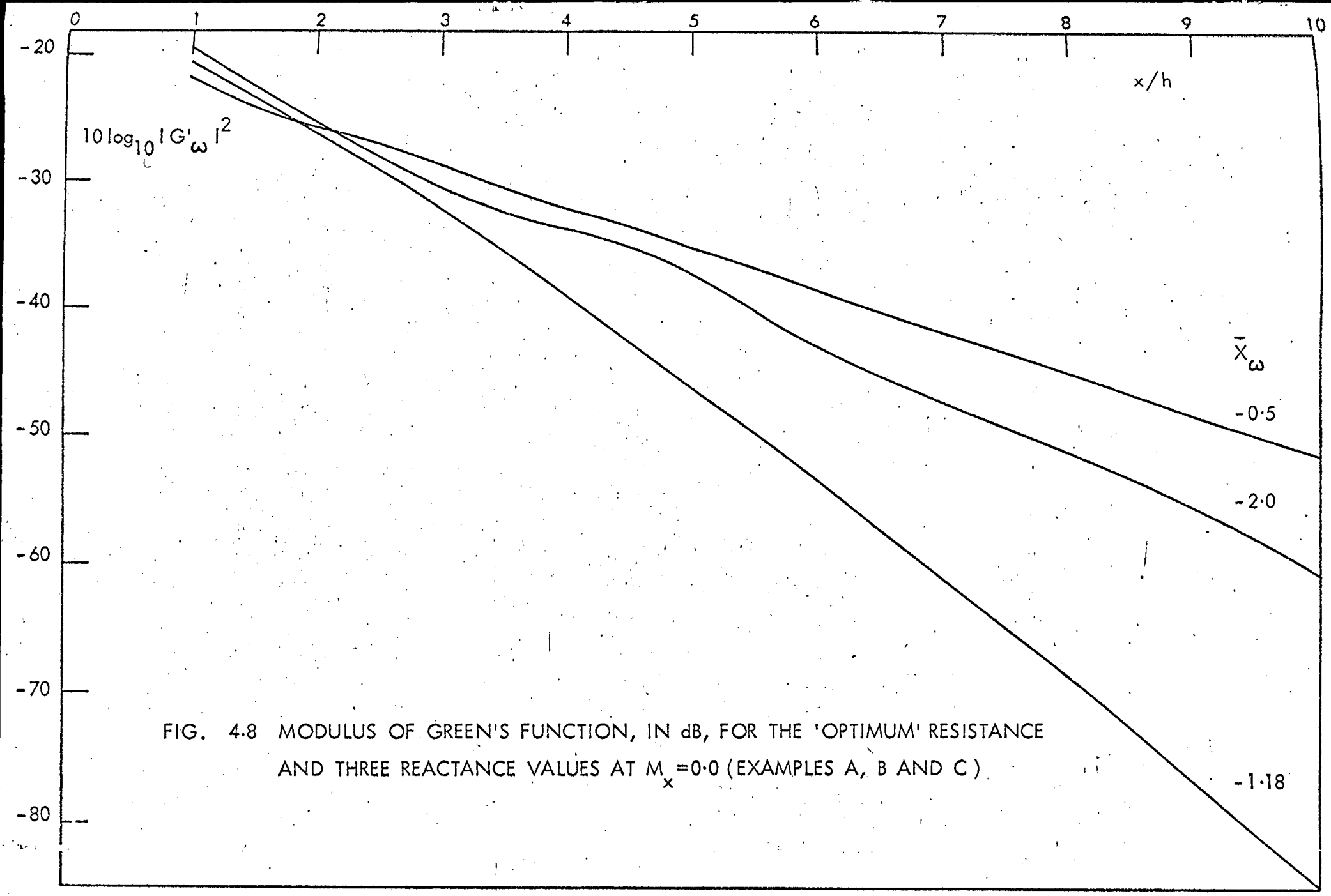

FIG. 4.8 MODULUS OF GREEN'S FUNCTION, IN dB, FOR THE 'OPTIMUM' RESISTANCE AND THREE REACTANCE VALUES AT $M_x = 0{\cdot}0$ (EXAMPLES A, B AND C)

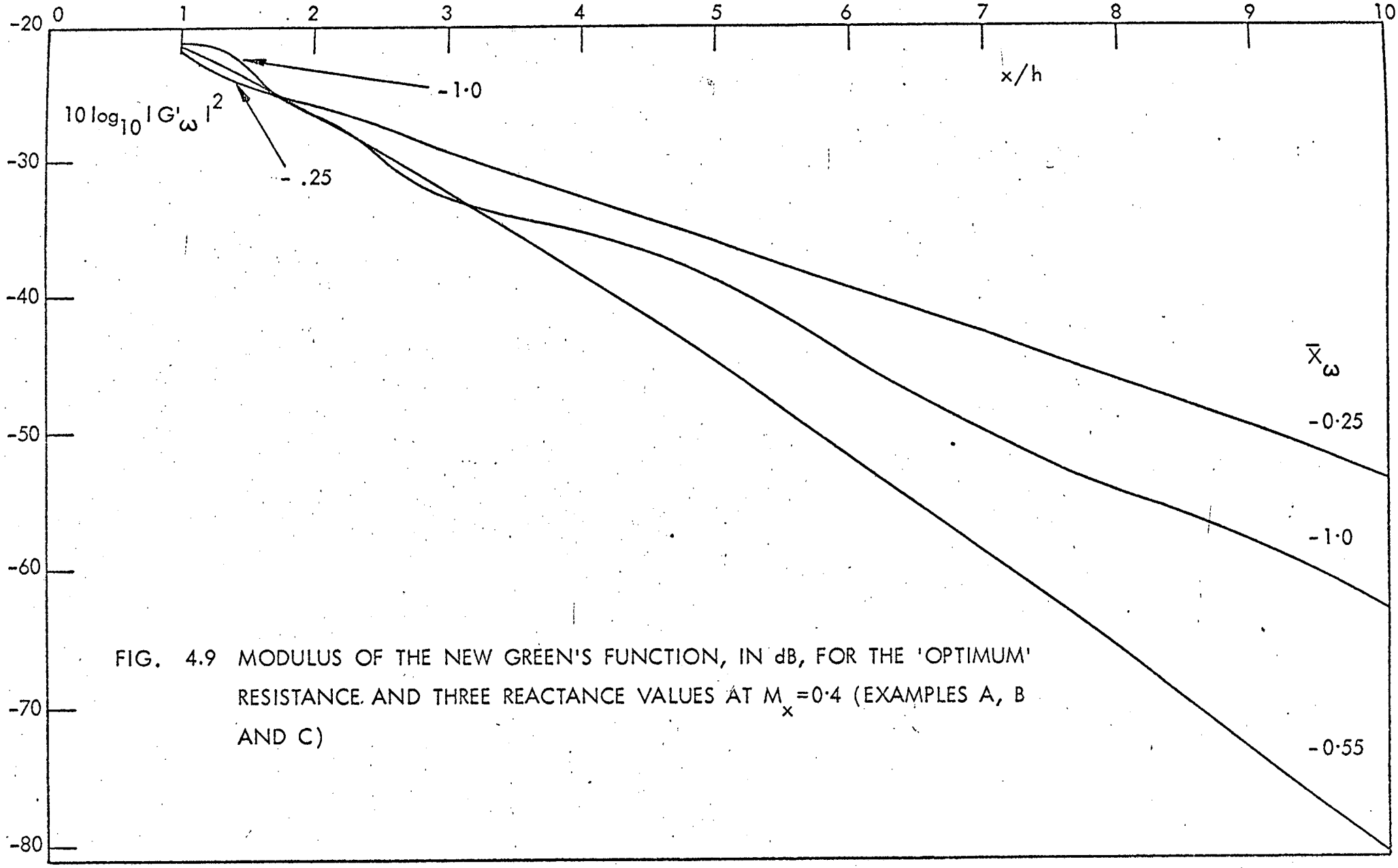

FIG. 4.9 MODULUS OF THE NEW GREEN'S FUNCTION, IN dB, FOR THE 'OPTIMUM' RESISTANCE AND THREE REACTANCE VALUES AT M_x=0·4 (EXAMPLES A, B AND C)

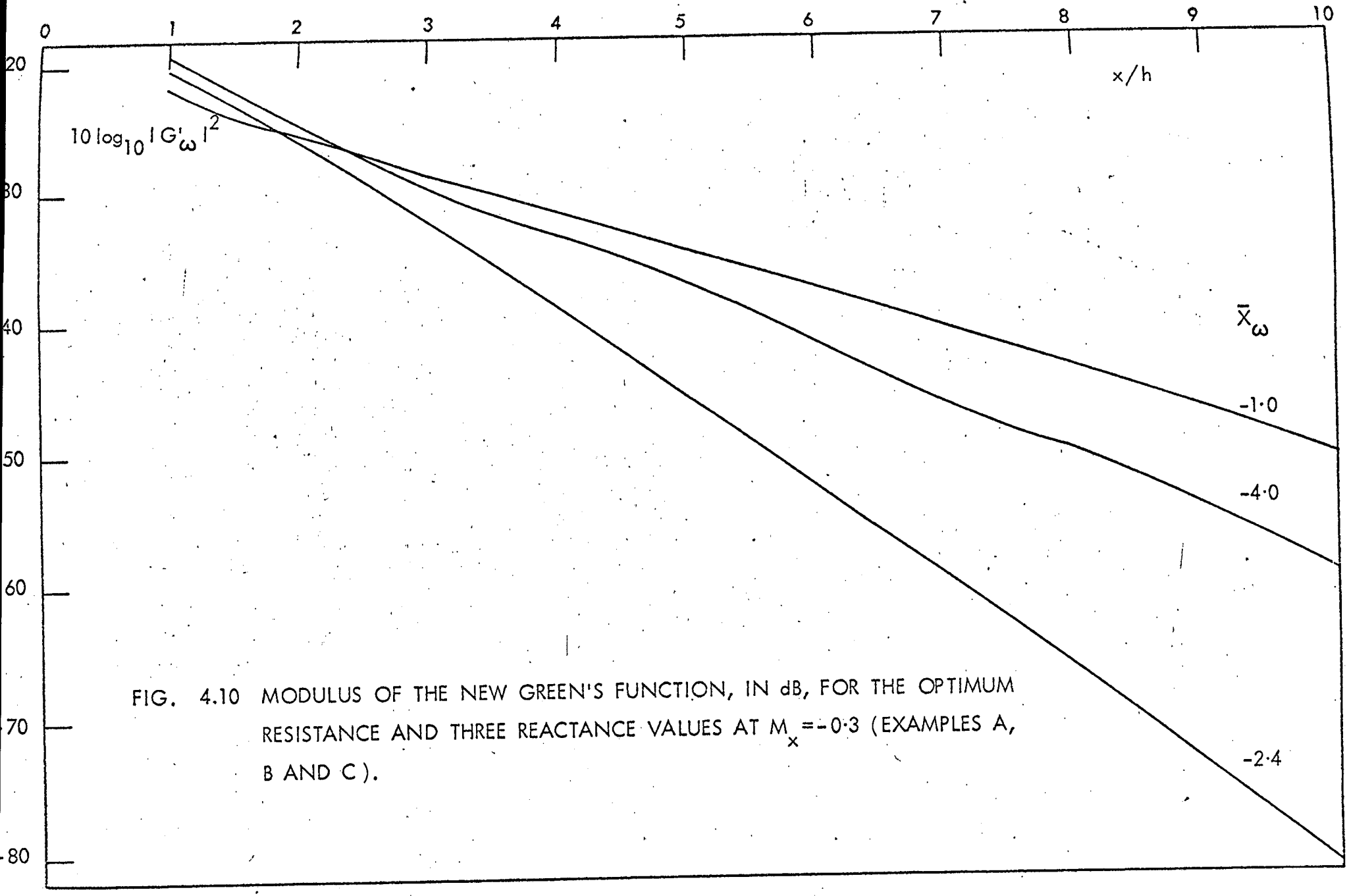

FIG. 4.10 MODULUS OF THE NEW GREEN'S FUNCTION, IN dB, FOR THE OPTIMUM RESISTANCE AND THREE REACTANCE VALUES AT $M_x = -0{\cdot}3$ (EXAMPLES A, B AND C).

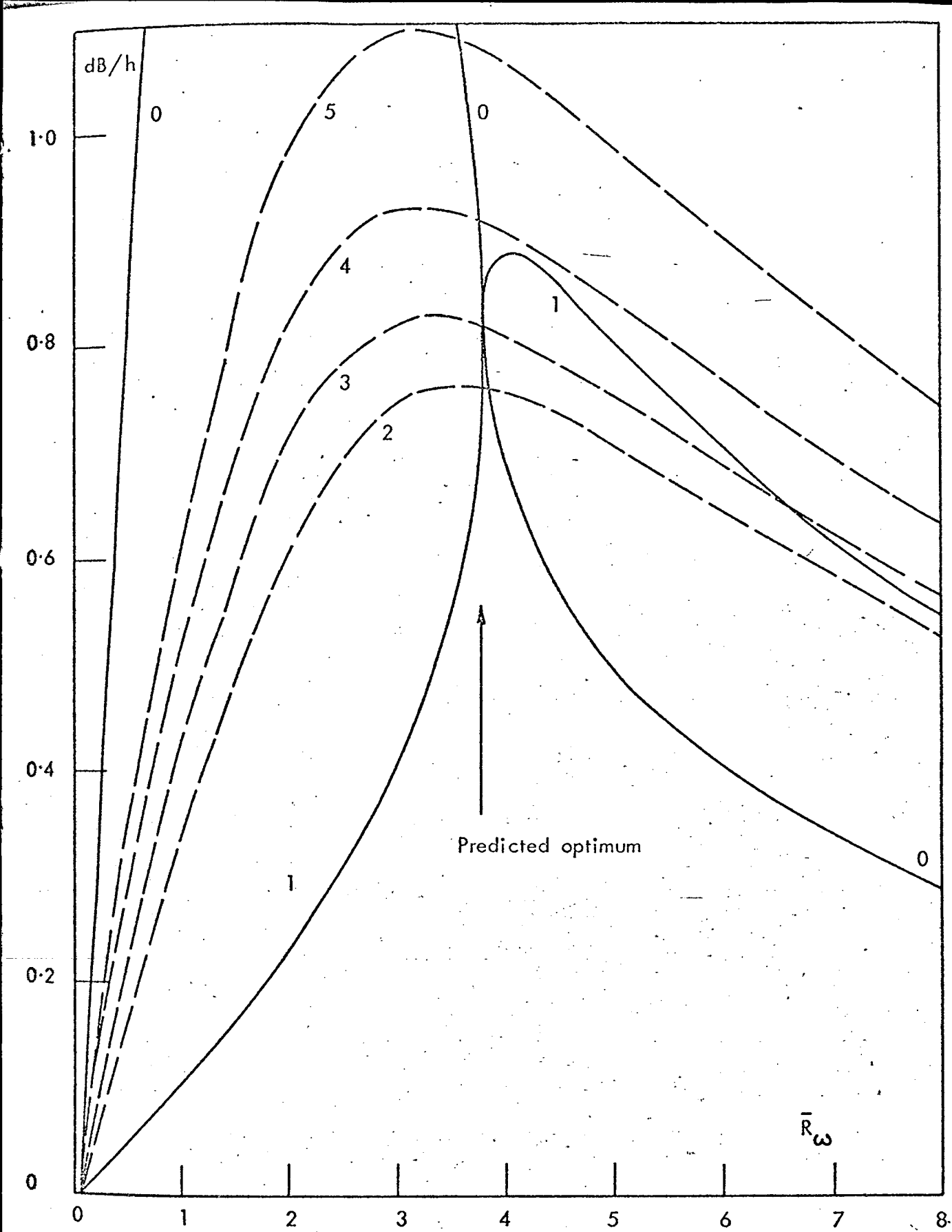

FIG. 4.11 VERIFICATION OF THE (0,1) OPTIMUM RESISTANCE, FOR $M_x = +0{\cdot}4$, AT $h/\lambda = 4$ (REACTANCE IS HELD CONSTANT AND EQUAL TO THE OPTIMUM VALUE).

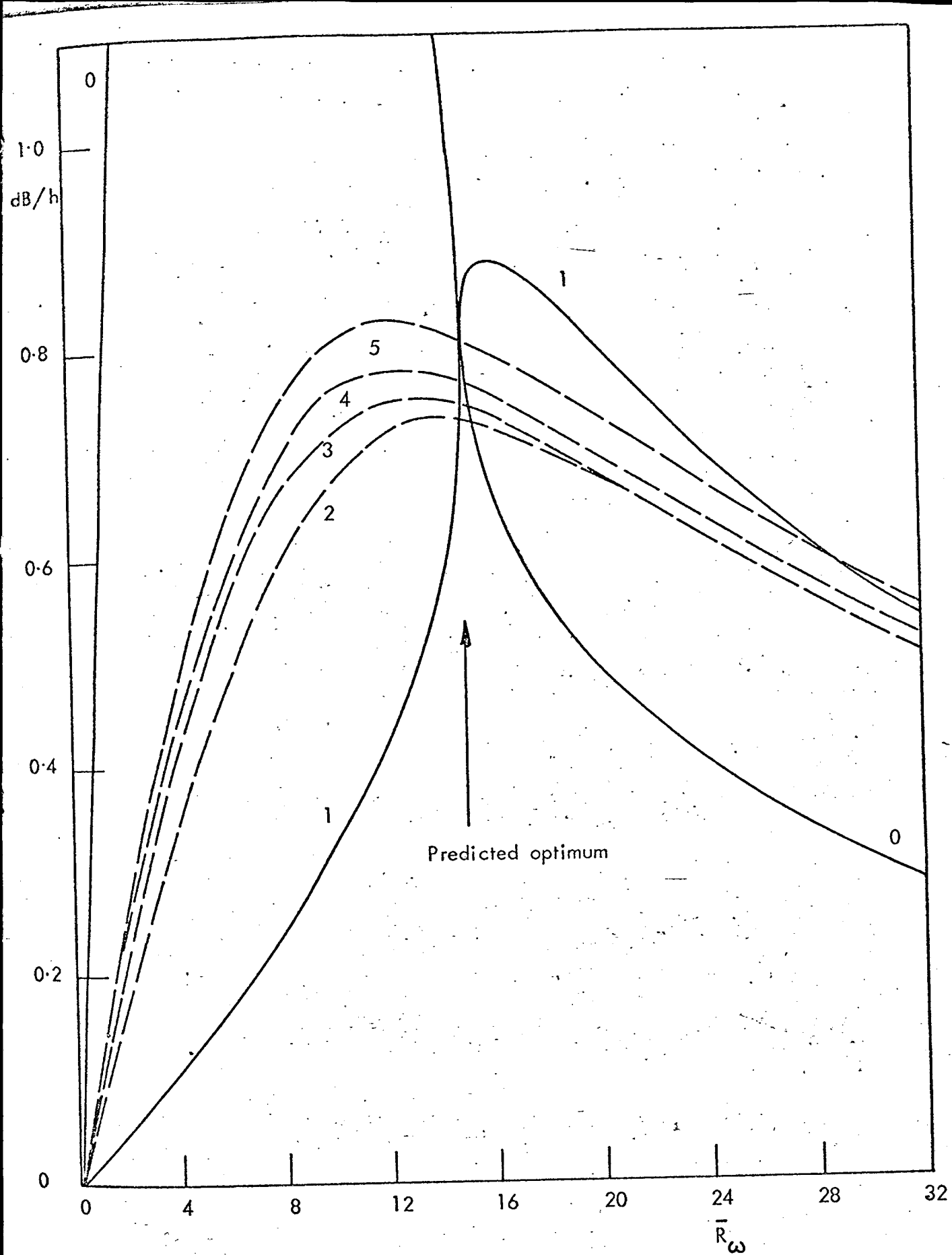

FIG. 4.12 VERIFICATION OF THE (0,1) OPTIMUM RESISTANCE, FOR $M_x = -0{\cdot}3$, AT $h/\lambda = 4$ (REACTANCE IS HELD CONSTANT AND EQUAL TO THE OPTIMUM VALUE).

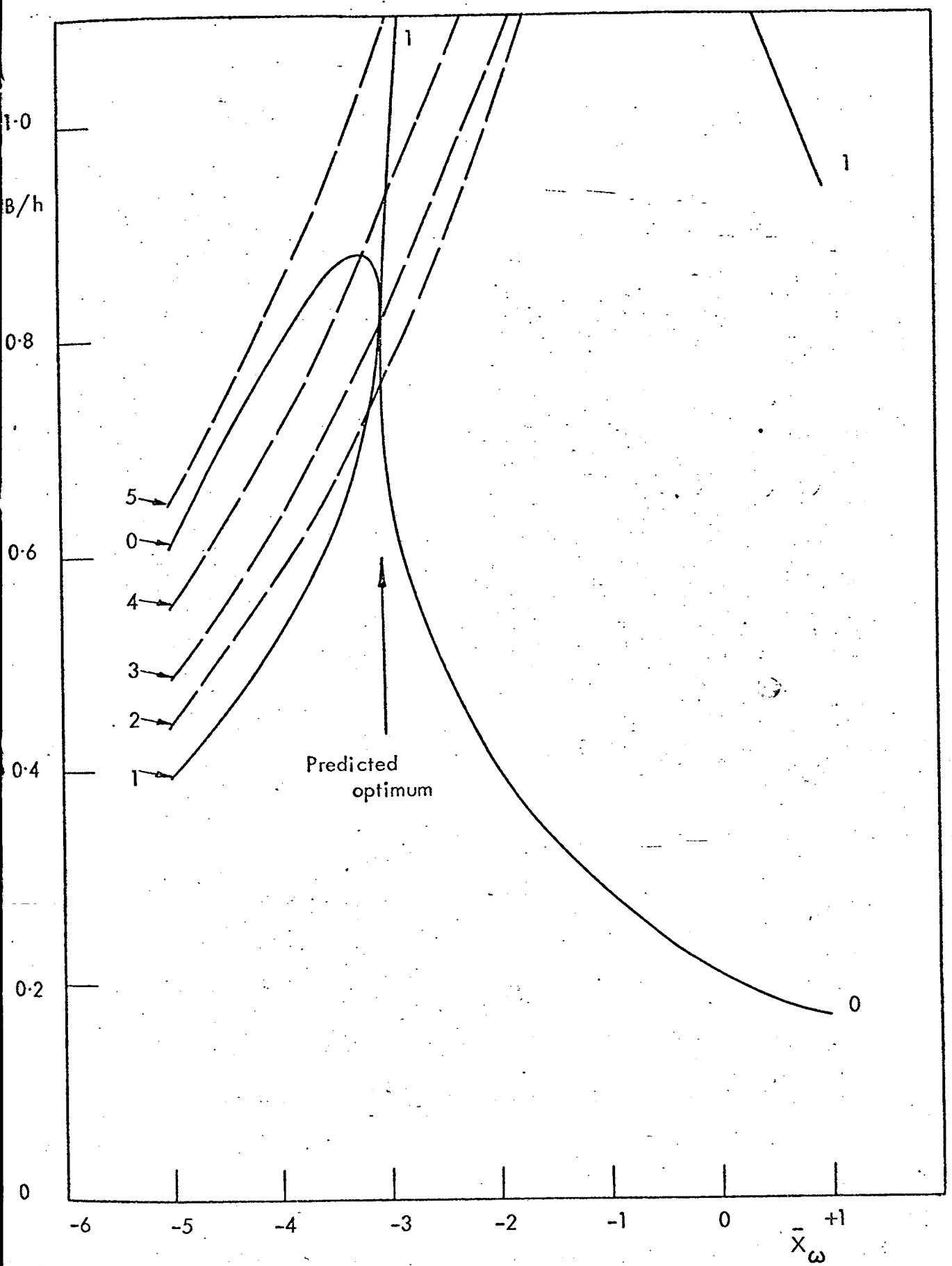

FIG. 4.13 VERIFICATION OF THE (0,1) OPTIMUM REACTANCE, FOR $M_x = +0{\cdot}4$, AT $h/\lambda = 4$ (RESISTANCE IS HELD CONSTANT AND EQUAL TO THE OPTIMUM VALUE)

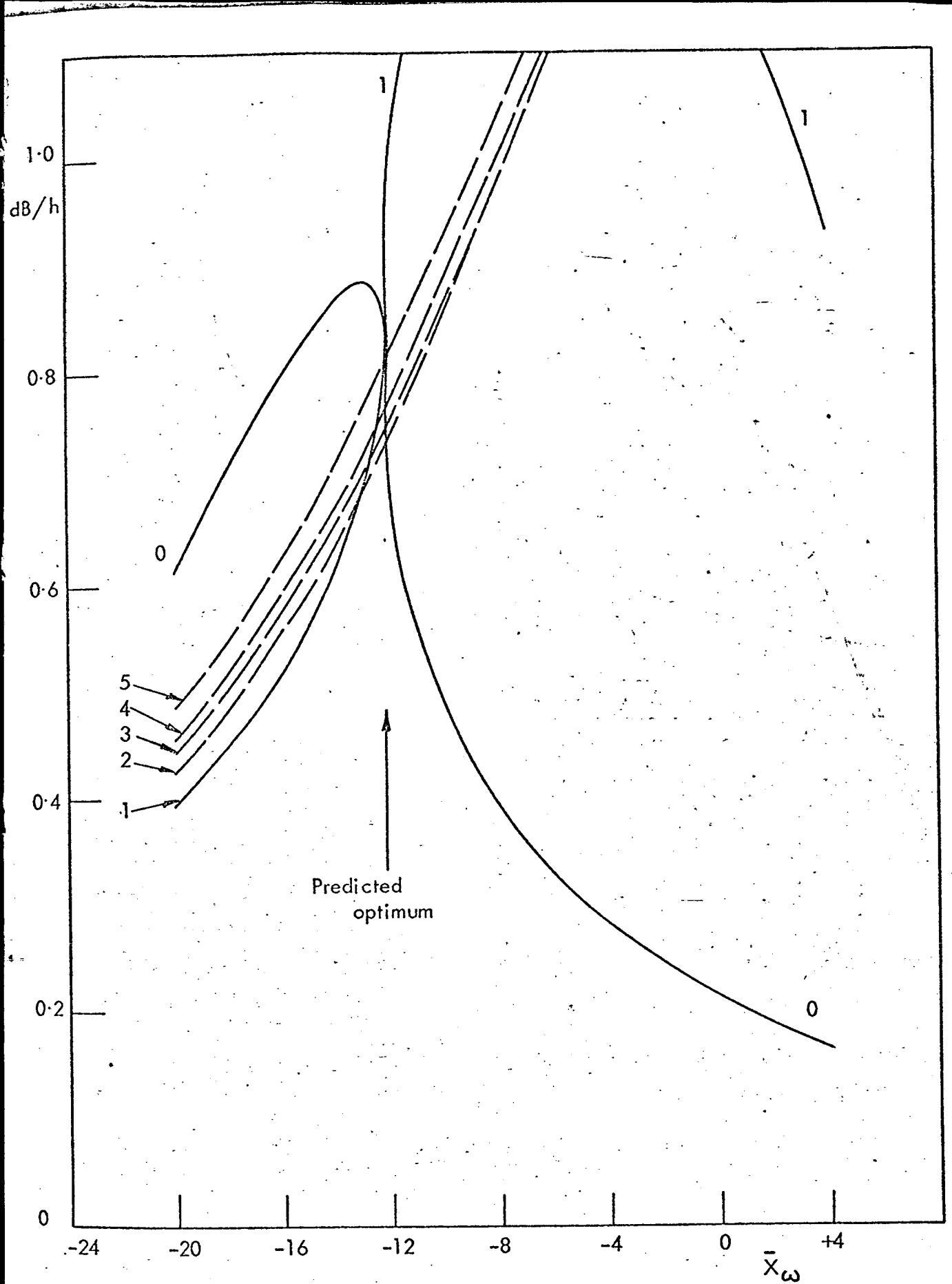

FIG. 4.14 VERIFICATION OF THE (0,1) OPTIMUM REACTANCE, FOR $M_x = -0{\cdot}3$, AT $h/\lambda = 4$ (RESISTANCE IS HELD CONSTANT AND EQUAL TO THE OPTIMUM VALUE).

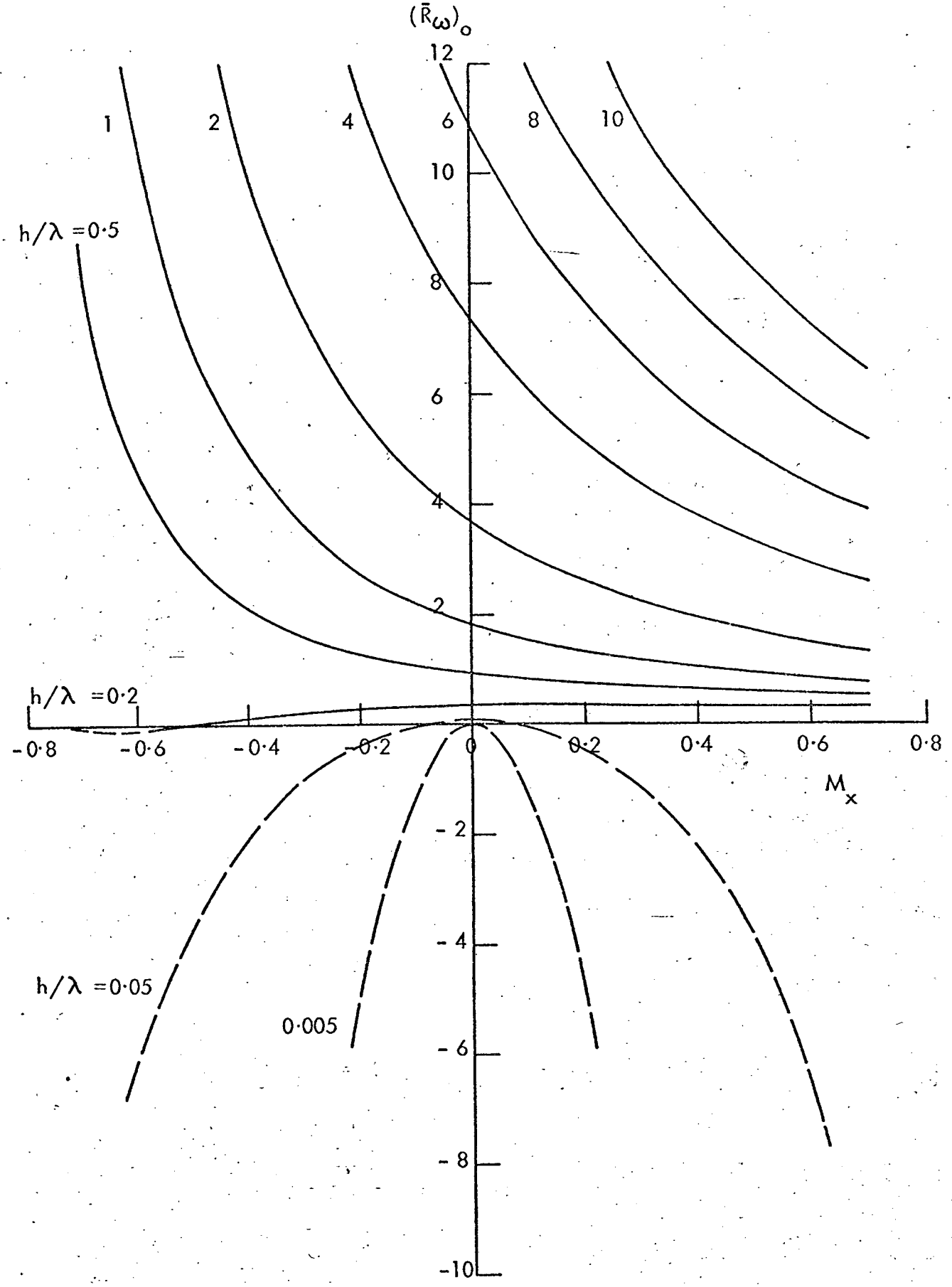

FIG. 4.15 VARIATION OF $(\bar{R}_\omega)_o$ WITH M_x AND h/λ ((0,1) MODE PAIR).

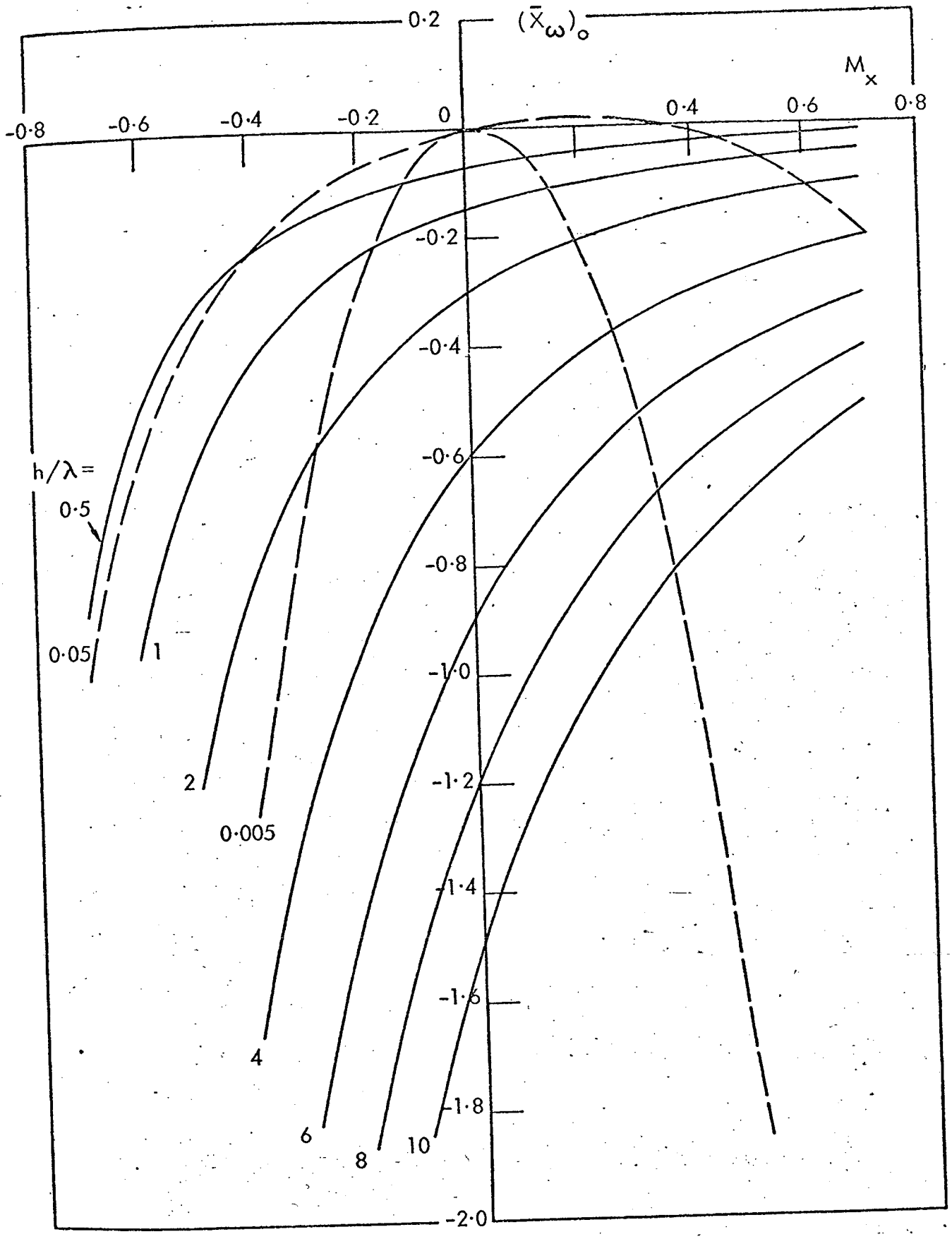

FIG. 4.16 VARIATION OF $(X_\omega)_o$ WITH M_x AND h/λ ((0,1) MODE PAIR).

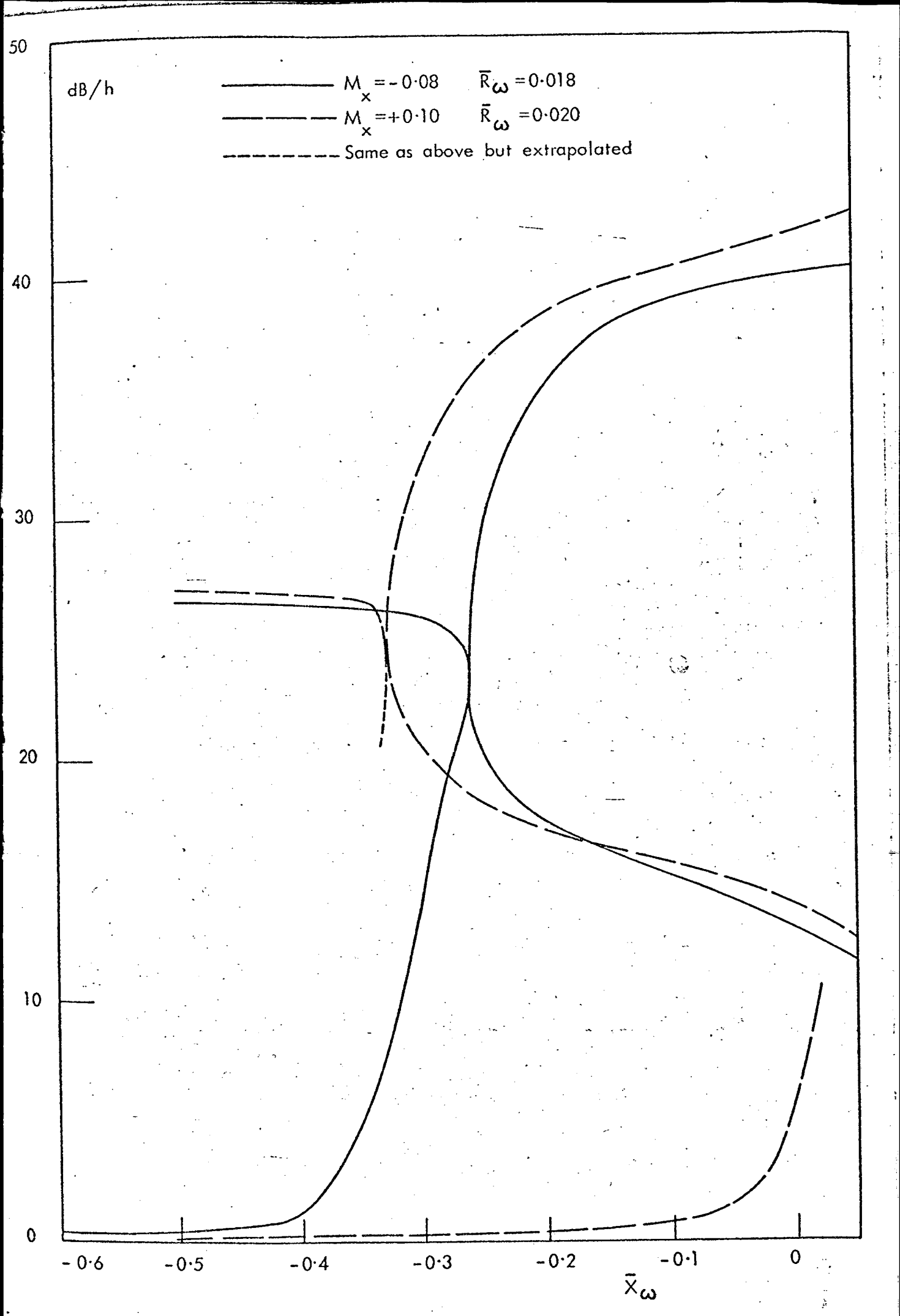
dB/h
$M_x = -0{\cdot}08$ $\bar{R}_\omega = 0{\cdot}018$
$M_x = +0{\cdot}10$ $\bar{R}_\omega = 0{\cdot}020$
Same as above but extrapolated
50
40
30
20
10
0
-0·6
-0·5
-0·4
-0·3
-0·2
-0·1
0
$\bar{X}_\omega$

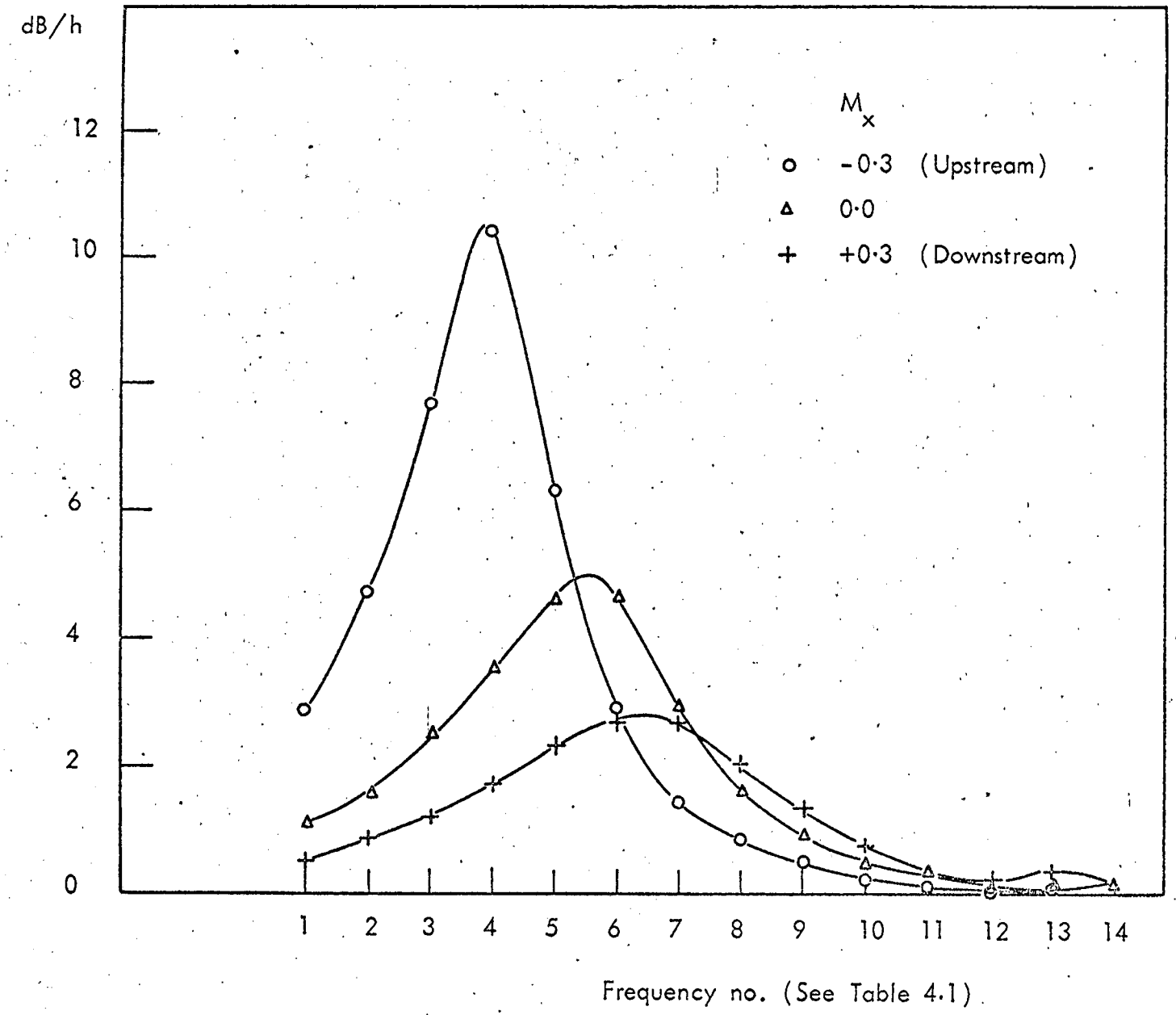

FIG. 4.18 CALCULATED LEAST DAMPED MODE ATTENUATIONS.

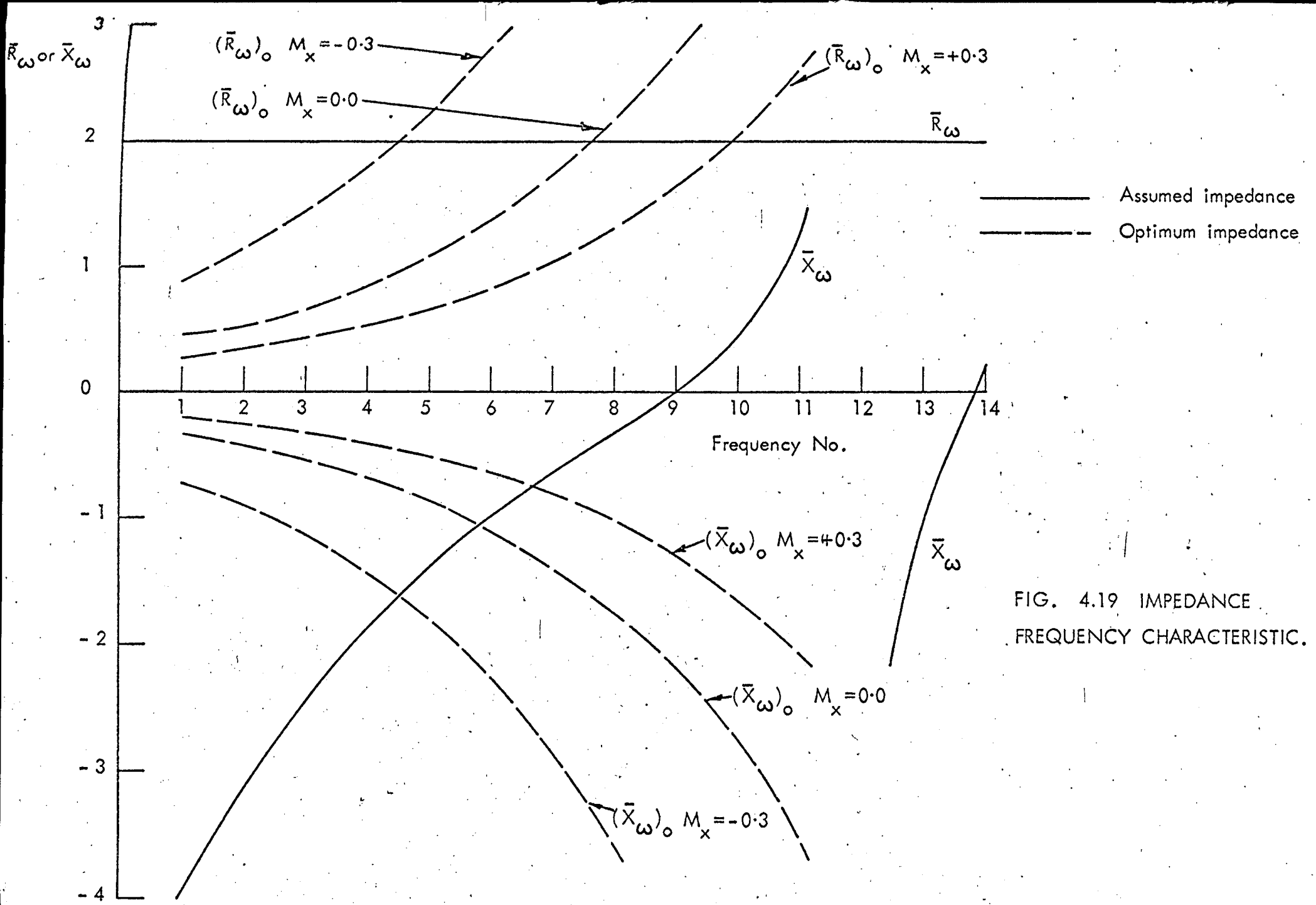

FIG. 4.19 IMPEDANCE FREQUENCY CHARACTERISTIC.

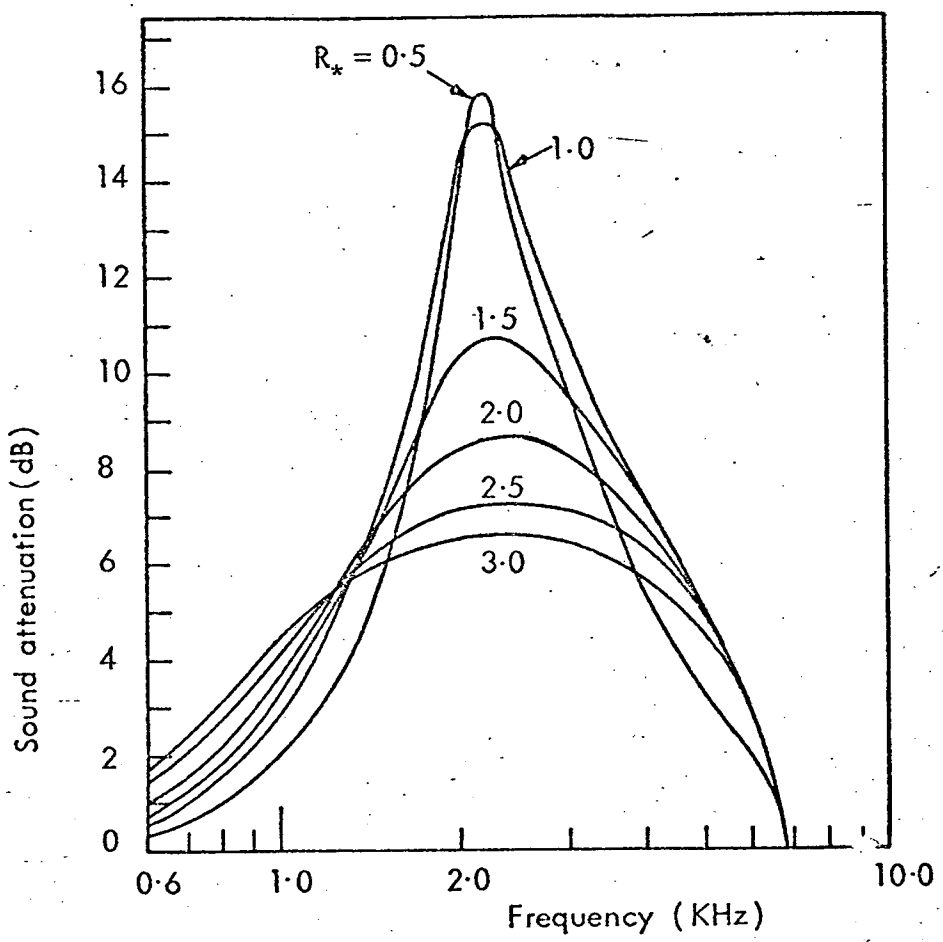

FIG. 4.20 TO DEMONSTRATE THAT MAXIMUM ATTENUATION OCCURS AT APPROXIMATELY THE SAME REACTANCE VALUE - AFTER Ko (30)

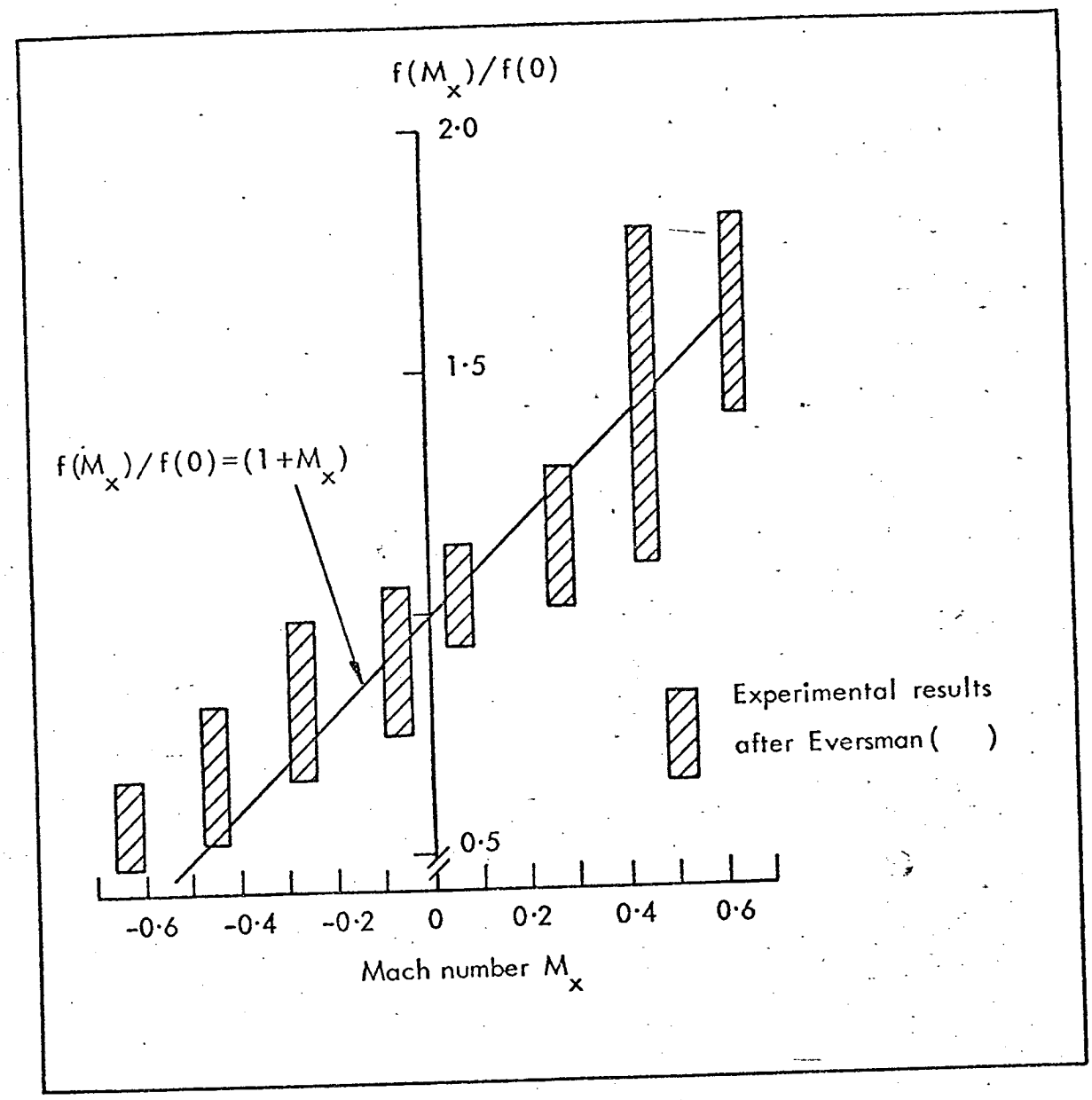

FIG. 4.21 COMPARISON OF EQUATION (4.5.6) FOR FREQUENCY $f(M_x)$, OF PEAK ATTENUATION WITH FLOW, WITH EVERSMAN'S (42) EXPERIMENTAL DATA.

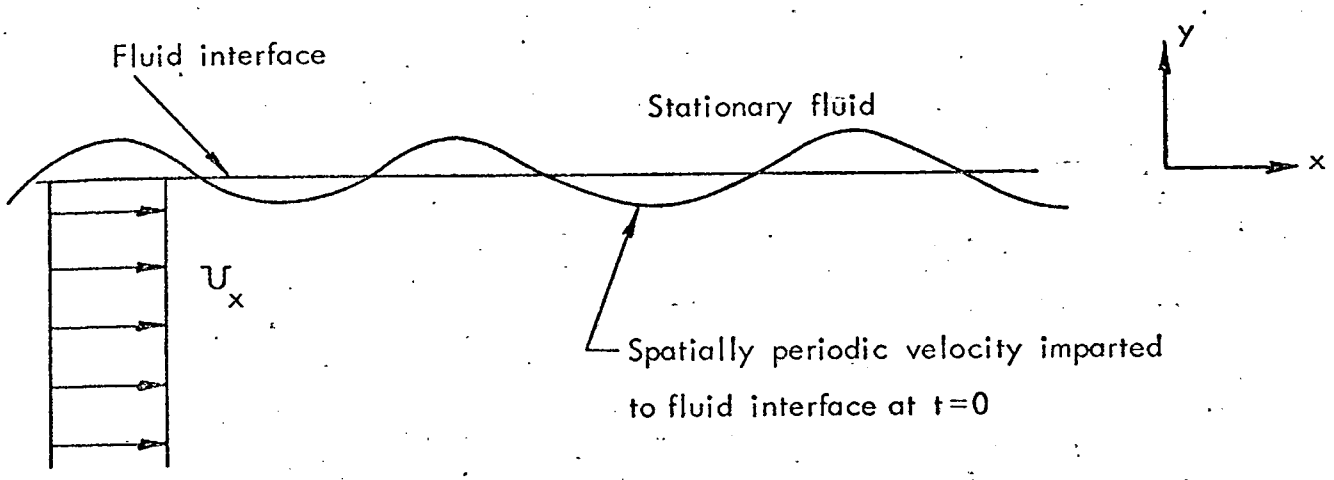

FIG. 4.22 THE MODEL ANALYSED BY MILES (45).

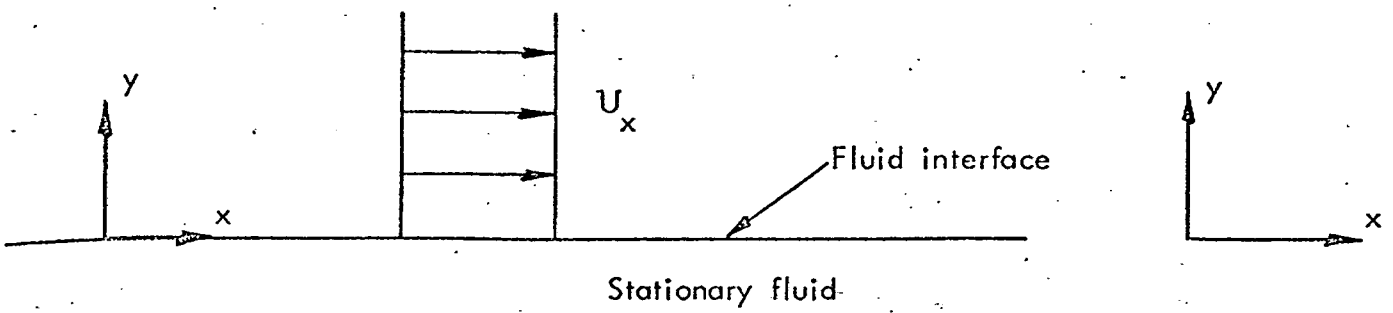

Line source emitting pulse at t=0

FIG. 4.23a THE MODEL ANALYSED BY FRIEDLAND AND PIERCE (46).

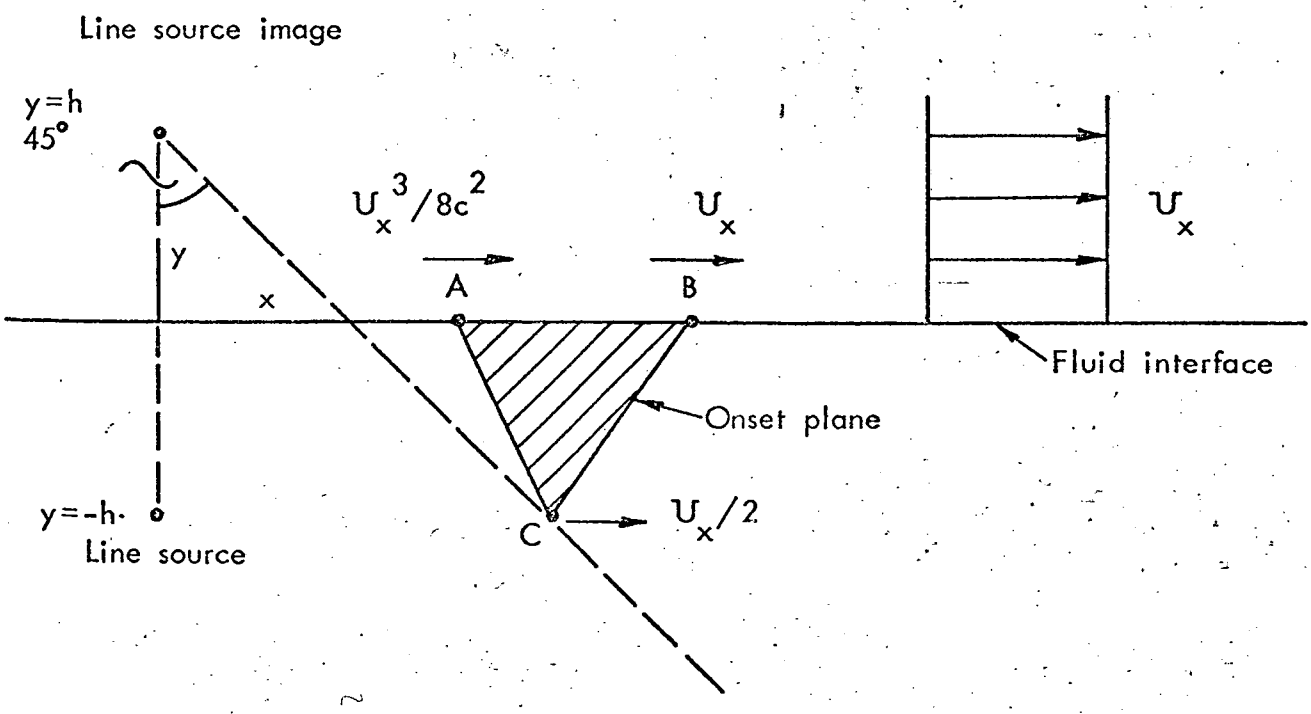

FIG. 4.23b THE MODEL ANALYSED BY FRIEDLAND AND PIERCE (46) AFTER ONSET OF THE 'SINGULAR SOLUTION'.

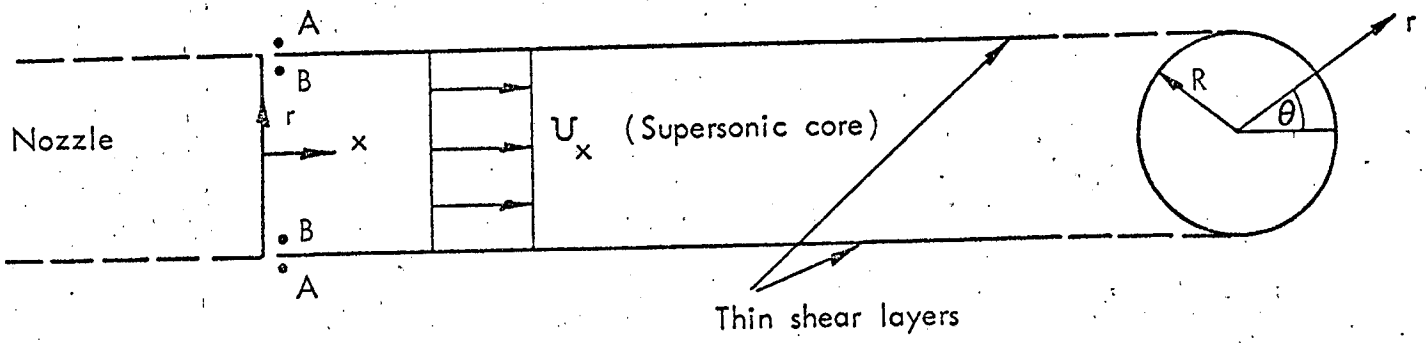

Localised pressure difference (at $x=0$) switched on at $t=0$: $p_A - p_B \propto \exp[in\theta - i\omega t]$

FIG. 4.24 THE MODEL ANALYSED BY TAM (47).

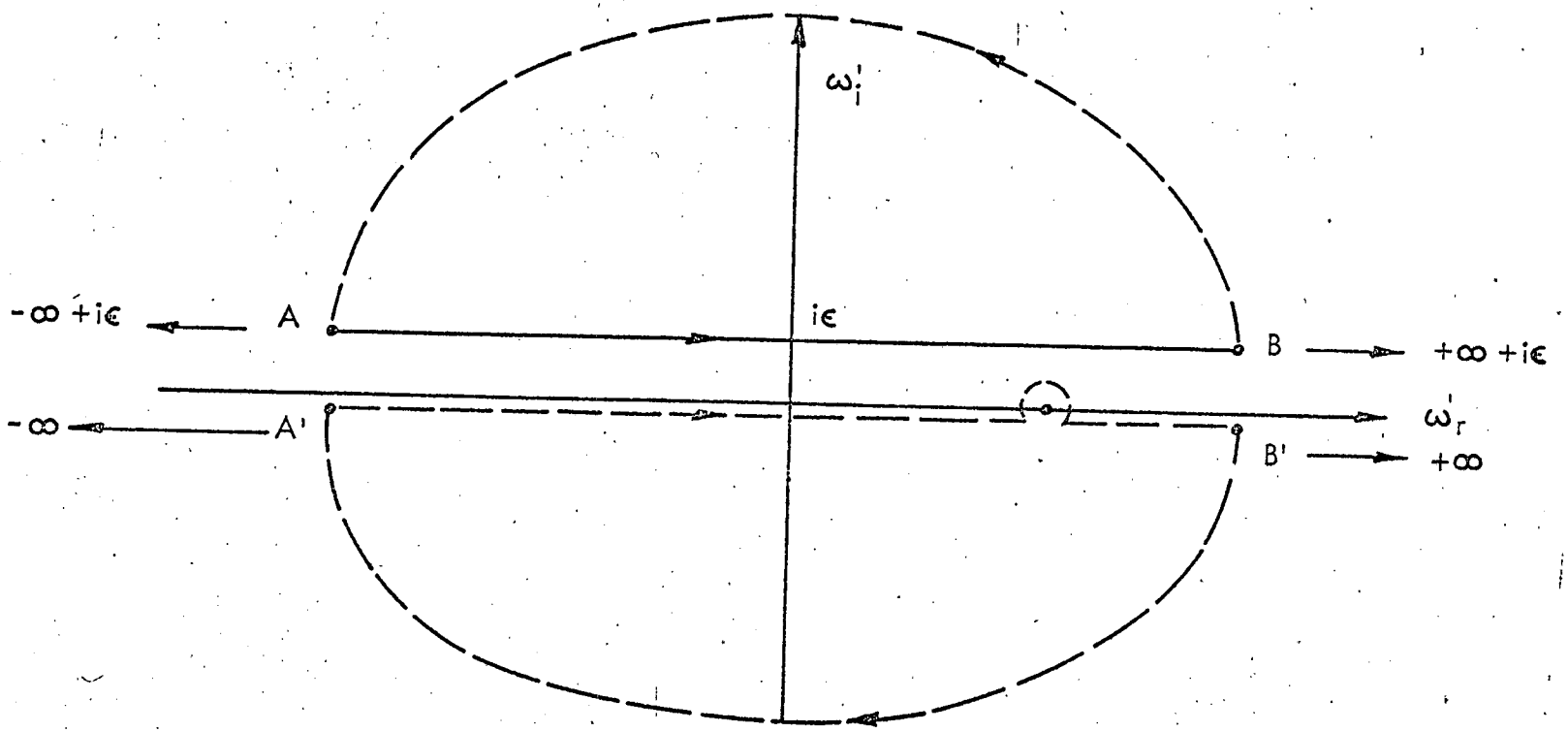

FIG. 4.25 INTEGRATION PATHS ON THE COMPLEX ω' PLANE.

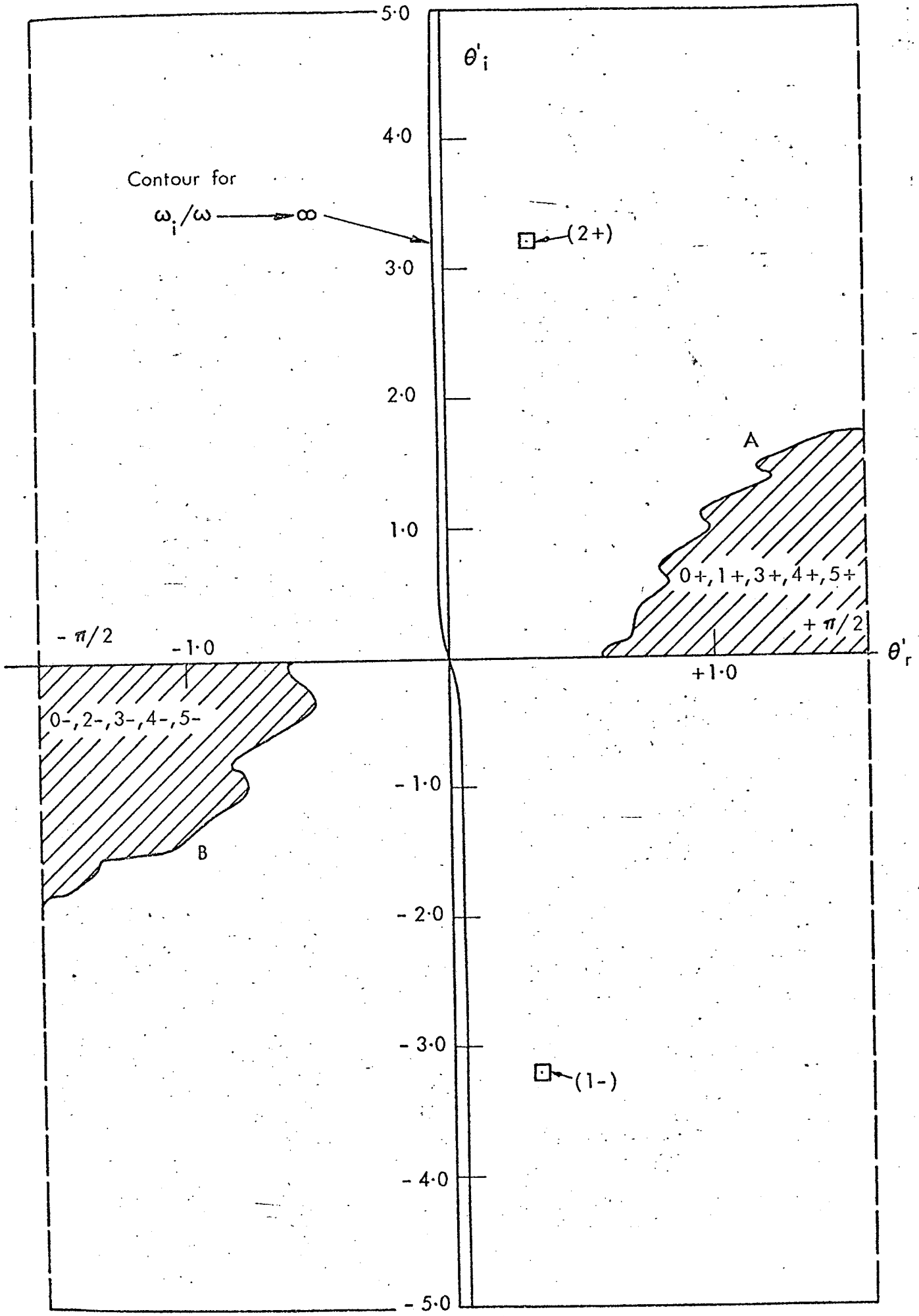

FIG. 4.26 CONTOUR AND LOCATION OF POLES AS $\omega_i/\omega \longrightarrow +\infty$ ON THE

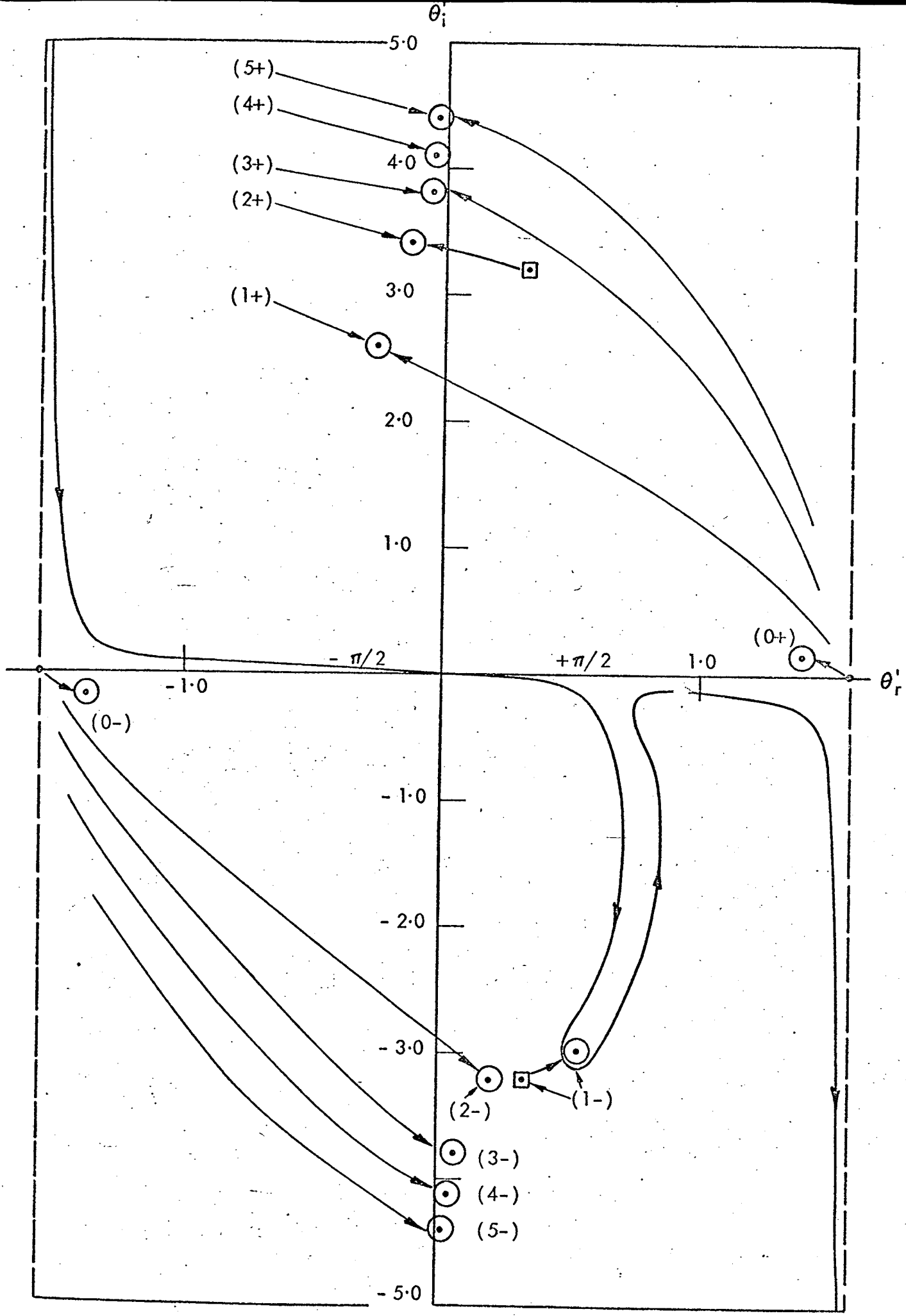

FIG. 4.27 CONTOUR AND LOCATION OF POLES AS $\omega_i/\omega \longrightarrow 0$ ON THE θ' PLANE.

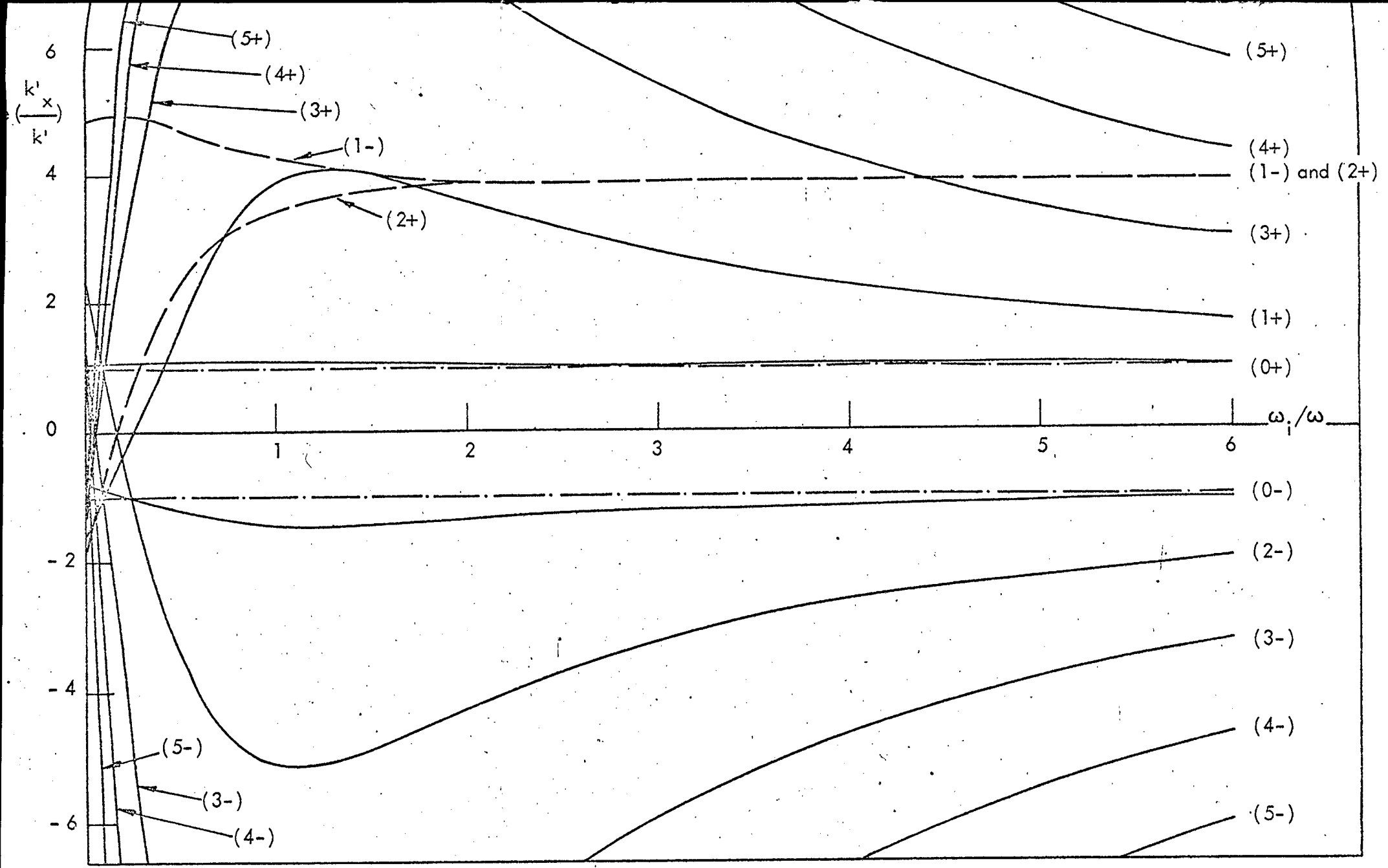

FIG. 4.28 VARIATION OF $\mathrm{Re}(k'_x/k')$ WITH ω_i/ω FOR THE FIRST TEN MODES.

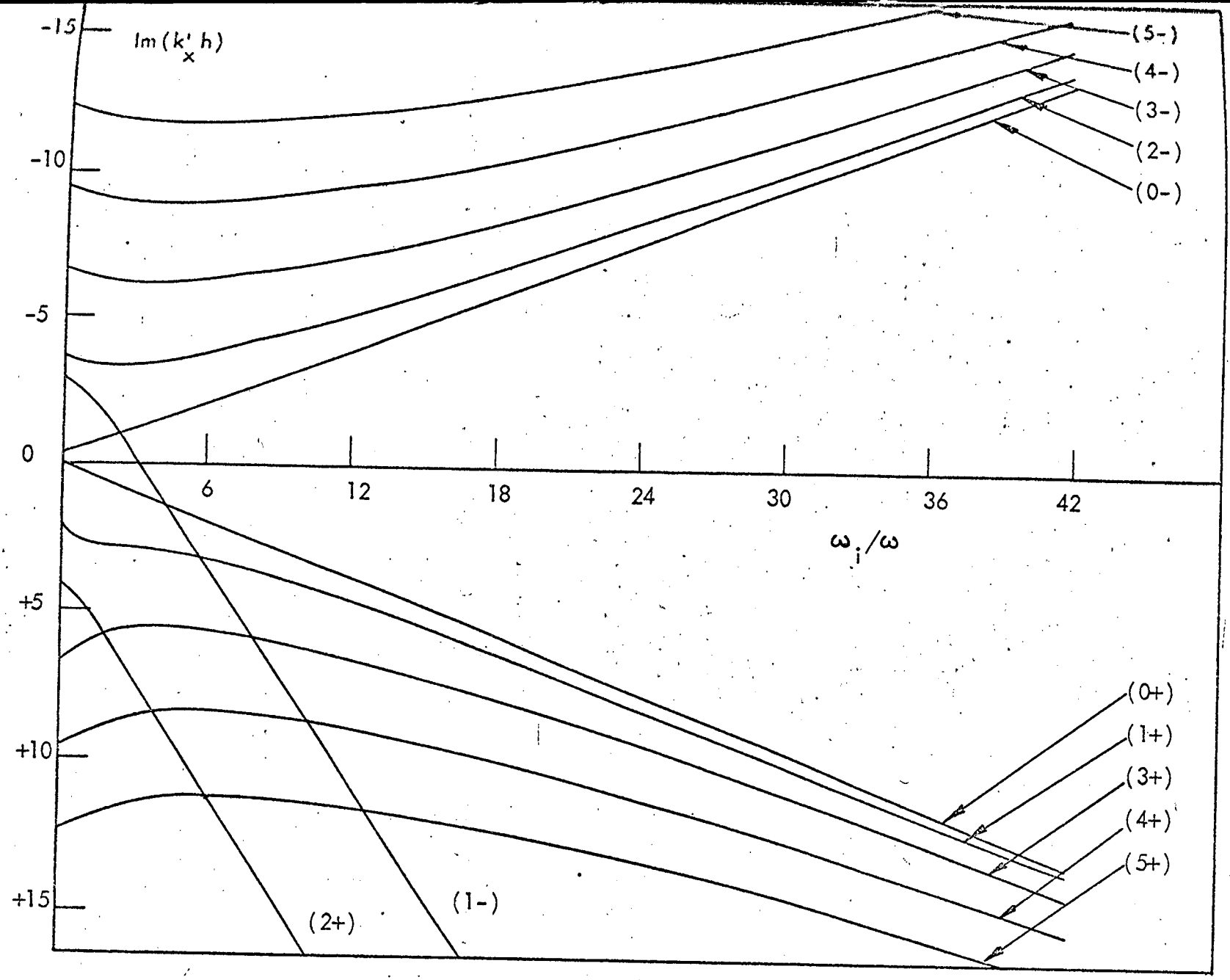

FIG. 4.29 VARIATION OF $\mathrm{Im}(k'_x h)$ WITH ω_i/ω FOR THE FIRST TEN MODES.

CHAPTER 5

ACOUSTIC ENERGY FLOW IN LINED DUCTS CONTAINING UNIFORM OR 'PLUG' FLOW

5.1 Discussion

In section (4.4) it is shown that (if certain conditions are satisfied) the Green's function for a lined duct containing uniform flow can contain an infinite number of 'strange' modes which decay away from the source but have phase velocities towards the source. In section (4.7) this solution is modified to satisfy the Causality requirement and in a particular example one of these 'strange' modes is identified as a mode existing downstream of the source with a phase velocity in the uniform flow direction and spatial amplification in that direction.

Prior to obtaining these two results an attempt was made to determine the role of the 'strange' modes by investigating their associated energy flows. 'To determine the role' in this context is to decide whether under assumed steady-state conditions, a 'strange' mode exists in $x - \bar{x}_0 > 0$ or in $x - \bar{x}_0 < 0$. To be precise it was hypothesised that given a particular 'strange' modal solution of the steady-state (real frequency) homogeneous wave equation, an energy radiation condition could be used to determine the role of that mode, without recourse to specification of the source distribution or to the Causality Law and a transient analysis.

Subsequently it was found that an energy radiation condition cannot be used for this purpose, particularly in the light of the result obtained in section (4.7), but it is of interest to outline the original approach and the obstacles encountered.

The basic energy radiation condition is that the total energy flow

of the acoustic 'far-field', radiated from the duct termination, is outward going, provided the unperturbed fluid in the 'far-field' is at rest relative to the termination. That is, the total energy flow, which is obtained by integrating the local intensity normal to a 'far-field' control surface, S, over that surface, shown schematically in Figure (5.1), must be directed out of the volume enclosed by the surface.

In order to derive from this basic energy radiation condition one that can be applied to a particular mode at some reference plane in the duct (say plane AB in Figure (5.1)) at least two requirements must be satisfied:

(i) the intensity or energy flux must be defined such that there are no associated sources of energy throughout the control volume and

(ii) it must be shown that the particular mode can exist in isolation at plane AB, that is, at a finite distance from the duct termination.

If the unperturbed fluid in the control volume is at rest, the classical energy flux, given by the time averaged product of the pressure and the acoustic particle velocity in the required direction, has no associated energy sources and hence the energy flow across plane AB can be equated with the energy absorbed at planes AD and BC plus the energy radiated to infinity across the control surface S*. As the wall admittances are passive the energy flow across plane AB must be directed into the control volume, that is, towards the duct termination.

---

*All exterior duct surfaces are assumed rigid for the purposes of this exercise and planes AD and BC are chosen to coincide with the duct walls.

If the unperturbed fluid is in motion so that, for example, there is a mean flow into the termination, and the entire flow field is irrotational and of uniform entropy everywhere within the control volume, the energy flux defined by Cantrell and Hart (40) has no associated energy sources, according to Morfey (49). Due to the presence of boundary layers a real 'inlet flow' cannot be completely irrotational but provided there is a smooth inlet geometry and the unperturbed fluid is at rest 'at infinity',* 'inlet flow' is likely to be irrotational everywhere outside the boundary layer regions.

In distinct contrast an outlet flow or jet has large unbounded regions of rotational flow and for such flows no general, explicit energy flux definition is available for which the associated energy sources are identically zero. Thus a simple energy radiation condition cannot be used to determine the role of a 'strange' mode in the region between the source plane and termination if the mean flow is directed towards and out of the termination.

To continue with the inlet flow case: the exterior irrotational mean flow can take any form as the exterior surfaces are rigid but it must match the uniform or 'plug' flow of the duct interior. It is here, within the duct, that energy sources, associated with the Cantrell and Hart (40) energy flux, appear at the walls (unless both walls have a zero admittance or impedance), despite the fact that the flow is defined to be uniform and hence irrotational. This major obstacle to the application of the energy radiation condition is discussed in section (5.3) with the aid of examples.

Superficially the recent work by Mohring (50), where an energy flux is explicitly defined which has no associated energy sources in

---

*This condition has already been assumed for the basic energy radiation condition.

parallel sheared (rotational) flow, would appear to overcome this obstacle. However an explicit definition of Möhring's (50) energy flux for the complete flow field, that is a parallel sheared duct flow matched to some exterior mean flow field is not available. In the present context, the Möhring (50) energy flux for an infinite parallel sheared duct flow is of little value although it is of some interest to evaluate this energy flux for uniform duct flow to see how the Cantrell and Hart (40) energy sources at the walls are replaced by a finite Möhring (50) energy flow parallel to the walls; this is the subject of section (5.4).

To summarise, a simple energy radiation condition cannot be obtained for a duct mode in uniform flow, unless both walls have a zero impedance or admittance, because an energy flux definition which satisfies the requirement that there are no associated energy sources throughout the control volume is not available. Even if such a definition were available it might be difficult to satisfy the second requirement (proof that the particular mode can exist in isolation at a finite distance from the termination) particularly in the light of the results of section (4.7). Investigations in this direction would require information on the reflection of modes at the termination and this, as yet, is not available, except for rigid walled ducts.

In view of the foregoing discussion one might question the validity of using duct axial energy flow in multi-mode wave guide models (30) to provide an estimate of the far-field energy insertion loss for comparison with measured values. Strictly speaking there is no justification for this practice, except for zero mean flow or for 'inlet flow ducts' with non-absorptive walls. However it is shown in section (5.3) that the wall energy sources associated with the

Cantrell and Hart (40) energy flux vanish for well 'cut-on' modes. As it is usual to restrict energy evaluations to the 'cut-on' modes in wave guide models and as the axial energy decay is likely to be controlled by a well 'cut-on' mode there is some justification for this practice, with the following qualifications: the Cantrell and Hart (40) definition must be used and then only for irrotational, uniform entropy 'inlet flows' at the termination. There is apparently no justification for using this (or any other) energy flux definition when there is a 'jet flow' at the termination, except, perhaps, in the high frequency limit where geometric acoustics is valid.

Expressions for individual modal energy flows, according to the Cantrell and Hart (40) definition, are given in section (5.3), for both the well 'cut-off' and well 'cut-on' limits; the former is used to demonstrate the existence of energy sources at the wall (with uniform flow) and the latter can be used, under certain conditions, to estimate the radiated energy. A preliminary discussion is given in section (5.2) of individual modal energy flows in the absence of mean flow.

5.2 Acoustic Energy Flow in Lined Ducts, Containing a Fluid at Rest Relative to the Duct Walls

Throughout this chapter the same basic duct geometry will be used as in previous chapters: an infinite two dimensional duct with a finite admittance wall at $y = h$ and a rigid wall at $y = 0$. The acoustic pressure due to a two dimensional point source is given by the Green's function of Chapter 2, which is of the form

$$p = \sum p_n = \sum_{n=0}^{\infty} a_n \psi_n(y) \exp[-jk_{xn}x], \qquad x > 0; \tag{5.2.1}$$

the $+j$ notation is used and the source is placed at $x = 0$. Acoustic energy flows in each direction (x, y) can be calculated for this pressure field, together with the appropriate velocity field, but this involves not only the individual modal energy flows but also cross-modal energy flows. However once the energy expressions are formulated for the individual modes it is a straightforward extension to formulate the cross-mode energy expressions and therefore this Chapter is restricted to simple mode energy flows.

The axial velocity field, u_n, associated with the pressure mode n is obtained from the momentum equation in that direction

$$\rho_o j\omega u_n = - \frac{\partial p_n}{\partial x}$$

so that

$$u_n = \frac{a_n}{\rho_o c} \psi_n(y) Y_n \exp[-jk_{xn}x] = \frac{p_n}{\rho_o c} . Y_n \tag{5.2.2}$$

where $Y_n = k_{xn}/k$, is termed the modal admittance. The velocity field normal to the duct walls, v_n, associated with the pressure mode n is obtained from the momentum equation in that direction

$$\rho_o j\omega v_n = - \frac{\partial p_n}{\partial y}$$

so that

$$v_n = \frac{a_n}{\rho_o c} \cdot j \frac{\psi_n'(y)}{k} \exp\left[-jk_{xn}x\right] \qquad (5.2.3)$$

The function satisfies the boundary condition $\psi_n'(y) = 0$ at $y = 0$, and $\psi_n'(y) = -jk\bar{\beta}_\omega \psi_n(y)$ at $y = h$, so that

$$v_n(h) = \frac{a_n}{\rho_o c} \bar{\beta}_\omega \psi_n(h) \exp\left[-jk_{xn}x\right]. \qquad (5.2.4)$$

The classical expression for the energy flux, I, is

$$I_x = \langle pu \rangle , \qquad I_y = \langle pv \rangle ,$$

where the $\langle\ \rangle$ denotes 'time averaged'. The expressions for the energy flux associated with mode n are therefore

$$I_{xn} = \tfrac{1}{2}\mathrm{Re}(p_n u_n^*) \qquad I_{ym} = \tfrac{1}{2}\mathrm{Re}(p_n v_n^*) \qquad (5.2.5)$$

and the energy flow, E_{xn}, in the axial direction (per unit width in the z direction) is

$$E_{xn} = \int_0^h I_{xn}\, dy. \qquad (5.2.6)$$

Substituting the expressions (5.2.1), (5.2.2) and (5.2.4) for p_n, u_n and v_n into the energy flux expressions gives

$$I_{xn} = \frac{a_n a_n^*}{2\rho_o c} \psi_n(y)\psi_n^*(y) \exp\left[-j(k_{xn} - k_{xn}^*)x\right] \mathrm{Re}(Y_n^*), \qquad (5.2.7)$$

$$I_{yn}(h) = \frac{a_n a_n^*}{2\rho_o c} \psi_n(h)\psi_n^*(h) \exp\left[-j(k_{xn} - k_{xn}^*)x\right] \mathrm{Re}(\bar{\beta}_\omega^*). \qquad (5.2.8)$$

The direction of the axial energy flux is given by the sign of the real part of the modal admittance or k_{xn}/k where

$$\frac{k_{xn}}{k} = (1 - \frac{k_y^2}{k^2})^{\frac{1}{2}}.$$

For $Re(\bar{\beta}_\omega) \geq 0$, $Re(Y_n^*)$ remains positive or zero and the energy flux direction is, everywhere in the interval $0 \leq y \leq h$, the same as that of the decay, which is given by

$$\exp[-x2\ Im(-\ k_{xn})].$$

The energy flux direction normal to the wall is given by the sign of $Re(\bar{\beta}_\omega)$, as would be expected.

The energy flow in the axial direction is

$$E_{xn} = h.\ \frac{a_n a_n^*}{2\rho_o c} \exp[-j(k_{xn} - k_{xn}^*)x] Re(Y_n^*)\Omega_n$$

where $$\Omega_n = \frac{1}{h} \int_o^h \psi_n(y)\psi_n^*(y)\ dy.$$

The reason for the appearance of cross-modal energy flows is that the functions $\psi_n(y)$ are not orthogonal to the functions $\psi_n^*(y)$ (except for $\bar{\beta}_\omega = 0$ and $\bar{\beta}_\omega \to \infty$), that is

$$\int_o^h \psi_n(y)\psi_m^*(y)\ dy \neq 0.$$

5.3 Acoustic Energy Flow in a Region of Uniform Axial Flow

In this section appropriate acoustic energy flow expressions are formulated for a particular mode in the presence of an axial mean flow field which is uniform in the y direction (normal to the propagation direction). The results indicate that 'plug' flow in a lined duct (that is, a duct having one or more walls with a finite, non-zero wall admittance) cannot be completely included in this category, and has to be considered as an example of a partly sheared mean velocity field in the following section.

The axial velocity field for pressure mode n is given by the momentum equation

$$\rho_o(j\omega + \frac{\partial}{\partial x})\, u_n = -\frac{\partial p_n}{\partial x}$$

or

$$u_n = \frac{a_n}{\rho_o c}\psi_n(y)\bar{Y}_n \exp[-jk_{xn}x] = \frac{p_n}{\rho_o c}\cdot\bar{Y}_n \qquad (5.3.1)$$

where

$$\bar{Y}_n = k_{xn}/(k - k_{xn}M_x). \qquad (5.3.2)$$

Similarly the normal velocity field at the point $y = h$ is given by

$$v_n(h) = \frac{a_n \bar{\bar{\beta}}_\omega \psi_n(y)}{\rho_o c(1 - Y_n M_x)} \exp[-jk_{xn}x] \qquad (5.3.3)$$

where, for 'plug' flow,

$$\bar{\bar{\beta}}_\omega = \bar{\beta}_\omega(1 - Y_n M_x)^2. \qquad (5.3.4)$$

A number of different definitions are available for the acoustic energy flux, in the presence of mean flows, each one having a set of particular conditions for which the acoustic energy is conserved (that is, the absence of energy sources). These have been

reviewed by Morfey (49) who adopts the definition given by Cantrell and Hart (40) and shows that the main conditions for conservation of this energy are that (i) the mean flow field is irrotational and (ii) the mean entropy is uniform. This definition will also be adopted here, partly because it is an explicit definition with the least restrictive conditions for energy conservation and partly because it is identical to Mohring's (50) definition for the particular case of uniform mean flow.

According to Cantrell and Hart's (40) definition the modal energy flux is given by

$$I_{xn} = \tfrac{1}{2}\mathrm{Re}\{p_n u_n^* + M_x \frac{p_n p_n^*}{\rho_o c} + M_x^2 p_n u_n^* + \rho_o c u_n u_n^* M_x\} \qquad (5.3.5)$$

and

$$I_{yn} = \tfrac{1}{2}\mathrm{Re}\{p_n v_n^* + \rho_o c\, M_x u_n v_n^*\} . \qquad (5.3.6)$$

These expressions can be rewritten in terms of the modal admittance, Y_n (see equations (5.3.1) and (5.3.2)),

$$I_{xn} = \frac{p_n p_n^*}{2\rho_o c}\ \mathrm{Re}\{\bar{Y}_n^*(1 + M_x^2 + M_x \bar{Y}_n) + M_x\}, \qquad (5.3.7)$$

$$I_{yn} = \tfrac{1}{2}\mathrm{Re}\{p_n v_n^*(1 + \bar{Y}_n M_x)\} , \qquad (5.3.8)$$

and after some manipulation these become

$$I_{xn} = \frac{p_n p_n^*}{2\rho_o c}\left\{\frac{M_x + (1 - M_x^2)\mathrm{Re}(Y_n)}{(1 - Y_n M_x)(1 - Y_n^* M_x)}\right\} ,$$

$$= \frac{p_n p_n^*}{2\rho_o c}\left\{\frac{\mathrm{Re}(Y_n')}{(1 - Y_n M_x)(1 - Y_n^* M_x)}\right\}, \qquad (5.3.9)$$

where $Y_n = k_{xn}/k$ and $Y_n' = k_{xn}'/k$, k_{xn}' being the Lorentz

axial wavenumber

$$k_{xn}' = k_x(1 - M_x^2) + kM_x,$$

$$I_{yn}(h) = \frac{p_n(h)p_n^*(h)}{2\rho_o c} \left\{ \frac{\mathrm{Re}(\bar{\bar{\beta}}_\omega^*)}{(1 - Y_n M_x)(1 - Y_n^* M_x)} \right\}. \qquad (5.3.10)$$

The direction of the axial energy flux is, everywhere in the interval $0 \leq y \leq h$, given by the sign of the real part of the Lorentz axial wavenumber: this can be negative for decay in the positive direction (see sections 4, 5 and 6 of the previous chapter) and appears to pose a paradox. That is, if energy is supposedly lost at the boundaries of the uniform flow region, the energy flow should decay whereas here the energy appears to be flowing in the negative axial direction and therefore to be amplified. The answer lies in the expression given by equation (5.3.10) for the energy flux normal to the boundary at $y = h$. The 'plug' flow boundary condition leads to the energy flux direction being determined by the real part of the effective admittance and not the actual admittance. Whenever k_{xn}' (or Y_n') has a negative real part, by definition the real part of $\bar{\bar{\beta}}_\omega$ is also negative. Thus these expressions are consistent in themselves but for 'plug' flow there is clearly a discontinuity in energy flux normal to the boundary: equation (5.3.10), in general, does not equal the energy flux 'absorbed' by the lined wall, which is still given by equation (5.2.8). This discrepancy is, essentially, the subject of the next section.

Expressions for the energy flows within the uniform region are of interest for 'well cut-on' modes; these are, subject to the condition

$$k \gg |k_{yn}|(1 - M_x^2)^{\frac{1}{2}},$$

$$I_{xn} = \frac{p_n p_n^*}{2\rho_o c} (1 + M_x)^2$$

$$E_{xn} = h. \frac{a_n a_n^*}{2\rho_o c} (1 + M_x)^2 \exp[-j(k_{xn} - k_{xn}^*)x] \Omega_n.$$

As the 'well cut-on' approximation leads to the same value for the real part of the axial wavenumber as for 'well cut-on' modes in rigid wall ducts, these expressions are similar to those given by Morfey (51).

With the same approximation, the energy flux normal to the flow boundary does reduce to the energy flux absorbed by the wall and thus the energy flux discontinuity is not important for well 'cut-on' modes; nor does this problem arise if $\bar{\beta}_\omega = 0$ or $\bar{\beta}_\omega \to \infty$ for then the energy flux is identically zero.

The reason for this energy flux discontinuity can be recognised if the slip motion at the duct walls is replaced by a thin boundary layer in which the transition can take place from the uniform mean flow Mach number M_x to a stationary non-slip motion at the lined wall. This region of sheared or rotational fluid then gives rise to energy source terms, according to Morfey (49), which are, before time averaging (the terms with a zero time average being ignored),

$$- M_x(y) \frac{dM_x(y)}{dy} (pv') - \rho u' \frac{\bar{D}u''}{Dt} - \rho v' \frac{\bar{D}v''}{Dt} - \rho_o c \frac{dM_x(y)}{dy} (u'v'')$$

where (u', v') are the irrotational components of the fluctuating velocity (u, v), (u'', v'') are the rotational components* and $\bar{D}/Dt = \partial/\partial t + U_x \frac{\partial}{\partial x}$.

---

*It is proved in Chapter 6 that the linearised fluctuating velocity field in the presence of mean shear has rotational components.

Such energy sources can be avoided by means of Mohring's (50) alternative formulation, which allows this energy production region to be replaced by an energy wave-guide for a modified energy flow. In the absence of mean shear this modified energy takes the same form as that defined by Cantrell and Hart (40). However it has only been defined explicitly by Mohring (50) for a parallel sheared flow and thus it cannot be related immediately to energy radiated from a duct termination.

In the vicinity of the termination the mean velocity field is likely to be irrotational for incoming flow, and thus the energy defined by Cantrell and Hart (40) is conserved and can be equated to the radiated energy.

5.4 Acoustic Energy in Lined Ducts Containing Plug Flow

Möhring's (50) energy flux expressions are

$$I_{xn} = \frac{1}{2\rho_o\omega^2} \mathrm{Re}\left\{ \frac{-U_x'(y)}{(1 - Y_n M_x(y))^2 (1 - Y_n^* M_x(y))^2} p_n^* \frac{dp_n}{dy} \right\}$$

$$+ \frac{p_n p_n^*}{2\rho_o c} \left\{ \frac{\mathrm{Re}(Y_n')}{(1 - Y_n M_x(y))(1 - Y_n^* M_x(y))} \right\}, \qquad (5.4.1)$$

$$I_{yn}(h) = \frac{p_n(h) p_n^*(h)}{2\rho_o c} \left\{ \frac{\mathrm{Re}(\bar{\bar{\beta}}_\omega^*)}{(1 - Y_n M_x)(1 - Y_n^* M_x)} \right\}. \qquad (5.4.2)$$

The second term in I_{xn} is identical to the energy flux defined by Cantrell and Hart (40), and $I_{yn}(h)$ remains exactly the same. The plane $y = h$ is defined to be the boundary of the uniform flow region and M_x, without a following (y), is defined as the Mach number of this uniform flow. $M_x(y)$ varies from M_x at $y = h$ to zero at $y = h + \varepsilon$ where ε is the boundary layer width (see Figure (5.2)). $M_x(y)$ is allowed to have any dependence on y in the interval $h \leq y \leq h + \varepsilon$.

The aim of this exercise is to use these energy flux definitions to present an alternative interpretation of the occurrence of the energy flux discontinuity normal to the wall as $\varepsilon \to 0$, (that is, as the realistic flow field sketched in Figure (5.2) approaches that of the 'plug flow' model), this normal energy flux <u>at</u> the wall being

$$I_{yn}(h + \varepsilon) = \frac{p_n(h + \varepsilon) p_n^*(h + \varepsilon)}{2\rho_o c} \mathrm{Re}(\bar{\beta}_\omega^*). \qquad (5.4.3)$$

It is clear that as $\varepsilon \to 0$, $U_x'(y) \to -\infty$ everywhere in the interval $h \leq y \leq h + \varepsilon$ and, thus, so does the energy flux I_{xn}.

However, the total energy flow, E_{xn}', within that interval remains finite, being of order $U_x'(y)\varepsilon$ which, in the limit $\varepsilon \to 0$, tends to a finite value, of order U_x. The second term in I_{xn} does vanish in this limit being of order ε. It is assumed of course that $Y_n \neq \{M_x(y)\}^{-1}$ in the interval $0 \leq y \leq h + \varepsilon$. The expression for E_{xn}' can be obtained by direct integration of the first term in I_{xn} if it is assumed that the pressure and normal particle displacement, ξ_y, are constant in this interval (a proof, for the case $\varepsilon \to 0$, is given in Chapter 6). On using the usual relation

$$\frac{dp_n}{dy} = -\rho_o j\omega(j\omega\xi_y)(1 - Y_n M_x(y))^2,$$

the first term (say I_{xn}') becomes

$$I_{xn}' = \tfrac{1}{2}\,\mathrm{Re}\left\{\frac{j(p_n^*(h).j\omega\xi_y(h))}{k_{xn}^*}\left[\frac{M_x'(y)Y_n^*}{(1 - Y_n^* M_x(y))^2}\right]\right\}$$

so that, with $j\omega\xi_y(h) = \bar{\beta}_\omega\, p_n(h)/\rho_o c$,

$$E_{xn}' = \int_h^{h+\varepsilon} I_{xn}(y)dy = \frac{p_n(h)p_n^*(h)}{2\rho_o c}\left\{\frac{\mathrm{Re}\left[-j\bar{\beta}_\omega M_x(1 - Y_n M_x)\right]}{k(1 - Y_n^* M_x)(1 - Y_n M_x)}\right\} + O(\varepsilon) \qquad (5.4.4)$$

In the limit as $\varepsilon \to 0$ this finite energy flow can be interpreted as the cause of the energy flux discontinuity at the wall. This can be demonstrated by forming an energy balance for a volume element of area $\Delta x \times \varepsilon$ in the (x, y) plane (see Figure (5.2)).

According to the present definition, this energy should be conserved in sheared flow. Therefore a check on the validity of the expression for E_{xn}' is that it should satisfy

$$\lim_{\substack{\Delta x \to 0 \\ \epsilon \to 0}} \{-E_{xn}'(x) + E_{xn}'(x + \Delta x) - E_{yn}(h) + E_{yn}(h + \epsilon)\} = 0^* \qquad (5.4.5)$$

From equation (5.4.4) the limiting difference between the sum of the outgoing axial energy flows is (with $\psi_n(h)$ assumed equal to $\psi_n(h+\epsilon)$)

$$E_{xn}'(x + \Delta x) - E_{xn}'(x) =$$

$$\frac{a_n a_n^*}{2\rho_o c} \psi_n(h)\psi_n^*(h)\left\{ \frac{\mathrm{Re}\left[-j\bar{\beta}_\omega M_x(1 - Y_n M_x)\right]}{k(1 - Y_n M_x)(1 - Y_n^* M_x)} \right\} \exp\left[-j(k_{xn} - k_{xn}^*)x\right]$$

$$\times \quad -j(k_{xn} - k_{xn}^*)\Delta x$$

and for the other outgoing energy flows

$$E_{yn}(h + \epsilon) - E_{yn}(h) =$$

$$\frac{a_n a_n^*}{2\rho_o c} \psi_n(h)\psi_n^*(h)\left\{\mathrm{Re}(\bar{\bar{\beta}}_\omega^*) - \frac{\mathrm{Re}(\bar{\bar{\beta}}_\omega^*)}{(1 - Y_n M_x)(1 - Y_n^* M_x)} \right\}$$

$$\times \exp\left[-j(k_{xn} - k_{xn}^*)x\right]\Delta x.$$

It is easily shown that

$$\mathrm{Re}\left\{\bar{\beta}_\omega^* - \frac{\bar{\beta}_\omega^*(1 - Y_n^* M_x)^2}{(1 - Y_n M_x)(1 - Y_n^* M_x)} \right\} = -j(k_{xn} - k_{xn}^*)$$

$$\times \frac{\mathrm{Re}\left[+j\bar{\beta}_\omega M_x(1 - Y_n M_x)\right]}{k(1 - Y_n M_x)(1 - Y_n^* M_x)}$$

so that equation (5.4.5) is clearly satisfied.

As an example of the relative values of these energy flows in

---

*This double limit is used for convenience: Δx and ϵ could be taken to be finite but the resulting expressions for the energy flows would be less simple.

the sheared and uniform flow regions, consider one of the approximate analytic solutions of the 'strange' modes derived in section (4.6):

$$k_{xn}h \doteq \frac{-khM_x}{(1 - M_x^2)} - \frac{n\pi}{(1 - M_x^2)^{\frac{1}{2}}} \left\{\frac{M_x^2\, Re(\bar{\beta}_\omega)}{kh(1 - M_x^2)} + j\left(1 + \frac{M_x^2 Im(\bar{\beta}_\omega)}{kh(1 - M_x^2)}\right)\right\}, \qquad (5.4.6)$$

$$k_{yn}h \doteq m\pi\left\{1 + \frac{M_x^2\, Im(\bar{\beta}_\omega)}{kh(1 - M_x^2)} - j\,\frac{M_x^2\, Re(\bar{\beta}_\omega)}{kh(1 - M_x^2)}\right\}. \qquad (5.4.7)$$

In the limit $\varepsilon \to 0$ the axial energy flow within the shear layer, E_{xn}', is

$$E_{xn}' = \frac{a_n a_n^*}{2\rho_o c}\,\psi_n(h)\psi_n^*(h)\,\exp\left[-j(k_{xn} - k_{xn}^*)x\right]\frac{Re\left[-j\bar{\beta}_\omega M_x(1 - Y_n M_x)\right]}{k(1 - Y_r^* M_x)(1 - Y_n M_x)}.$$

As $k_{yn}h \doteq n\pi$ and $|Y_n M_x| \gg 1$ this reduces to

$$E_{xn}' \doteq \frac{a_n a_n^*}{2\rho_o c}\exp\left[-j(k_{xn} - k_{xn}')\right]\frac{Re\left[j\bar{\beta}_\omega Y_n M_x^2\right]}{k(1 - Y_n^* M_x)(1 - Y_n M_x)}.$$

Within the uniform flow region $0 \leq y \leq h$ the axial energy flow, E_{xn}, is

$$E_{xn} = \frac{a_n a_n^*}{2\rho_o c}\left\{\int_0^h \psi_n(y)\psi_n^*(y)dy\right\}\exp\left[-j(k_{xn} - k_{xn}^*)x\right]\frac{Re(Y_n')}{(1 - Y_n M_x)(1 - Y_n^* M_x)}.$$

As $\psi_n(y) \doteq \cos(n\pi\, y/h)$ the integral is approximately $h/2$. Thus the ratio of the two energy flows is

$$\frac{E_{xn}'}{E_{xn}} \doteq \frac{2Re\left[j\bar{\beta}_\omega Y_n M_x^2\right]}{kh\; Re\left[Y_n'\right]}.$$

With the approximation

$$Y_n \doteq \frac{-jn\pi}{(kh(1 - M_x^2)^{\frac{1}{2}})}$$

and with

$$Re(Y_n') \doteq \frac{-M_x^2\, Re(\tilde{\beta}_\omega)}{(kh)^2(1 - M_x^2)^{\frac{1}{2}}} ,$$

clearly

$$\frac{E_{xn}'}{E_{xn}} \doteq -2.$$

That is, the axial energy flow within the shear layer is approximately twice that within the uniform flow and is in the opposite direction, thus counteracting that energy flow and (also) providing a net energy flow in the decay direction as it must with passive walls. It has been assumed, for this example, that no boundary layer exists at $y = 0$, and thus the plane $y = 0$ could be regarded as a plane of symmetry. Alternatively a boundary layer can be assumed at $y = 0$ but as the wall admittance is zero there, the axial and normal energy flows within this boundary layer are identically zero.

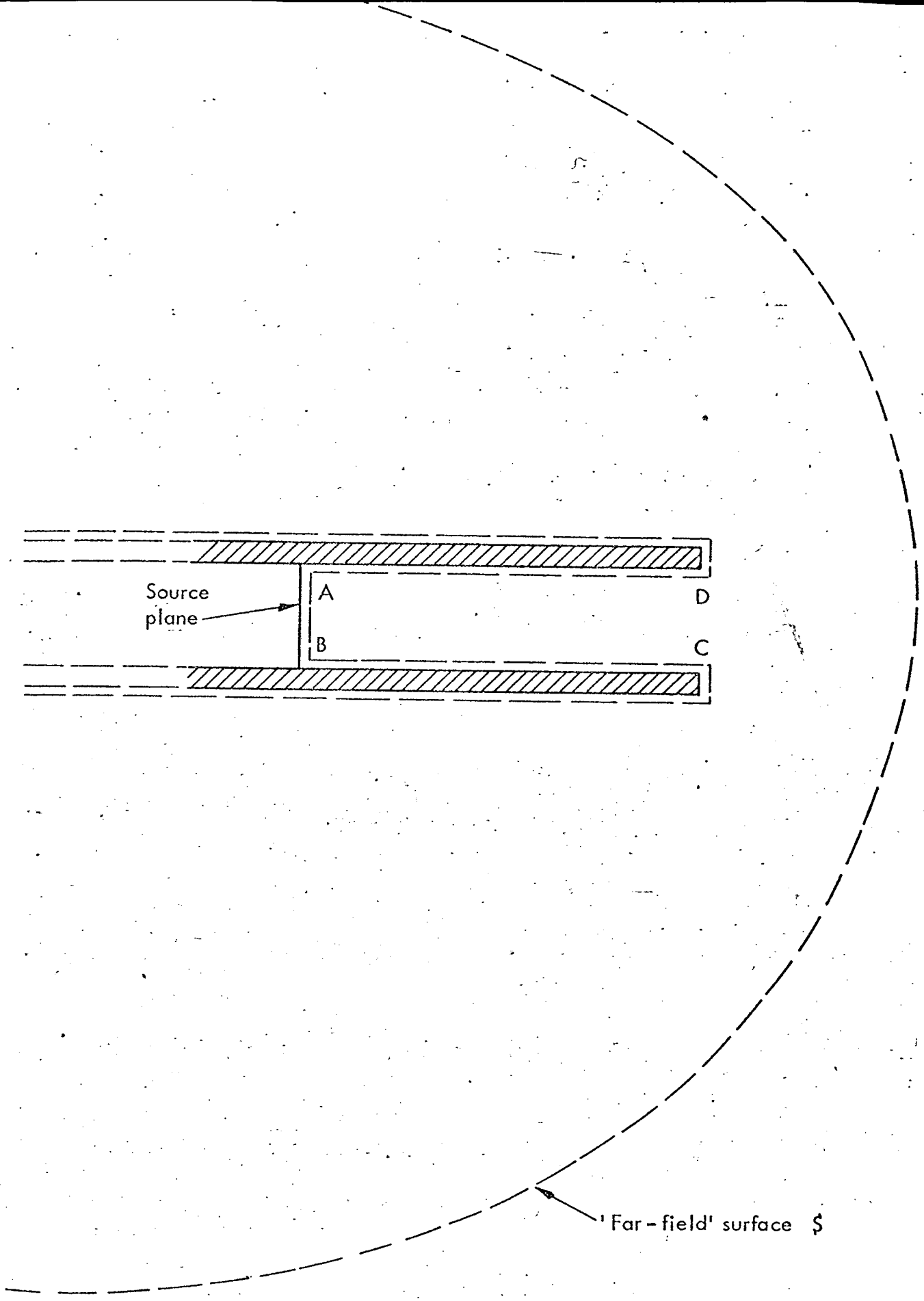

FIG. 5·1 A SEMI-INFINITE DUCT FOR ENERGY CONSIDERATIONS.

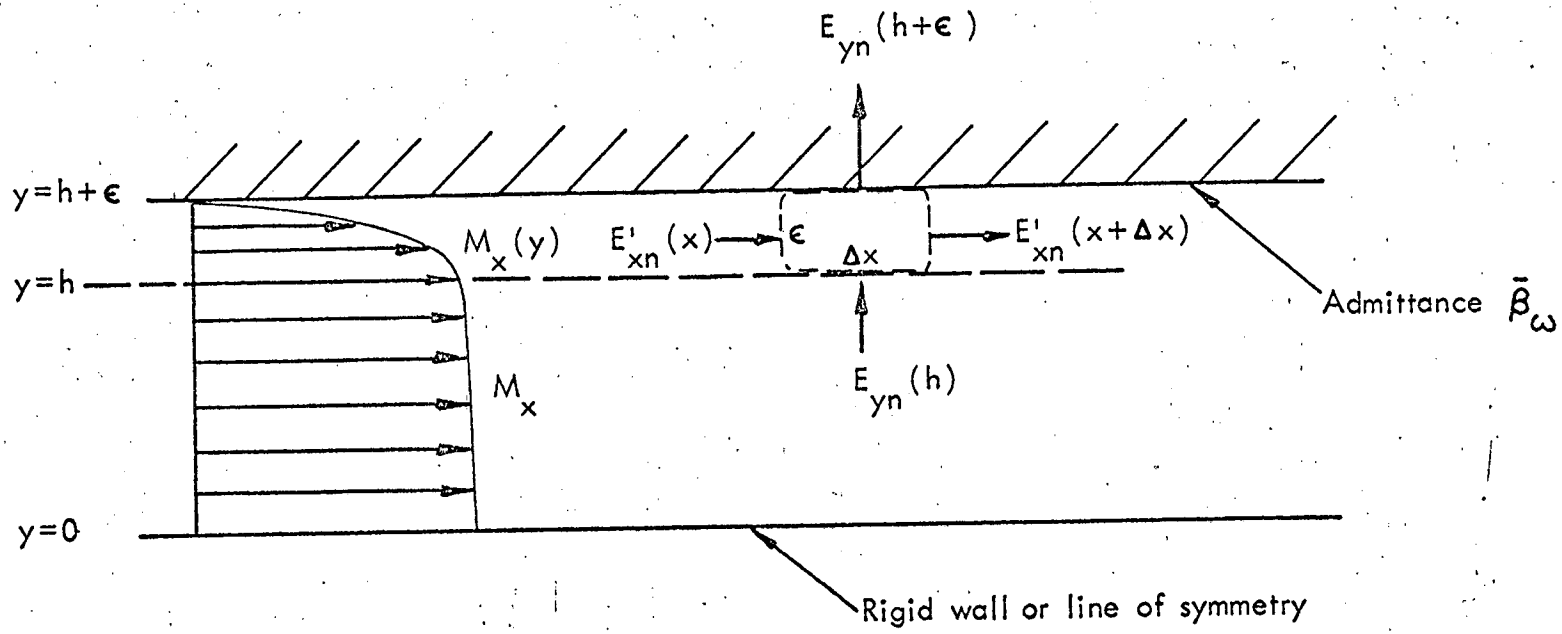

FIG. 5.2 AN ENERGY BALANCE VOLUME IN THE SHEARED FLOW REGION.

CHAPTER 6

SOME ASPECTS OF 'SOUND' ATTENUATION IN LINED DUCTS CONTAINING INVISCID MEAN FLOWS WITH BOUNDARY LAYERS

6.1 Discussion

In Chapter 4 it was assumed that the influence of a realistic subsonic mean flow on the propagation and attenuation of sound in a lined duct could be investigated, in the first instance, by using a mathematical model in which the mean flow is uniform across the duct. A uniform profile with 'slip' at the boundaries is clearly never found in practice, but as a model for the duct acoustic field it may lead to realistic modal solutions under certain conditions. These conditions have never been specified in quantitative terms: usually it is argued that this model is realistic if the boundary layer thickness is small compared with the sound wavelength or quarter wavelength. In many applications this qualitative condition is not satisfied and hence recent work on wave-guide models (52)-(58), in particular for aero-engine applications, has concentrated on developing computer programs which can solve the wave equation for sheared flow.

However since analytical work, such as that presented in Chapter 4 and the transient analysis by Eversman (41), would be complicated, if not impossible, without the uniform flow model, it is clearly desirable that a study should be made of the limits within which this model can be realistically used. In addition a controversy still apparently exists (59) concerning the correct acoustic boundary conditions for the uniform flow model.

In section (6.2) the uniform flow model is viewed as a limiting case of a more general model, consisting of a uniform flow region

separated from the duct walls by boundary layers of arbitrary profile with the boundary layer widths tending to zero. It is then verified analytically that the acoustic boundary conditions used in Chapters 4 and 5 for the uniform flow model are indeed correct. Approximate analytic expressions are also obtained for the boundary conditions, to be applied at the edge of the uniform flow region in the finite boundary layer wall; these are correct to first order in a parameter proportional to boundary layer thickness. This makes it possible to investigate the validity of the uniform flow model in representing the effects of 'thin' boundary layers on sound propagation and attenuation in flow ducts.

In section (6.3) the differential equations for 'sound' propagation in sheared flow are solved exactly, by numerical integration, for a particular example in which the boundary layers have linear profiles. The results confirm that modal solutions converge to the uniform flow solutions as the boundary layer thickness tends to zero and, with the aid of the analytic approximations obtained in section (6.2), an interpretation is given of the dependence of each mode axial wavenumber on boundary layer thickness.

Derivation of the Green's function for sheared duct flow is discussed in section (6.4), with the restriction that the line source is located within a uniform flow region. Further examples are given to show the influence of finite width boundary layers on the mode identified in section (4.7) as one which is spatially amplified in the downstream direction. In these examples it is recognised that a singularity of the differential equations is about to appear and as in stability theory (60) a correct procedure for the treatment of this singularity should be established before further work in this area can continue.

6.2 An Analytical Approach for Thin Boundary Layers

Consider Figure (6.1): the two-dimensional duct now contains some realistic flow profile with a boundary layer region between $y = 0$ and $y = \delta$, of arbitrary profile, $U_x(y)$, and a uniform flow region between $y = \delta$ and $y = H$. The plane $y = H$ can be taken to be a rigid wall, in which case the flow is unrealistic in that no boundary layer exists adjacent to it, or it can be regarded as a plane of symmetry such that the duct is of width $2H$ and contains a symmetrical flow profile. This particular model is adopted here for simplicity but later it will be generalised to the case of a boundary layer adjacent to the rigid wall.

The usual method of investigating sound propagation and attenuation in such a flow field is to solve the equations for the entire region $0 \leq y \leq H$. However it is clear from the preceding analysis that the solutions are known for the uniform region $\delta \leq y \leq H$ provided the boundary conditions can be specified at $y = \delta$. For the special case, where δ vanishes, so that 'slip' is said to occur at the wall, the boundary conditions have been given, for example by Morse and Ingard (14), although no proof is given of their validity: for real duct flows it is usually argued that this uniform flow model should be realistic provided the boundary layer thickness is small compared with the sound wavelength or quarter wavelength.

If the equations can be solved in the region $0 \leq y \leq \delta$, for small values of δ (suitably non-dimensionalised) it should then be possible to

(i) establish whether or not the uniform flow boundary conditions are the same as those for a realistic profile with boundary layer widths tending to zero (as was assumed for the purposes of the energy analysis in Chapter 5).

(ii) specify in quantitative terms the conditions under which the zero boundary layer thickness boundary conditions remain valid for realistic flows, and

(iii) specify the boundary condition at $y = \delta$ for the uniform flow region in terms of δ, as a first approximation, with associated restrictions.

These aims have effectively been accomplished by the following analysis, although it will be seen that for (ii) there is no simple specification.

For a single mode at radian frequency ω the dependence of the acoustic quantities on time t and axial distance x are expressed by the usual factor*

$$\exp\left[j\omega t - jk_x x\right] \quad **$$

and the linearised, compressible, inviscid flow equations for this mode are

(Continuity)

$$j(\omega - k_x U_x(y))\rho - j\rho_o k_x u + \rho_o \frac{dv}{dy} = 0 \qquad (6.2.1)$$

(Momentum - x)

$$\rho_o j(\omega - k_x U_x(y))u + \rho_o v \frac{dU_x(y)}{dy} = jk_x p \qquad (6.2.2)$$

(Momentum - y)

$$\rho_o j(\omega - k_x U_x(y))v = -\frac{dp}{dy} \qquad (6.2.3)$$

(Energy)

$$p = c^2\rho \quad . \qquad (6.2.4)$$

---

*The Green's function is discussed in section (6.4).

**The n subscript in k_{xn}, denoting a modal solution is omitted throughout this chapter.

$U_x(y)$ is the mean velocity and ρ_o, the mean density, is constant; c is the (constant) speed of sound.

For the uniform flow region, $\delta \leq y \leq H$, where $U_x(y) = U_x$ is a constant, these equations combine to give

$$\frac{d^2p}{dy^2} + p\left\{\left(\frac{\omega - k_x U_x}{c}\right)^2 - k_x^2\right\} = 0. \qquad (6.2.5)$$

The appropriate solution for $dp/dy = 0$ at $y = H$ is

$$p(y) = A \cos k_y(y - H) \qquad (6.2.6a)$$

where

$$k_y^2 = \left(\frac{\omega - k_x U_x}{c}\right)^2 - k_x^2. \qquad (6.2.6b)$$

'A' is a constant (determined by boundary conditions given as a function of y) and k_y must satisfy the boundary condition at $y = \delta$ which, if given as an admittance $\beta_{\omega\delta}$, will be obtained as solutions of the equation

$$j\rho_o\omega h\left(1 - \frac{k_x U_x}{\omega}\right)\beta_{\omega\delta} = (k_y h)\tan(k_y h). \qquad (6.2.7)$$

$\beta_{\omega\delta}$ is taken to be the ratio of the velocity (normal to the plane $y = \delta$) in the negative y direction and the pressure, both at $y = \delta$.

For the non-uniform flow region, $0 \leq y \leq \delta$, the equations, after some manipulation (see Appendix (6A) for details), reduce to a pair of simultaneous, first order ordinary differential equations in the pressure, p, and velocity, v:

$$\frac{dv}{dY} = \left[\frac{1}{1 - \frac{k_x U_x(y)}{\omega}} \frac{d}{dY}\left(\frac{-k_x U_x(y)}{\omega}\right)\right]v + \left[\frac{k_y^2(y)\delta}{j\rho_o(\omega - k_x U_x(y))}\right]p, \qquad (6.2.8)$$

$$\frac{dp}{dY} = \left[-\rho_o j(\omega - k_x U_x(y))\delta\right]v + [0]p, \qquad (6.2.9)$$

where $k_y^2(y)$ is still defined by equation (6.2.6b), but with U_x

replaced by $U_x(y)$, and Y is the non-dimensionalised coordinate y/δ.

Equations (6.2.8) and (6.2.9) can be replaced by a second order differential equation in p alone but these equations are in the most suitable form for the following type of analysis and, apparently, are to be preferred for numerical integration (see section (6.3)). This is not surprising, however, as they were originally derived for numerical integration, to obtain solutions of ω/k_x or k_x in compressible stability analysis (24).

The first objective, to derive the variations of $v(Y)$ and $p(Y)$ in the region $0 \leq Y \leq 1$ in the limit $\delta \to 0$, is accomplished by neglecting the terms proportional to δ in equations (6.2.8) and (6.2.9); the latter reduces to

$$\frac{dp(Y)}{dY} \doteq 0$$

$$\text{or} \qquad p(Y) \doteq p(0); \qquad (6.2.10)$$

that is, the pressure is approximately uniform through the boundary layer. Equation (6.2.8) becomes

$$\frac{dv}{dY} \doteq \left[\frac{1}{1 - \frac{k_x U_x(y)}{\omega}} \frac{d}{dY}\left(\frac{-k_x U_x(y)}{\omega}\right)\right] v$$

which is integrated from $Y = 0$ to $Y = Y'$ with the proviso that $\omega/k_x = c_x \neq U_x(y)$ in this interval:

$$\int_{v(0)}^{v(Y')} \frac{dv}{v} \doteq \int_{U_x(0)}^{U_x(Y')} \frac{d(-k_x U_x(Y)/\omega)}{(1 - k_x U_x(Y)/\omega)}$$

or

$$\log_e\left\{\frac{v(Y')}{v(0)}\right\} \doteq \log_e\left\{1 - \frac{k_x U_x(Y')}{\omega}\right\}$$

or, dropping the Y' notation

$$v(Y) \doteq v(0)\,(1 - \frac{k_x U_x(Y)}{\omega}). \qquad (6.2.11)$$

As $v(Y)$ is related to the time derivative of the displacement, $\dot{\bar{\xi}}_y$, by

$$v(Y) = \dot{\bar{\xi}}_y(1 - k_x U_x(Y)/\omega)$$

equation (6.2.11) means that the displacement is approximately constant through the boundary layer and equal to the displacement at the wall. Equations (6.2.10) and (6.2.11) show that the variations of pressure and displacement through <u>any</u> realistic boundary layer, in the limit of vanishing thickness, are consistent with the uniform flow model boundary conditions of continuity of pressure and displacement. This result has been obtained on the assumption that c_x does not equal the mean velocity anywhere within the boundary layer (see section (6.4) for a discussion related to this point).

The next step is to retain terms in the differential equations which are proportional to δ: equation (6.2.11) for $v(Y)$ is substituted into equation (6.2.9) for dp/dY and the result is integrated to give (see Appendix (6B) for the derivation of the following results)

$$p(Y) \doteq p(0)\{1 + j(k_x\delta)\frac{\omega}{k_x}\rho_o\beta_\omega \int_0^Y (1 - \frac{k_x U_x(y)}{\omega})^2\, dY\}. \qquad (6.2.12)$$

Similarly equation (6.2.10) for $p(Y)$ is substituted into equation (6.2.8) for dv/dY and the result integrated to give

$$v(Y) \doteq v(0)\,\{1 - \frac{k_x U_x(Y)}{\omega}\}\{1 - (\frac{\omega\delta}{c})\frac{Y}{j\rho_o\beta_\omega} + (k_x\delta)\frac{k_x}{j\rho_o\beta_\omega}$$

$$\times \int_0^Y (1 - \frac{k_x U_x(y)}{j\rho_o\beta_\omega})^{-2}\, dY\}. \qquad (6.2.13)$$

Up to this point the speed of sound has been retained explicitly; this is because the case $c \to \infty$ (incompressible fluid) is to be considered in the following section. If the above expressions are written in terms of the usual non-dimensional admittance $\rho_o c\beta_\omega = \bar{\beta}_\omega$ the non-dimensional perturbation parameter emerges as $k\delta$:

$$p(Y) \doteq p(0)\{1 + j(k\delta)\bar{\beta}_\omega \int_0^Y (1 - K_x M_x(Y))^2 dY\}, \qquad (6.2.14)$$

$$v(Y) \doteq v(0)\{1 - K_x M_x(Y)\}\{1 - \frac{(k\delta)Y}{j\bar{\beta}_\omega} + (k\delta)\frac{K_x^2}{j\bar{\beta}_\omega}\int_0^Y (1 - K_x M_x(Y))^{-2} dY\}, \qquad (6.2.15)$$

where $K_x = k_x/k$, $M_x = U_x/c$.

For a compressible (finite c) fluid, equations (6.2.14) and (6.2.15) for the variation of $p(Y)$ and $v(Y)$ should be accurate to first order in $k\delta$. For the incompressible case the perturbation parameter can be taken to be $k_x\delta$.

These equations have been checked* (see Appendix (6C)) with Graham and Graham's (61) series expansion for the pressure in a <u>linear</u> profile boundary layer which is of the form

$$p(Y) = \sum_{n=1}^{\infty} a_n (1 - \frac{k_x U_x Y}{\omega})^n . \qquad (6.2.16)$$

In this case the integrals in equations (6.2.14) and (6.2.15), for $Y = 1$, are

$$\int_0^1 (1 - \frac{k_x U_x Y}{\omega})^2 dY = \frac{\omega}{3k_x U_x}\left[1 - (1 - \frac{k_x U_x}{\omega})^3\right]$$

---

*The equations have also been checked in the incompressible limit by taking the exact solutions for the linear profile and retaining terms to first order in $k_x\delta$: see Appendix (6D).

$$\int_0^1 (1 - \frac{k_x U_x Y}{\omega})^{-2}\, dY \;=\; (1 - \frac{k_x U_x}{\omega})^{-1},$$

so that the total changes in p and v across the boundary layer are given by

$$p(1) \doteq p(0)\,\{1 + j(k_x\delta)\,\frac{\omega}{k_x}\cdot\rho_o\beta_\omega\cdot\frac{\omega}{3k_xU_x}\,[1 - (1 - \frac{k_xU_x}{\omega})^3]\}, \qquad (6.2.17)$$

$$v(1) \doteq v(0)\,\{1 - \frac{k_xU_x}{\omega}\}\,\{1 - (\frac{\omega\delta}{c})\,\frac{1}{j\rho_o c\beta_\omega} + k_x\delta\,\frac{k_x}{j\omega\rho_o\beta_\omega}\,(1 - \frac{k_xU_x}{\omega})^{-1}\}, \qquad (6.2.18)$$

or in the 'compressible form'

$$p(1) \doteq p(0)\,\{1 + \frac{j(k\delta)\bar\beta_\omega}{3K_xM_x}\,[1 - (1 - K_xM_x)^3]\} \qquad (6.2.19)$$

$$v(1) \doteq v(0)\,\{1 - K_xM_x\}\{1 - \frac{(k\delta)}{j\bar\beta_\omega} + \frac{(k\delta)K_x^2}{j\bar\beta_\omega}\,(1 - K_xM_x)^{-1}\}. \qquad (6.2.20)$$

The final step is to match this pressure and velocity with that in the uniform flow region via the usual admittance method:

$$\beta_{\omega\delta} \doteq -\frac{v(1)}{p(1)}$$

$$\doteq \frac{-v(0)(1 - K_xM_x)\{1 - k\delta/j\bar\beta_\omega + k\delta K_x^2/j\beta_\omega(1 - K_xM_x)\}}{p(0)\qquad\{1 + jk\,\bar\beta_\omega[1 - (1 - K_xM_x)^3]/3K_xM_x\}}$$

or

$$\frac{\rho_o c\beta_{\omega\delta}}{(1 - K_xM_x)} \doteq \bar\beta_\omega + jk\delta\,\{1 - \frac{K_x^2}{(1 - K_xM_x)} - \frac{\bar\beta_\omega^2}{3K_xM_x}\,[1 - (1 - K_xM_x)^3]\}.$$

This expression for $\beta_{\omega\delta}$, the admittance at the edge of the uniform flow region, is substituted into equation (6.2.7) to give

$$\frac{(k_y h)}{jkh}\tan(k_y h) = \bar{\beta}_\omega(1 - K_x M_x)^2 + jk\delta(1 - K_x M_x)^2\left\{1 - \frac{K_x^2}{(1 - K_x M_x)}\right.$$

$$\left. - \frac{\bar{\beta}_\omega^2}{3K_x M_x}\left[1 - (1 - K_x M_x)^3\right]\right\}$$

$$= (\bar{\beta}_\omega + \bar{\beta}_\delta)(1 - K_x M_x)^2 \qquad (6.2.21)$$

where

$$\bar{\beta}_\delta = jk\delta\left\{1 - \frac{K_x^2}{(1 - K_x M_x)} - \frac{\bar{\beta}_\omega^2}{3K_x M_x}\left[1 - (1 - K_x M_x)^3\right]\right\} \qquad (6.2.22)$$

Equation (6.2.21) is one of the objectives of this section: the first term on the right hand side corresponds to the uniform flow model of Chapter 4 and is the only term if $k\delta \to 0$. It represents an adequate boundary condition for realistic profiles provided the remaining terms are negligible by comparison. If they are not these terms can be used as an approximation, valid to first order in $k\delta$, to the actual boundary condition. In principle these terms should present no further difficulties when solving for the solutions of K_x, in that, like the uniform flow model, the terms are a function of K_x, M_x and $\bar{\beta}_\omega$ plus one constant parameter, $k\delta$. However it has to be remembered that this approximation is for a linear profile: for any other profile the integrals in equations (6.2.12) and (6.2.13) must be re-evaluated. These, in general, would require numerical integration and then it may be preferable to integrate the exact equations instead and avoid approximations of this kind. Nevertheless work has been carried out (58) on estimating, by comparisons, the appropriate thickness of linear profile boundary layers which can be used instead of the complicated profiles found in practice and here the approximation given above may be of use. As a rough estimate the linear profile thickness should be taken to be $\frac{1}{8}$ of the actual turbulent boundary layer thickness.

The other objective of this section - to specify the conditions under which the uniform flow model boundary conditions can be used to obtain realistic solutions of K_x - is, in general, unattainable. Ironically the example which best explains the reason for this is the condition where the solution has been optimised for the maximum attenuation, which is defined by

$$\frac{d}{d(k_y h)} \left\{ \frac{(k_y h)\tan(k_y h)}{(1 - K_x M_x)^2} \right\} = 0 \qquad (6.2.23)$$

or

$$\frac{d(\bar{\beta}_\omega + \bar{\beta}_\delta)}{d(k_x h)} = 0 ;$$

that is, any change in $(\bar{\beta}_\omega + \bar{\beta}_\delta)$ brings about a large change in $(k_x h)$. Thus at and near this extreme condition it is <u>not</u> sufficient to state that "the uniform flow model is realistic provided it predicts the admittance within a certain error". The allowable error is variable, being extremely small at the optimum condition and roughly proportional to the error induced in $k_x h$ elsewhere, except at local maxima and minima.

(With this result the optimisation results are placed in their intended perspective: their value lies in the indicated trends and not in the absolute values. Any perturbation, be it in duct width, liner impedance, frequency or flow, inevitably causes an abrupt change away from the optimised attenuation rate.)

Away from 'optimum' conditions the terms proportional to $k\delta$ can be meaningfully evaluated for two examples:

(a) $K_x \doteq \frac{1}{1 + M_x}$ (the 'well cut-on' approximation)

and

(b) $(1 - K_x M_x) \doteq -K_x M_x$ (the 'well cut-off' approximation).

For example (a) the right hand side of equation (6.2.21) becomes

$$\frac{\bar{\beta}_\omega}{(1+M_x)^2} + \frac{jk\delta}{(1+M_x)^2}\left\{\frac{1}{(1+M_x)} - \frac{\bar{\beta}_\omega^2(1+M_x)}{3M_x}\right.$$

$$\left.\times\left[1 - \left(\frac{1}{1+M_x}\right)^3\right]\right\}$$

and the ratio of the terms proportional to $k\delta$ and the first term is, for low subsonic Mach numbers, approximately

$$\frac{jk\delta}{(1+M_x)}\left(M_x\bar{Z}_\omega - \bar{\beta}_\omega\right). \qquad (6.2.24)$$

The effect of a finite thickness boundary layer for a 'well cut-on' mode is minimised for a wall admittance such that $\bar{\beta}_\omega^2 \doteq M_x$ and, due to the term $(1+M_x)$, is larger for negative Mach numbers (sound propagation upstream) than for positive Mach numbers of the same magnitude.

For example (b) the ratio of the terms is, approximately,

$$jk\delta\left\{\bar{Z}_\omega\frac{K_x}{M_x} + \bar{\beta}_\omega\frac{K_x^2M_x^2}{3}\right\} \qquad (6.2.25)$$

and thus the 'well cut-off' solutions of K_x are expected to be sensitive to boundary layer thickness (as K_xM_x can be large).

In the following section some numerical solutions are presented for K_x to illustrate and verify some of the conclusions reached in this section.

6.3 Some Exact Solutions Obtained by Numerical Integration of the Differential Equations

6.3.1 Some exact solutions which converge to the uniform flow solutions as $\delta \to 0$

The linearised equations for unsteady, compressible, inviscid motion in parallel sheared flow have been solved numerically by, among others, Mack (24), Mungur and Gladwell (52) and Kurze (17), Mungur's (52) computer program being available within the Institute of Sound and Vibration (52). The occurrence of the strange mode solutions in the uniform flow model, during the optimisation work described in Chapter 4, prompted the author to request Mungur to investigate the behaviour of these solutions in flows with boundary layers adjacent to the duct walls. In the first instance Mungur checked a chosen uniform flow solution and then replaced the uniform flow regions adjacent to the walls by linear profile boundary layers to variable thickness. The rather disturbing result emerged that even for thin boundary layers the solution for K_x was markedly different from the agreed uniform flow solution. Thus a paradox appeared which could only be explained if it were to be established that the K_x solution for a trapezoidal flow profile does not converge to that for a uniform flow profile, in the limit as the 'boundary layer' width tends to zero.

This was regarded as an unacceptable argument and two investigations were initiated, one being the subject of the previous section. The other, described here, is essentially a repetition of Mungur's preliminary investigation but using a completely independent computer program specially written for the purpose.

The model used by Mungur is shown in Figure (6.2): the duct width is held constant and δ, which will be expressed relative to H, is varied. The parameter values are identical to those used in section (4.7), that is,

$kH = \pi/10$; $M_x = 0.5$; $\bar{\beta}_\omega = 0.28 + j.039$

$(\bar{Z}_\omega = 3.5 - j.4892)$

These values are close to those that give rise to a uniform flow double pole (or an 'optimum' condition), which are: the same reduced frequency, Mach number and reactance but with $Re(\bar{Z}_\omega) = 3.982$.

Mungur checked the uniform flow solution for the (1-) mode (the minus sign indicates attenuation in the upstream, negative x direction*, a plus sign, attenuation in the downstream positive x direction) which is

$$K_x = 5.800 + j\ 11.95$$

but failed to find similar values for K_x with any finite δ/H value.

Here the variation of K_x with δ/H will be shown for the (1-) mode and also for the modes (0-), (2-), (0+), (1+) and (2+), which have the following uniform flow solutions:

Mode	K_x	
0+	.7417	-j.1597
1+	-2.764	-j8.893
2+	-3.109	-j18.22
0-	-1.731	j1.569
1-	5.800	j11.95
2-	2.536	j15.67

The variation of $|Im(K_x)|$ with δ/H for these 6 modes is shown in Figure (6.3) for $\delta/H = 0$ to $\delta/H = 6\%$**; the variation of $Re(K_x)$ with /H, for the same range, is shown in Figure (6.4). All these solutions converge to the uniform flow solutions as $\delta/H \to 0$. These

---

*This notation is for convenience and does not define which side of the source plane the mode exists, that is, whether it is attenuating away from a source plane in the upstream direction - see section (4.7).

**According to the crude rule that this linear profile, representing the turbulent boundary layer, is $\frac{1}{8}$ of the total boundary layer thickness, $\delta/H = 6\%$ corresponds approximately to the maximum possible total boundary layer thickness of $H/2$.

results together with the analytic results of the previous section provide adequate proof that the uniform flow model represents the effects of real velocity profiles on sound propagation and attenuation in lined ducts, if the shear or boundary layer regions are sufficiently thin.

The rest of this section is devoted to interpreting the behaviour of K_x, the normalised axial wavenumber, with boundary layer thickness, apart from the following brief discussion on the differences between the present computer program and the one written by Mungur and Gladwell (52).

The essential difference is that the present program numerically integrates differential equations of the form

$$\frac{dp}{dy} = (A)p + (B)v \qquad (6.3.1)$$

$$\frac{dv}{dy} = (C)p + (D)v \qquad (6.3.2)$$

whereas Mungur's program integrates the equations

$$\frac{dp}{dy} = (E)X + (F)p \qquad (6.3.3)$$

$$\frac{dX}{dy} = (G)X + (H)p \qquad (6.3.4)$$

where A, B, ..., H are functions of k, K_x and $M_x(y)$ and $A \equiv F \equiv 0$.

Numerical integration is carried out by evaluating the right hand sides of these equations at a number of evenly spaced points, 0, Δy, $2\Delta y$, ..., called integration points, and this number has to be specified, in advance, for the standard integration subroutine. (Advanced subroutines determine this number by iteration but these have not been used here or by Mungur (52).) The accuracy of integration depends on the chosen number of integration points and strictly speaking the required number, n, has to be determined by simply increasing n until K_x (or any other parameter of interest) ceases to change, up to so many significant figures. As the dependent variables differ in the two programs the required number of integration points will, in general, be different. To illustrate this point a second program was written to integrate the

form of the differential equations used by Mungur and the number of integration points was varied from 2 to 20 in both programs for the (2-) mode in the δ/H range 0.05-5%. The resulting variations of $Re(K_x)$ with δ/H are shown in Figure (6.5): this second program requires twenty integration points before $Re(K_x)$ ceases to change whereas the original program requires only two. It is suggested that this unexpected sensitivity of $Re(K_x)$ to the number of integration points is the main reason for Mungur's failure to obtain convergence to the uniform flow solution, although originally another reason was confusion between the (1-) and (2-) modes. The reasons for the order of magnitude difference in required integration points between each program are not yet established.

6.3.2 Interpretation of the dependence of axial wavenumbers on boundary layer thickness

Returning to Figures (6.3) and (6.4), note first that the lowest order modes (0+) and (0-) are almost entirely independent of δ/H, as might be expected from equation (6.1.24); the same will be true in further examples. The most rapid variations of K_x with δ/H are exhibited by the (1-) and (2-) modes: even at $\delta/H = 0.5\%$ for the (1-) mode the change in $Re(K_x)$ is 45% and in $Im(K_x)$ is 14%, relative to their values at $\delta/H = 0$. An inspection of the pressure and displacement variation through the boundary layer reveals that the total changes are not large and, therefore, that this large change in $Re(K_x)$ is a good example of the predicted sensitivity of K_x for modes near 'optimum' conditions (the chosen impedance is near the 'optimum' value for the (1-, 2-) mode pair).

Examples of displacement variation through the boundary layer for the (1-) mode are shown in Figure (6.6). Here the real part of the ratio

of the displacement to its value at the wall (at $Y = 0$) is shown for the slightly different model sketched in Figure (6.7), although this has negligible effect on these particular results, as will be seen later. The imaginary part of the normalised displacement (not shown) is zero, by definition, at y/δ but through most of the boundary layer has a value approximately equal to 10% of the real part. The pressure variation is almost negligible, and is therefore not shown, the total change across the boundary layer being 0.5% for the case of $\delta/h = 0.4\%$. Thus a change of approximately 10% in the modulus of ratio of pressure and displacement at the edge of the boundary layer brings about a change in $Re(K_x)$ approaching 50%, although the change in $|K_x|$ is only about 19%.

These changes in pressure and displacement can also be obtained from the approximate analytic expressions given in the previous sections: from equation (6.2.19) the total change across a linear profile boundary layer is

$$\frac{p(1)}{p(0)} = \{1 + j \frac{k\delta\bar{\beta}_\omega}{3K_x M_x} [1 - (1 - K_x M_x)^3]\} \qquad (6.3.5)$$

which for large $|K_x|$ and $|Im(K_x)| > |Re(K_x)|$ is

$$\left| \frac{p(1)}{p(0)} - 1 \right| \doteq kh\left(\frac{\delta}{h}\right) \frac{|\bar{\beta}_\omega|}{3} |K_x|^2 M_x .$$

For the values

$$kh = \pi/10 \doteq 0.3$$

$$\delta/h = 0.004$$

$$|\beta_\omega| \doteq 0.28$$

$$M_x = 0.5$$

$$|K_x| \doteq 16$$

the above expression yields

$$\left|\frac{p(1) - p(0)}{p(0)}\right| \doteq 0.7\%$$

From equation (6.2.20) the total displacement change is

$$\left|\frac{\xi_y(1)}{\xi_y(0)}\right| \doteq 1 - \frac{k\delta}{j\bar{\beta}_\omega} + \frac{k\delta K_x^2}{j\bar{\beta}_\omega}(1 - K_x M_x)^{-1} \qquad (6.3.6)$$

which for large $|K_x|$ and $|\mathrm{Im}(K_x)| > |\mathrm{Re}(K_x)|$ is

$$\left|\frac{\xi_y(1)}{\xi_y(0)} - 1\right| \doteq kh\,\frac{\delta}{h}\,\frac{|K_x|}{M_x\,|\beta_\omega|}$$

(the omission of the term $k\delta/j\bar{\beta}_\omega$ is justified below). For the above parameter values the above expression yields

$$\left|\frac{\xi_y(1) - \xi_y(0)}{\xi_y(0)}\right| \doteq 14\%.$$

The omitted term $k\delta/j\bar{\beta}_\omega$ is of order 0.5%. In view of the approximations these are in good agreement with the computed values.

As the ratios $|p(1)/p(0)|$ and $|\xi_y(1)/\xi_y(0)|$ are proportional to $|K_x|^2$ and $|K_x|$, respectively, much larger changes will occur in pressure and displacement for the (2+) mode, for example ($|K_x| \doteq 18$) but there is a less rapid variation in K_x with δ/H. In fact it will be seen that the variation that does exist is not due to the change in thickness of the boundary layer adjacent to the finite admittance wall but is due to the other boundary layer adjacent to the rigid wall.

To illustrate this and to be able to compare results with analytic approximations, the model is changed to that shown in Figure (6.7): the boundary layer adjacent to the rigid wall is now absent and the model can be thought of as a duct of twice the width (2H) with an identical boundary layer adjacent to an identical wall admittance at $y = 2H$.

The variation of K_x with δ/H for the same modes as before is shown in Figures (6.8) and (6.9) where the previous results are entered for comparison. The variation of $Im(K_x)$ with δ/H for the (2+) mode is now almost entirely removed, and although $Re(K_x)$ changes by 10% between $\delta/H = 0$ and $\delta/H = 0.4\%$ this is small in comparison with the 45% change in $Re(K_x)$ for the (1-) mode; of course $|K_x|$ for the (2+) mode does not change, significantly, throughout the δ/H range as $|Re(K_x)| << |Im(K_x)|$ and $|K_x| \doteq |Im(K_x)|$. Clearly a boundary layer adjacent to the rigid wall has a strong influence on both the (2-) and (2+) modes. To understand this the approximation expressions in the previous section would have to be re-derived with the finite admittance at $y = H - \delta$ being taken into account. Another striking feature of the comparisons in Figures (6.8) and (6.9) is the almost complete insensitivity of the (1-) mode to the removal of the boundary layer adjacent to the rigid wall. This is not surprising in view of the conclusion of section (4.7), that this mode is associated with the instability of the shear layer adjacent to the finite admittance wall. This particular mode is discussed further in section (6.4).

Actually the model in Figure (6.7) with the duct width, H, kept constant is still not quite comparable with the model used for the analytic approximations. There it is implicitly assumed that the width of the uniform flow region, h, is a constant although it is not difficult to re-derive equation (6.2.21), for example, with $h = H - \delta$. In Figures (6.11) and (6.12) the K_x variation with δ/H or δ/h for the same 6 modes is shown with H constant and h constant, there being very little difference between the two. This might appear to contradict a previous statement that the near 'optimum' modes (1-) and (2-) are sensitive to the value of parameters like kh. However at low frequencies

it is known, even from the zero flow case (see Figure 2.15), that the wavenumber is nearly independent of kh although it still remains sensitive to boundary conditions.

Finally as a means of identifying the important terms in equation (6.2.21), which in its 'incompressible' form is

$$\frac{(k_y h)}{j\omega h}\tan(k_y h) = \rho_o\beta_\omega(1 - \frac{k_x U_x}{\omega})^2$$

$$-j(k_x\delta)\frac{k_x}{\omega}(1 - \frac{k_x U_x}{\omega}) - j(k_x)\frac{\omega^2\rho_o^2\beta_\omega^2}{k_x^2.3U_x}(1 - \frac{k_x U_x}{\omega})^2$$

$$\times\left[1 - (1 - \frac{k_x U_x}{\omega})^3\right], \qquad (6.3.7)$$

the boundary layer region is taken to be incompressible ($c \to \infty$) while the uniform flow region remains compressible. The results are shown in Figures (6.12) and (6.13). There is very little difference between K_x values for the compressible and incompressible boundary layer and the values can only just be distinguished, graphically, for the (0-), (1-) and (2-) modes.

It can therefore be deduced that where the K_x solutions do exhibit any significant dependence upon the boundary layer thickness, the important terms in equation (6.2.21) are (with the uniform flow region speed of sound being used, if required)

$$\frac{k_y h}{jkh}\tan(k_y h) = \bar{\beta}_\omega(1 - K_x M_x)^2 + jk\delta(1 - K_x M_x)^2\{ - \frac{K_x^2}{(1 - K_x M_x)}$$

$$- \frac{\bar{\beta}_\omega^2}{3K_x M_x}\left[1 - (1 - K_x M_x)^3\right]\} \qquad (6.3.8)$$

It is not possible to simplify the right hand side of this equation for the (1-) mode over the entire range of δ/h values, because $\mathrm{Im}(K_x)$ dominates $|K_x|$ for small values and $\mathrm{Re}(K_x)$ for large values.

For the (2-) mode, however, where $K_x \doteq j|\mathrm{Im}(K_x)|$ the right hand

side, $\bar{\bar{\beta}}_{\omega\delta}$, is, approximately,

$$\bar{\bar{\beta}}_{\omega\delta} \doteq -\mathrm{Re}(\bar{\beta}_\omega)\,|\mathrm{Im}(K_x)|^2\,M_x^2 + (kh)\left(\frac{\delta}{h}\right)\,|\mathrm{Im}(K_x)|^3\,M_x$$
$$-j(kh)\left(\frac{\delta}{h}\right)\,|\mathrm{Im}(K_x)|^4\,M_x^4\,\frac{\mathrm{Re}(\bar{\beta}_\omega)^2}{3} \qquad (6.3.9)$$

The (2-) mode is particularly interesting because at $\delta/h = 0$, like the (1-), (1+) and (2+) modes over the entire range, it is an example of a 'strange' mode, but at a value of $\delta/h \doteq 2.5\%$ $\mathrm{Re}(K_x) = 0$; at $\delta/h \doteq 3.3\%$ $\mathrm{Re}(K_x) = -0.66$ and the real part of the Lorentz wavenumber, k_x, is zero: that is, within the uniform flow region,

$$K_x = -\frac{M_x}{1 - M_x^2} + \frac{k_x'}{k(1 - M_x^2)}.$$

Thus when $\mathrm{Re}(k_x') = 0$

$$\mathrm{Re}(K_x) = \frac{-M_x}{1 - M_x^2} = -0.66 \qquad (\text{for } M_x = 0.5).$$

The reason for these 'strange' modes* is the appearance of a negative real part of the effective admittance, $\bar{\bar{\beta}}_{\omega\delta}$. In the present example, for $\delta/h = 3.3$, the component of $\bar{\bar{\beta}}_{\omega\delta}$ which is independent of δ/h according to equation (6.3.9) takes the value

$$-\mathrm{Re}(\bar{\beta}_\omega)\,|\mathrm{Im}(K_x)|^2\,M_x^2 = -10.8 \qquad (|\mathrm{Im}(K_x)| = 12.4).$$

This <u>negative</u> value, and similar values at lower δ/h values, is the reason for the 'strange' mode. However the second term in $\bar{\beta}_{\omega\delta}$ is real and takes the value

*'Strange' in the sense that the Lorentz phase velocity $(\omega/\mathrm{Re}(k_x'))$ is in the opposite direction to that of decay.

$$(kh)\left(\frac{\delta}{h}\right)\left|\mathrm{Im}(K_x)\right|^3 M_x = +9.9 \quad (\delta/h = 3.3\%); \quad +10.8 \ (\delta/h = 3.6\%).$$

Thus the approximate analytic formula (6.3.9) for $\bar{\bar{\beta}}_{\omega\delta}$ predicts that $\mathrm{Re}(\bar{\bar{\beta}}_{\omega\delta}) = 0$ at a δ/h value correct to within 10%; for larger values of δ/h $\mathrm{Re}(\bar{\bar{\beta}}_{\omega\delta})$ is positive and the mode is 'well behaved'. The third term in $\bar{\bar{\beta}}_{\omega\delta}$ is, in this approximation, imaginary and while it can be important in determining the actual value of K_x it does not play any direct part in the transition from a 'strange' to a 'well behaved' mode.

This concludes a preliminary interpretation of the dependence of modal wavenumbers on boundary layer thickness; the (1-) mode is considered further in section (6.4).

6.4 Discussion: The Role of Duct Modes, the Green's Function and Other Mode Solutions in Sheared Flow

The influence of a finite boundary layer thickness on the mode axial wavenumbers has been determined for a particular example, but it cannot be immediately assumed that each mode in sheared flow plays the same role as it does in 'plug' flow. For example, in Figure (6.4), the change in sign of $Re(K_x)$ for the (2-) mode and, in Figure (6.3), the rapid reduction in $|Im(K_x)|$ with increasing δ/H for the (1-) mode, possibly leading to a change in sign of $Im(K_x)$, may indicate a change of role for these modes. Strictly speaking it appears that Briggs' (23) procedure must be repeated for each duct mean velocity profile. This requires the expression for the Fourier transform (in space and time) of the field due to a source or source distribution (e.g. the Green's function) in sheared flow. To the author's knowledge such an expression is not available but in some unpublished work Möhring (12) claims to have obtained the Fourier x transform*, $P(y, k_x)$ of the field due to an arbitrary source distribution (at $x = \bar{x}_0$) in a rigid walled, semi-infinite duct containing mean flow with a symmetric velocity profile. The function $P(y, k_x)$ has an "infinite number of poles above and below the real k_x-axis and branch points on the real axis" on the complex k_x plane. In the inversion of $P(y, k_x)$ the contribution from these branch points is a 'far-field' which grows in the downstream direction like $x^{3/2}$.

It seems reasonable to assume that the poles in Möhring's (12) analysis are equivalent to those defined in section (4.4) (on the complex θ' plane) for the Green's function, but with the effective admittance, $\bar{\bar{\beta}}_{\omega'}(1 - M_x \sin\theta')$, replaced by $\bar{\bar{\beta}}_{\omega'\delta}$ which depends on the properties of the shear region as well as on ω', M_x and θ'. In other words the

---

*Or, possibly, an approximation.

analysis of section (4.4), based on the Lorentz transform and the Brekhovskikh (20) method, can still be applied to the uniform flow region but with modified boundary conditions for that region and the restriction that the line source is contained within the region. In effect, all that is required are the modified pole locations (that is the mode solutions - the subject of the previous section) and the evaluation of

$$\left[\frac{d\bar{\beta}_{\omega'\delta}}{d\theta'}\right]_{\theta'=\theta'_n}$$

to determine the residue or mode amplitude.

This approach apparently overlooks the existence of branch points and, therefore, of part of the solution like that obtained by Möhring(12) which grows like $x^{3/2}$ in a rigid walled duct. However if the approach is correct in all other respects, it would allow one to use Briggs' (23) procedure to determine the role of each mode and hence to obtain the Green's function (for $x - \bar{x}_o \lesssim 0$) with the restriction, of course, that the line source is located somewhere in the uniform flow region. The full Briggs' (23) procedure has not been applied in this section; instead it is, in effect, carried out for a one particular mode, the (1-) mode, and the results confirm an intuitive understanding of the role of this mode in sheared flow.

In section (4.7) the (1-) mode in 'plug' flow is identified as a mode that exists downstream of the source and is spatially amplified. It is clearly associated with the incompressible Helmholtz temporal instability of an inviscid fluid interface or vortex sheet (in the absence of all boundaries). In this classical model it is known that if the step velocity profile is replaced by a finite width shear region the time amplification rate, for a given real axial wavenumber, (k_x), is modified, and eventually tends to zero with increasing $k_x\delta$. Rayleigh (44) shows that for a linear profile shear region the time amplification rate

reduces to zero when $k_x\delta \doteq 1.3$.

Although the present model differs considerably, it is suggested that the reduction in $|Im(K_x)|$ for the (1-) mode is simply a reduction in the spatial amplification rate; that is, the mode is tending to be stabilised by the increased boundary layer widths.

This suggestion could be tested by applying Briggs'(23) procedure; that is, by increasing the imaginary part of the frequency (time amplification) and seeing if the sign of the imaginary part of k_x changes. If it does, the mode <u>is</u> unstable and is, therefore, a spatially amplified mode with the (real) source frequency time dependence. To avoid this tedious procedure (considerably lengthened by the fact that a transcendental equation is now replaced by differential equations) a simpler method can be used, if

$$|Im(k_x)| << |Re(k_x)|,$$

which will be referred to as condition A. If 'A' is satisfied then, according to Gaster (62), given a solution with a real frequency $\omega = \omega_r$ and a complex wavenumber $k_x = k_{xr} + jk_{xi}$, another solution is

$$\omega = \omega_r + j\omega_i$$

$$k_x = k_{xr}$$

where

$$\omega_i = -k_{xi}\frac{\partial\omega_r}{\partial k_{xr}}.$$

If this solution gives $\omega_i < 0$ (time amplification) then <u>it is the equivalent</u> of Briggs' (23) procedure because the real part of the frequency is the same and the imaginary part of k_x is zero, that is, <u>it is about to change sign.</u>

Actually it is easier to solve the equations directly for ω, with

$k_x = k_{xr}$, than to work out the group velocity c_g where

$$c_g = \frac{\partial \omega_r}{\partial k_{xr}} ;$$

of course it is necessary to check that the solution gives $Re(\omega) \doteq \omega_r$, the original real frequency. Solutions could also be obtained when 'A' is not satisfied but then, in general, the solution $Re(\omega)$ would differ from the original frequency of interest.

To obtain k_x solutions which satisfy 'A', the δ/H range has been extended for the (1-) mode and solutions for the model shown in Figure (6.2) are shown in Figure (6.14); the range $0 \lesssim \delta/H \lesssim 6\%$ covered by Figures (6.3) and (6.4) is also included. Of course velocity profiles for δ/H values larger than 6% bear little relation to those found in practice but they do allow principles to be demonstrated and, in any case, other more realistic profiles and different parameter values may well yield k_x solutions satisfying 'A'. With these larger δ/H values considerably more integration points are required to obtain solution convergence, as might be expected: some examples are given below in Table A. In addition some difficulty was experienced in establishing the sign of $Im(K_x)$ at $\delta/H = 40\%$ and this will be discussed later.

The imaginary frequency solutions have been obtained for three δ/H values and are given in Table B below in terms of K_x. The real k_x solutions are amplifying with time and hence the real ω solutions for the (1-) mode play the same role as did the (1-) mode in 'plug' flow. It is not unreasonable to assume that the same is true throughout the entire δ/H range. The similarity of K_x values in Table B means that the group velocity is approximately equal to the phase velocity, which at $\delta/H = 40\%$ equals 80% of the uniform flow velocity.

	Re(K_x)			
δ/H%/N	5	10	20	40
6.3	9.059	9.126	9.126	9.125
8.0	8.233	8.150	8.141	8.142
10.0	7.275	7.071	7.072	7.072
12.5	8.344	6.071	6.058	6.059
16.0	7.955	5.157	5.153	5.153
20.0	7.652	4.341	4.349	4.349
25.0	7.498	3.619	3.639	3.639
31.5	7.488	3.016	3.018	3.016
40.0	7.634	2.477	2.472	2.469

	Im(K_x) (+j notation)			
δ/H%/N	5	10	20	40
6.3	2.121	2.051	2.043	2.042
8.0	1.517	1.391	1.403	1.402
10.0	0.6755	0.9246	0.9191	0.9193
12.5	0.5273	0.6170	0.6189	0.6191
16.0	0.3854	0.4072	0.4137	0.4134
20.0	0.2626	0.2693	0.2613	0.2613
25.0	0.1736	0.1471	0.1478	0.1479
31.5	0.1272	0.08421	0.06815	0.06780
40.0	0.1232	-0.02056	-0.02093	0.01699

Table A. Variation of K_x solutions for the (1-) mode with number of integration points, N.

δ/H%	K_x(real ω)	K_x (real k_x)
25.0	3.639 + j.1479	3.632 + j.1511
31.5	3.016 + j.06780	3.014 + j.06828
40.0	2.469 + j.01699	2.469 + j.01712

Table B. Comparison of K_x solutions for real ω and real k_x (N = 40).

For larger δ/H values $Im(K_x)$ will presumably continue to decrease but it is not known whether it will remain positive or change sign. The latter alternative would be difficult to understand in view of the fact that one wall has a passive impedance. In either case further computation must be ruled out until the following problem is resolved.

Both terms on the right hand side of the differential equation (6.1.8) have the denominator

$$1 - K_x M_x(Y).$$

As $|Im(K_x)| \to 0$ this term tends to zero at some point, Y_c, in the interval $0 \leq Y \leq 1$ $(0 \leq y \leq \delta)$ if $Re(K_x)M_x > 1$: that is, if the phase velocity is less than the uniform flow velocity and in the same direction. This condition is satisfied by the (1-) mode solutions and hence the probable cause of the computational difficulty is the appearance, in the limit $|Im(K_x)| \to 0$, of a singularity at $Y = Y_c$.

Correct treatment of this problem is clearly essential and although it does not appear to have arisen in previous studies of 'sound' propagation and attenuation in sheared flows, not surprisingly a large part of the theory developed for stability analysis is concerned with this problem.

According to stability theory (60) to obtain a K_x solution of the inviscid equations which is a valid solution of the viscous equations in the limit of vanishing viscosity, it is necessary to introduce the concept of a path of integration between $Y = 0$ and $Y = 1$ in the complex Y plane. The most important feature of the correct path of integration is its position relative to the location of the singularity of the differential equation at $Y = Y_c$, where Y_c is defined by

$$1 - K_x M_x(Y_c) = 0.$$

This singularity cannot be ignored just because K_x, and hence Y_c, is complex. It has been deduced (60) that for k_x real, ω complex and rigid wall boundary conditions, the correct path of integration is along the real (Y) axis only if the mode amplifies with time. If it decays with time (and this includes the neutral case, $Im(\omega) = 0$*) the integration path must not pass between the singularity and the real axis. For example if the mode decays with time and $Im(Y_c) > 0$ the integration path must be of the type shown in Figure (6.15a); if it amplifies with time and $Im(Y_c) < 0$ the path is along the real (Y) axis as in Figure (6.15b). A definition of the correct paths for the complex k_x case does not appear to be available, but clearly must be established before complete computation studies can be carried out in this field. In the particular examples considered above the 'equivalence' of the $Re(k_x)$ and $Re(\omega)$ cases presumably means that the present** definition <u>can</u> be used and hence computational difficulties avoided by making a detour around the singularity, which lies close to the Re(Y) axis. However this requires extensive changes to the computer programs and has not been attempted.

---

*In the sense that the path can be moved off the real (Y) axis to avoid the singularity at $Y = Y_c$.

**That is, the definition of integration paths given above for $Re(k_x)$ and complex ω.

Appendix 6A

Derivation of the Simultaneous Differential Equations for the Pressure and Normal Velocity

The continuity, momentum and energy equations are:

$$j(\omega - k_x U_x(y))\rho - j\rho_o k_x u + \rho_o \frac{dv}{dy} = 0 , \tag{1}$$

$$\rho_o j(\omega - k_x U_x(y))u + \rho_o v \frac{dU_x(y)}{dy} = jk_x p , \tag{2}$$

$$\rho_o j(\omega - k_x U_x(y))v = - \frac{dp}{dy}, \tag{3}$$

$$p = c^2 \rho . \tag{4}$$

First substitute for ρ in equation (1) using equation (4):

$$\frac{j(\omega - k_x U_x(y))p}{c^2} - j\rho_o k_x u + \rho_o \frac{dv}{dy} = 0. \tag{5}$$

From (2), u is given by

$$u = \frac{k_x p}{\rho_o(\omega - k_x U_x(y))} + \frac{jv}{(\omega - k_x U_x(y))} \frac{dU_x(y)}{dy} \tag{6}$$

so that u can be eliminated from equation (5) to give

$$\frac{dv}{dy} = \left[\frac{-k_x}{(\omega - k_x U_x(y))} \frac{dU_x(y)}{dy}\right] v + \left[\frac{(\omega - k_x U_x(y))^2 - c^2 k_x^2}{j\rho_o c^2 (\omega - k_x U_x(y))}\right] p. \tag{7}$$

Putting $Y = y/\delta$ and using the notation

$$\frac{(\omega - k_x U_x(y))^2}{c^2} - k_x^2 = k_y^2(y)$$

gives equation (6.2.8).

Equation (6.2.9) is equation (3) above with $Y = y/\delta$.

Appendix 6B

Derivation of the Expressions for the Variation of the Pressure and Normal Velocity to First Order in $k_x\delta$ or $k\delta$

To obtain equation (6.2.12) the zeroth order expression for v,

$$v(Y) \doteq v(0)(1 - k_x U_x(y)/\omega),$$

is substituted into the differential equation for dp/dy,

$$\frac{dp}{dy} \doteq [-\rho_o j(\omega - k_x U_x(y))\delta]\ v(0)(1 - k_x U_x(y)/\omega),$$

which is integrated to give

$$p(Y) - p(0) \doteq -j\omega\rho_o v(0) \int_0^Y (1 - k_x U_x(y)/\omega)^2\, dY$$

and, with $-v(0) = p(0)\beta_\omega$, this gives equation (6.2.12).

To obtain equation (6.2.13) the zeroth order expression for p

$$p(Y) \doteq p(0)$$

is substituted into the differential equation for dv/dY to give

$$\frac{dv}{dY} + P(Y)v = Q(Y) \qquad (8)$$

where

$$P(Y) = -\left[\frac{1}{(1 - k_x U_x(y)/\omega)} \frac{d}{dY}\left(-\frac{k_x U_x(y)}{\omega}\right)\right],$$

$$Q(Y) = \frac{k_y^2(Y)\delta\, p(0)}{j\rho_o(\omega - k_x U_x(y))}.$$

Equation (8) has the standard solution

$$v = A \exp\left[-\int P\, dY\right] + \exp\left[-\int P\, dY\right] \int \exp\left[\int P\, dY\right] Q\, dY$$

and with $\exp\left[-\int P\, dY\right] = (1 - k_x U_x(Y)/\omega)$ this becomes

$$v = A(1 - k_x U_x(Y)/\omega) + (1 - k_x U_x(Y)/\omega) \int \frac{k_y^2(Y)\delta p(0)\, dY}{j\rho_o\omega(1 - k_x U_x(Y)/\omega)^2} \cdot \tag{9}$$

As $v = v(0)$ at $Y = 0$ so that

$$v(0) = A + \int \frac{k_y^2(Y)\, \delta p(0)\, dY}{j\rho_o\omega(1 - k_x U(Y)/\omega)^2}$$

equation (9) becomes

$$v(Y) = v(0)\ (1 - k_x U_x(Y)/\omega) + (1 - k_x U_x(Y)/\omega)\ \frac{\delta p(0)}{j\rho_o\omega} \int_0^Y \frac{k_y^2(Y)dY}{(1 - k_x U_x(Y)/\omega)^2} \tag{10}$$

By using $p(0) = -v(0)/\beta_\omega$ and the expression for $k_y^2(Y)$ equation (6.2.12) is derived.

Appendix 6C

To Check the Expressions for the Pressure and Velocity Variations through a Linear Profile Boundary Layer with Graham and Graham's (61) Result, to First Order in $k\delta$.

Graham and Graham's (61) expression for the pressure in a linear profile region is given in the form of an expansion about the critical point:

$$p(Y) = \sum_{n=0}^{\infty} a_n \left(1 - \frac{k_x U_x}{\omega}\right)^n$$

or, explicitly, in Graham and Graham's (61) notation,

$$p(\zeta) = a\{1 - \frac{K_x^2}{2B^2}(1 - B\zeta)^2 - [\frac{1}{4B^2} + \ldots](1 - B\zeta)^4 \ldots\}$$

$$+ b\{(1 - B\zeta)^3 + \frac{K_x^2}{10B^2}(1 - B\zeta)^5 - [\frac{1}{28B^2} \ldots](1 - B\zeta)^7 \ldots\} \quad (11)$$

where $B = K_x M_x/k\delta$, $\zeta = k\delta.Y$ and $M_x = U_x/c$ and where terms up to B^{-2} have been retained so that $v(\zeta)$, which is given by

$$v(\zeta) = \frac{-1}{j\rho_o c(1 - B\zeta)} \frac{dp}{d\zeta}, \quad (12)$$

will be correct to order B^{-1}. The ratio of the constants a and b are determined by the boundary condition $v(0) = -\beta_\omega p(0)$. From equations (11) and (12), $v(\zeta)$ is given by

$$v(\zeta) = \frac{-1}{j\rho_o c(1 - B\zeta)}\{a[\frac{K_x^2}{B}(1 - B\zeta) + \frac{(1 - B\zeta)^3}{B} + O(\frac{1}{B})^2]$$

$$+ b[-3B(1 - B\zeta)^2 - \frac{K_x^2}{B}(1 - B\zeta)^4 + \frac{(1 - B\zeta)^6}{4B} + O(\frac{1}{B})^2]\}. \quad (13)$$

Application of the boundary condition at $\zeta = 0$ gives

$$b \doteq a \frac{\{\frac{K_x^2}{B} + \frac{1}{B} - j\rho_o c\beta_\omega\}}{\{j\rho_o c\beta_\omega + 3B + \frac{K_x^2}{2B} - \frac{1}{4B}\}}. \quad (14)$$

The constant b is needed correct to B^{-2} because it multiplies a term of order B in the expression for $v(\zeta)$. But for the pressure an adequate approximation is

$$b \doteq a\{\frac{-j\rho_o c\beta_\omega}{3B}\}$$

so that

$$p(0) \doteq a + b = a - \frac{j\rho_o c\beta_\omega}{3B},$$

$$p(k\delta) \doteq a + b(1 - Bk\delta)^3 = a + b(1 - K_x M_x)^3,$$

and after some manipulation

$$p(k\delta) \equiv p(1) \doteq p(0)\{1 + \frac{j(k\delta)\bar{\beta}_\omega}{3K_x M_x}[1 - (1 - K_x M_x)^3]\},$$

which agrees with equation (6.2.19). An expression for $v(k\delta) \equiv v(1)$ identical to that given by equation (6.2.20) is derived in a similar fashion.

Appendix 6D

To Check the Expressions for the Pressure and Velocity Variations through a Linear Profile, Incompressible Boundary Layer with the Exact Solutions, to First Order in $k_x\delta$

In the limit $c \to \infty$ the velocity $v(Y)$ satisfies the equation

$$\frac{d^2v}{dY^2} - (k_x\delta)^2 v = 0, \tag{15}$$

a solution being of the form

$$v(Y) = A \cos(k_y\delta.Y) + B \sin(k_y\delta.Y) \tag{16}$$

where $k_y^2 = -k_x^2$ and the ratio of the constants is determined by the boundary condition at $Y = 0$. The pressure at $Y = 0$ can be obtained from the momentum equation in the x direction, having substituted for u, with the incompressible continuity equation being used:

$$p(Y) = \frac{\omega\rho_o}{jk_x(k_x\delta)}\left(1 - \frac{k_xU_x}{\omega}Y\right)\frac{dv}{dY} + \frac{\rho_o v}{j(k_x\delta)}.U_x \tag{17}$$

Using equation (16) then gives $p(0)$ as

$$p(0) = \frac{\omega\rho_o(k_y\delta)}{jk_x(k_x\delta)}B + \frac{\rho_oU_x}{jk_x\delta}A$$

and with application of the boundary condition at $Y = 0$, B is related to A by

$$B = -A\left(1 + \frac{\beta_\omega\rho_oU_x}{jk_x\delta}\right) j(k_x\delta)k_x/\rho_o\omega\beta_\omega k_y\delta. \tag{18}$$

Substituting equation (18) for B into equation (16) and recognising that $A \equiv v(0)$ gives

$$v(Y) = v(0)\{\cos(k_y\delta Y) - \left[\frac{j(k_x\delta)k_x}{\rho_0\beta_\omega\omega(k_y\delta)} + \frac{k_xU_x}{\omega k_y\delta}\right]\sin(k_y\delta Y)\}, \qquad (19)$$

which in the limit of small $|k_x\delta|$ or $|k_y\delta|$, so that $\cos k_y\delta Y \doteq 1$, $\sin k_yY \doteq k_y\delta Y$, reduces to equation (6.2.18) with $Y = 1$ and $c \to \infty$. In the same limit equation (6.2.17) for $p(1)$ has also been checked, by using equation (17) above, although it is a laborious procedure involving the expansion of the cosine and sine functions to second and third powers of $k_y\delta$.

Appendix 6E

Concerning the Existence of a Rotational (Time Dependent) Velocity Field in Sheared Mean Flow

In Chapter 5 it was noted that the energy source terms identified by Morfey (49) for the energy expression defined by Cantrell and Hart (40) consisted of interactions between (i) the irrotational velocity field and the mean shear, (ii) the mean shear and the rotational velocity field and (iii) the rotational velocity field and itself. In (i) the interaction is also with the associated pressure field.

Inviscid acoustic motion in the absence of mean flow or in the presence of uniform mean flow always has an associated irrotational velocity field and it therefore seems appropriate to briefly note the reasons for the appearance of a rotational field for linearised (acoustic ?) motion in sheared mean flow.

It can be shown that any vector function of position such as $\underline{u} \equiv (u, v, 0)$ can always be uniquely separated* into an irrotational part $\underline{u}_\ell$, for which curl $\underline{u}_\ell = 0$ and a rotational part $\underline{u}_t$, for which div $\underline{u}_t = 0$. For the present two dimensional field

$$(\text{curl } \underline{u})_z = (\text{curl } (\underline{u}_\ell + \underline{u}_t))_z = (\text{curl } \underline{u}_t)_z = \frac{\partial v_t}{\partial x} - \frac{\partial u_t}{\partial y}$$

$$= -jk_x v_t - \frac{du_t}{dy},$$

$$\text{div } \underline{u} = \text{div}(\underline{u}_\ell + \underline{u}_t) = \text{div } \underline{u}_\ell = -jk_x u_\ell + \frac{dv}{dy}$$

and

$$-jk_x v_\ell - \frac{du_\ell}{dy} = 0,$$

$$-jk_x u_t + \frac{dv_t}{dy} = 0.$$

---

*Apart from components such that curl $\underline{u}$ = div $\underline{u}$ = 0

Thus if an expression is formed for curl $\underline{u}$ the 'sources' of this rotational field can be identified: this is done by taking the momentum equations of section (6.2),

$$\rho_o j(\omega - k_x U_x(y))u + \rho_o v \frac{dU_x(y)}{dy} = jk_x p, \qquad (20)$$

$$\rho_o j(\omega - k_x U_x(y))v = -\frac{dp}{dy}, \qquad (21)$$

and differentiating equation (20) with respect to y, multiplying equation (21) by $-jk_x$ and subtracting to give

$$\rho_o j(\omega - k_x U_x(y))(-jk_x v - \frac{du}{dy}) = \rho_o \frac{dU_x(y)}{dy}(-jk_x u + \frac{dv}{dy}); - \rho_o v \frac{d^2U_x(y)}{dy^2}$$

or with the above definitions:

$$-jk_x v_t - \frac{du_t}{dy} = \frac{1}{j(\omega - k_x U_x(y))} \frac{dU_x(y)}{dy} (-jk_x u_\ell + \frac{dv_\ell}{dy}) - \frac{v}{j(\omega - k_x U_x(y))} \frac{d^2U_x(y)}{dy^2} \qquad (22)$$

Thus the 'sources' of the rotational field can be recognised as an interaction between (i) the mean shear and the irrotational field, and (ii) an interaction between the total normal velocity and the first derivative of the mean shear. It is of interest to note that for an incompressible linear gradient flow the right hand side of equation (22) is zero, as div $\underline{u}$ is zero.

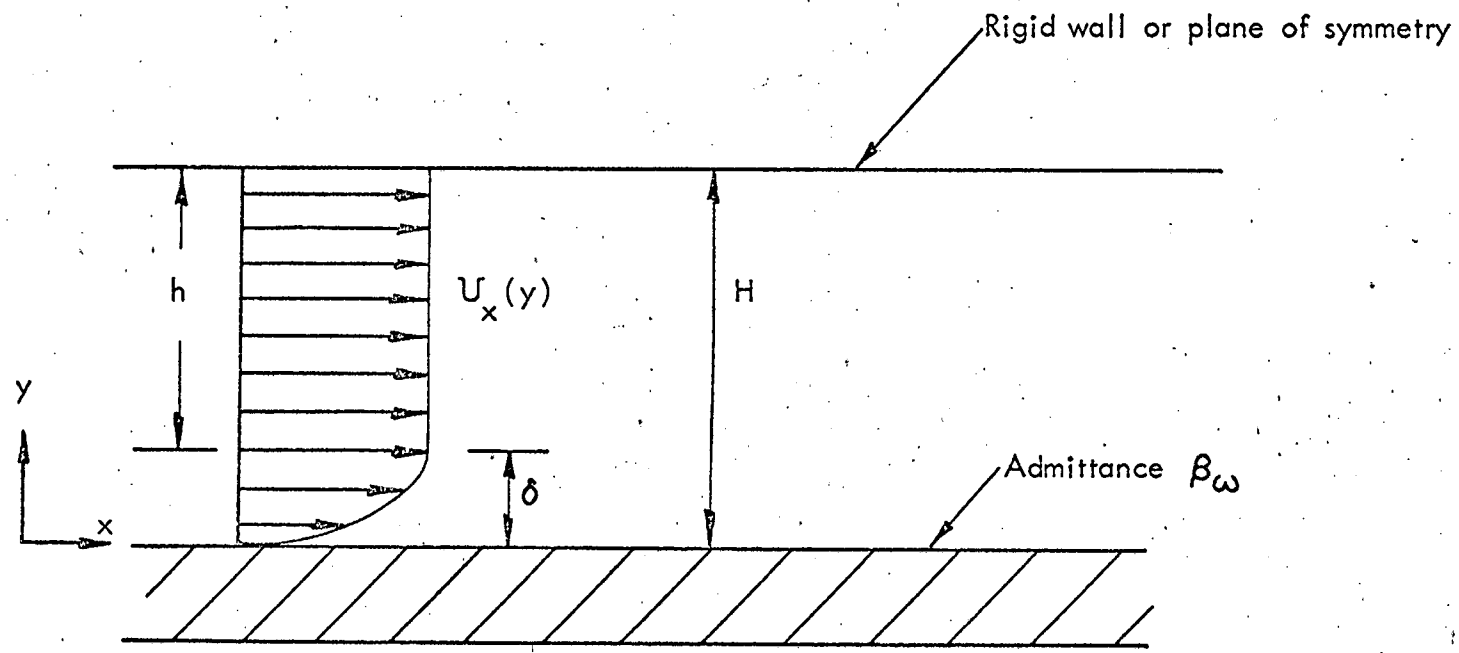

FIG. 6.1 TWO-DIMENSIONAL DUCT CONTAINING MEAN FLOW WITH A REALISTIC VELOCITY PROFILE.

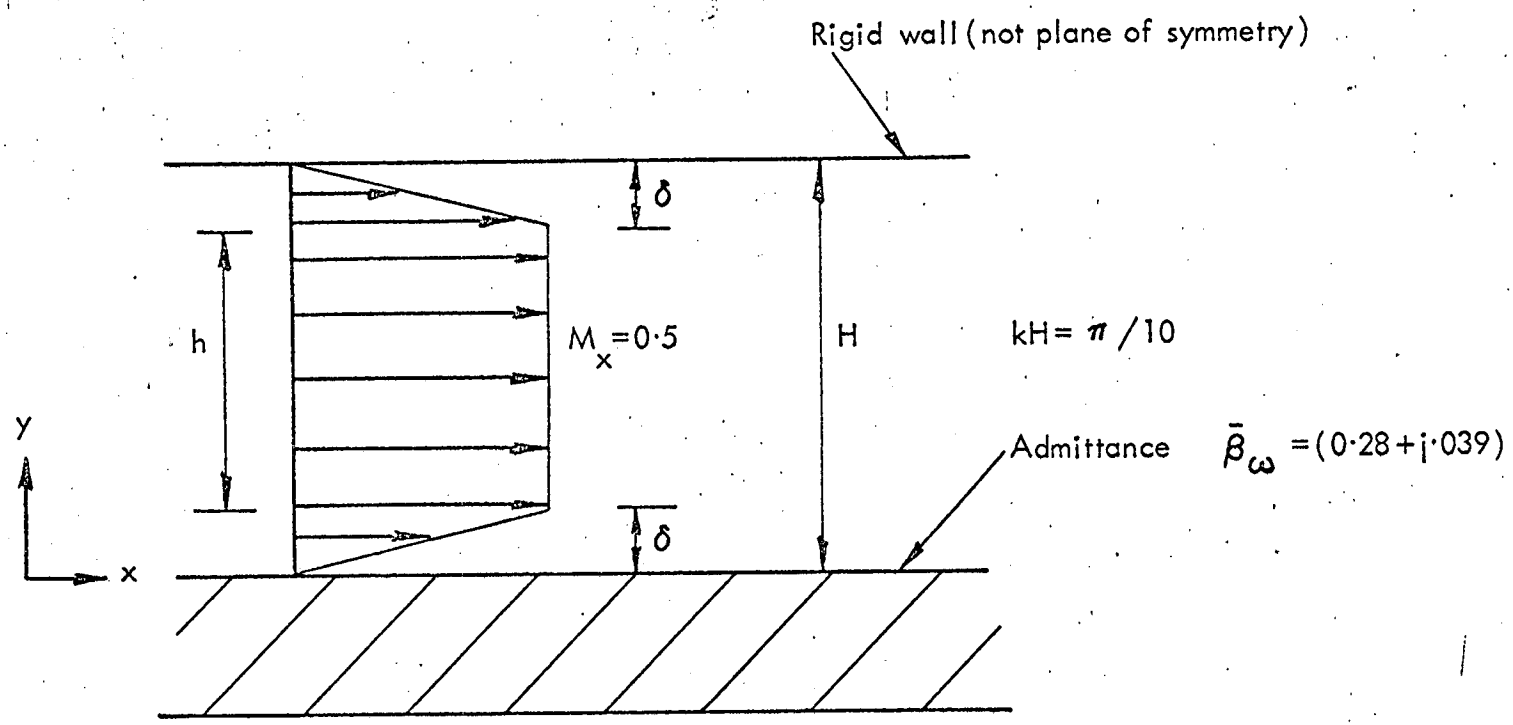

FIG. 6.2 INITIAL EXAMPLE USED TO INVESTIGATE DEPENDENCE OF AXIAL WAVENUMBER ON δ/H, (THE ASYMMETRIC MODEL).

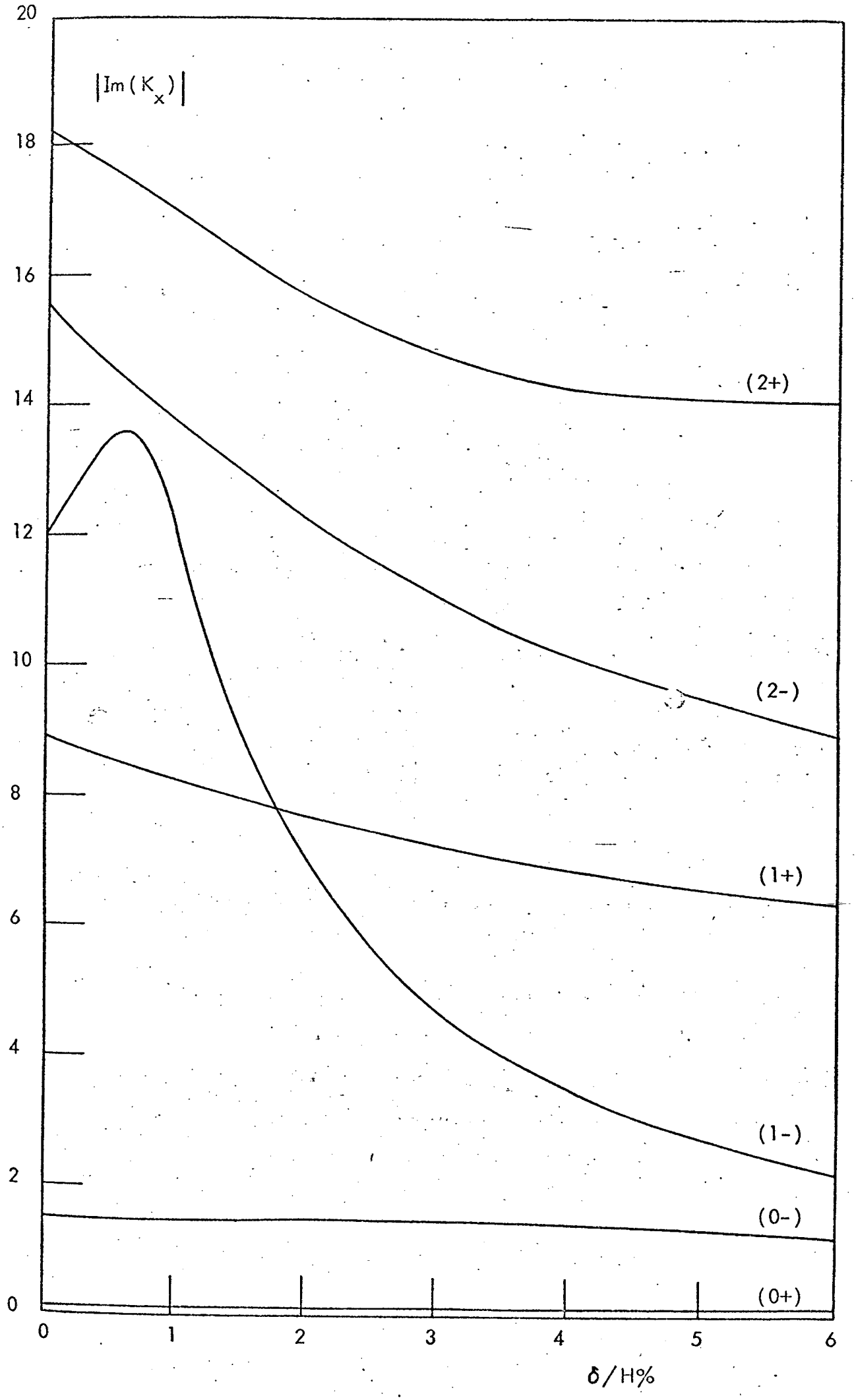

FIG. 4.9 VARIATION OF $|Im(K_x)|$ WITH δ/H FOR THE FIRST SIX MODE

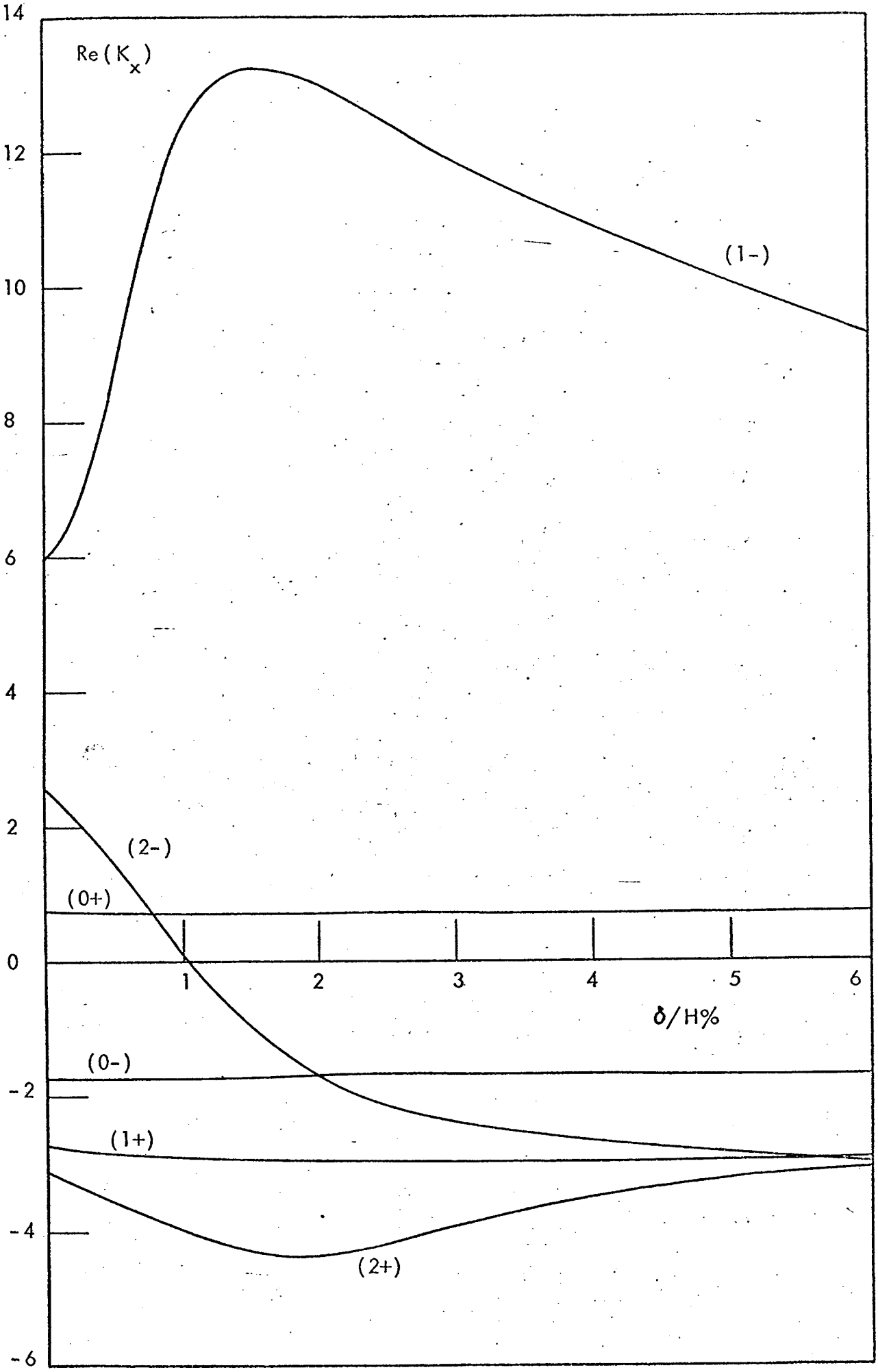

FIG. 6.4 VARIATION OF Re (K_x) WITH δ/H FOR THE FIRST SIX MODE SOLUTIONS OF THE EXAMPLE SHOWN IN FIGURE (6.2).

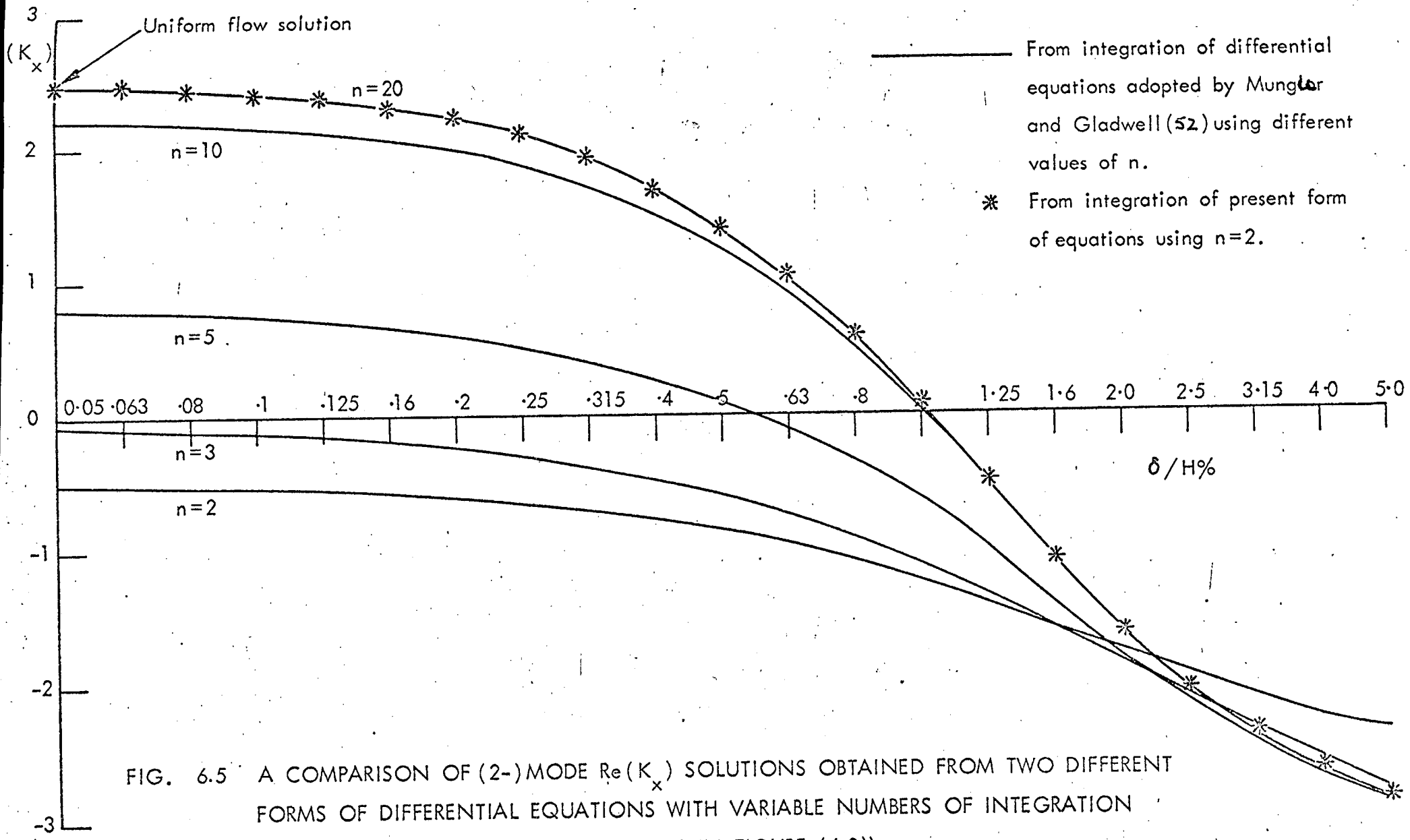

FIG. 6.5 A COMPARISON OF (2-) MODE $Re(K_x)$ SOLUTIONS OBTAINED FROM TWO DIFFERENT FORMS OF DIFFERENTIAL EQUATIONS WITH VARIABLE NUMBERS OF INTEGRATION POINTS, n. (FOR THE EXAMPLE SHOWN IN FIGURE (6·2)).

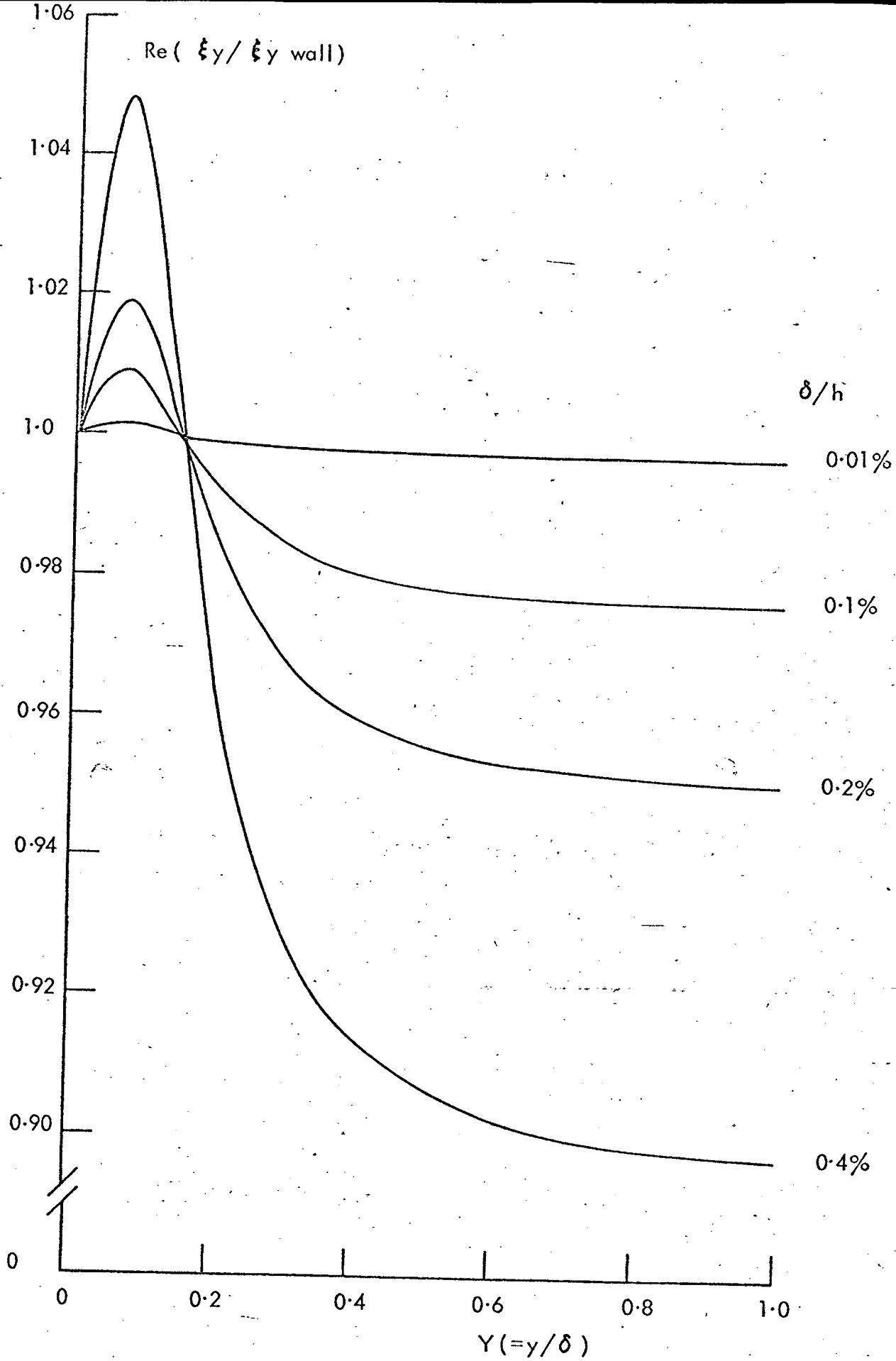

FIG. 6.6 EXAMPLES OF NORMAL DISPLACEMENT VARIATION THROUGH THE LINEAR PROFILE BOUNDARY LAYER FOR DIFFERENT δ/h VALUES. ((1-) MODE, CONSTANT h, FOR MODEL SHOWN IN

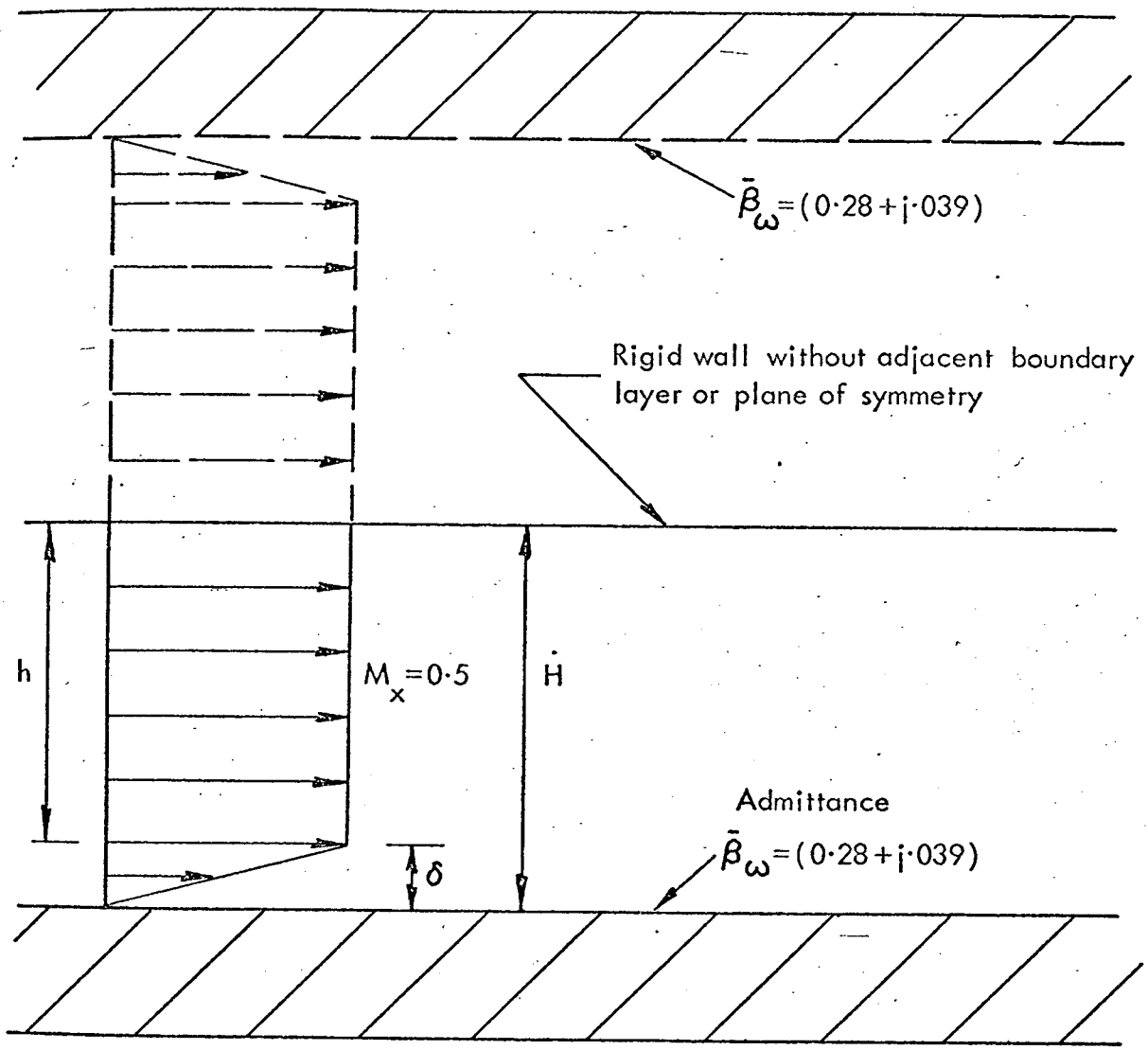

kh or kH = $\pi/10$, whichever is held constant.

FIG. 6.7 THE SYMMETRIC MODEL.

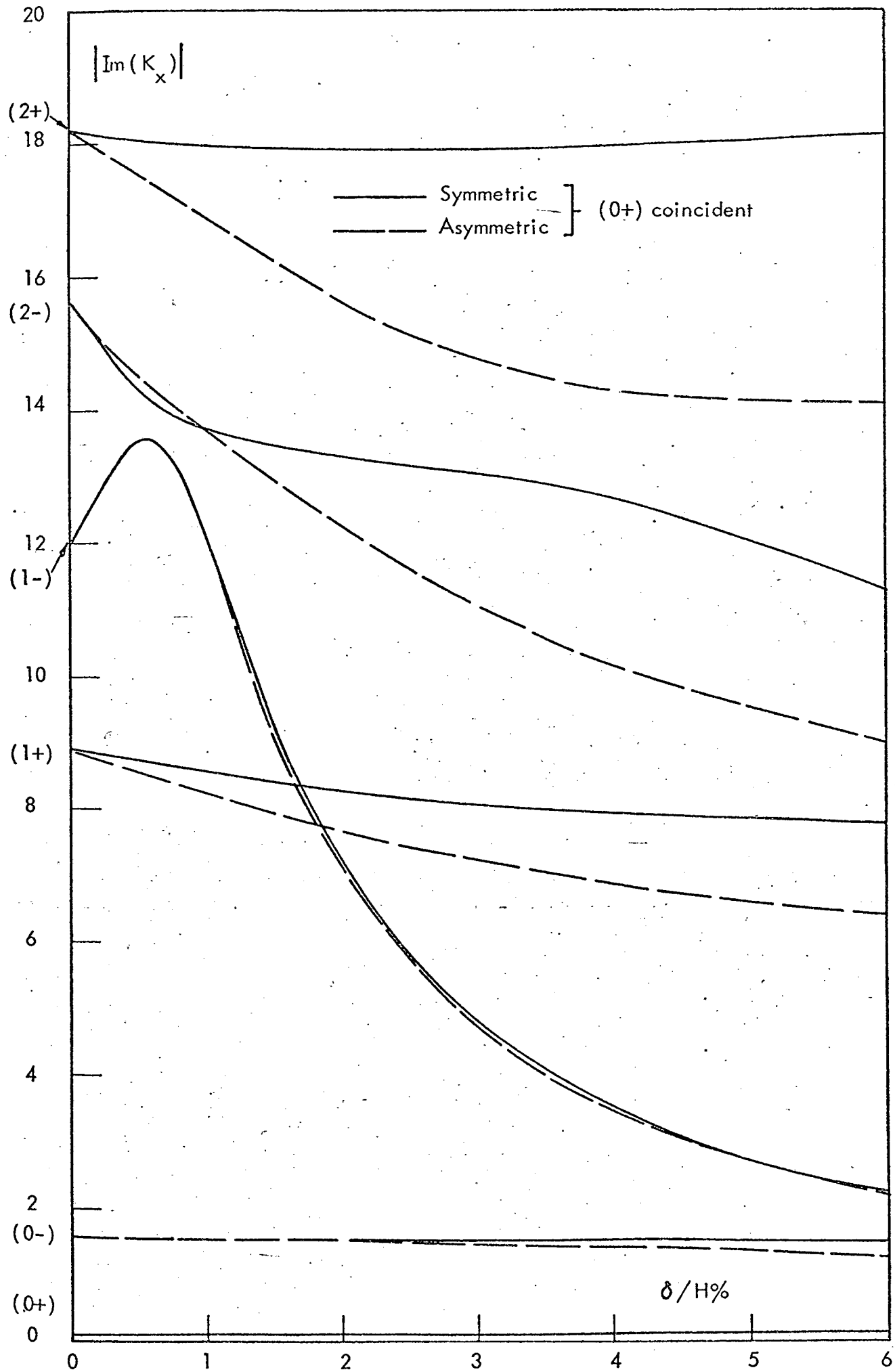

FIG. 6.8 COMPARISON OF Im(K_x) SOLUTIONS FOR THE ASYMMETRIC (FIGURE

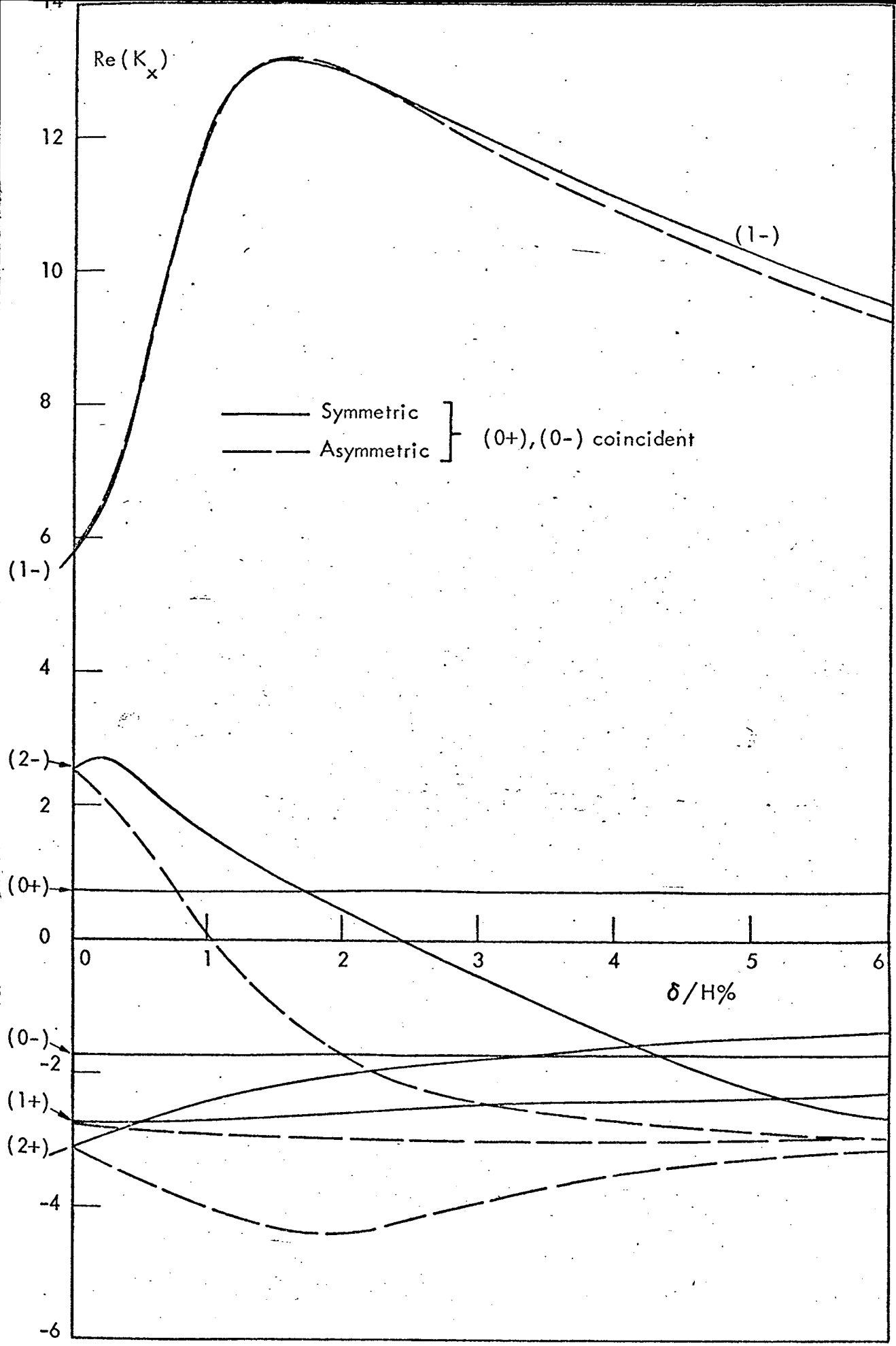

FIG. 6.9 COMPARISON OF $Re(K_x)$ SOLUTIONS FOR THE ASYMMETRIC (FIGURE 6.2)) AND SYMMETRIC (FIGURE (6.7)) MODELS (CONSTANT H).

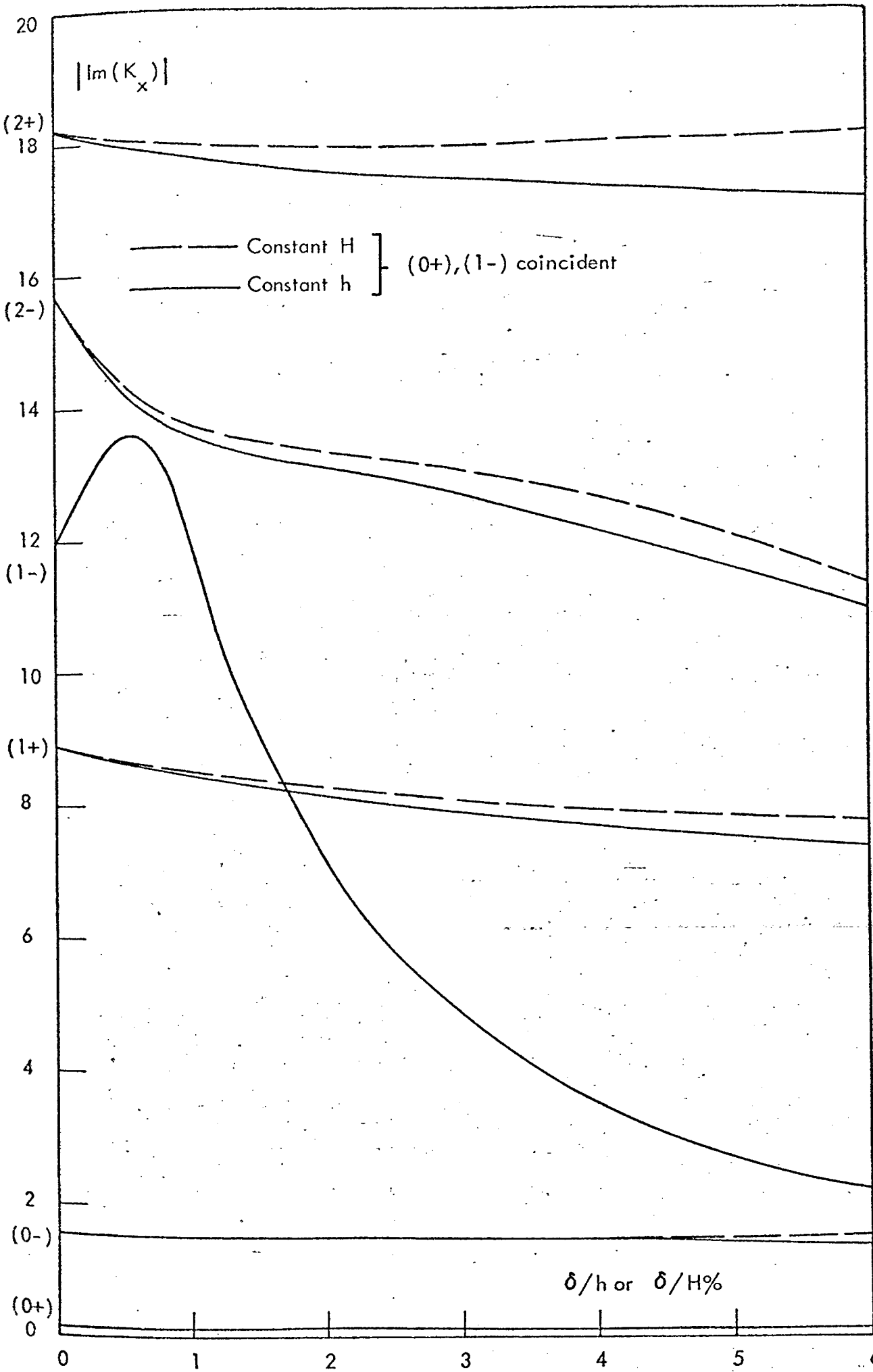

FIG. 6.10 COMPARISON OF $Im(K_x)$ SOLUTIONS FOR CONSTANT DUCT WIDTH (H) AND CONSTANT UNIFORM FLOW WIDTH (h) (SYMMETRIC MODEL,

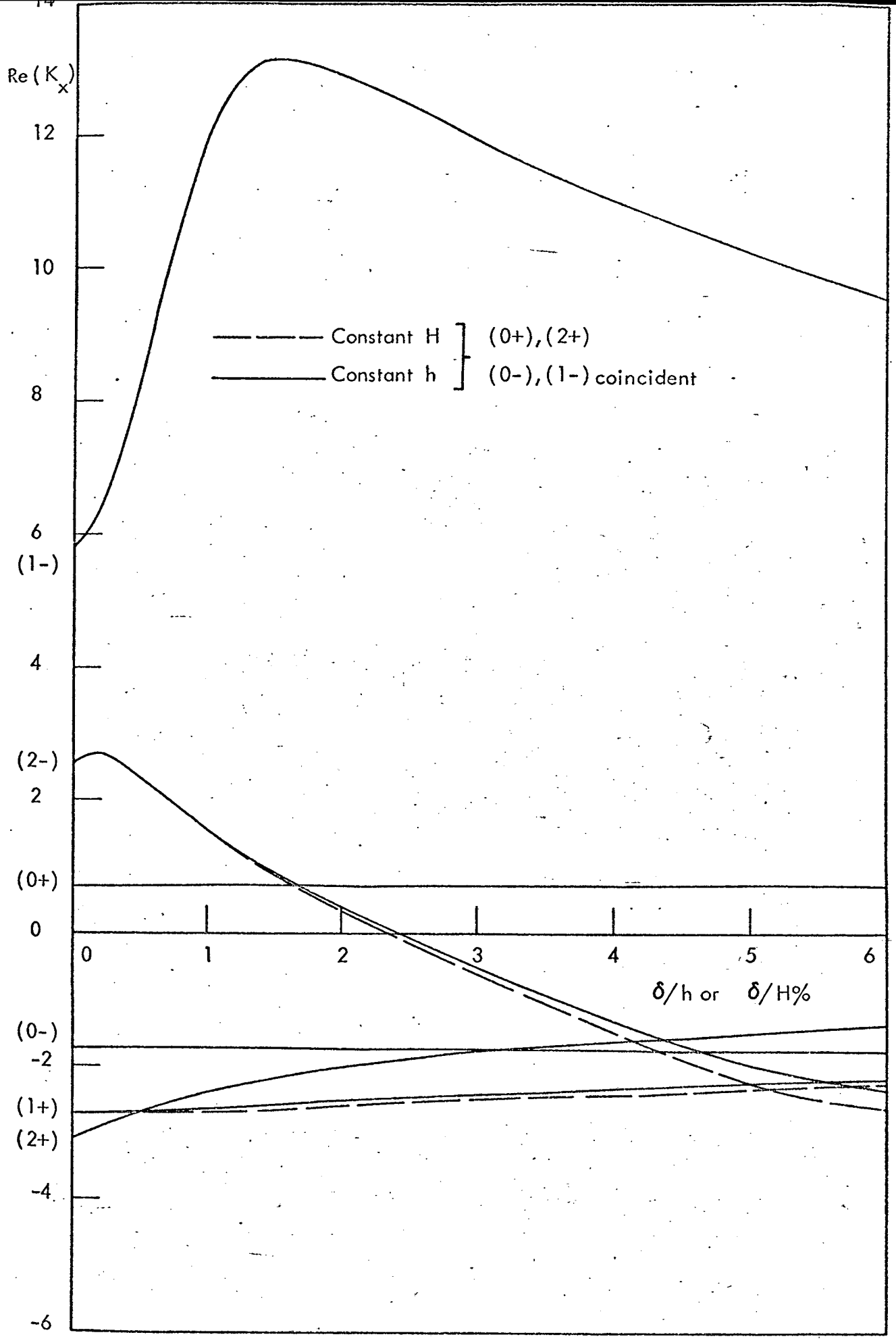

FIG. 6.11 COMPARISON OF Re (K_x) SOLUTIONS FOR CONSTANT DUCT WIDTH (H) AND CONSTANT UNIFORM FLOW WIDTH (h) (SYMMETRIC MODEL, FIGURE (6.7)).

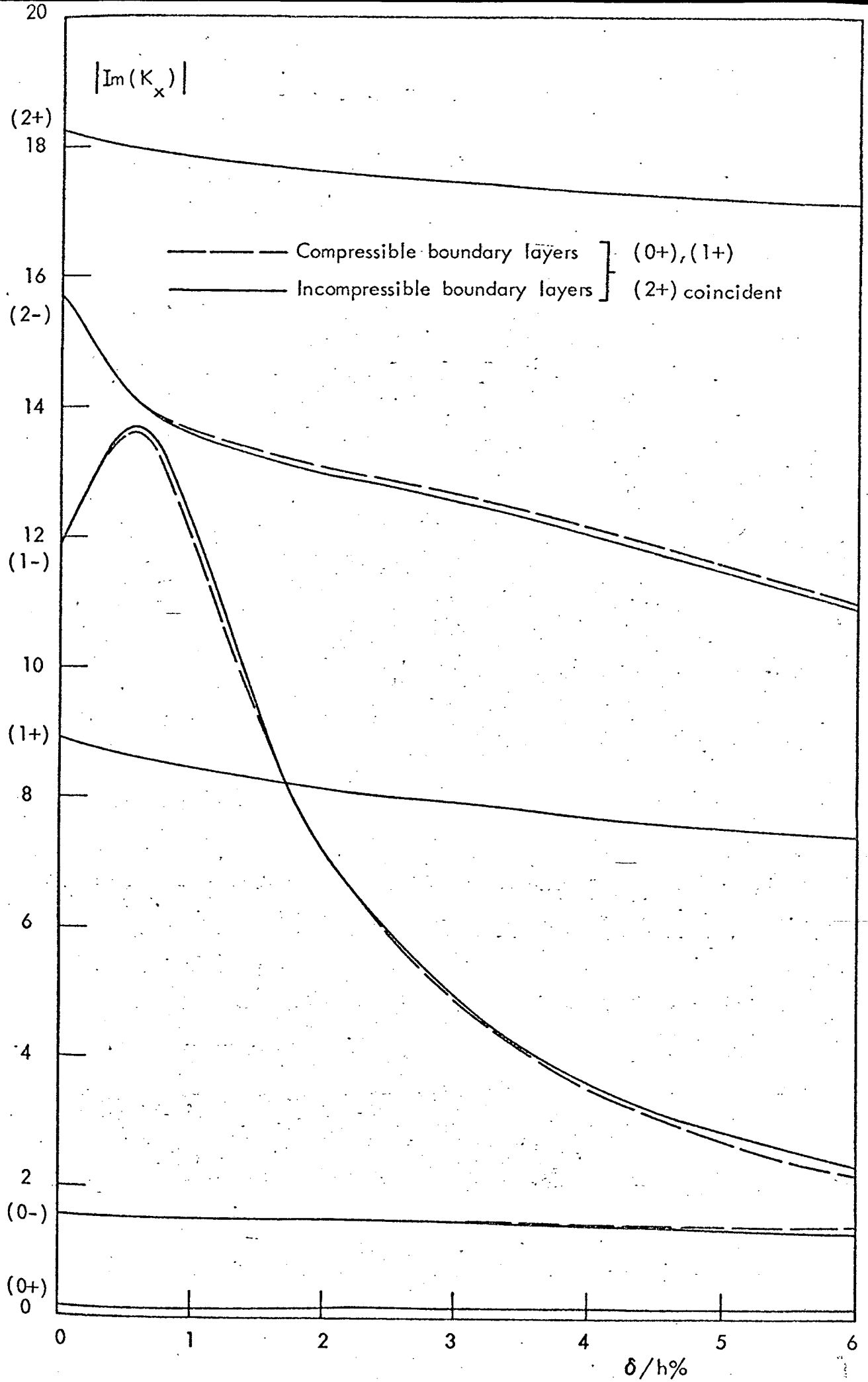

FIG. 6.12 COMPARISON OF Im(K_x) SOLUTIONS FOR COMPRESSIBLE AND

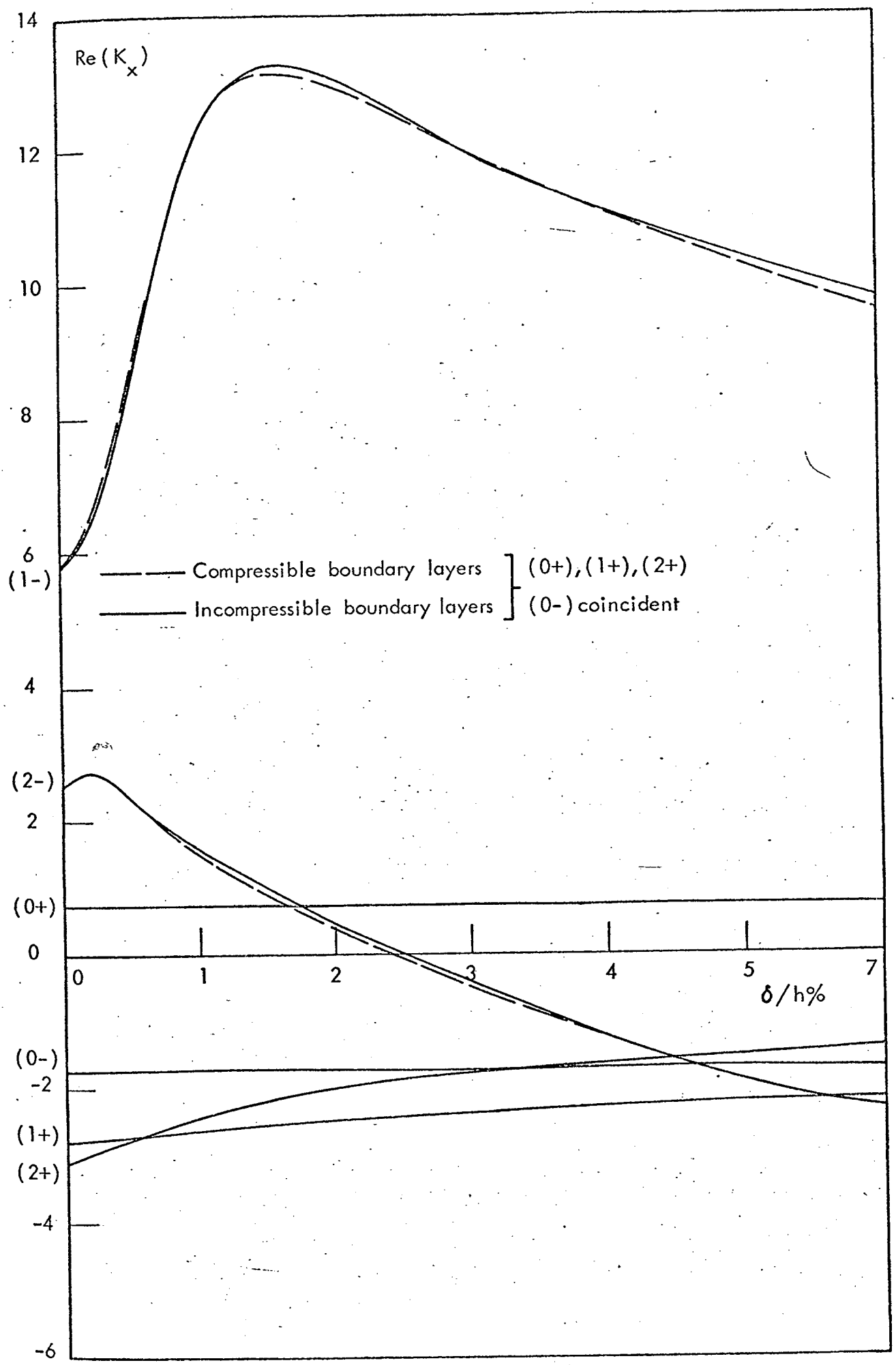

FIG. 6.13 COMPARISON OF Re (K_x) SOLUTIONS FOR COMPRESSIBLE AND INCOMPRESSIBLE BOUNDARY LAYERS (SYMMETRIC MODEL, FIGURE

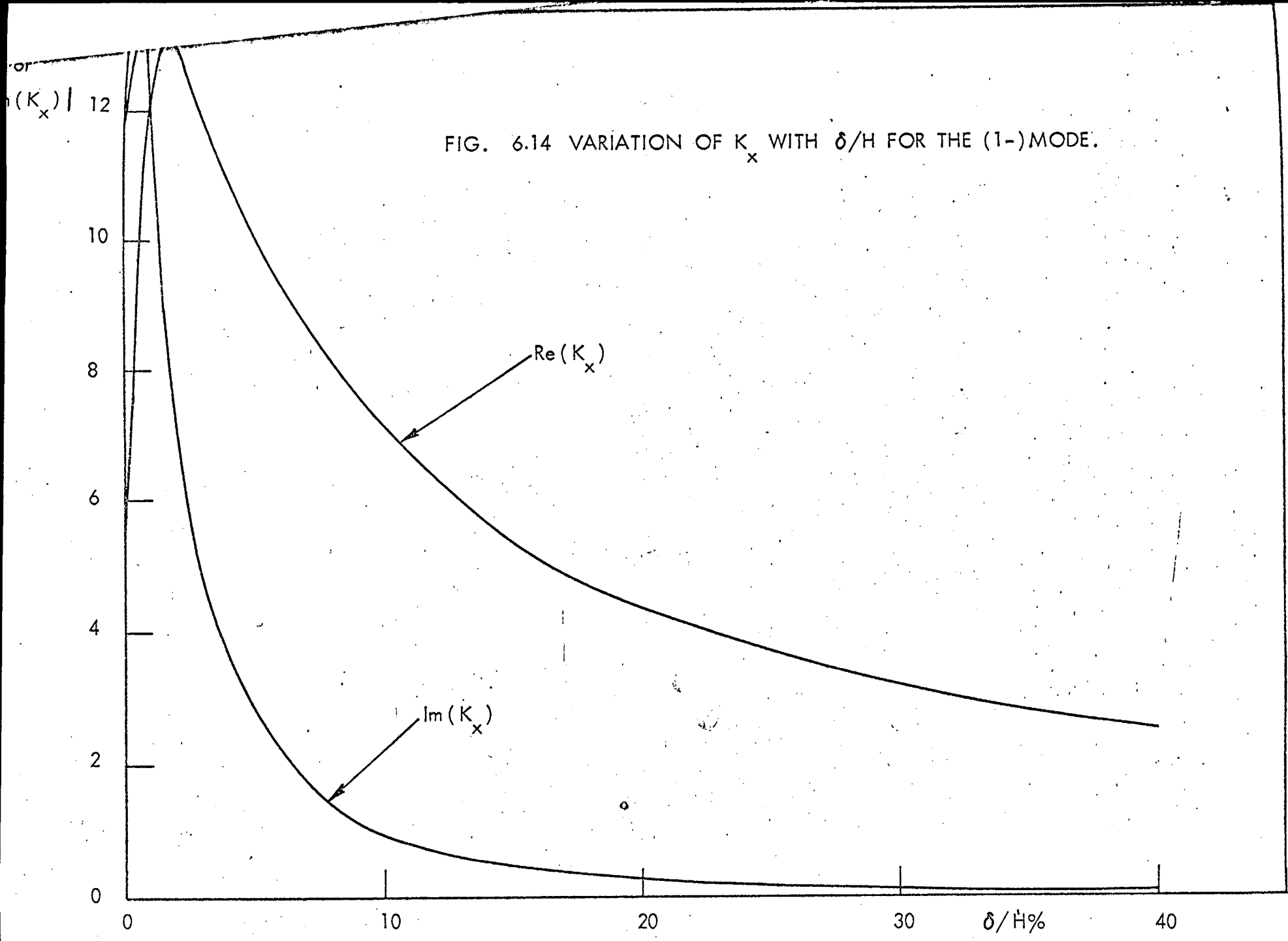

FIG. 6.14 VARIATION OF K_x WITH δ/H FOR THE (1-)MODE.

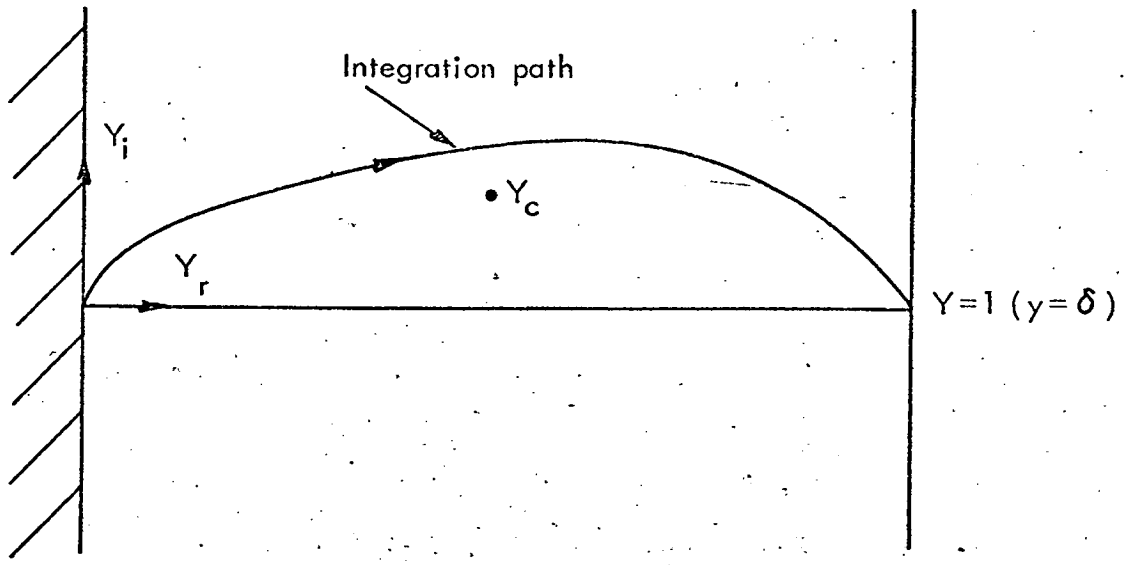

FIG. 6.15a INTEGRATION PATH IF MODE DECAYS WITH TIME AND $Im(Y_c) > 0$ (+j notation).

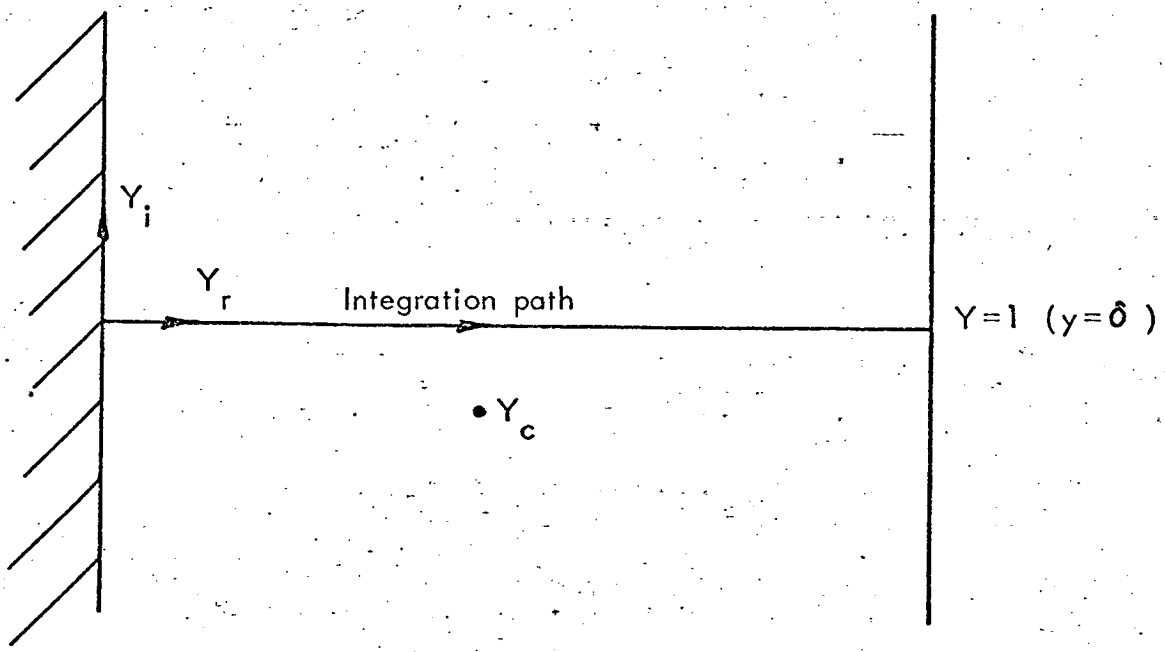

FIG. 6.15b INTEGRATION PATH IF MODE AMPLIFIES WITH TIME AND $Im(Y_c) < 0$ (+j notation)

CHAPTER 7

CONCLUSIONS

7.1 Summary and Discussion

A theoretical investigation has been carried out into certain aspects of sound attenuation in lined ducts containing subsonic mean flow. The investigation has concentrated on the analysis of the perturbed or acoustic field in an infinite, uniformly lined, two-dimensional duct of constant cross-section in which the unperturbed fluid properties, other than its mean velocity, are constant across the duct cross-section. The idealised duct geometry and other features were chosen because it has been previously demonstrated that these can provide the foundation for the construction of a theoretically based model which, in certain cases, can accurately predict the experimentally observed acoustic 'performance' of duct linings in finite length rectangular flow ducts in terms of an estimated insertion loss.

A convenient but not necessarily complete mathematical description of the perturbed duct field at a particular frequency, ω, is usually assumed to be in the form of an infinite sum of modes: each mode has a unique axial phase velocity $\omega/\mathrm{Re}(k_x)$ and an exponential attenuation $\exp[\mathrm{Im}(k_x)x]$ in the positive or negative x direction. The relative amplitude or weighting of each mode in the infinite summation is partly determined by the source distribution within the duct (and, in finite length ducts, by the boundary conditions associated with the duct termination). In this investigation the source distribution is an infinite, uniform line source of unit strength running parallel to the duct walls and normal to the duct axes so that the problem remains two-dimensional. The function describing the perturbed or acoustic field is therefore the two-dimensional duct Green's function and once this is

defined the field due to any two-dimensional source distribution can be constructed by superposition.

The results of this investigation are essentially concerned with the optimisation of modal attenuation rates and the derivation of the Green's function for the case where the unperturbed duct fluid has a uniform, subsonic, mean velocity relative to the duct walls; but in addition preliminary considerations are given to the case where the fluid mean velocity is uniform across the entire duct cross section except for boundary layer regions adjacent to the duct walls.

The optimisation of modal attenuation rates is based on Cremer's (19) result for the lowest order mode pair (0, 1) in a two-dimensional duct of width h containing a fluid otherwise at rest and with one wall lined, having a locally reacting impedance, Z_ω, (at frequency ω); the other wall is rigid. Cremer (19) claims to have shown that the optimum impedance, $Z_{\omega opt}$, which gives rise to the maximum attenuation of the least attenuated mode is

$$Z_{\omega opt} = (0.91 - j0.76)(\frac{\omega h}{c})(\frac{1}{\pi})\rho_o c$$

where ρ_o and c are respectively the unperturbed, uniform, mean fluid density and speed of sound.

A more accurate value has been obtained, that is,

$$Z_{\omega opt} = (0.929 - j0.744)(\frac{\omega h}{c})(\frac{1}{\pi})\rho_o c$$

and it has been shown how Cremer's (19) result can be generalised and hence extended to higher order mode pairs in the same duct and to mode pairs in other duct geometries. For example a good approximation to the optimum impedance for the mode pair (m, m+1) in the same duct is

$$Z_{\omega opt} \doteq [(m + \tfrac{3}{4})\pi + j\tfrac{1}{2}\ell n(4m + 3)\pi]^{-1} \ (\frac{\omega h}{c})\rho_o c$$

and in a circular duct the optimum impedance for the zeroth circumferential, lowest order radial mode pair is

$$Z_{\omega opt} \doteq (0.88 - j0.38)(\frac{2\omega b}{c})(\frac{1}{2\pi})\rho_o c.$$

Optimum impedances have also been given for a two-dimensional duct which contains uniform flow as a function of the flow Mach number, M_x, and $\omega h/c$: a simple rule emerges which is valid for any duct geometry provided the axial wavenumber satisfies the well 'cut-on' condition:

$$|k_x| \doteq \frac{k}{(1 + M_x)} \ ; \quad k = \omega/c.$$

The rule is this: the optimum impedance for a mode pair in uniform flow is equal to the optimum impedance for the same mode pair in zero flow divided by $(1 + M_x)^2$. In symbols,

$$Z_{\omega opt}|_{M_x} \doteq \frac{Z_{\omega opt}}{(1 + M_x)^2} .$$

Some of these optimum impedance results have been shown to be of considerable use in interpreting and classifying results from theoretically based insertion loss models and also from experimental facilities. However, for at least two reasons, the real value of this type of optimum impedance lies in the trends exhibited, for example, the linear dependence on the reduced frequency, kh, and the approximate Mach number dependence, $(1 + M_x)^{-2}$, rather than the exact numerical values. One reason is that rate of change of attenuation rate of the mode pair with liner impedance is large near this optimum impedance value. In fact the mathematical definition of the optimum condition is that this rate of change tends to infinity. Thus any perturbation in the impedance and other parameter values can bring about a large change in

modal attenuation rates. The other reason is discussed later. With aero-engine applications in mind, it is recommended that further work in this area should be carried out to establish the dependence of the optimum impedance for the lowest order radial mode pair on the circumferential mode order in circular and annular ducts and on the 'hub-tip ratio' of annular ducts.

In an attempt to understand the reason for the apparently arbitrary numerical constants which appear in the optimum impedance expressions, and also its linear dependence on the reduced frequency, an alternative but approximate method of representing the Green's function, based on a suggestion by Morfey (21), has been evaluated. The method consists of explicitly retaining the free-field Green's function in its original form and representing the influence of each duct wall by the free-field of one, or more, image sources. The image source in the first approximation has a strength given by the plane wave reflection coefficient evaluated at an angle defined by the ray paths joining the source, its image and the observation point. In the simplest ray model the axial attenuation of the sound field is realised by the usual 'radial spreading' decay of the source free-field and destructive interference caused by the source-image free-fields or, in other words, by reflections from the duct walls. Examples have been given to demonstrate that this simple ray model gives results which agree qualitatively with those from the exact (modal) duct Green's function in terms of the axial decay of the pressure field; in particular, at distances from the source where the field is adequately described by the (0, 1) mode pair the ray model axial 'decay' or destructive interference increases as the impedance is varied and approaches the optimum value for the (0, 1) mode pair. Thus the following qualitative but simple, physical interpretation is advanced for the mechanism by which the (0, 1) mode pair optimum

impedance gives rise to a maximum attenuation*: this mode pair describes the 'far-field' of a line source in a two-dimensional duct and such a field can be approximately represented by a direct ray from the source and two reflected rays from the duct walls. The maximum axial 'decay' of this field occurs when the liner impedance is such that the two reflected rays cause the most efficient destructive interference with the direct ray. Using this definition of an optimum impedance it has been shown that the reactive part of this impedance must be negative (+j notation, that is, 'stiffness controlled') and must be proportional to the reduced frequency; therefore those features of the modal optimum impedance are understood but nothing can be deduced immediately about the real part.

The potential of more refined ray models has also been assessed and their accuracy is found to be sufficient to suggest with some justification, that these refined ray models could be used as an alternative to the exact but relatively complicated mode models, particularly for aero-engine applications where the duct length rarely exceeds four to five duct widths. For other applications where duct lengths exceed this value and where the typical wavelength is smaller than the duct width the ray models may not be adequate. Further work is strongly recommended in this field to assess, in general the true potential of these and other ray models particularly in situations where the modal description becomes even more complicated, for example, where the liner impedance is a function of position and where the duct cross-section varies along the duct axis.

The line source Green's function for a duct containing a fluid otherwise at rest is well known but it has been re-derived using Brekhovskikh's (20) method to demonstrate that the now generalised

---

*But see the qualification to this below.

optimum condition is a special case of mode degeneracy: for example the (0, 1) mode pair optimum impedance is that impedance value which causes the (0) and (1) mode solutions to merge and become identical. In the Brekhovskikh (20) method the correct treatment of this degeneration is clear: instead of evaluating a residue at a simple pole, the residue must be evaluated at a double pole. However, contrary to Cremer's (19) implied assumption, the degenerate or double pole solution gives rise to a mode with an exponential dependence on the axial coordinate, x, multiplied by a factor which has a linear dependence on x and which also depends on the transverse coordinate. The simple exponential decay of the individual degenerate modes is offset by a linear amplification at this optimum condition and the maximum attenuation rates claimed by Cremer (19) are modified. This is the other reason, referred to above, why the optimum impedances defined by Cremer (19) and in the present work should be used only as a qualitative guide to liner impedance specification in practical problems. In one particular example it has been shown that the effective axial attenuation rate of the Green's function for the 'optimum' liner impedance is only 75% of the value claimed by Cremer (19) (that is, due to exponential decay alone and ignoring the linear amplification); also, in the same example, the true optimum reactance differs from Cremer's (19) value by approximately 12% although this result may be modified if the resistance is allowed to vary.

The derivation of the line source Green's function for a duct containing a fluid with a uniform mean flow relative to the duct walls has been attempted in the first instance on the basis that, with the application of the Lorentz transform, the problem is identical, with modified boundary conditions, to the zero flow case. The Green's function has been obtained, without rigorous proof of the validity of every mathematical

:p, as an infinite sum of non-orthogonal modes. Despite the non-thogonality of this infinite set of mode functions it appears to a complete solution. Evidence to support the validity of this new een's function has been presented in the form of comparisons between luated examples of this function and of a refined ray model, modi-d to include uniform mean flow. Close to the line source the vergence of the mode Green's function - composed of a finite sum of es - as the number of modes is increased, to the ray Green's ction were found to be similar to the convergence rate of the zero w Green's function. Further away from the source the differences ween the ray and mode Green's functions were found to be similar the differences that occur for zero flow. The uniform flow Mach ber used in these examples ranged from -0.3 to +0.4 (plus sign - al decay in the downstream direction, minus sign - axial decay in upstream direction).

In response to some comments by Ffowcs-Williams (22) the method deriving the Green's function was modified to take into account the ssibility that the (modulus of) Green's function does not tend to o at large distances from the source. The modification is based on procedure formulated in the study of electron stream interaction with asmas and in effect defines the correct path of integration for the version of the Fourier spatial transform in the axial direction. The ocedure has been outlined with the aid of an example and the Green's nction was found to contain a spatially amplified mode existing wnstream of the line source; this mode is closely related to the ll known incompressible Helmholtz temporal instability of a fluid jacent to a simple flexible wall. This type of result needs careful terpretation and qualification before it is compared with experimental servations.

First, at some distance from the source a spatially amplified mode will be large enough to invalidate the assumption that the linearised equations of mass, momentum and energy conservation describe the perturbed field. In other words the equations do not necessarily hold in this case throughout the spatial region between the source and some observation point downstream of the source. Second, the absence of duct terminations at a finite distance from the source is now clearly one simplification in the idealised duct geometry which may have to be removed in order to obtain a realistic description of the perturbed field in a finite length duct. If the finite region between a source and termination can be described by a combination of (linear) spatially amplifying and decaying modes, then the perturbed field near the source may be controlled by modes usually associated with the reflection, by the termination, of the infinite duct field.

Third, the idealised model contains no perturbation sources other than the acoustic line source, whereas in reality, a flow duct contains many pre-existing fluctuations which can excite the amplified mode, as well as all other modes. Where amplification does not take place, there is no real objection to the idealised model because the strength of the defined acoustic source and its mode field usually exceed that of the other pre-existing sources. With mode amplification one could argue that the pre-existing sources have triggered all possible types of instability and a stable possibly non-linear perturbed flow field is created. The defined acoustic source is then switched on and that part of the excited field which decays away from this source is superimposed on the pre-existing perturbed field whereas the amplified part is discarded because it represents a physical process which has already taken place.

These points need to be considered in more detail before any attempt is made to relate spatially amplified 'acoustic' modes to experimental observations like those, for example, reported by Meyer et al (16). In addition it may be necessary to include some effects of viscosity and thermal conductivity and also to investigate the influence of realistic mean velocity profiles on the properties of the amplified modes. This is common practice in stability analysis and the computational methods are well established (24). The difficulty mentioned above concerning non-linearity has been studied (63) to some extent but the effects of duct terminations and the true role of spatially amplified modes in models of real flow ducts urgently require further research.

The influence of finite width shear of boundary layer regions adjacent to the duct walls has been investigated with the aid of analytic approximations and these have shown that mode solutions obtained for a duct containing uniform mean flow are identical to those obtained for the same duct with arbitrary profile boundary layers, in the limit as the boundary layer thicknesses tend to zero. This has been confirmed with examples of numerical solutions of the appropriate ordinary differential equations for linear velocity profile boundary layers. The influence of boundary layer thickness, with the same profile, on the axial wavenumber of the spatial amplified mode has been considered and found to be in qualitative agreement with Rayleigh's (44) result for the temporal stability of a linear profile incompressible free shear layer: the spatial amplification rate decreases significantly with increasing boundary layer thickness but unlike Rayleigh's (44) result, the mode is not completely stabilised and remains slightly amplified for the range of boundary layer thickness considered.

In the present context this work on ducts containing non-uniform mean flow is incomplete without the derivation of the Green's function

It has been argued that this function could be obtained by using the same methods as used for the uniform flow case, provided the line source is located within a uniform flow region. However, according to the work by Möhring (12) an infinite sum of simple modes may not be a complete solution and this requires further investigation.

Finally, concerning the method (used in simple insertion loss models) of relating, approximately, the perturbed duct field to the acoustic field radiated from the duct termination, expressions have been formulated for the energy flows associated with individual modes, according to certain definitions. It has been shown that the axial energy flow in a uniform flow duct can only be equated with the radiated energy if: the radiation is from an 'inlet flow' termination, the axial energy flow is calculated according to the energy flux defined by Cantrell and Hart (40) and the duct walls are non-absorptive. If the duct walls are absorptive the duct and radiated energy flows are approximately identical if the duct energy flow is primarily due to the existence of well 'cut-on' modes.

7.2 Main Conclusions and Recommendations for Future Work

7.2.1 Lined ducts containing a fluid at rest

1. Cremer (19) has defined the optimum, locally reacting liner impedance for the maximum exponential attenuation rate of the lowest order mode pair in a one-side-lined two-dimensional rectangular duct and not, as claimed, the maximum attenuation rate of the least attenuated mode pair.

2. This optimum condition is defined in Chapter 2 in mathematical terms and hence the optimum impedance can now be obtained for any mode pair in any duct of uniform rectangular, circular or annular cross-section.

3. It has been shown that at the optimum condition the mode pair degenerates into a single mode with the expected exponential attenuation rate but this is offset by an amplification rate which is directly proportional to the distance from the source. Thus the actual attenuation rate is less than that given by Cremer (19). This may help to explain why the large predicted exponential attenuations have not been observed in practice.

4. Under certain conditions these 'optimum' impedances alone can be used to guide liner design although, ideally, theoretical optimisation should be carried out with an appropriate wave-guide model and a specification of the source distribution.

5. The physical mechanism by which large attenuation rates occur at and near the optimum condition has been understood, qualitatively, with the aid of a ray model.

Recommendations

(a) Optimum impedances and corresponding exponential attenuation rates have been worked out for higher order modes in rectangular ducts

and for the zero circumferential, lowest order radial mode pair in a circular duct. Calculation of these quantities for other mode pairs in circular ducts and in annular ducts is recommended as these would be particularly useful for aero-engine applications.

(b) A general study of the ray model, with appropriate refinements, should be carried out to assess its potential as an alternative method of calculating sound fields in ducts.

7.2.2 Lined ducts containing subsonic, uniform mean flow

1. With the application of the Lorentz transformation the Brekhovskikh (20) method has been used (see Chapter 4) to obtain a line source Green's function for the two-dimensional duct in the form of an infinite sum of non-orthogonal modes.

2. The optimum condition has been defined and the conclusions (2), (3) and (4) for the zero flow case carry over to the uniform flow case. A simple relationship has been established between zero and uniform flow optimum impedances for well 'cut-on' modes which can be used to interpret trends in theoretical and experimental results.

3. Steady-state modes can have phase velocities in the opposite direction to that of attenuation. The direction of the phase velocity, or attenuation cannot be used to determine the role of these 'strange' modes, that is, whether, in an infinite duct, the mode exists upstream or downstream of the harmonic source or source distribution, nor can energy radiation conditions be used for this purpose, except under special circumstances.

4. Briggs' (23) method, which is based on the Causality Law can be used to determine the role of each 'strange' mode and hence the correct Green's function. In a particular example (Chapter 4) it has been shown that one of the 'strange' modes exists downstream of the source and is spatially amplified in this direction. This steady-

state duct mode is a modified form of the well known temporal instability of an incompressible vortex sheet adjacent to a single flexible wall. The remaining 'strange' modes in the Green's function decay away from the source in the upstream or downstream directions and play the same role as 'cut-off' modes in a zero flow duct.

5. The theoretical existence of spatially amplified duct modes may form the basis for an explanation of the occurrence of spatial amplification, when observed in practice (16).

Recommendations

(a) The point source Green's function is required for two- and three-dimensional ducts in order to construct more realistic models of practical problems.

(b) Further theoretical work on spatial amplification in ducts should concentrate on investigating the effects of real boundary layer flow profiles, viscosity and thermal conduction, non-linearity and duct terminations at a finite distance from the source or source distribution. However this work should be contemplated only if spatial amplification is established as a common occurrence in the lined ducts used in practice. At present this does not appear to be the case.

7.2.3 Lined ducts containing subsonic, non-uniform mean flow

1. An analytical study of the simultaneous first order differential equations for the perturbed field in sheared flow has revealed that the pressure and normal particle displacement are constant through a shear layer of arbitrary profile, in the limit as the shear layer thickness tends to zero. Thus the uniform or 'plug' flow model can be regarded as the valid limiting case of a model in which the flow is uniform across the duct but is separated from the duct walls by 'thin' boundary

layers. The physical effects of 'thin' boundary layers on mode solutions are therefore correctly included in the uniform flow model. In this sense the accepted concept that the uniform flow model implies 'slip' at the boundaries, and must therefore be unrealistic, is misleading.

2. Approximate analytic solutions have been obtained (Chapter 6) for the pressure and normal velocity variations through boundary layers to first order in a parameter proportional to boundary layer thickness. These have been used to interpret trends in the dependence of mode axial wavenumbers on boundary layer thickness.

3. The analytic approximations can be used to predict the influence of thin but finite thickness linear profile boundary layers on mode axial wavenumbers except at and near optimum conditions.

4. The equations used here to describe the perturbed field in sheared flow are identical to those used in studies of compressible boundary stability. These are in a different form to those generally used in sheared flow duct acoustics. Although mathematically equivalent the stability form of the equations can have an advantage over the usual form in terms of a reduction in the computer time taken for their numerical integration. The stability equations are also preferable because the dependent variables are the familar pressure and normal velocity (as opposed to the pressure and normal pressure gradient).

5. It has been shown that an increasing boundary layer thickness of linear profile tends to stabilise the spatially amplified mode.

Recommendations

(a) Work should continue on the influence of non-uniform flow on perturbed duct fields although for many practical problems the uniform flow model, in the present context, represents most of the important

physical processes.

(b) In further work emphasis should be placed on distinguishing the 'acoustic', or perturbed field which decays away from the source or source distribution, from the 'non-acoustic', or amplified field, in order that the physical mechanisms can be identified and properly described in theoretical models.

REFERENCES

1. Conference on Progress of NASA Research Relating to Noise Alleviation of Large Subsonic Jet Aircraft. 1968. N.A.S.A. Langley Research Centre.

2. C.K.W. Tam. 1971. J. Sound Vib. Vol. 16, No. 3, pp. 393-405. On finite amplitude spinning acoustic modes and subsonic choking.

3. C.L. Morfey and M.J. Fisher. 1970. J. Roy. Aeron. Soc., Vol. 74, pp. 579-585. Shock-wave radiation from a supersonic ducted rotor.

4. U. Ingard. 1968. J.A.S.A. Vol. 43, No. 1, pp. 167-168. Nonlinear attenuation of sound in a duct.

5. U. Kurze. 1968. Doktor-Ingenieur Dissertation, Berlin. Schallausbreitung im Kanal mit periodischer Wandstruktur unter Berücksichtigung seitlicher Kopplingen in den Feldern hinter der Wand.

6. P.G. Vaidya. 1972. Paper presented at the symposium on the Acoustics of Flow Ducts, Southampton University. Some developments in the theory of sound attenuation.

7. R.A. Scott. 1946. Proc. Phys. Soc. Vol. LVIII, pp. 358-368. The propagation of sound between walls of porous material.

8. H.K. Liu and A.J. Martenson. To appear in J.A.S.A. Propagation of the discrete frequency noise from fans and compressors in axisymmetrical ducts of arbitrary shape.

9. A. Eisenberg and T.W. Kao. 1971. J.A.S.A. Vol. 49, No. 1, pp.169-175. Propagation of sound through a variable-area duct with a steady compressible flow.

10. P. Mungur. 1971. ISVR Annual Report, Southampton University. Propagation of sound in a flow duct with a varying boundary layer thickness.

11. A. Cummings, A. Kapur and P. Mungur, 1972. Paper presented at the symposium on the Acoustics of Flow Ducts, Southampton University. Sound propagation in a combustion can with axial temperature and density gradients.

12. W. Möhring. 1972. Paper presented at the symposium on The Acoustics of Flow Ducts, Southampton University. On the resolution into modes of sound fields in ducts with shear flow.

13. P.M. Morse. 1948. McGraw-Hill. Vibration and Sound.

14. P.M. Morse and K.U. Ingard. 1968. McGraw-Hill. Theoretical Acoustics.

15. D.C. Pridmore-Brown. 1958. J. Fluid Mech. Vol. 4, pp. 393-406. Sound propagation in a fluid flowing through an attenuating duct.

16. E. Meyer, F. Mechel and G. Kurtze. 1958. J.A.S.A. Vol. 30, No. 3, pp. 165-174. Experiments on the influence of flow on sound attenuation in absorbing ducts.

16a. P.D. Dean. 1970. ISVR Memo. No. 411. Research on the design of silencer elements.

17. U.J. Kurze and C.H. Allen. 1971. J.A.S.A. Vol. 49, No. 5 (part 2) pp. 1643-1654. Influence of flow and high sound level on the attenuation in a lined duct.

18. D.J. Snow. 1972. M.Sc. Thesis, Loughborough University. Attenuation of plane and high order modes in a circular and annular lined duct.

19. L. Cremer. 1953. Acustica, Vol. 3, pp. 249-263. Theory regarding the attenuation of sound transmitted by air in a rectangular duct with an absorbing wall, and the maximum attenuation constant produced during this process. (In German)

20. L.M. Brekhovskikh. 1960. Academic Press. Waves in Layered Media.

21. C.L. Morfey. 1971. Personal Communication.

22. J.E. Ffowcs-Williams. 1971. Personal Communication.

23. R.J. Briggs. 1964. Research Monograph No. 29. M.I.T. Press. Electron-stream interaction with plasmas.

24. L.M. Mack. 1965. Contribution to Methods of Computational Physics, Vol. 4. Academic Press. Computation of the stability of the laminar compressible boundary layer.

25. L.S. Wirt. 1972. J.A.S.A. Vol. 51, No. 5 (Part 1), pp. 1448-1463. Analysis, testing and design of lined ducts.

26. B. Barry and C.J. Moore. 1971. J. Sound Vib. Vol. 17, No. 2, pp. 207-220. Subsonic fan noise.

27. J.M. Tyler and T.G. Sofrin. 1961. S.A.E. 345D. Axial flow compressor noise.

28. J. Dyer. 1958. J.A.S.A. Vol. 30, No. 9, pp. 833-841. Measurement of noise sources in ducts.

29. C.L. Morfey. 1968. I.S.V.R. Memo. No. 218. Some thoughts on broad-band noise generation in fans.

30. Sung-Hwan Ko. 1971. J.A.S.A. Vol. 50, No. 6 (Part 1), pp.1418-1432. Sound attenuation in lined rectangular ducts with flow and its application to the reduction of aircraft engine noise.

31. C.L. Morfey. 1972. Personal Communication.

32. H.E. Plumblee, J.S. Gibson and L.W. Lassiter. 1962. WADD-TR-61-75. A theoretical and experimental investigation of the acoustic response of cavities in an aerodynamic flow.

33. B. Pye and S. Jones. 1970. University of Southampton Computer Service.

34. M.J. Benzakein, R.E. Kraft and E.B. Smith. 1969. Paper 69-WA/GT-11 presented at A.S.M.E. Winter Meeting, Los Angeles, Calif. Sound attenuation in acoustically treated turbomachinery ducts.

35. D.J. Snow. 1970. Rolls Royce Ltd. Personal Communication.

36. E.J. Rice. 1968. N.A.S.A. TM X-52442. Attenuation of sound in soft walled circular ducts.

37. B.J. Tester. 1971. Paper 20P7 presented at the 7th I.C.A., Budapest. The optimisation of sound attenuation in lined ducts containing uniform, axial, subsonic, mean flow.

38. L.B. Felsen and H.Y. Yee. 1968. J.A.S.A. Vol. 44, No. 4, pp. 1028-1039. Ray method for sound-wave reflection in an open-ended circular pipe.

39. C.L. Morfey. 1971. Personal Communication.

40. R.H. Cantrell and R.W. Hart. 1964. J.A.S.A. Vol. 36, No. 4, pp. 697-706. Interaction between sound and flow in acoustic cavities: mass, momentum and energy considerations.

41. W. Eversman. 1971. J.A.S.A. Vol. 50, No. 2 (Part 1), pp. 421-425. Signal velocity in a duct with flow.

42. W. Eversman. 1970. J.A.S.A. Vol. 48, No. 2 (Part 1), pp. 425-428. The effect of mach number on the tuning of an acoustic lining in a flow duct.

43. P.E. Doak and P.G. Vaidya. 1970. J. Sound Vib. Vol. 12, No. 2, pp. 201-224. Attenuation of plane wave and higher order mode sound propagation in lined ducts.

44. J.W.S. Rayleigh. 1887. Dover Publications, Vol. 2, The Theory of Sound.

45. J.W. Miles. 1958. J. Fluid Mech. Vol. 4, pp. 538-552. On the disturbed motion of a plane vortex sheet.

46. A.B. Friedland and A.D. Pierce. 1969. Physics of Fluids, Vol. 12, No. 6, pp. 1148-1159.

47. C.K.W. Tam. 1971. J. Fluid Mech. Vol. 46, part 4, pp. 757-768. Directional acoustic radiation from a supersonic jet generated by shear layer instability.

48. R. Betchov and W.O. Criminale. 1967. Academic Press. Stability of parallel flows.

49. C.L. Morfey. 1971. J. Sound Vib. Vol. 14, No. 2, pp. 159-170. Acoustic energy in non-uniform flows.

50. W. Möhring. 1971. J. Sound Vib. Vol. 18, No. 1, pp. 101-109. Energy flux in duct flow.

51. C.L. Morfey. 1971. J. Sound Vib., Vol. 14, No. 1, pp. 37-55. Sound transmission and generation in ducts with flow.

52. P. Mungur and G.M.L. Gladwell. 1969. J. Sound Vib. Vol. 9, No. 1, pp. 28-48. Acoustic wave propagation in a sheared fluid contained in a duct.

53. P. Mungur and H.E. Plumblee. 1969. Paper presented at the NASA Basic Noise Research Conference, Washington. Propagation and attenuation of sound in a soft-walled annular duct containing a sheared flow.

54. G.A. Wynne and H.E. Plumblee. 1970. Paper presented at 79th Spring Meeting of the Acoustical Society of America. Calculation of eigenvalues of the finite difference equations describing sound propagation in a duct carrying sheared flow.

55. W. Eversman. 1971. J.A.S.A. Vol. 49, No. 5 (Part 1), pp. 1372-1380. Effect of boundary layer on the transmission and attenuation of sound in an acoustically treated circular duct.

56. P.N. Shankar. 1971. J. Fluid Mech., Vol. 47, part 1, pp. 81-91. On acoustic refraction by duct shear layers.

57. S. Mariano. 1971. J. Sound Vib., Vol. 19, No. 3, pp. 261-275. Effect of wall shear layers on the sound attenuation in acoustically lined rectangular ducts.

58. S.D. Savkar. 1971. J. Sound Vib., Vol. 19, No. 3, pp. 355-372. Propagation of sound in ducts with shear flow.

59. W. Eversman. 1971. Paper presented at the AIAA/SAE 7th Propulsion Joint Specialists Conference, Utah. Theoretical and experimental analysis of acoustic linings for ducts with flow.

60. C.C. Lin. 1955. C.U.P. The Theory of Hydrodynamic Stability.

61. E.W. Graham and B.B. Graham. 1969. J.A.S.A. Vol. 46, No. 1 (Part 2), pp. 169-175. Effect of a shear layer on plane waves of sound in a fluid.

62. M. Gaster. 1962. J. Fluid Mech., Vol. 14, pp. 222-224. A note on the relation between temporally-increasing and spatial-increasing disturbances in hydrodynamic stability.

63. K. Stewartson and J.T. Stewart. 1971. J. Fluid Mech., Vol. 48, p. 529. A non-linear instability theory for a wave system in plane Poiseuille flow.